Stony Brook University

OFFICIAL COPY

The official electronic file of this thesis or dissertation is maintained by the University Libraries on behalf of The Graduate School at Stony Brook University.

© All Rights Reserved by Author.

Synthesis and Positron Emission Tomography Studies of Radioligands Targeting α7 Nicotinic Acetylcholine Receptors in the Central Nervous System

A Dissertation Presented

by

Sung Won Kim

to

The Graduate School

In Partial fulfillment of the

Requirements

for the Degree of

Doctor of Philosophy

in

Chemistry

Stony Brook University

August 2007

Stony Brook University

The Graduate School

Sung Won Kim

We, the dissertation committee for the above candidate
for the Doctor of Philosophy degree, hereby recommend
acceptance of this dissertation.

Dr. Joanna S. Fowler, Principle Advisor
Department of Chemistry

Dr. Yu-Shin Ding, Advisor
Department of Chemistry

Dr. Joseph W. Lauher, Advisor
Department of Chemistry

Dr. Andreas Mayr, Chairperson
Department of Chemistry

Dr. Francis Johnson, Third member
Department of Chemistry

Dr. Charles M. Fortmann, Outside reader
Department of Applied Mathematics & Statistics

This dissertation is accepted by the Graduate School

Lawrence Martin
Dean of the Graduate School

Abstract of the Dissertation

Synthesis and Positron Emission Tomography Studies of Radioligands Targeting α7 Nicotinic Acetylcholine Receptors in the Central Nervous System

by

Sung Won Kim

Doctor of Philosophy

In Chemistry

Stony Brook University

2007

The pharmacological effects of the action of nicotine on nicotinic acetylcholine receptors (nAChR) have been implicated in many diseases such as Alzheimer's disease, schizophrenia, and tobacco dependence. Brain imaging using positron emission tomography (PET) for each nAChR subtype provides biological information on subtype-specific function and pathological change. While PET studies for the α4β2 nAChR have progressed, the development of PET for α7 nAChR has been hampered due to the lack of suitable radioligands. It is, therefore, important to develop α7 nAChR-selective PET tracers for *in vivo* imaging studies to better understand the role of α7 nAChR in specific CNS disorders. Furthermore, positron emitter labeled drug that targets α7 nAChR can also contribute to drug development by providing information on *in vivo* pharmacokinetics.

In this work, we first investigated the drug pharmacokinetics of GTS-21, a partial α7 nAChR agonist drug, using PET in the baboon and rat. GTS-21 was labeled at two

different positions with the short-lived isotope C-11. In addition, the two corresponding demethylated metabolites, which have themselves been considered as contributing to the therapeutic effects of GTS-21, were synthesized and labeled with C-11. PET studies revealed extremely rapid uptake and clearance of [2-methoxy-^{11}C]GTS-21 from the brain, and significant brain uptake of the metabolite 2-OH-GTS-21, suggesting that it might contribute to the therapeutic effects of GTS-21.

Second, in order to describe α7 nAChR distribution, we synthesized C-11 labeled des-N-ethyl-N-methylmethyllycaconitine based on the known selective antagonist, methyllycaconitine. In its PET study, des(N-ethyl)-N-^{11}C-methylmehtyllycaconitine showed lack of blood brain barrier permeability at a tracer dose level, possibly due to high molecular weight and low lipophilicity. We also synthesized C-11 nicotine for primate PET study to show nicotine action in conjunction with the cigarette smoking. For [^{11}C]nicotine, compared with maternal brain, slow fetal brain entry and clearance of [^{11}C]nicotine was observed, indirectly indicating [^{11}C]nicotine transfer from the maternal to fetal brain during prenatal smoking.

Third, we have been developing putative quinuclidine-based α7 nAChR ligands with the aim of achieving selectivity and binding affinity. We synthesized a PET ligand candidate through reliable Pd catalyzed cross-coupling reactions of heteroaryl bromides and heteroaryl carboxylic acid, which might be useful for the parallel synthesis of quinuclidine-based derivatives.

This dissertation also provides insight for ligand interaction toward α7 nAChR through homology model of mouse α7 nAChR. For rational PET tracer design, a

quantitative structure-activity relationship study was performed to provide a putative ligand candidate for α7 nAChR.

Table of Contents

List of Figures····x

List of Schemes····xii

List of Tables····xiii

List of Abbreviations····xiv

Chapter 1 Introduction····1

1.1 α7 nicotinic acetylcholine receptor····1

1.1.1 α7 nicotinic acetylcholine receptor····1

1.1.2 The biodistribution of α 7 nAChR····5

1.1.3 Implications in diseases····8

1.1.4 CNS drugs related with α7 nicotinic acetylcholine receptor····10

1.1.5 The development of α7 nAChR radiotracers ····12

1.1.5.1 nAChR PET tracers····12

1.1.5.2 α7 nAChR PET tracers····14

1.2 Positron Emission Tomography (PET) ····16

1.2.1 Introduction····16

1.2.2 Common PET radionuclides····17

1.2.3 Development of PET tracer····19

1.2.3.1 C-11 PET chemistry ····21

1.2.3.2 F-18 PET Chemistry····23

1.2.4 The mechanistic view and properties of CNS PET tracers····25

1.2.5 The Drug development and PET ····29

1.3 Objectives····31

1.4 References····33

Chapter 2 C-11 labeled isotopomers and metabolites of GTS-21····45

2.1 Background····47

2.2 Objectives····49

2.3 Synthesis·····50
2.4 Radiolabeling, log D and free fraction in plasma·····50
2.5 Biological study·····53
2.5.1 Brain and torso imaging of 2-^{11}C-GTS-21(2-^{11}C-2) in baboon ·····54
2.5.2 Plasma analysis for radiotracer in baboon·····57
2.5.3 Comparison of dynamic PET images of two isotopomers·····60
2.5.4 Comparison of dynamic PET images of two C-11 labeled metabolites·····62
2.5.5 Effect of co-administration of a therapeutic dose of GTS-21·····63
2.5.6 Micropet and ex vivo studies in mouse ·····65
2.6 Conclusion·····68
2.7 Experimental·····69
2.7.1 General·····69
2.7.2 Sythesis·····70
2.7.3 Measurement of free fraction in plasma and log D·····72
2.7.4 PET studies in baboon·····74
2.7.5 Image Analysis ·····75
2.7.6 Plasma Analysis of [^{11}C]GTS-21 (2-^{11}C-2 and 4-^{11}C-2) ·····75
2.7.7 Plasma Analysis of ^{11}C-3 and ^{11}C-4 ·····76
2.7.8 Mouse Studies·····77
2.8 References·····79
Chapter 3 The development of quinuclidine-based α7 nAChR PET tracer·····83
3.1 Background·····83
3.2 Objectives ·····90
3.3 The synthesis of quinuclidine-based dihydroxyfuropyridine·····91
3.3.1 Initial design····· 91
3.3.2 Synthesis of precursor·····92
3.3.2.1 Alternative synthetic approaches via selective lithiation·····94
3.3.3 The synthesis of reference compound·····98
3.4 The synthesis of quinuclidinyl carboxamide derivatives·····99
3.4.1 Initial design of PET tracer·····99
3.4.2 The synthesis of precursor and reference compound·····100

3.4.3 Radiosynthesis ····· 102
3.4.4 PET studies ····· 102
3.4.5 Strategy for parallel synthesis ····· 103
3.4.6 Suzuki reaction ····· 104
3.5 Strategy for parallel synthesis ····· 112
3.5.1 Suzuki reaction of heteroarylthiophenecarboxylic acids ····· 112
3.6 Homology modeling of α7 nAChR ····· 112
3.6.1 background ····· 112
3.6.2 Homology modeling ····· 113
3.6.3 Docking ····· 116
3.7 Quantitative Structure-Activity Relationship (QSAR) study ····· 116
3.7.1 PET tracer candidates ····· 121
3.8 Experimental ····· 122
3.9 References ····· 138
Chapter 4 The PET study and synthesis of des-N-ethyl-^{11}C-methylMLA ····· 141
4.1 Background ····· 141
4.2 Objectives ····· 143
4.3 Synthesis ····· 144
4.4 Baboon study ····· 146
4.5 Experimental ····· 147
4.6 References ····· 150
Chapter 5 PET study of C-11 labeled nicotine ····· 153
5.1 Background ····· 153
5.2 Objectives ····· 156
5.3 Radiotracer chemistry ····· 158
5.4 PET studies ····· 160
5.4.1 Baboon study ····· 160
5.4.2 Pharmacokinetics ····· 161
5.4.3 Dosimetry ····· 163
5.4.4 Pregnant macaque study ····· 163
5.5 Materials and Experimental Methods ····· 165

5.5.1 Radiosynthesis·····165
5.5.2 Baboon study·····166
5.6 References·····167
Appendix·····171

List of Figures

Figure 1.1 The acetylcholine and subtype-selective AChR alkaloids

Figure 1.2 α-bungarotoxin (α-BTX) and ^{125}I-methyllycaconitine (MLA

Figure 1.3 α7 nAChR targeting drug candidates

Figure 1.4 PET tracers for nAChR (methy**l**-NFEP)

Figure 1.5 alpha7 nAChR-targeting PET tracers

Figure 1.6 The synthetic transformations of C-11 labeled carbon dioxide.

Figure 1.7 ^{18}FDG, epibatidine, [^{18}F]epibatidine

Figure 1.8 The structure of Kryptofix® $_{222}$

Figure 1.9 PET tracer for MAO A, B and mechanistic view.

Figure 2.1 The structures of anabaseine and GTS-21.

Figure 2.2 The metabolic route of GTS-21

Figure 2.3 The HPLC profiles of [^{11}C] GTS-21.

Figure 2.4 Time-activity curves for selected regions of interest of **2-^{11}C-2**.

Figure 2.5 Time-activity curves for baboon torso after administration of **2-^{11}C-2**.

Figure 2.6 Time-activity curves for baboon plasma.

Figure 2.7 Time-activity curves for [^{11}C]GTS-21 and their labeled metabolites

Figure 2.8 The PET image in baboon summed [^{11}C]GTS-21 and their labeled metabolites

Figure 2.9 The effect of therapeutic dose of GTS-21

Figure 2.10 Time-activity curves of **2-^{11}C-2**, B) **4-^{11}C-2** in mouse

Figure 3.1 The three dimensional structures of acetylcholine and nictine.

Figure 3.2 The strategy for SAR study

Figure 3.3 Comparison of azacylic systems for cationic center for α7 nAChR[7]

Figure 3.4 Stereochemistry at 3-postion of quinuclidine ring for α7 nAChR binding

Figure 3.5 Effect of substituent of the hydrophobic group of quinuclidine carboxamide on affinity for α7 nAChR.

Figure 3.6 Effect of substituents at 2-positon of quinuclidine ring on α7 nAChR binding affinity.

Figure 3.7 spirodihydrofuropyridine derivatives for α7 nAChR

Figure 3.8 The selective α7 nAChR ligands

Figure 3.9 Target compounds

Figure 3.10 Uptake of quinuclidinyl 2-(6-^{18}F-fluoropyridinyl) thiophene-5-carboxamide (3-21) in the baboon brain.

Figure 3.11 The nicotinic acetylcholine receptor of *Torpedo marmorata* (PDB ID: 2BG9) generated by MOE (Moleculer operation Environment).

Figure 3.12 The binding pocket of sea hare AChBP with epibatidine (PDB ID: 2BYQ)

Figure 3.13 Comparison of epibatidine binding pockets between sea hare AChBP (A, PDB ID: 2BYQ) and the homology model of mouse nAChR (B).

Figure 3.14 Correlation plot of QSAR model and training set.

Figure 3.15 Cross-validation plot of QSAR model.

Figure 3.16 The validation of QSAR model by a test set.

Figure 4.1 The structure of methyllycaconitine derivatives

Figure 4.2 The PET image in baboon summed from time of injection through 90 min for [^{11}C]des-N-ethyl-N-methylMLA

Figure 5.1 Nicotine and imidacloprid

Figure 5.2 Synthesis of [^{11}C] nicotine. i, [^{11}C]methyl iodide, PMP, DMF

Figure 5.3 HPLC profiles of [^{11}C]nicotine in the different HPLCsystems.

Figure 5.4 The time-activity curves for [^{11}C]nicotine in the baboon brain

Figure 5.5 The time-activity curve for peripheral organs in the baboon

Figure 5.6 The time-activity curve of [^{11}C]nicotine in the pregnant macaque

Figure 5.7 The PET image in baboon summed from time of injection.

Figure 5.8 The area under the curves (AUC) in the plasma for [^{11}C]nicotine

List of Schemes

Scheme 2.1 The synthetic scheme for GTS-21 and its metabolites. a, ethanol, reflux

Scheme 2.2 The radiosynthesis of C-11 labeled GTS-21 and its metabolites.

Scheme 3.1 The synthesis of precursor **3-2** and unlabeled target compound **3-1**

Scheme 3.2 The total synthesis of compound **3-2**

Scheme 3.3 The ring closure to dihydrofuropyridine ring using sodium hydride/DMF

Scheme 3.4 The synthetic route via lithiation of pyridine derivatives **3-10.**

Scheme 3.5 The synthetic pathway of F-18 labeled **3-2.**

Scheme 3.6 The synthesis of 5'-(2-Methyl-3-furanyl)spiro[1-azabicyclo[2.2.2]octane-3,2'(3'H)-furo[2,3-b]pyridine].

Scheme 3.7 The synthetic route for **3-21** and **3-25**.

Scheme 3.8 The radiosynthesis of **3-21**

Scheme 3.9 Strategy for parallel synthesis of quinuclindin-3-yl heteroarylthiophenyl carboxamide derivatives.

Scheme 3.10 Suzuki coupling of furan-3-boronic acid using 3-bromopyridine derivatives.

Scheme 3.11 Palladium-catalyzed cross-coupling reaction of pyridine-4-boronic acid.

Scheme 4.1 Synthesis of Des(N-ethyl)-N-methylMLA

Scheme 4.2 Synthesis of Des-N-ethylmethylMLA

Scheme 4.3 Radiosynthesis of Des-N-ethyl-^{11}C-methylMLA.

List of Tables

Table 1.1 The nAChR and mAChR subtypes

Table 1.2 The biodistribution of α7 and α4β2 nAChR

Table 1.3 The common positron emitting radionuclides for PET[93]

Table 2.1 Summary of baboon PET studies.

Table 2.2 The reproducibility of 2-^{11}C-2 PET study in the baboon brain.

Table 2.3 Effect of therapeutic dose of GTS-21 (0.031 mg/kg)* in the baboon brain.

Table 2.4 Whole body biodistribution of [2-methoxy-^{11}C]GTS-21 and [4-methoxy-^{11}C]GTS-21 in mouse.

Table 3.1 SAR study of AR-R17779 derivatives for nAChR subtype binding

Table 3.2 Comparison of cross binding activity (Ki) of 5-HT_3R drugs

Table 3.3 Binding profile (Ki) of spirodihydrofuropyridine derivatives

Table 3.4 Conditions for selective lithiation of 2-chloro-5-(furan-3-yl)pyridine

Table 3.5 Palladium catalyzed cross coupling reactions with 5-bromothiophene-2-carboxylic acid and palladium acetate

Table 3.6 Palladium catalyzed cross coupling reaction with 5-bromothiophene-2-carboxylic acid and various palladium catalysts and bases

Table 3.7 Palladium catalyzed cross coupling reaction with 5-(dihydroxyboryl) thiophene-2- carboxylic acid and 2-bromopyridine derivatives

Table 3.8 Palladium catalyzed cross coupling reaction with 2-bromopyridine and non-carboxyl aryl boronic acid

Table 3.9 Palladium catalyzed cross coupling reaction with 2-bromo-6-fluoropyridine and non-carboxyl aryl boronic acid

Table 3.10 Comparison of ligand interactions between sea hare AChBP (PDB ID: 2BYQ) and homology model of mouse α7 nicotinic acetylcholine receptor

Table 3.11 The PET ligand candidates calculated by QSAR model.

Table 5.1 The radiosynthesis and properties of [^{11}C] nicotine

Table 5.2 Summary of [^{11}C]nicotine PET studies.

Table 5.3 The dosimetry of [^{11}C]nicotine in the baboon

List of Abbreviations

Ach	Acetylcholine
AchBP	Acetylcholine binding protein
ACN	Acetonitrile
AD	Alzheimer's disease
ADHD	Attention deficit and hyperactivity disorder
mAChR	Muscarinic acetylcholine receptor
BBB	Blood-brain barrier
α-BTX	α-bungarotoxin
Bu	Butyl
BNL	Brookhaven national laboratory
CNS	central nervous system
DBU	1,8-Diazabicyclo[5.4.0]undec-7-ene
DME	1,2-Dimethoxyethane
DMF	*N*,*N*-Dimethylformamide
DMSO	Dimethyl sulfoxide
DV	Distribution volumn
EOB	End of cyclotron bombardment
TH	thalamus
PBS	Phosphate buffered saline
EP	Epibatidine
Et	Ethyl
fMRI	Functional magnetic resonance imaging
^{18}FDG	2-Deoxy-2-[^{18}F]fluoro-D-glucose
K_{222}	4, 7, 13, 16, 21, 24 -hexaoxa-1, 10-diazabicyclo [8.8.8] hexacosane
HOBT	3-hydroxybenzotriazole hydrate
HPLC	High-performance liquid chromatography
LBD	Ligand binding domain
LDA	Lithium diisopropylamide
Me	Methyl
MLA	Methyllycacotinine
MRI	Magnetic resonance imaging
nAChR	Nicotinic acetylcholine receptor
NMR	Nuclear magnetic resonance
QSAR	PQunantitative structure-activity relationship
PD	Parkinson's disease
PEG	Polyethylene glycol
PET	Positron emission tomography
PNS	Peripheral nervous system
PMP	1,2,2,6,6-pentamethylpiperidine
R_f	Retention factor
RCY	Radiochemical yield
ROI	Region of interest
RT	Room temperature

SA	Specific activity
SAR	Structure activity relationship
MAO	Monoamine oxidase
BP	Binding potential
SPECT	Single photon emission computed tomography
TBAB	Tetrabutylammonium bromide
TBTU	*N,N,N′,N′*-Tetramethyl-*O*-(benzotriazol-1-yl)uronium tetrafluoroborate
THF	Tetrahydrofuran
TLC	Thin-layer chromatography
TMS	Tetramethylsilane

Acknowledgments

With a Master degree from Korean University in 1995, I never planned to study again. My first trip to the United States, however, was to pursue studies in chemistry. What happened in my life? I sometimes question God as to my avocation. I stopped smoking and learned English both of which are prerequisites for survival in the US and started student life in my new surroundings. Fortunately, during the course of my Ph. D. degree, there have been special people to help me. I thank Dr. Joanna S. Fowler for her all thoughtful and kind efforts in my research as well as in my life. I will never forget your kindness, generosity and sincere care but also your scientific passion and dedication. In desperate times, you gave me encouragement and offered advice. When I found it difficult to balance the demands of family life and research, you were like a mother providing gentle support. You gave me the freedom to speak my mind without hesitation, which rarely happened previously in my academic career. It was an honor to be your Ph.D. student.

I extend my sincerest gratitude to:

Dr. Bong Young Chung, my thesis advisor for my Master's degree in Korea University, introduced me to the exciting world of chemistry.

Dr. Yu-Shin Ding gave me a wonderful experience in medical imaging and showed what chemistry can do. Ironically, you introduced me to the nicotine project, a previous smoker of 10 years. When I struggled with my synthetic problems, you encouraged me to get through all difficulty without any criticism. Even when you moved to the University of Yale, you still kept me in your schedule.

Dr. Joseph W. Lauher, a great consultant and scientist, opened my eyes wide enough to see the whole picture.

Dr. Andreas Mayr, the chairperson for the Ph.D. committee, treated me very kindly when I came to Stony Brook and later encouraged me to finish this work.

Dr. Francis Johnson, a third committee member, advised on critical problems in my thesis. I was most impressed by your knowledge and the laboratory skills you continue to perfect.

Dr. Charles M. Fortmann, an outside committee member, graciously accepted to read my dissertation. Thank you.

Mr. David Alexoff has been my consultant and mentor for small animal PET work and my personal life. Thank you for your strong and frank opinions and scientific criticism.

Dr. Stephen L. Dewey taught me anatomy and how to have fun. Your awesome humor made us all happy.

Dr. Jean Logan taught me PET modeling and help with my paper work.

Dr. Wynn Shiffer assisted me with PET image analysis.

I also thank all the cyclotron and PET people at BNL. Dr. Michael Schueller and Dr. Rich Ferrieri helped and taught me working with hot atoms. Especially, I thank Colleen Shea, Youwen Xu, Lisa Muench for their support for PET chemistry and correction of our article. I thank Dr. Gene-Jack Wang who is an unbelievably kind and enthusiastic scientist.

I thank Drs. David Grills, Andy Hwang in the Chemistry Department for teaching me LS-MS and NMR and your friendships.

Kun-eek Kil, my Korean friend and colleague, who introduced me a BNL PET group. You are such good man and shared all my emotions. I also thank Dr. Myung-hwa Kim and Dr. Namjun Kim who guided my wife to study here and always encouraged my confidence.

Dr. Alicia Reid, a synthetic chemist as well as wonderful woman who shared her knowledge in chemistry.

Dr. Zachery E. Katsamanis is a sincere friend as well as a good chemist, who helped me to revise this thesis and our article.

Dr. Jacob Hooker, a new friend in science.

Dr Kuo-shyan Lin, thank you for teaching me nuclear medicine.

I also thank our laboratory members Martine Mirrione, Vinal Patel and the German students.

I also thank all staff members in the Chemistry Department of BNL and Stony Brook University, Katherine Hughes, Jene Patterson, Steve Howell, Lee Wallcott and Jim Anselmini.

My family: Jong Sang Kim (father), Jung Shin Hwang (mother), Mi-Kyung Kim (sister), Duk-Won Kim (brother), Heejung Kim (sister), Oksun Park (mother-in-law) for all your love and support from my starting point. I also thank my best friend in Korea, Min-Seok Cho who is very smart and passionate.

My son, Ryan Joowon Kim. I will always remember my debt for the time when you were in the daycare. You are a wonderful gift in my life.

Last but not least, my wife, Dr. Yeon Joo Jang is my supporter, faithful friend, sweetheart. You gave me a chance to change my life. Your love for me is most important gift from God.

Chapter 1. Introduction

1.1 α7 nicotinic acetylcholine receptor

1.1.1 α7 nicotinic acetylcholine receptor

Brain cholinergic system Acetylcholine is the endogenous neurotransmitter for the cholinergic system. The level of acetylcholine is controlled by metabolic components such as cholinesterase (anabolic) and choline acetyltransferase (catabolic) and cholinergic neural transmission which is mediated by the acetylcholine receptor. This acetylcholine receptor in the nervous system was historically classified to nicotinic acetylcholine receptor (nAChR) and muscarinic acetylcholine receptor (mAChR) by binding characteristics for the two natural alkaloids, nicotine and muscarine under the Sir. Henry Dale's observation, respectively (Figure 1.1).[1] The brain cholinergic system has been of particular interest in medicine because of its involvement in memory and cognition. Cholinergic deterioration in Alzheimer's disease (AD) has resulted in the development of the cholinergic hypothesis; in other words, cognitive deficit of AD brain may be due to a deficiency of cholinergic neurotransmission and degeneration of cholinergic neuron.[2]

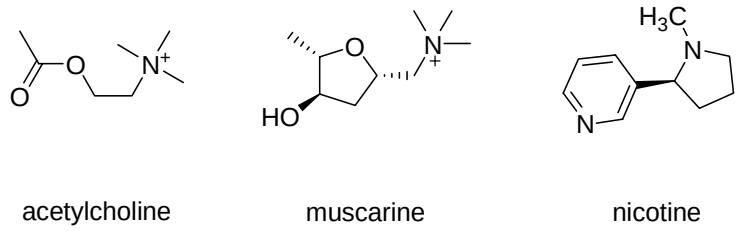

Figure 1.1 The acetylcholine and subtype-selective AChR alkaloids.

Structure and Classification While mAChR is one of guanine nucleotide (G protein) coupled metabotropic receptor family with 5 subclasses, nAChR is a ligand-

gated ion channel (LGIC) assembling with five subunits (Table 1). The subunits of the nAChR are known to be α2-7, α9, α10, β2- β4 in the mammalian CNS and include α8 in avian species.[3] Diverse pentameric combinations of these subunits present in the nervous system mediate a variety of intrinsic biochemical functions as well as physiological functions. In fact, along with different subunit combinations, a heterogeneous pattern of subunits expression in the developmental stage and distinctive electrophysiological properties for nicotinic drugs have been observed.[4-6]

Table 1.1 The nAChR and mAChR subtypes

	Subtypes	Structure	Class	Related diseases
mAChR	M_1, M_2, M_3, M_4, M_5	single peptide with seven transmembrane domains	G protein-coupled receptors	Schizophrenia AD, PD
nAChR	$\alpha_4\beta_2$, α_7, $\alpha_4\alpha_5\beta_2$ (CNS) α_7, $\alpha_3\alpha_5\beta_4\beta_X$ (PNS) $\alpha_1\beta_1\gamma\delta$, $\alpha_1\beta_1\gamma\delta$ (Muscle)	Pentamer with five subunits	Ligand-gated ion channel	Auditory gating Schizophrenia, AD, PD, ADHD

PNS (peripheral nervous system)
PD (Parkinson's disease)
ADHD (attention-deficit hyperactivity disorder)

Structurally, nAChR is a prototype of Cys loop receptor family of the LGIC super family[7] which includes 5-hydroxytryptamine type 3A receptor (5-HT_{3A}), γ-aminobutyric acid receptor type A and C ($GABA_A$ and $GABA_C$), and glycine receptor (GlyR). α subunits have a sdisulfide bond of the conserved vicinal two Cys in the extracellular domain. The agonist, nicotine was known to bind the pocket between α and adjacent subunit and thus the number of binding sites depends on the number of α subunits. To date, the α2- α7, α10, β2-β4 subunits have been found in human neuronal nAChRs. The

α4β2 ($(\alpha4)_2(\beta2)_3$) and α7 ($(\alpha7)_5$) nAChR subtypes are the most abundant two subtypes in the CNS. Though α7 nAChR can be assembled in heteromeric form with β2 [8], it is generally accepted to be a homomeric subtype as $(\alpha7)_5$ (Table 1.1).

Binding characterization Over several decades, the discovery and characterization of subtype specific radioligands have been based on natural products-based research.[9, 10] Compared with α4β2 nAChR which shows high binding affinity for nicotine and low binding affinity for α-bungarotoxin (α-BTX) extracted from snake venom, the venom of the banded krait, *Bungarus multicinctus*,[11, 12] the α7 nAChR has low binding affinity for nicotine and high binding affinity for α-BTX (Figure 1.2).[10, 13] Based on its similar binding pattern with α7 subunit protein or mRNA distribution as well as its high binding affinity, ^{125}I-α-BTX binding assay is a gold standard for α7 nAChR,[13-15] even though it was recently reported that α-BTX binds to $GABA_AR$ containing the GABRβ3 subunit.[16]

The other standard compound for α7 nAChR binding is methyllycaconitine (MLA), a natural alkaloid isolated from larkspurs species. It showed competitive binding profile for ^{125}I-α-BTX binding in nanomolar level and almost identical pattern of distribution in the CNS.[17-20]

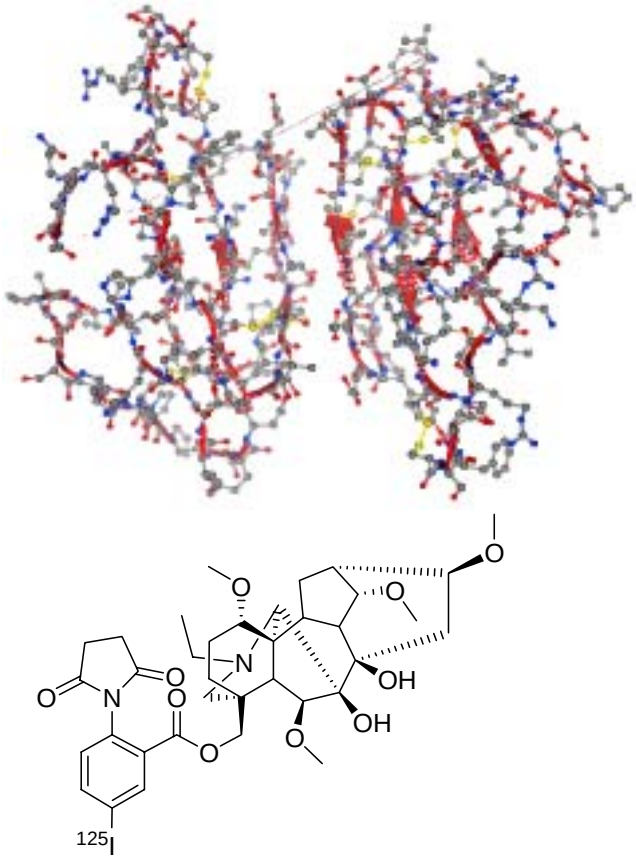

Figure 1.2 α-bungarotoxin (α-BTX) and ^{125}I-methyllycaconitine (^{125}I-MLA)

Function Electrophysiologically, α7 nAChR showed fast desensitization and high calcium permeability by activation through binding with agonists such as acetylcholine and nicotine. At the cellular level, the α7 nAChR is present in the nerve terminal the presynpase. It has been hypothesized that the α7 nAChR is linked with cellular Ca^{2+} related signaling events such as protein kinase C-dependent apoptotic process, neurite growth, synaptic transmission, and neurotrophic effects. In the synapse, α7 nAChR has been known to mediate fast synaptic transmission and to modulate the release of other neurotransmitters.

Pharmacologically, the α7 nAChR in the central nervous system (CNS) is known to be involved in sensory gating and cognitive functions such as attention, spatial memory.[21, 22] There is evidence for critical role of α7 nAChR for learning and memory. For example, nicotine-induced memory enhancement has been suggested to be due to α7 nAChR consistent with high density in the hippocampus. α7 nAChR knock-out mice showed impaired attention[23] and episodic memory dysfunction.[24] α7 nAChR agonists have been shown to contribute to the working memory.[25] In addition, several studies showed that the CNS α7 nAChR is involved in neuroprotection through α7 nAChR-selective agonists.[26] However, addiction, one of side effect of nicotine, may not be involved with α7 nAChR.[25]

1.1.2 The biodistribution of α 7 nAChR

In case of α4β2 nAChR, in vivo imaging in humans with several PET tracers has shown high specificity, sensitivity, and correlation with known α4β2 nAChR distribution in the brain. However, to date, α7 nAChR PET tracers are still under development. In addition to shortage of ligands with selectivity and high affinity, the task of developing suitable α7 nAChR ligands appears even more challenging due to the fact that α7 density in mammalian brain is less (only 30~50%) than that of α4β2 nAChR.[27, 28]

The biodistribution studies of α7 nAChR in the brain has been performed by autoradiography with selective ligands ([I^{125}]α-BTX,[29] [^{3}H] MLA,[27] [I^{125}]iodoMLA[30]), in situ hybridization[31, 32], RT-PCR[33], and immunohistochemistry.[34]

Compared with [^{3}H]nicotine binding which is high in thalamus and low in hippocampus, [I^{125}]α-BTX binding sites in the rat brain showed distinctive pattern[35].

They are high in the hippocampus and absent in the thalamus. Whiteaker et al. showed in their autoradiography study with [^{3}H]MLA that α7 nAChR binding is high in the dorsal tegmental nucleus of the pons, colliculi, and hippocampus (58.8 fmol/mg protein) in the rat brain.[27] [^{125}I]-BTX binding was also quite identical with binding sites for [^{3}H]MLA and Bmax of whole brain was 45.6 fmol/mg protein. Binding sites for radiolabeled ligands is low (5.45 fmol/mg protein) in cerebellum and thus this brain region may be suitable as a reference region in a PET study in rat.

The distribution pattern of α7 nAChR in the brain is different from $\alpha_4\beta_2$ nAChR. In monkey, while [^{3}H]cytisine (a specific radioligand for the α4β2 nAChR) binding for is highest in thalamus, and lower in striatum, hippocampus, amygdala, [I^{125}]α-BTX (a specific radioligand for the a7 nAChR) is rich in thalamus, hippocampus, moderate in amygdala and very low in putamen and caudate.[29] Recently, Kulak et al. also reported a high density region for [^{125}I]-BTX binding analysis in thalamic nuclei, compared with hippocampus, basal ganglia, cortex area in monkey brain.[30] In contrast with monkey, [I^{125}]α-BTX binding of rat thalamus is almost not detected,[13] indicating the distribution of α7 nAChR is species-specific in thalamus. Hans et al. also suggested that neuronal function of α7 nAChR in primate is more complex than in rodent, presumably because of its wide distribution in the monkey.[29]

Table 1.2 The biodistribution of α7 and α4β2 nAChR

	α7 nAChR (fmol/mg protein)			α4β2 nAChR (fmol/mg protein)		
	Human	Rat	monkey	Human	Rat	Monkey
Cortex	10.6[36]	48.4[37]	22.4[38]	12.5[36]	98.4[37]	41.6[38]
Cerebellum	11[33]	5.45[39]	-	-	45[40]	-
Striatum	-	47.0[36]	12.1[38]	55.0[36]	154[37]	-
Hippocampus	18.2[33]	83.6[36]	-	-	44.5[39]	-

In the human brain, the order of [I^{125}]α-BTX binding density was reported to be hippocampus (18.2 fmol/mg protein), temporal cortex (15 fmol/mg protein) cerebellum (11.0 fmol/mg protein) (Table 1.2).[33] Consistently, Court et al. demonstrated that α7 nAChR was high in hippocampus, widely distributed in cerebral cortex, very low in striatum, absent in globus pallidus, contrasting with the distribution in non-primate brain.[41] In contrast, while [^{3}H]nicotine binding in striatum was higher than that in hippocampus and thalamus, [I^{125}]α-BTX also showed much higher binding in hippocampus and thalamus than in striatum. Martin-Ruiz et al. reported that [I^{125}]α-BTX binding in cerebellum was slightly higher than that in frontal and parietal cortex.[42] Interestingly, Falk et al. reported that expression of the α7 nAChR in the fetal brain was higher than in adult brain, indicating its role in the brain development.[5]

A potentially interfering molecular target to be considered in the design of radiotracers with specificity for the α7 nAChR for PET tracer development is 5-HT_{3A} receptor in that they share high homology (~30%) in protein sequence as a structurally similar pentameric ligand-gated ion channel.[43] Therefore, many α7 nAChR ligands showed cross reactivity with 5-HT_3.[44] The order of high binding sites for 5-HT_{3A} observed by [^{3}H]GR65630 were area postrema (13.1 ± 9.7 fmol/mg protein), striatum (4.8 ± 2.4 fmol/mg protein), amygdala, hippocampus, cerebral cortex and cerebellum in human brain.[45]

1.1.3 Implications in diseases

During the normal aging, the level of brain nAChR decreases gradually in the most brain regions. However, in disease the degree of brain nAChR change is subtype-specific with distinctive regional trends in the neurodegerative diseases and developmental disorders.

Alzheimer's disease & Parkinson's disease Pharmacologically, α7 nAChR has been considered to be associated with cognitive function and neuroprotection. Hellstrom-Lindahl et al. reported transcriptional and translational alteration of α7 expression in hippocampus of AD brain, with higher level of α7 mRNA of AD brain and less expression of [I^{125}]α-BTX binding sites than that of control.[33] An increase of [I^{125}]α-BTX binding sites in cerebellum (39%)[33] and thalamus[46] with AD was also reported. While significant deterioration of α4β2 nAChR in the temporal cortex of the AD brain was observed, α7 nAChR was not changed significantly except for Davies et al.[47] and Wevers et al.'[48] observations in their biodistribution studies.[49, 50] It is also known that β amyloid binds to α7 nAChR with high affinity. α7 nAChR agonist induced neuroprotection against β amyloid or glutamate has been reported, suggesting α 7 nAChR-related cell survival kinase mechanism.[51]

In Parkinson's disease, there are significantly increased [I^{125}]α-BTX binding sites in temporal cortex[52] and decreased binding sites in cerebellum.

In order to ameliorate the symptoms of these neurocognitive diseases, α7 nAChR is a potential target for the CNS drug development because it is intact compared with α4β2 nAChR.

Schizophrenia In epidemiological studies, 80% of schizophrenics are heavy smokers. Therefore, this is considered self-medication of high concentration of nicotine, which showed agonistic activity to α7 nAChR. In fact, GTS-21 (so called DMXB, Figure 1.3), a functionally selective agonist to α7 nAChR, showed its efficacy for schizophrenia in a clinical study.[53] α7 nAChR-related pathological change in schizophrenia was observed in hippocampus[54] and thalamic reticular nucleus[55] of schizophrenics without change of [^{3}H]nicotine binding sites. In conjunction with gene abnormality, chromosome 15q13–14 which is a locus of α7 nAChR (CHRNA7), has been implicated in schizophrenia.[56] Recently, α7 nAChR-knock out mouse generated as an animal model of schizophrenia showed severe attention deficit.[23]

Autism Attention deficit in autistic human is believed to be associated with alteration of cholinergic system in cortical area. In conjunction with α7 nAChR, while [^{125}I]BTX binding increase in cerebellum,[42] α7 immunoreactivity decreased in thalamus with autisum.[57]

Small cell lung cancer (SCLC) Peripherally, it has been shown that SCLC cells express high level of [I^{125}]α-BTX binding sites.[12, 58, 59] SCLC has been considered to be associated with tobacco smoking. This carcinogenesis was suggested to be caused by 4-(N-nitroso-N-methylamino)-1-(3-pyridyl)-1-butanone (NNK) which is a potent carcinogen contained in tobacco products.[60] α7 nAChR is also known to be expressed in malignant pleural mesothelioma (MPM) which is induced by asbestos.[61] α-Cobratoxin, an inhibitor for α7 nAChR showed efficacy for MPM cancer cell lines.[62]

1.1.4 CNS drugs related with α7 nicotinic acetylcholine receptor

Diversity of nAChR subtypes in the CNS implies their various pharmacological effects. For example, nicotine-induced favorable and adverse effects may be due to these diverse functional activities of nAChR subtypes. To reduce the adverse effect and maximize therapeutic effect of nicotine, selective ligands have been developed. Even though fast electrophysiological desensitization of α7 nAChR may limit its therapeutic effect, several agonists have been under the clinical trials. The first leading drug candidate targeting α7 nAChR is GTS-21 (Figure 1.3), a functionally selective agonist for α7 nAChR, which has been shown to normalize auditory gating for schizophrenics[53], and to enhance memory in healthy humans.[63]

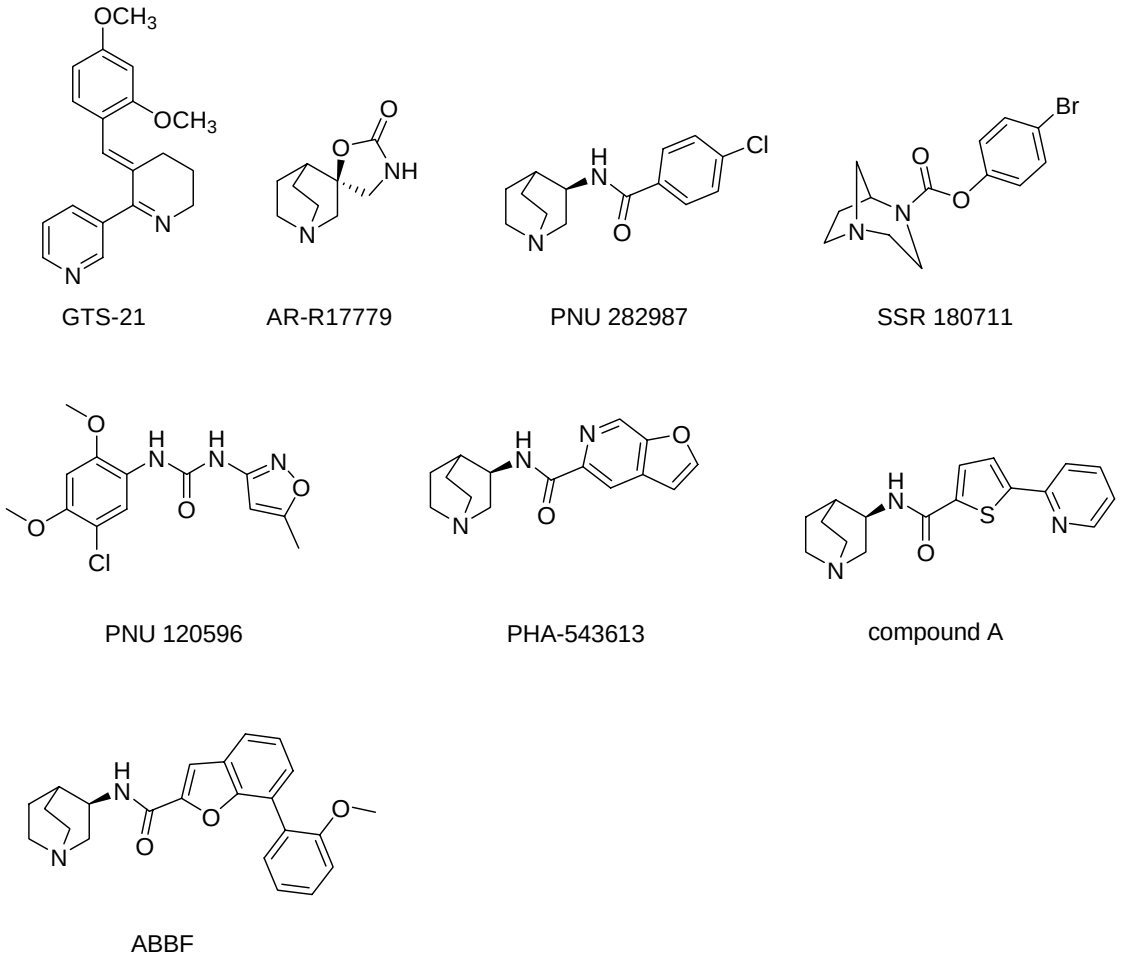

Figure 1.3 α7 nAChR targeting drug candidates

Stimulated by these antipsychotic and cognitive effects of GTS-21, many pharmaceutical companies have been involved in the development of new α7 nAChR selective agonists in the last 10 years. AR-R17779[64] and PNU 282987[65] showed cognitive efficacy in the many animal models as selective agonists.[66] However, AR-R17779 failed to demonstrate appropriate bioavailability in the target tissue and PNU-282987 is later known to be an active inhibitor for the human *Ether-a-go-go* (hERG) K^+ channel which is contra-indicated in drug development. Another quinuclidine-based agonist, Compound

A [67] showed efficacy for sensory gating deficit rat model. In 2006, Wishka et al. reported a new drug candidate, PHA-543613 (Ki= 8.8 nM)[68], which showed rapid brain penetration and moderate oral bioavailability as well as efficacy for auditory sensory gating and cognition. In 2007, Biton et al. and Pichat et al. reported that SSR 180711[69], a selective partial agonist for α7 nAChR (Ki= 14 nM, EC_{50}= 4.4 uM for human α7 nAChR), showed efficacy for various mouse models with cognition deficits such as memory and attention for schizophrenia.[70] Another quinuclidine-based agonist, ABBF was reported by Boess et al. to induce memory enhancement in rat, which was blocked by MLA, indicating α7 nAChR involvement.[25] An allosteric modulator, PNU120596 was known to prolong the electrophysiological response of agonists.[71] In addition to these compounds, PH-399733, MEM 3453 are in clinical trials.[72]

1.1.5. The development of α7 nAChR radiotracers

1.1.5.1 _nAChR PET tracers

Since nicotine was first labeled with [^{11}C]methyl iodide[73], many non-selective nAChR or selective α4β2 nAChR PET tracers have been developed intensively for last ten years. In the beginning, [^{11}C]nicotine, [^{11}C]N-methylcytisine were synthesized, showing a high non-specific binding in vivo and relatively homogenous distribution. [^{11}C]ABT-418 and [^{11}C]MPA showed a moderate degree of specificity compared [^{11}C]nicotine (Figure 1.4). Based on epibatidine (EP), which is a very potent natural product isolated from the South American Ecuadoran poison frog, the BNL PET group developed F-18 labeled epibatidine ([^{18}F]NFEP) in which F-18 was substituted for the chlorine atom which occurs in the natural product. 6-[^{18}F]NFEP provide a high signal-to-

noise[74, 75] ratio and high sensitivity to changes in acetylcholine[76]. Though it showed high specific binding and signal-to-noise *in vivo*[74], its use for human was not possible due to high toxicity.[77] Subsequently, in order to reduce toxicity, the modification of [^{18}F]NFEP by N-methylation was performed and gave a similar biodistribution profile to [^{18}F]NFEP in baboon; however, it changed cardiorespiratory parameters indicating binding to the peripheral nicotinic receptor precluding translation to humans.

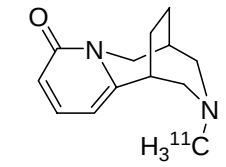

N-methylcyticine

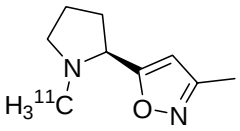

[^{11}C]ABT-418

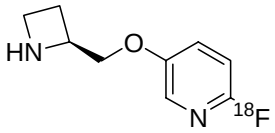

6-[^{18}F]Fluoro-A-85380

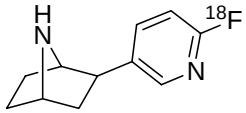

[^{18}F]NFEP

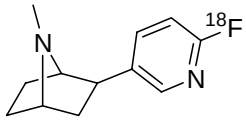

[^{18}F]N-methy-NFEP

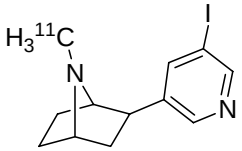

[^{11}C]NMI-EPB

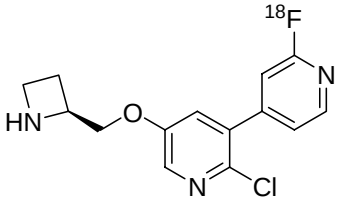

[^{18}F]NIDA52189

Figure 1.4 PET tracers for nAChR (methyl-NFEP)

Based on the A-85380, which shows subnanomolar affinity and moderately low toxicity[78], F-18 labeled 2- and 6-fluoro-A-85380 (Figure 1.4) have been shown to maintain high affinity towards α4β2 nAChR with a lower toxicity than epibatidine derivatives.[79] Currently, these labeled compounds have been tested for human α4β2 nAChR system in the CNS[80] and interestingly, ^{125}I version of A85380 for SPECT was tested for human brain with Parkinson's disease, showing the significant loss of striatal binding sites.[81] However, F-18 labeled A-85380 is still not considered as an optimal PET tracer in that it showed slow brain kinetics, which interfered the quantitative analysis and required a long acquisition time to reach a equilibrium for receptor binding. To overcome low binding potential for cortical and striatal area, [^{18}F]NIDA52189 (name it or put structure in a figure; Ki= 4.9 pM) has been developed by Zhang et al., showing 2.5 times higher binding potential than F-18 labeled A-85380.[82]

In 2005, a C-11 version of epibatidine derivative, [^{11}C]NMI-EPB (functional antagonist for nAChR) was developed to overcome limitation of toxicity shown by agonists such as epibatidine.[83]

1.1.5.2 α7 nAChR PET tracer

Compared with α4β2 nAChR PET tracers, the development of α7 nAChR PET tracer has been hampered by lack of suitable structural templates which would be potent and selective.

In 2001, Dolle et al. synthesized C-11 labeled quinuclindinyl carbamate derivative ([^{11}C]quinuclidin-3-yl 4-bromophenylcarbamate, **1-1**) and performed a rat *ex vivo* study, demonstrating homogenous distribution in the brain and no specificity (Figure 1.5). In

2005, Dannals et al. published the study of three quinuclidine-based ligands. Notwithstanding their high affinity *in vitro* study, compound (**1-2**) and (**1-3**) showed poor specificity and lack of site selectivity[84] and compound () showed very fast clearance in all brain regions.[85]

To our knowledge, up to date, a suitable α7 nAChR PET tracer has not been reported.

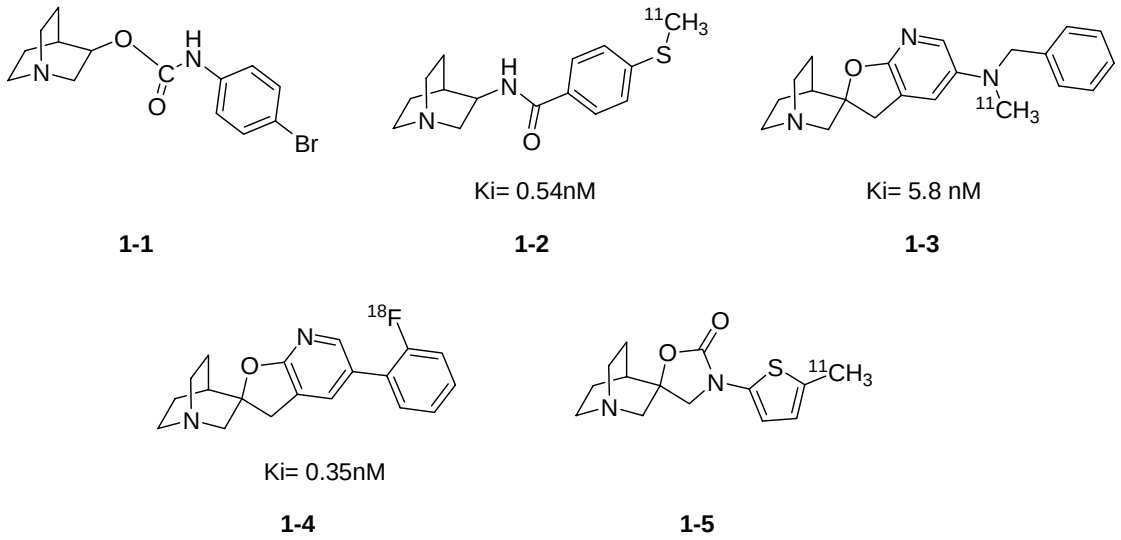

Figure 1.5 alpha7 nAChR-targeting PET tracers

1.2 Positron Emission Tomography (PET)

1.2.1 Introduction

Positron emission tomography (PET) is a non-invasive medical imaging technology that tracks temporal and spatial concentration of positron-emitter-labeled compound in living organisms, providing information on biochemical transformations and the distribution and movement of drugs.

In common, while magnetic resonance imaging (MRI) and X-ray computed tomography (CT) delineate mainly anatomical detail *in vivo* system, PET is a functional and molecular imaging tool for a specific biological target of interest. Functional magnetic resonance imaging (fMRI) can also observe the oxygen metabolism and blood flow changes. However, it is limited as functional imaging which does not show a direct specific molecular interaction. The other molecular imaging tools have their advantages, but they have their respective limitation (Figure 1.6). For the last two decades, PET has been intensively developed not only as a research tool to investigate drug action and disease-specific pathological change for biological components such as neuronal receptors, enzymes, but also as a clinical diagnostic tool for cancer[86], epilepsy[87], cardiovascular diseases, and cognitive impairment.[88, 89] PET is also a unique tool for evaluating drug pharmacokinetics and pharmacodynamics in humans and animals and is used increasingly for drug research and development.

As a probe for drug induced pharmacodynamic change in the CNS, PET is highly sensitive to detect of the availability of endogenous neurotransmitter receptors and transporters without any perturbation of the system. For example, while the concentration

of neurotransmitter is generally in the micro to nanomolar range per gram[90], the concentration of PET tracer in the brain is from picomolar to femtomolar range per gram. As the pharmacologically effective dose of CNS drugs is likely generally to be even much higher, the biological effect of PET tracer dosage is negligible and thus PET is a true tracer method. In fact, several evidences showed that the change [^{11}C]raclopride binding in the baboon and human brain correlated with the change of dopamine level in striatum induced by nicotine or tobacco smoking.[91, 92]

In view of pharmacokinetics, PET and a labeled drug provides a direct measure of drug distribution and kinetics over the course of time *in vivo* system. Owing to its non-invasiveness, PET human pharmacokinetic study is feasible especially in the early stage of drug development. This has the potential to facilitate the drug discovery in human by reducing cost and time. In the later phases of drug development, PET can be utilized to determine drug doses and target occupancy.

1.2.2 Common PET radionuclides

The physical characteristics of positron emitters suitable for PET are their short-half life and positron emission which results in the production of two photons energetic enough to penetrate the body barrier (511 keV). There are several common positron emitters produced routinely in a modern cyclotron (Table 1.3). While F-18 in the forms of 2-deoxy-2-[^{18}F]fluoro-D-glucose (FDG) can be purchased and delivered within several hours after its production, most of positron emitters such as C-11, N-13, O-15 must be generated at the side of the experiment from a cyclotron due to their short half life.

Table 1.3 The common positron emitting radionuclides for PET[93]

Nuclide	Half-life(min)	Production	Range (mm)**	Specific Activity (Max. SA*) (Ci/μmol)	Decay Product
^{11}C	20.4	$^{14}N(p,\alpha)^{11}C$	4.1	< 20 (9.22×10^3)	^{11}B
^{13}N	9.98	$^{16}O(p,\alpha)^{13}N$	5.4	< 10.8 (1.89×10^4)	^{13}C
^{15}O	2.03	$^{14}N(d,n)^{15}O$	8.2	(9.08×10^4)	^{15}N
^{18}F	109.8	$^{18}O\ (p,n)^{18}F$ $^{20}Ne(d, \alpha)^{18}F$	2.4	< 5.4 (1.71×10^3)	^{18}O

* Theoretically calculated.

** Maximum range in the water.

In principle, the positron (β^+) emitted by decay of a positron emitter moves a certain distance depending on its kinetic energy, and then annihilates with an electron to generate two photons at 180° apart. The PET camera detects coincident photons to give spatial and temporal quantitative information of radionuclide concentration. The physically intrinsic resolution depends on the traveled distance of positron in the tissue and the angular deviation of two γ-ray (±0.25 °). The maximum distances to travel for ^{11}C, ^{18}F are 4.1mm, 2.4mm, respectively.[93]

Specific Activity The quality of positron emitters is determined by specific activity which defines as the unit of radioactivity/unit of mass (commonly, Ci/μmol). Theoretically, since each position emitter is produced from different element and thus present as a pure isotopic form, maximum specific activity would be achieved (also called, carrier-free). For example, C-11 produced by N-14 should not contain C-12. However, in reality, the elimination of C-12 in the [^{14}N] nitrogen is impossible and therefore, specific activity is very low (typically, C-12/C-11= 5000~10000), which means

carrier-free C-11 is not achievable. The major sources of C-12 are hydrocarbons in the nitrogen gas which is irradiated in the cyclotron as well as atmospheric carbon dioxide in target and delivery line and chemical reagents for precursor synthesis. In general, specific radioactivity of C-11 ranges 1-20 Ci/μmol at the end of bombardment as a form of [^{11}C] methyl iodide at BNL cyclotron. In the batch type synthesis (wet synthesis) using lithium aluminum hydride with C-11 labeled carbon dioxide, the specific activity is significantly lower due to the unintentional introduction of CO_2 from the air. Therefore, the specific activity of a final product depend on mainly what kind of C-11 labeled precursor one chooses and what kind of reagents are used for the chemical transformation. In case of [^{18}F]F_2 production, for the purpose of delivery of the radioactive fluorine gas out of the target, the natural fluorine gas is intentionally added (Carrier-added), resulting in low specific activity labeled fluorine gas. In contrast, the production of [^{18}F]F^- from [^{18}O]H_2O does not need carrier (No- carrier-added). However, stable fluoride ($^{19}F^-$) is still present and comes from various components used in production and synthesis.

The specific activity also reduces naturally by decay of positron emitters after the end of bombardment. Obviously, the specific activity of shorter half-lived radionuclide is reduced faster than that of longer half-lived radionuclide.

1.2.3 Development of PET tracers

The work flow of PET consists of four main categories; radionuclide production in the cyclotron, synthesis of precursor, radiolabeling in a radiotracer laboratory, biological study (PET scan), and image analysis and evaluation. Generally, there are

several unique factors to be considered in the field of PET chemistry, distinguished from normal synthetic chemistry or radiochemistry.

First, the major factors governing PET chemistry is time for the entire labeling process including purification. For example, compared with common radiochemistry with C-14 (half-life= 5730 years, β^- decay), C-11 PET chemistry must be completed within less than 60 minutes in order to have sufficient radiotracer for a human PET study because of its short half-life. In view of the design of precursor, the labeling step is preferred to be the last step of all synthetic schemes. Reaction kinetics in the labeling step is pseudo first order kinetics of labeled precursor which is limiting reagent (less than 0.01-0.06 equivalency (in case of [^{11}C] methyl iodide). Usually, this reaction rate is optimized by controlling temperature, solvent, chemical additives, and catalysts. Maximum radiochemical yield depends on the rate for both labeling and decomposition of product which can occur at high temperatures which are frequently used. To reduce time for purification, preparative HPLC and solid-phase extraction[94] are commonly used for product purification. In particular, solid-phase extraction is advantageous for commercial production in view of short purification time as well as better reproducibility. In case of F-18, due to its comparatively longer half-life, several steps and purifications are possible.

Recently, some techniques have been developed to increase the reaction rate. The efficiency of microwave reactor was reported[95] and currently, microfluidics technology has been introduced to improve radiochemical yield and product selectivity by efficient heat and mass transfer (diffusion). However, it still needs to be verified whether it works for C-11 with flexibility to various reaction condition.[96]

Second, one should consider what kind of labeled precursor is available for the labeling step, by which synthetic strategy would be determined. Considering the limited number of labeled precursors available either from the cyclotron target or via some simple steps, the general synthetic organic transformation is used for labeling. Less commonly, catalytic enzyme reactions have been adopted. Recently, transition metal catalysts such as cross coupling reaction have broadened labeling methodology.[97, 98] The functional groups that are labile or reactive at high temperature and certain pH should be routinely protected by the appropriate protecting group. The deprotection step must also be rapid.

For the PET study, the decay uncorrected yield at the end of synthesis should be also taken into account to produce enough of radioactivity for the PET study.

In a view of safety, radiation exposure for PET chemist is minimized during the radiosynthesis. All procedure are planned carefully to reduce the exposure to radiation under the proper engineering control such as proper protective gear, automated devices, on- line purification system, and shielding. These controls are indispensable not only to prevent unnecessary handling of radioactive material but to improve the reproducibility of yield and product quality.

1.2.3.1. C-11 PET chemistry

Carbon is one of the most ubiquitous elements in biologically active molecules. The isotopic substitution of C-11 for C-12 allows the direct measurement of behavior of a molecule of interest. Of the six unstable carbon isotopes of which half-life are known, Only C-11 has the practically appropriate half-life and decay mode for PET. Though

kinetic isotope effect was reported in the previous literature ($^{11}C/^{14}C$)[99-102], it is generally assumed that C-11 has the same properties of C-12 in the biological experiment set-up.

Since C-11 was observed by Crane and Lauritsen[103] in 1934 by proton beam bombardment onto boron oxide, the first application to biological system was performed by Ruben et al. to show incorporation of C-11 labeled carbon dioxide into plants by photosynthesis in 1939.[104] Six years later, Tobias reported the first human study with C-11 labeled carbon monoxide.[105] However, since C-14 was discovered in 1940 by Ruben et al.,[106] it began widely to be used for biological application instead C-11. After the development of PET instrument, C-11 PET chemistry has intensively been developed.

In view of the synthetic design of unlabeled precursor, one should consider a reliably available C-11 labeled precursor (Figure 1.6) for the labeling step. The common chemical forms from nuclear reaction are C-11 labeled carbon dioxide, methane, and rarely carbon monoxide. Mostly, these are released to a dry on-line reactor (solvent free) or cold trapping in a batch reactor (wet) for transformation to a reactive C-11 labeled precursor. Recently, borane was reported as trapping reagent of C-11 labeled carbon monoxide. In the BNL PET facility, routinely accessible C-11 labeled precursors are carbon dioxide, methyl iodide, methyl triflate, and cyanide. C-11 labeled methyl iodide is frequently used for alkylation of amine, phenolic –OH, thiol group and amide. C-11 labeled methyl triflate is an alternative precursor for the functional groups which are less reactive.

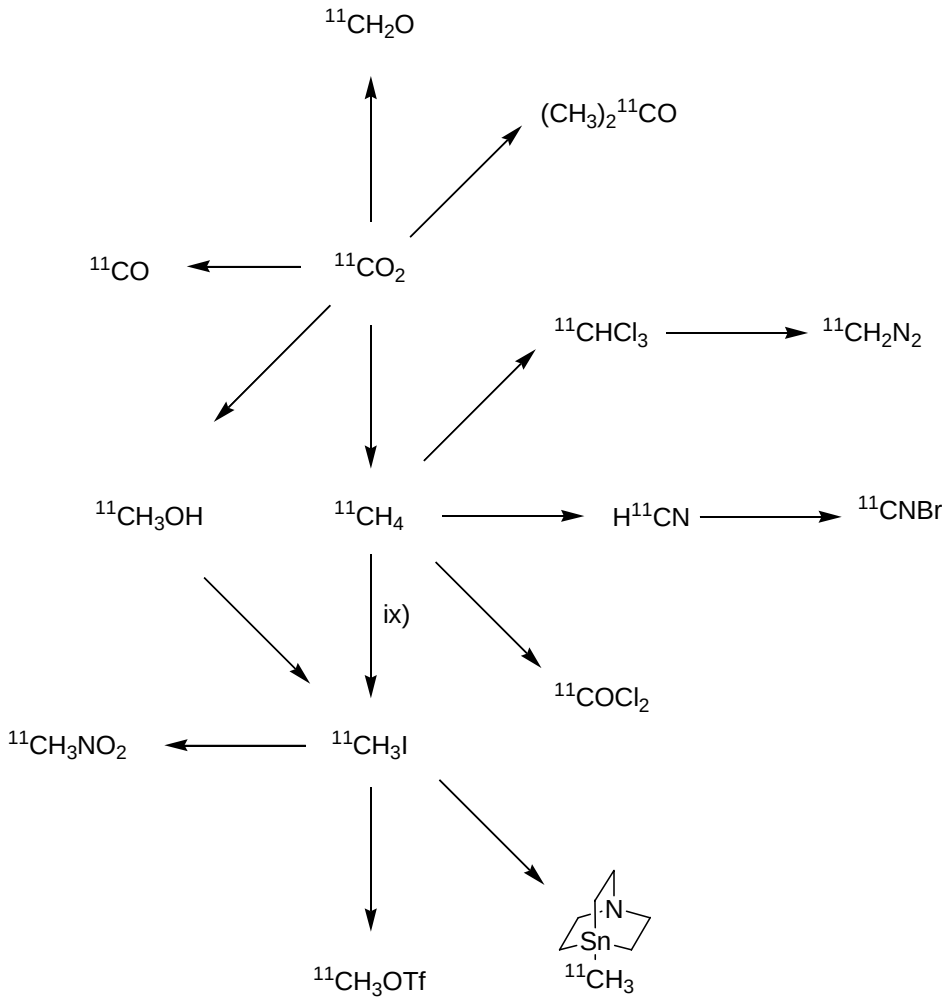

Figure 1.6 The synthetic transformations of C-11 labeled carbon dioxide.

Compared with F-18, the advantages of C-11 are 1) that the labeled chemical structure would usually be identical with unlabeled compound 2) that PET studies can be performed repeatedly in the same day due to its 20.4 min half-life allowing the same subject (animal or human) to serve as its own control.

1.2.3.2 F-18 PET Chemistry

In 1937, Snell reported first his observation of fluorine-18. [107] He wrote 'When neon gas is bombarded with 5 MV deuterons, an active product is formed which emits

positive electrons and decays with a period 112±4 minutes. This active substance behaves chemically like fluorine'. Later this F-18 labeled fluorine production has been fully exploited and described by BNL PET group[108] and the first organic compound labeled with F-18 was [^{18}F]cholesterol.[109] During 1970th, the most widely used PET tracer, 2-deoxy-2-[^{18}F]fluoro-D-glucose (^{18}FDG) was first synthesized by BNL PET group for the measurement of glucose metabolism in the human brain and in tumors (Figure 1.7).

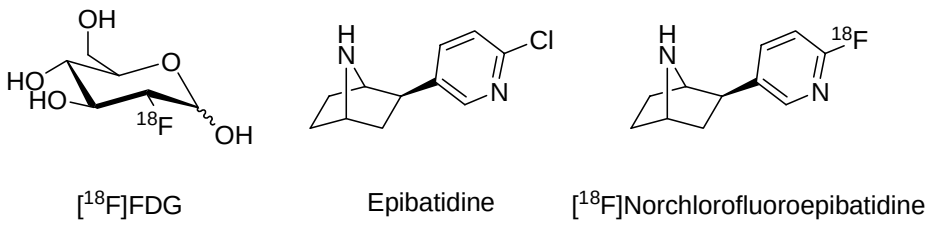

Figure 1.7 ^{18}FDG, epibatidine, [^{18}F]epibatidine

F-18 can replace stable fluorine in a number of fluorine-containing pharmaceuticals. But, due to its small size and similar bond length with C-H, it may be useful for isosteric replacement for hydrogen atom or hydroxyl group. However, high electronegativity of fluorine should be also considered for alteration of molecular interaction for biological target. In some cases, a functional group which has little effect on biological activity can be replaced with ^{18}F. For example, in the PET study for epibatidine which binds with high affinity to the nicotinic receptor, chloride was replaced with ^{18}F, based on similar affinity data observed in vitro binding study (Figure 1.7).[74, 110]

Primary chemical forms of F-18 from the cyclotron are elemental fluorine (F_2), fluoride (F^-). Clearly, elemental fluorine and fluoride are used for the electrophilic reaction and nucleophilic substitution, respectively. Therefore, while [^{18}F]F_2 fluorine has been used for labeling of alkene, electron-rich aromatic ring, [^{18}F]F^- was used for

nucleophilic substitution reactions of the aliphatic or aromatic halides. To increase solubility and reactivity of $[^{18}F]F^-$, potassium, cesium, tetraalkylammonium cations have been used. Kryptofix (2.2.2) (4, 7, 13, 16, 21, 24 -hexaoxa-1, 10-diazabicyclo [8.8.8] hexacosane (K_{222}) chelated potassium is widely used. For the nucleophilic aromatic substitution on pyridine, the trimethylammonium group in the pyridine ring is preferable as a leaving group, compared with nitro and halides.[111]

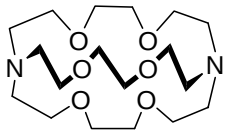

Figure 1.8 The structure of Kryptofix® $_{222}$

During the general production of $[^{18}F]F_2$, the carrier gas (F_2, 0.1%) is inevitably added for the recovery of F-18, resulting in low specific activity (< 0.015 Ci/μmol) and low maximum yield (50%). $[^{18}F]F^-$ using water also has limitation for the nucleophilic fluorination due to water because hydrated fluoride anion is much less nucleophilic than anhydrous fluoride. Therefore, strong heating is sometimes required and often generates side products.

Compared with C-11, the longer half-life of F-18 gives the opportunity for more synthetic manipulations almost up to 5.5 hrs, but it can limit repeated PET studies on the same day and imaging study with F-18 is usually longer than C-11 PET study.

1.2.4 The mechanistic view and properties of CNS PET tracers

The starting point of PET tracer development is identifying biological target which is usually a neurotransmitter receptor, transporter or and enzyme. The *ex vivo* data

and autoradiography may provide complementary information for binding site and biodistribution. It is important that ligand behavior on a particular target is well-characterized in vitro study, especially by SAR (structure-activity relationship). For example, the mechanism-based design of FDG comes from the fact that 2-deoxy-D-glucose-6-phosphate is trapped inside of the cell. More specifically, 2-deoxy-D-glucose undergoes the same transport into the cell and phosphorylation by hexokinase as D-glucose. However, unlikely D-glucose, it was trapped because it could not be further metabolized by phosphohexose isomerase. Structurally, hydroxyl group at C-2 is essential for this step. The substitution of fluoride at C-2 showed the same biological behavior as 2-deoxy-D-glucose.

In the CNS, the modes of ligand binding are largely classified by kinetics as either reversible or irreversible. [^{11}C] clorgyline and [^{11}C] deprenyl are typical irreversibly binding PET tracers which bind monoamine oxidase A and B, respectively.[112] These irreversible PET tracers showed the primary kinetic isotope effect in vivo imaging with deuterium substitution for hydrogen in the propargyl group (Figure 1.9). Compared with reversible binding kinetics, different kinetic modeling method is applied for irreversible binding. Currently, most of CNS PET tracers target neuronal receptors or transporter in the reversible binding manner.

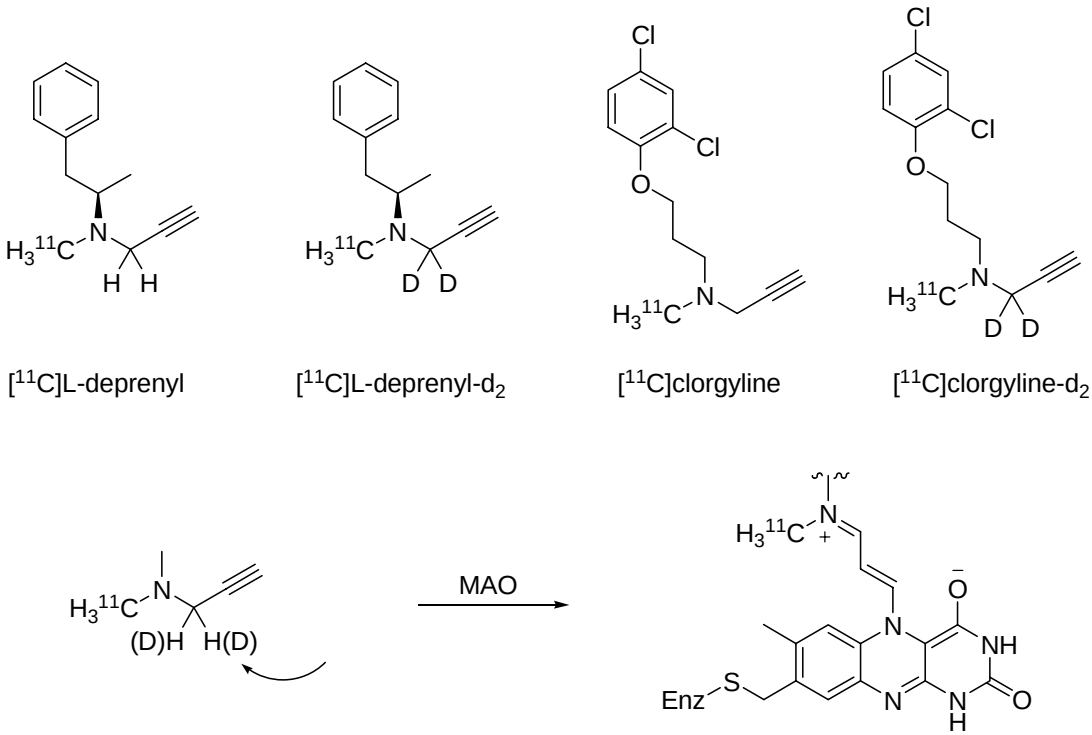

Figure 1.9 PET tracer for MAO A, B and mechanistic view.

Potential ligands for PET tracer are selected by *in vitro* binding affinity and are determined with several basic considerations such as the potential for labeling, molecular weight, and calculated lipophilicity. Empirically, molecular weight and lipophilicity can often be used to predict blood-brain penetration though there are many other factors which come into play such as metabolism and binding to plasma proteins. Based on the known distribution pattern and concentration of the biological target, a PET tracer candidate pre-evaluated by considering binding potential:

Binding potential = Bmax/Kd,

where Bmax and Kd represent concentration of biological target, dissociation constant.[113] Specifically localized distribution and high concentration of biological target of interest are important for obtaining high to signal-to-noise in the PET image.

Specific signal / non specific signal = B'max/Kd(1+Kn)[114]

In general, the important criteria of CNS PET tracer during PET study include:

1) Specific binding in brain regions known to contain the molecular target. Saturability is usually evaluated by blocking study with co-injection or pre-injection of identical non-radioactive compound in a dose dependent manner.

2) Selectivity for target of interest against the other homologous molecular component, which can be validated by the pretreatment of known selective compound for the target in a dose dependent manner.

3) Acceptable toxicity within tracer-dose level and radiation dosimetry for within regulatory guidelines

4) Penetration of BBB at a tracer-dose level, which is related to plasma protein binding, molecular weight, and lipophilicity (log P = 1-3)[17] of PET tracer candidate.

5) Proper pharmacokinetics profile to be quantifiable in the brain, mostly showing discrimination between non-target region and target regions,

6) Slow metabolic rate and high free fraction in blood or fast kinetics for dissociation from plasma protein, allowing accumulation in the CNS

7) Absence of labeled metabolites in the brain

8) Specific activity, which should be high enough to avoid perturbing the living system; it is especially important for low receptor concentration because saturation.

High specific activity as well as relatively low biological potency and toxicity of the unlabeled parent compound are important factors in avoiding perturbing the process under investigation and also in obtaining approval for using a new radiotracer for human

PET studies. In general, the toxicity of the parent compound can be used as guidance but all new labeled compounds must undergo extensive toxicology studies prior to approval for human studies if the compound has never been administered to humans. Some compounds have unacceptably high toxicity and cannot be administered to humans. For example, epibatidine has a low LD_{50} (0.2 mg/kg).[115] While the F-18 labeled epibatidine study was successful for baboon study, but it could not proceed to human study due to narrow margin of safety. For blood-brain barrier permeation, efflux system such as p-glycoprotein,[116] which is known as a main membrane protein for multi-drug resistance, is likely to limit PET tracer availability in the brain. Furthermore, the influence by this efflux system is higher in a extremely low tracer dose level than a therapeutic dose level which may saturate it.

For the evaluation of PET tracer, the change in radiotracer concentration over time is measured to give basic time-radioactivity curve. In many cases, one may need more sophisticated kinetic modeling[117], whereby the quantitative information on the interaction between PET tracer and target of interest is extracted from the other physiological influences such as blood flow, metabolism, and non-specific binding. Quantitative unchanged tracer analysis in blood samples eliminates study-to-study and subject-to-subject blood input variability by metabolism. Mostly, the labeled metabolites are precluded by BBB due to narrow range of chemical properties for BBB penetration.

1.2.5 The Drug development and PET

Currently, the cost of new drug development including failed cases was estimated around US$ 500 million up to $ 2 billion over 15 years per new drug.[118] This cost

increases significantly as a drug candidates proceeds to one phase to the next. One of the crucial points for the cost and risk management is the effective decision-making in each pre- or clinical phase from the multiple drug candidates, which should bear the safety as well as therapeutic efficacy. Moreover, of particular need is safety, toxicity which require more stringent regulation.

PET is a non-invasive tool to show drug candidate action by imaging quantitatively its pharmacodynamics and pharmacokinetics. First, by labeling the drug candidate with a positron-emitter, drug distribution over time can be evaluated to give bioavailability in target tissue. Simultaneously, PET also provides the delivery and residence time and concentration of labeled drug and its labeled metabolites to the other non-target region which may be valuable for drug safety issue. Second, PET measures physiological changes by drug action such as metabolic rate and blood perfusion. Moreover, using specific interaction between PET tracer and target molecule, PET allows temporal quantitative information on mechanism-based biological event such as neurotransmitter release, receptor occupancy, and gene expression. In other words, depending on what one investigates and the radiotracer which is used, the drug efficacy or drug induced cellular events can be measured without perturbation by the PET tracer. From small animal to primate model, PET can be performed longitudinally and repeatedly in the same animal. Moreover, due to its non-invasiveness, PET may be cost-effective tool in that PET human study is relatively feasible in the early stage of drug development; It also may contribute to reduce risk for decisions to move the clinical stage by providing direct comparison or translation between animal and human.

However, PET has several limitations. The biological event which need longer time than several half-lives may not be appropriate for PET though by running serial studies with a short-half life tracer, one can follow a process that occurs over several hours or days. Nonetheless, the very short-lived isotopes like ^{13}N, ^{15}O are rarely used as drug labels because the half-life is too short for many syntheses and for tracking biological processes.

1.3 Objectives

The pharmacological effects by nicotine action on nAChR have been implicated in many diseases such as Alzheimer's disease (AD), schizophrenia, and tobacco dependence.[9] Brain imaging using PET for each nAChR subtype allows us biological information on subtype-specific function and pathological change. While α4β2 nAChR PET tracers have been developed, the development of PET for α7 nAChR has been hampered due to the lack of suitable radioligands. It is, therefore, important to develop α7 nAChR-selective PET tracers for *in vivo* imaging studies to better understand the role of α7 nAChR in specific CNS disorders. Furthermore, PET imaging of drug targeting α7 nAChR can also contribute drug development by providing information on drug movement and occupncy *in vivo*. This project was performed in collaboration with BNL PET group, specially, under the direction of Joanna S. Fowler and Yu-Shin Ding. Though the main goal for α7 nAChR-selective tracer development was not achieved, this work can be synthetic and pharmacologic research basis for the further development.

We have following specific aims:

Specific Aim 1: Development of new α7 nAChR related PET radioligands including novel synthetic procedures to prepare suitable precursors, which are then used to prepare C-11 ($t_{1/2}$ = 20.4min.) and F-18 ($t_{1/2}$ = 109.8min.) labeled analogues

1a. Synthesis of C-11 labeled GTS-21 and its labeled metabolites

1b. Synthesis of furopyridine derivatives

1c. Synthesis of carboxamide derivative and F-18 labeling

1d. Synthesis of C-11 labeled Norethyl-N-methyl-methyllycaconitine

1e. Synthesis of C-11 labeld nicotine

Specific Aim 2: Characterization of radiotracer binding *in vivo*

2a. *In vivo* studies with PET to determine the biodistribution, pharmacokinetics for evaluation of positron-emitter labeled compound

1.4 References

1. Dale, H. H. The action of certain esters and ethers of choline, and their relation to muscarine. *Journal of Pharmacology and Experimental Therapeutics* **1914,** 6, 147-190.

2. Bartus, R. T.; Dean, R. L., 3rd; Beer, B.; Lippa, A. S. The cholinergic hypothesis of geriatric memory dysfunction. *Science* **1982,** 217, 408-414.

3. Lukas, R. J.; Changeux, J. P.; Le Novere, N.; Albuquerque, E. X.; Balfour, D. J.; Berg, D. K.; Bertrand, D.; Chiappinelli, V. A.; Clarke, P. B.; Collins, A. C.; Dani, J. A.; Grady, S. R.; Kellar, K. J.; Lindstrom, J. M.; Marks, M. J.; Quik, M.; Taylor, P. W.; Wonnacott, S. International Union of Pharmacology. XX. Current status of the nomenclature for nicotinic acetylcholine receptors and their subunits. *Pharmacol Rev* **1999,** 51, 397-401.

4. Papke, R. L. The kinetic properties of neuronal nicotinic receptors: genetic basis of functional diversity. *Prog Neurobiol* **1993,** 41, 509-31.

5. Falk, L.; Nordberg, A.; Seiger, A.; Kjaeldgaard, A.; Hellstrom-Lindahl, E. The alpha 7 nicotinic receptors in human fetal brain and spinal cord. *Journal of Neurochemistry* **2002,** 80, 457-465.

6. Slotkin, T. A.; Pinkerton, K. E.; Auman, J. T.; Qiao, D.; Seidler, F. J. Perinatal exposure to environmental tobacco smoke upregulates nicotinic cholinergic receptors in monkey brain. *Developmental Brain Research* **2002,** 133, 175-179.

7. Romanelli, M. N.; Gualtieri, F. Cholinergic nicotinic receptors: Competitive ligands, allosteric modulators, and their potential applications. *Med Res Rev* **2003,** 23, 393-426.

8. Khiroug, S. S.; Harkness, P. C.; Lamb, P. W.; Sudweeks, S. N.; Khiroug, L.; Millar, N. S.; Yakel, J. L. Rat nicotinic ACh receptor alpha7 and beta2 subunits co-assemble to form functional heteromeric nicotinic receptor channels. *J Physiol* **2002,** 540, 425-34.

9. Holladay, M. W.; Dart, M. J.; Lynch, J. K. Neuronal nicotinic acetylcholine receptors as targets for drug discovery. *J Med Chem* **1997,** 40, 4169-94.

10. Marks, M. J.; Collins, A. C. Characterization of nicotine binding in mouse-brain and comparison with the binding of alpha-bungarotoxin and quinuclidinyl benzilate. *Molecular Pharmacology* **1982,** 22, 554-564.

11. Wilson, S. P.; Kirshner, N. Acetylcholine-receptor of adrenal-medulla. *Journal of Neurochemistry* **1977,** 28, 687-&.

12. Garciaguzman, M.; Sala, F.; Sala, S.; Camposcaro, A.; Stuhmer, W.; Gutierrez, L. M.; Criado, M. Alpha-bungarotoxin-sensitive nicotinic receptors on bovine chromaffin cells - molecular-cloning, functional expression and alternative splicing of the alpha-7 subunit. *European Journal of Neuroscience* **1995,** 7, 647-655.

13. Clarke, P. B.; Schwartz, R. D.; Paul, S. M.; Pert, C. B.; Pert, A. Nicotinic binding in rat brain: autoradiographic comparison of [3H]acetylcholine, [3H]nicotine, and [125I]-alpha-bungarotoxin. *J. Neurosci.* **1985,** 5, 1307-1315.

14. Marks, M. J.; Stitzel, J. A.; Romm, E.; Wehner, J. M.; Collins, A. C. Nicotinic binding-sites in rat and mouse-brain - comparison of acetylcholine, nicotine, and alpha-bungarotoxin. *Molecular Pharmacology* **1986,** 30, 427-436.

15. Seguela, P.; Wadiche, J.; Dineleymiller, K.; Dani, J. A.; Patrick, J. W. Nicotinic binding-sites in rat and mouse-brain - comparison of acetylcholine, nicotine, and alpha-bungarotoxin . *Journal of Neuroscience* **1993,** 13, 596-604.

16. McCann, C. M.; Bracamontes, J.; Steinbach, J. H.; Sanes, J. R. The cholinergic antagonist {alpha}-bungarotoxin also binds and blocks a subset of GABA receptors. *PNAS* **2006,** 103, 5149-5154.

17. Whiteaker, P.; Davies, A. R. L.; Marks, M. J.; Blagbrough, I. S.; Potter, B. V. L.; Wolstenholme, A. J.; Collins, A. C.; Wonnacott, S. An autoradiographic study of the distribution of binding sites for the novel alpha 7-selective nicotinic radioligand [H-3]methyllycaconitine in the mouse brain. *European Journal of Neuroscience* **1999,** 11, 2689-2696.

18. Davies, A. R. L.; Hardick, D. J.; Blagbrough, I. S.; Potter, B. V. L.; Wolstenholme, A. J.; Wonnacott, S. Characterisation of the binding of [H-3]methyllycaconitine: a new radioligand for labelling alpha 7-type neuronal nicotinic acetylcholine receptors. *Neuropharmacology* **1999,** 38, 679-690.

19. Salminen, O.; Whiteaker, P.; Grady, S. R.; Collins, A. C.; McIntosh, J. M.; Marks, M. J. The subunit composition and pharmacology of alpha-Conotoxin MII-binding nicotinic acetylcholine receptors studied by a novel membrane-binding assay. *Neuropharmacology* **2005,** 48, 696-705.

20. Baker, E. R.; Zwart, R.; Sher, E.; Millar, N. S. Pharmacological properties of alpha 9 alpha 10 nicotinic acetylcholine receptors revealed by heterologous expression of subunit chimeras. *Molecular Pharmacology* **2004,** 65, 453-460.

21. Levin, E. D.; Bradley, A.; Addy, N.; Sigurani, N. Hippocampal alpha 7 and alpha 4 beta 2 nicotinic receptors and working memory. *Neuroscience* **2002,** 109, 757-65.

22. Pitsikas, N.; Borsini, F. Different effects of tropisetron and ondansetron in learning and memory paradigms. *Pharmacol Biochem Behav* **1997,** 56, 571-6.

23. Young, J. W.; Crawford, N.; Kelly, J. S.; Kerr, L. E.; Marston, H. M.; Spratt, C.; Finlayson, K.; Sharkey, J. Impaired attention is central to the cognitive deficits observed in alpha 7 deficient mice. *European Neuropsychopharmacology* **2007,** 17, 145-155.

24. Fernandes, C.; Hoyle, E.; Dempster, E.; Schalkwyk, L. C.; Collier, D. A. Performance deficit of α7 nicotinic receptor knockout mice in a delayed matching-to-place task suggests a mild impairment of working/episodic-like memory doi:10.1111/j.1601-183X.2005.00176.x. *Genes, Brain and Behavior* **2006,** 5, 433-440.

25. Boess, F. G.; De Vry, J.; Erb, C.; Flessner, T.; Hendrix, M.; Luithle, J.; Methfessel, C.; Riedl, B.; Schnizler, K.; van der Staay, F. J.; van Kampen, M.; Wiese, W. B.; Koenig, G. The novel alpha 7 nicotinic acetylcholine receptor agonist N-[(3R)-1-azabicyclo[2.2.2]oct-3-yl]-7-[2-(methoxy)phenyl]-1-benzofuran- 2-carboxamide improves working and recognition memory in rodents. *Journal of Pharmacology and Experimental Therapeutics* **2007,** 321, 716-725.

26. Meyer, E. M.; Kuryatov, A.; Gerzanich, V.; Lindstrom, J.; Papke, R. L. Analysis of 3-(4-hydroxy, 2-Methoxybenzylidene)anabaseine selectivity and activity at human and rat alpha-7 nicotinic receptors. *J Pharmacol Exp Ther* **1998,** 287, 918-25.

27. Whiteaker, P.; Davies, A. R. L.; Marks, M. J.; Blagbrough, I. S.; Potter, B. V. L.; Wolstenholme, A. J.; Collins, A. C.; Wonnacott, S. An autoradiographic study of the distribution of binding sites for the novel α7-selective nicotinic radioligand [3H]-methyllycaconitine in the mouse brain. *European Journal of Neuroscience* **1999,** 11, 2689-2696.

28. Hellstrom-Lindahl, E.; Court, J. A. Nicotinic acetylcholine receptors during prenatal development and brain pathology in human aging. *Behavioural Brain Research* **2000,** 113, 159-168.

29. Han, Z. Y.; Zoli, M.; Cardona, A.; Bourgeois, J. P.; Changeux, J. P.; Le Novere, N. Localization of [3H]nicotine, [3H]cytisine, [3H]epibatidine, and [125I]alpha-bungarotoxin binding sites in the brain of Macaca mulatta. *J Comp Neurol* **2003,** 461, 49-60.

30. Kulak, J. M.; Schneider, J. S. Differences in [alpha]7 nicotinic acetylcholine receptor binding in motor symptomatic and asymptomatic MPTP-treated monkeys. *Brain Research* **2004,** 999, 193-202.

31. Ryan, R. E.; Loiacono, R. E. Nicotine regulates alpha 7 nicotinic receptor subunit mRNA: implications for nicotine dependence. *Neuroreport* **2001,** 12, 569-572.

32. Quik, M.; Polonskaya, Y.; Gillespie, A.; Jakowec, M.; Lloyd, G. K.; Langston, J. M. Localization of nicotinic receptor subunit mRNAs in monkey brain by in situ hybridization. *Journal of Comparative Neurology* **2000,** 425, 58-69.

33. Hellstrom-Lindahl, E.; Mousavi, M.; Zhang, X.; Ravid, R.; Nordberg, A. Regional distribution of nicotinic receptor subunit mRNAs in human brain: comparison between Alzheimer and normal brain. *Molecular Brain Research* **1999,** 66, 94-103.

34. Araki, C. M.; Hamassaki-Britto, D. E. Motion-sensitive neurons in the chick retina: a study using Fos immunohistochemistry. *Brain Research* **1998,** 794, 333-337.

35. Clarke, P. B.; Schwartz, R. D.; Paul, S. M.; Pert, C. B.; Pert, A. Nicotinic binding in rat brain: autoradiographic comparison of [3H]acetylcholine, [3H]nicotine, and [125I]-alpha-bungarotoxin. *J Neurosci* **1985,** 5, 1307-15.

36. Gotti, C.; Zoli, M.; Clementi, F. Brain nicotinic acetylcholine receptors: native subtypes and their relevance. *Trends in Pharmacological Sciences* **2006,** 27, 482-491.

37. Zoli, M.; Moretti, M.; Zanardi, A.; McIntosh, J. M.; Clementi, F.; Gotti, C. Identification of the nicotinic receptor subtypes expressed on dopaminergic terminals in the rat striatum. *Journal of Neuroscience* **2002,** 22, 8785-8789.

38. Quik, M.; Vailati, S.; Bordia, T.; Kulak, J. M.; Fan, H.; McIntosh, J. M.; Clementi, F.; Gotti, C. Subunit composition of nicotinic receptors in monkey striatum: Effect of treatments with 1-Methyl-4-phenyl-1,2,3,6-tetrahydropyridine or L-DOPA. *Molecular Pharmacology* **2005,** 67, 32-41.

39. Gotti, C.; Clementi, F. Neuronal nicotinic receptors: from structure to pathology. *Progress in Neurobiology* **2004,** 74, 363-396.

40. Turner, J. R.; Kellar, K. J. Nicotinic cholinergic receptors in the rat cerebellum: Multiple heteromeric subtypes. *Journal of Neuroscience* **2005,** 25, 9258-9265.

41. J.A.[1], C.; C., M.-R.; A., G.; E., P. Nicotinic receptors in human brain: topography and pathology. *Journal of Chemical Neuroanatomy* 20, 281-298.

42. Martin-Ruiz, C. M.; Lee, M.; Perry, R. H.; Baumann, M.; Court, J. A.; Perry, E. K. Molecular analysis of nicotinic receptor expression in autism. *Molecular Brain Research* **2004,** 123, 81-90.

43. Maricq, A. V.; Peterson, A. S.; Brake, A. J.; Myers, R. M.; Julius, D. Primary structure and functional expression of the 5ht3 receptor, a serotonin-gated ion channel. *Science* **1991,** 254, 432-437.

44. Broad, L. M.; Felthouse, C.; Zwart, R.; McPhie, G. I.; Pearson, K. H.; Craig, P. J.; Wallace, L.; Broadmore, R. J.; Boot, J. R.; Keenan, M.; Baker, S. R.; Sher, E. PSAB-OFP, a selective alpha 7 nicotinic receptor agonist, is also a potent agonist of the 5-HT3 receptor. *European Journal of Pharmacology* **2002,** 452, 137-144.

45. Marazziti, D.; Betti, L.; Giannaccini, G.; Rossi, A.; Masala, I.; Baroni, S.; Cassano, G. B.; Lucacchini, A. Distribution of [H-3]GR65630 binding in human brain postmortem. *Neurochemical Research* **2001,** 26, 187-190.

46. Nordberg, A.; Winblad, B. *Alzheimer's and Parkinson's Diseases*. New York 1986.

47. Davies, P.; Feisullin, S. Postmortem stability of alpha-bungarotoxin binding-sites in mouse and human-brain. *Brain Research* **1981,** 216, 449-454.

48. Wevers, A.; Monteggia, L.; Nowacki, S.; Bloch, W.; Schutz, U.; Lindstrom, J.; Pereira, E. F. R.; Eisenberg, H.; Giacobini, E.; de Vos, R. A. I.; Steur, E.; Maelicke, A.; Albuquerque, E. X.; Schroder, H. Expression of nicotinic acetylcholine receptor subunits in the cerebral cortex in Alzheimer's disease: histotopographical correlation with amyloid plaques and hyperphosphorylated-tau protein. *European Journal of Neuroscience* **1999,** 11, 2551-2565.

49. Martin-Ruiz, C. M.; Court, J. A.; Molnar, E.; Lee, M.; Gotti, C.; Mamalaki, A.; Tsouloufis, T.; Tzartos, S.; Ballard, C.; Perry, R. H.; Perry, E. K. Alpha4 but not alpha3 and alpha7 nicotinic acetylcholine receptor subunits are lost from the temporal cortex in Alzheimer's disease. *J Neurochem* **1999,** 73, 1635-40.

50. Court, J. A.; Martin-Ruiz, C.; Graham, A.; Perry, E. Nicotinic receptors in human brain: topography and pathology. *Journal of Chemical Neuroanatomy* **2000,** 20, 281-298.

51. Wang, H. Y.; Lee, D. H.; D'Andrea, M. R.; Peterson, P. A.; Shank, R. P.; Reitz, A. B. beta-Amyloid(1-42) binds to alpha7 nicotinic acetylcholine receptor with high affinity. Implications for Alzheimer's disease pathology. *J Biol Chem* **2000,** 275, 5626-32.

52. Guan, Z. Z.; Nordberg, A.; Mousavi, M.; Rinne, J. O.; Hellstrom-Lindahl, E. Selective changes in the levels of nicotinic acetylcholine receptor protein and of corresponding mRNA species in the brains of patients with Parkinson's disease. *Brain Research* **2002,** 956, 358-366.

53. Olincy, A.; Harris, J. G.; Johnson, L. L.; Pender, V.; Kongs, S.; Allensworth, D.; Ellis, J.; Zerbe, G. O.; Leonard, S.; Stevens, K. E.; Stevens, J. O.; Martin, L.; Adler, L. E.; Soti, F.; Kem, W. R.; Freedman, R. Proof-of-concept trial of an alpha 7 nicotinic agonist in schizophrenia. *Archives of General Psychiatry* **2006,** 63, 630-638.

54. Freedman, R.; Hall, M.; Adler, L. E.; Leonard, S. evidence in postmortem brain-tissue for decreased numbers of hippocampal nicotinic receptors in schizophrenia. *Biological Psychiatry* **1995,** 38, 22-33.

55. Court, J.; Spurden, D.; Lloyd, S.; McKeith, I.; Ballard, C.; Cairns, N.; Kerwin, R.; Perry, R.; Perry, E. Neuronal nicotinic receptors in dementia with Lewy bodies and schizophrenia: alpha-bungarotoxin and nicotine binding in the thalamus. *Journal of Neurochemistry* **1999,** 73, 1590-1597.

56. Sherry Leonard et al. Further investigation of a chromosome 15 locus in schizophrenia: Analysis of affected sibpairs from the NIMH genetics initiative. *American Journal of Medical Genetics* **1998,** 81, 308-312.

57. Ray, M. A.; Graham, A. J.; Lee, M.; Perry, R. H.; Court, J. A.; Perry, E. K. Neuronal nicotinic acetylcholine receptor subunits in autism: An immunohistochemical investigation in the thalamus. *Neurobiology of Disease* **2005,** 19, 366-377.

58. Codignola, A.; Tarroni, P.; Cattaneo, M. G.; Vicentini, L. M.; Clementi, F.; Sher, E. Serotonin release and cell-proliferation are under the control of alpha-bungarotoxin-sensitive nicotinic receptors in small-cell lung-carcinoma cell-lines. *Febs Letters* **1994,** 342, 286-290.

59. Quik, M.; Chan, J.; Patrick, J. Alpha-bungarotoxin blocks the nicotinic receptor-mediated increase in cell number in a neuroendocrine cell-line. *Brain Research* **1994,** 655, 161-167.

60. Schuller, H. M.; Orloff, M. Tobacco-specific carcinogenic nitrosamines - Ligands for nicotinic acetylcholine receptors in human lung cancer cells. *Biochemical Pharmacology* **1998,** 55, 1377-1384.

61. Trombino, S.; Cesario, A.; Margaritora, S.; Granone, P.; Motta, G.; Falugi, C.; Russo, P. alpha 7-nicotinic acetylcholine receptors affect growth regulation of human mesothelioma cells: Role of mitogen-activated protein kinase pathway. *Cancer Research* **2004,** 64, 135-145.

62. Russo, P.; Cesario, A.; Catassi, A.; Paolucci, M.; Ognio, E.; Michele, C.; Doria-Miglietta, G.; Servent, D.; Dominioni, L.; Granone, P. Preclinical antitumor activity of alpha-Cobratoxin, an alpha7-nicotinic receptor inhibitor, in human malignant

mesothelioma: A potential drug against a fatal cancer disease? *Lung Cancer* **2005,** 49, S388-S388.

63. Kitagawa, H.; Takenouchi, T.; Azuma, R.; Wesnes, K. A.; Kramer, W. G.; Clody, D. E.; Burnett, A. L. Safety, pharmacokinetics, and effects on cognitive function of multiple doses of GTS-21 in healthy, male volunteers. *Neuropsychopharmacology* **2003,** 28, 542-551.

64. Mullen, G.; Napier, J.; Balestra, M.; DeCory, T.; Hale, G.; Macor, J.; Mack, R.; Loch, J., 3rd; Wu, E.; Kover, A.; Verhoest, P.; Sampognaro, A.; Phillips, E.; Zhu, Y.; Murray, R.; Griffith, R.; Blosser, J.; Gurley, D.; Machulskis, A.; Zongrone, J.; Rosen, A.; Gordon, J. (-)-Spiro[1-azabicyclo[2.2.2]octane-3,5'-oxazolidin-2'-one], a conformationally restricted analogue of acetylcholine, is a highly selective full agonist at the alpha 7 nicotinic acetylcholine receptor. *J Med Chem* **2000,** 43, 4045-50.

65. Bodnar, A. L.; Cortes-Burgos, L. A.; Cook, K. K.; Dinh, D. M.; Groppi, V. E.; Hajos, M.; Higdon, N. R.; Hoffmann, W. E.; Hurst, R. S.; Myers, J. K.; Rogers, B. N.; Wall, T. M.; Wolfe, M. L.; Wong, E. Discovery and structure - Activity relationship of quinuclidine benzamides as agonists of alpha 7 nicotinic acetylcholine receptors. *Journal of Medicinal Chemistry* **2005,** 48, 905-908.

66. Hajos, M.; Hurst, R. S.; Hoffmann, W. E.; Krause, M.; Wall, T. M.; Higdon, N. R.; Groppi, V. E. The selective alpha 7 nicotinic acetylcholine receptor agonist PNU-282987[N-[(3R)-1-azabicyclo[2.2.2]oct-3-yl]-4-chlorobenzamide hydrochloride] enhances GABAergic synaptic activity in brain slices and restores auditory gating deficits in anesthetized rats. *Journal of Pharmacology and Experimental Therapeutics* **2005,** 312, 1213-1222.

67. Cilia, J.; Cluderay, J.; Robbins, M.; Reavill, C.; Southam, E.; Kew, J.; Jones, D. Reversal of isolation-rearing-induced PPI deficits by an α7 nicotinic receptor agonist. *Psychopharmacology* **2005,** 182, 214-219.

68. Wishka, D. G.; Walker, D. P.; Yates, K. M.; Reitz, S. C.; Jia, S.; Myers, J. K.; Olson, K. L.; Jacobsen, E. J.; Wolfe, M. L.; Groppi, V. E.; Hanchar, A. J.; Thornburgh, B. A.; Cortes, L. A.; Wong, E. H. F.; Staton, B. A.; Raub, T. J.; Higdon, N. R.; Wall, T. M.; Hurst, R. S.; Walters, R. R.; Hoffmann, W. E.; Hajos, M.; Franklin, S.; Carey, G.; Gold, L. H.; Cook, K. K.; Sands, S. B.; Zhao, S. X.; Soglia, J. R.; Kalgutkar, A. S.; Arneric, S. P.; Rogers, B. N. Discovery of N-[(3R)-1-azabicyclo[2.2.2]oct-3-yl]furo[2,3-c]pyridine-5-carboxamide, an agonist of the alpha 7 nicotinic acetylcholine receptor, for the potential treatment of cognitive deficits in schizophrenia: Synthesis and structure-activity relationship. *Journal of Medicinal Chemistry* **2006,** 49, 4425-4436.

69. Biton, B.; Bergis, O. E.; Galli, F.; Nedelec, A.; Lochead, A. W.; Jegham, S.; Godet, D.; Lanneau, C.; Santamaria, R.; Chesney, F.; Leonardon, J.; Granger, P.; Debono,

M. W.; Bohme, G. A.; Sgard, F.; Besnard, F.; Graham, D.; Coste, A.; Oblin, A.; Curet, O.; Vige, X.; Voltz, C.; Rouquier, L.; Souilhac, J.; Santucci, V.; Gueudet, C.; Francon, D.; Steinberg, R.; Griebel, G.; Oury-Donat, F.; George, P.; Avenet, P.; Scatton, B. SSR180711, a novel selective alpha 7 nicotinic receptor partial agonist: (I) binding and functional profile. *Neuropsychopharmacology* **2007,** 32, 1-16.

70. Pichat, P.; Bergis, O. E.; Terranova, J. P.; Urani, A.; Duarte, C.; Santucci, V.; Gueudet, C.; Voltz, C.; Steinberg, R.; Stemmelin, J.; Oury-Donat, F.; Avenet, P.; Griebel, G.; Scatton, B. SSR180711, a novel selective alpha 7 nicotinic receptor partial agonist: (II) efficacy in experimental models predictive of activity against cognitive symptoms of schizophrenia. *Neuropsychopharmacology* **2007,** 32, 17-34.

71. Hurst, R. S.; Hajos, M.; Raggenbass, M.; Wall, T. M.; Higdon, N. R.; Lawson, J. A.; Rutherford-Root, K. L.; Berkenpas, M. B.; Hoffmann, W. E.; Piotrowski, D. W.; Groppi, V. E.; Allaman, G.; Ogier, R.; Bertrand, S.; Bertrand, D.; Arneric, S. P. A Novel Positive Allosteric Modulator of the {alpha}7 Neuronal Nicotinic Acetylcholine Receptor: In Vitro and In Vivo Characterization. *J. Neurosci.* **2005,** 25, 4396-4405.

72. Mazurov, A.; Hauser, T.; Miller, C. H. Selective alpha 7 nicotinic acetylcholine receptor ligands. *Current Medicinal Chemistry* **2006,** 13, 1567-1584.

73. Langstrom, B.; Antoni, G.; Halldin, C.; Svard, H.; Bergson, G. Synthesis of Some C-11-Labeled Alkaloids. *Chemica Scripta* **1982,** 20, 46-48.

74. Ding, Y. S.; Gatley, S. J.; Fowler, J. S.; Volkow, N. D.; Aggarwal, D.; Logan, J.; Dewey, S. L.; Liang, F.; Carroll, F. I.; Kuhar, M. J. Mapping nicotinic acetylcholine receptors with PET. *Synapse* **1996,** 24, 403-407.

75. Ding, Y. S.; Molina, P. E.; Fowler, J. S.; Logan, J.; Volkow, N. D.; Kuhar, M. J.; Carroll, F. I. Comparative studies of epibatidine derivatives [F-18]NFEP and [F-18]N-methyl-NFEP: Kinetics, nicotine effect, and toxicity. *Nuclear Medicine and Biology* **1999,** 26, 139-148.

76. Ding, Y. S.; Logan, J.; Bermel, R.; Garza, V.; Rice, O.; Fowler, J. S.; Volkow, N. D. Dopamine receptor-mediated regulation of striatal cholinergic activity: Positron emission tomography studies with norchloro[F-18]fluoroepibatidine. *Journal of Neurochemistry* **2000,** 74, 1514-1521.

77. Molina, P. E.; Ding, Y. S.; Carroll, F. I.; Liang, F.; Volkow, N. D.; Pappas, N.; Kuhar, M.; Abumrad, N.; Gatley, S. J.; Fowler, J. S. Fluoro-norchloroepibatidine: Preclinical assessment of acute toxicity. *Nuclear Medicine and Biology* **1997,** 24, 743-747.

78. Abreo, M. A.; Lin, N. H.; Garvey, D. S.; Gunn, D. E.; Hettinger, A. M.; Wasicak, J. T.; Pavlik, P. A.; Martin, Y. C.; DonnellyRoberts, D. L.; Anderson, D. J.; Sullivan, J. P.; Williams, M.; Americ, S. P.; Holladay, M. W. Novel 3-pyridyl ethers with subnanomolar affinity for central neuronal nicotinic acetylcholine receptors. *Journal of Medicinal Chemistry* **1996,** 39, 817-825.

79. Valette, H.; Bottlaender, M.; Dolle, F.; Guenther, I.; Fuseau, C.; Coulon, C.; Ottaviani, M.; Crouzel, C. Imaging central nicotinic acetylcholine receptors in baboons with [F-18]fluoro-A-85380. *Journal of Nuclear Medicine* **1999,** 40, 1374-1380.

80. Ding, Y. S.; Fowler, J. S.; Logan, J.; Wang, G. J.; Telang, F.; Garza, V.; Biegon, A.; Pareto, D.; Rooney, W.; Shea, C.; Alexoff, D.; Volkow, N. D.; Vocci, F. 6-[F-18]fluoro-A-85380, a new PET tracer for the nicotinic acetylcholine receptor: Studies in the human brain and in vivo demonstration of specific binding in white matter. *Synapse* **2004,** 53, 184-189.

81. Quik, M.; Bordia, T.; Forno, L.; McIntosh, J. M. Loss of alpha-conotoxinMII- and A85380-sensitive nicotinic receptors in Parkinson's disease striatum. *Journal of Neurochemistry* **2004,** 88, 668-679.

82. Zhang, Y.; Pavlova, O. A.; Chefer, S. I.; Hall, A. W.; Kurian, V.; Brown, L. L.; Kimes, A. S.; Mukhin, A. G.; Horti, A. G. 5-substituted derivatives of 6-halogeno-3-((2-(S)-azetidinyl)methoxy)pyridine and 6-halogeno-3-((2-(S)-pyrrolidinyl)methoxy)pyridine with low picomolar affinity for alpha 4 beta 2 nicotinic acetylcholine receptor and wide range of lipophilicity: Potential probes for imaging with positron emission tomography. *Journal of Medicinal Chemistry* **2004,** 47, 2453-2465.

83. Ding, Y. S.; Kil, K. E.; Lin, K. S.; Ma, W.; Yokota, Y.; Carroll, I. F. A novel nicotinic acetylcholine receptor antagonist radioligand for PET studies. *Bioorganic & Medicinal Chemistry Letters* **2006,** 16, 1049-1053.

84. Pomper, M. G.; Phillips, E.; Fan, H.; McCarthy, D. J.; Keith, R. A.; Gordon, J. C.; Scheffel, U.; Dannals, R. F.; Musachio, J. L. Synthesis and biodistribution of radiolabeled alpha(7) nicotinic acetylcholine receptor ligands. *Journal of Nuclear Medicine* **2005,** 46, 326-334.

85. Ravert H.T., D. P., Foss C.A., Fan H., Holmquist C.R., Phillips E.,; McCarthy D.J., H. R., Holt D., Dannals R.F., Pomper M.G. Synthesis of 5'-(2-[18f]fluorophenyl)-spiro[1-azabicyclo [2.2.2.]octane]-3,2'(3'h)-furo[2,3-b]pyridine ([18f]fps), an agonist at the α7 nicotinic acetylcholine receptor. *Journal of Labelled Compounds and Radiopharmaceuticals* **2005,** 48, S168.

86. Kubota, K. From tumor biology to clinical Pet: a review of positron emission tomography (PET) in oncology. *Ann Nucl Med* **2001,** 15, 471-86.

87. Van Paesschen, W.; Dupont, P.; Sunaert, S.; Goffin, K.; Van Laere, K. The use of SPECT and PET in routine clinical practice in epilepsy. *Current Opinion in Neurology* **2007,** 20, 194-202.

88. Jelic, V.; Nordberg, A. Early diagnosis of Alzheimer disease with positron emission tomography. *Alzheimer Disease & Associated Disorders* **2000,** 14, S109-S113.

89. Klunk, W. E.; Engler, H.; Nordberg, A.; Wang, Y. M.; Blomqvist, G.; Holt, D. P.; Bergstrom, M.; Savitcheva, I.; Huang, G. F.; Estrada, S.; Ausen, B.; Debnath, M. L.; Barletta, J.; Price, J. C.; Sandell, J.; Lopresti, B. J.; Wall, A.; Koivisto, P.; Antoni, G.; Mathis, C. A.; Langstrom, B. Imaging brain amyloid in Alzheimer's disease with Pittsburgh Compound-B. *Annals of Neurology* **2004,** 55, 306-319.

90. Buxton, D. A.; Brimblecombe, R. W.; French, M. C.; Redfern, P. H. Brain acetylcholine concentration and acetylcholinesterase activity in selectively bred strains of rats. *Psychopharmacology* **1976,** 47, 97-99.

91. Schiffer, W. K.; Alexoff, D. L.; Shea, C.; Logan, J.; Dewey, S. L. Development of a simultaneous PET/microdialysis method to identify the optimal dose of C-11-raclopride for small animal imaging. *Journal of Neuroscience Methods* **2005,** 144, 25-34.

92. Brody, A. L.; Olmstead, R. E.; London, E. D.; Farahi, J.; Meyer, J. H.; Grossman, P.; Lee, G. S.; Huang, J.; Hahn, E. L.; Mandelkern, M. A. Smoking-induced ventral striatum dopamine release. *American Journal of Psychiatry* **2004,** 161, 1211-1218.

93. Fowler, J. S.; Wolf, A. P. Working against time: Rapid radiotracer synthesis and imaging the human brain. *Accounts of Chemical Research* **1997,** 30, 181-188.

94. Pascali, C.; Bogni, A.; Iwata, R.; Decise, D.; Crippa, F.; Bombardieri, E. High efficiency preparation of L-[S-methyl-C-11]methionine by on-column [C-11]methylation on C18 Sep-Pak. *Journal of Labelled Compounds & Radiopharmaceuticals* **1999,** 42, 715-724.

95. Thorell, J. O.; Stoneelander, S.; Elander, N. Use of a microwave cavity to reduce reaction-times in radiolabeling with [c-11] cyanide. *Journal of Labelled Compounds & Radiopharmaceuticals* **1992,** 31, 207-217.

96. Lee, C.-C.; Sui, G.; Elizarov, A.; Shu, C. J.; Shin, Y.-S.; Dooley, A. N.; Huang, J.; Daridon, A.; Wyatt, P.; Stout, D.; Kolb, H. C.; Witte, O. N.; Satyamurthy, N.; Heath, J. R.; Phelps, M. E.; Quake, S. R.; Tseng, H.-R. Multistep Synthesis of a Radiolabeled Imaging Probe Using Integrated Microfluidics. *Science* **2005,** 310, 1793-1796.

97. Hostetler, E. D.; Terry, G. E.; Burns, H. D. An improved synthesis of substituted [C-11]toluenes via Suzuki coupling with [C-11] methyl iodide. *Journal of Labelled Compounds & Radiopharmaceuticals* **2005,** 48, 629-634.

98. Suzuki, M.; Doi, H.; Bjorkman, M.; Andersson, Y.; Langstrom, B.; Watanabe, Y.; Noyori, R. Rapid coupling of methyl iodide with aryltributylstannanes mediated by palladium(0) complexes: A general protocol for the synthesis of (CH3)-C-11-labeled PET tracers. *Chemistry-a European Journal* **1997,** 3, 2039-2042.

99. Axelsson, B. S.; Bjurling, P.; Matsson, O.; Langstrom, B. C-11/C-14 kinetic isotope effects in enzyme mechanism studies - c-11/c-14 kinetic isotope effect of the tyrosine phenol-lyase catalyzed alpha,beta-elimination of l-tyrosine. *Journal of the American Chemical Society* **1992,** 114, 1502-1503.

100. Axelsson, B. S.; Matsson, O.; Langstrom, B. The C-11/C-14 kinetic isotope effect method - the c-11/c-14 kinetic isotope effect in the sn2 reaction of n,n-dimethyl-para-toluidine with labeled methyl-iodide.*Journal of Physical Organic Chemistry* **1991,** 4, 77-86.

101. Axelsson, B. S.; Matsson, O.; Langstrom, B. Primary c-11/c-14-kinetic and secondary h-1/h-2-kinetic isotope effects in the sn2 reaction of hydroxide ion with methyl-iodide - the relationship between different carbon isotope effects. *Journal of the American Chemical Society* **1990,** 112, 6661-6668.

102. Axelsson, B. S.; Langstrom, B.; Matsson, O. C-11/C-14 Kinetic isotope effects. *Journal of the American Chemical Society* **1987,** 109, 7233-7235.

103. Crane, H. R.; Lauritsen, C. C. Further Experiments with Artificially Produced Radioactive Substances. *Physical Review* **1934,** 45, 497.

104. Ruben, S.; Hassid, W. Z.; Kamen, M. D. Radioactive Carbon in the Study of Photosynthesis. *J. Am. Chem. Soc.* **1939,** 61, 661-663.

105. Tobias, C.; Lawrence, J.; Roughton, F.; Root, W.; Gregersen, M. The elimination of carbon monoxide from the human body with reference to the possible conversion of CO to CO_2. *American Journal of Physiology* **1945,** 145, 253.

106. Ruben, S.; Kamen, M. D. Long-Lived Radioactive Carbon: C^{14}. *Physical Review* **1941,** 59, 349.

107. Snell, A. A new radioactive isotope of fluorine. *PHYSICAL REVIEW* **1937,** 51, 143.

108. Casella, V.; Ido, T.; Wolf, A. P.; Fowler, J. S.; Macgregor, R. R.; Ruth, T. J. Anhydrous f-18 labeled elemental fluorine for radiopharmaceutical preparation. *Journal of Nuclear Medicine* **1980,** 21, 750-757.

109. Nagai, T. Programs aimed at development of a radiopharmaceutical for adrenal scanning. *Journal of Nuclear Medicine* **1970,** 11, 217-&.

110. Liang, F.; Navarro, H. A.; Abraham, P.; Kotian, P.; Ding, Y. S.; Fowler, J.; Volkow, N.; Kuhar, M. J.; Carroll, F. I. Synthesis and Nicotinic Acetylcholine Receptor Binding Properties of exo-2-(2'-Fluoro-5'-pyridinyl)-7-azabicyclo- [2.2.1]heptane: A New Positron Emission Tomography Ligand for Nicotinic Receptors. *J. Med. Chem.* **1997,** 40, 2293-2295.

111. Dolci, L.; Dolle, F.; Jubeau, S.; Vaufrey, F.; Crouzel, C. 2-[F-18]fluoropyridines by no-carrier-added nucleophilic aromatic substitution with [F-18]FK-K-222 - A comparative study. *Journal of Labelled Compounds & Radiopharmaceuticals* **1999,** 42, 975-985.

112. Fowler, J.; Logan, J.; Volkow, N.; Wang, G.-J. Translational Neuroimaging: Positron Emission Tomography Studies of Monoamine Oxidase. *Molecular Imaging and Biology* **2005,** 7, 377-387.

113. Eckelman, W. C.; Mathis, C. A. Targeting proteins in vivo: in vitro guidelines. *Nuclear Medicine and Biology* **2006,** 33, 161-164.

114. Sihver, W.; Nordberg, A.; Langstrom, B.; Mukhin, A. G.; Koren, A. O.; Kimes, A. S.; London, E. D. Development of ligands for in vivo imaging of cerebral nicotinic receptors. *Behav Brain Res* **2000,** 113, 143-57.

115. Fitch, R. W.; Pei, X.-F.; Kaneko, Y.; Gupta, T.; Shi, D.; Federova, I.; Daly, J. W. Homoepiboxidines: further potent agonists for nicotinic receptors. *Bioorganic & Medicinal Chemistry* **2004,** 12, 179-190.

116. Sharom, F. J. Shedding light on drug transport: structure and function of the P-glycoprotein multidrug transporter (ABCB1). *Biochemistry and Cell Biology-Biochimie Et Biologie Cellulaire* **2006,** 84, 979-992.

117. Logan, J. Graphical analysis of PET data applied to reversible and irreversible tracers. *Nucl Med Biol* **2000,** 27, 661-70.

118. Adams, C. P.; Brantner, V. V. Estimating the cost of new drug development: Is it really $802 million? *Health Affairs* **2006,** 25, 420-428.

Chapter 2. C-11 labeled isotopomers and metabolites of GTS-21

Abstract[1]

Introduction: GTS-21 ((3*E*)-3-[(2,4-dimethoxyphenyl)methylene]-3,4,5,6-tetrahydro-2,3'-bipyridine), a partial α7 nicotinic acetylcholine receptor agonist drug, has recently been shown to improve cognition in schizophrenia and Alzheimer's disease. One of its two major demethylated metabolites, 4-OH-GTS-21, has been suggested to contribute to its therapeutic effects.

Methods: We labeled GTS-21 in two different positions with carbon-11 ([2-methoxy-^{11}C]GTS-21 and [4-methoxy-^{11}C]GTS-21) along with two corresponding demethylated metabolites ([2-methoxy-^{11}C]4-OH-GTS-21 and [4-methoxy-^{11}C]2-OH-GTS-21) for pharmacokinetic studies in baboons and mice with PET.

Results: Both [2-methoxy-^{11}C]GTS-21 and [4-methoxy-^{11}C]GTS-21 showed similar initial high rapid uptake in baboon brain, peaking from 1-3.5 min (0.027-0.038 %ID/cc) followed by rapid clearance ($t_{1/2}$ <15 min), resulting in low brain retention by 30 min. However, after 30 min, [2-methoxy-^{11}C]GTS-21 continued to clear while [4-methoxy-^{11}C]GTS-21 plateaued, suggesting the entry of a labeled metabolite into the brain. Comparison of the pharmacokinetics of the two labeled metabolites confirmed expected higher brain uptake and retention of [4-methoxy-^{11}C]2-OH-GTS-21 (the labeled metabolite of [4-methoxy-^{11}C]GTS-21) relative to [2-methoxy-^{11}C]4-OH-GTS-21 (the labeled metabolite of [2-methoxy-^{11}C]GTS-21) which had negligible brain uptake. *Ex vivo* studies in mice showed that GTS-21 is the major chemical form in the mouse brain.

Whole body dynamic PET imaging in baboon and mouse showed that the major route of excretion of C-11 is through the gallbladder.

Conclusions: The major findings are (1) extremely rapid uptake and clearance of [2-methoxy-^{11}C]GTS-21 from the brain which may need to be considered in developing optimal dosing of GTS-21 for patients, and (2) significant brain uptake of 2-OH-GTS-21, suggesting that it might contribute to the therapeutic effects of GTS-21. This study illustrates the value of comparing different label positions and labeled metabolites to gain insight on the behavior of a CNS drug and its metabolites in the brain providing an important perspective on drug pharmacokinetics.

2.1 Background

GTS-21 (3-[2,4-dimethoxybenzylideneanabaseine, **2-2**) is a "functionally" selective partial agonist drug for α7 nAChR (Ki= 211 nM against [^{125}I]α-bungarotoxin). It is also known to bind to the 5-HT_{3A} (Ki= 0.53 ± 0.9 μmol against [^{3}H]GR65630) and α4β2 nAChR (Ki= 84 nM against [^{3}H]Cytisine).[2-4] It was first synthesized in 1993 from anabaseine, a natural product isolated from a marine worm, nemertines and *Aphaenogaster* ant (Fig. 2.1).[5, 6] While anabaseine is a full agonist for α7 nAChR and muscular nAChR, GTS-21 is a partial agonist for α7 nAChR and an antagonist for muscular nAChR and α4β2 nAChR. This α7 nAChR functionally selective agonism of GTS-21has led to interest in the pharmacological effects of α7 nAChR last ten years.

Anabaseine (**2-1**) GTS-21(**2-2**)

Figure 2.1 The structures of anabaseine and GTS-21.

Many preclinical studies documenting its efficacy in cognition, learning and its neuroprotective properties[7, 8] set the stage for investigations in humans for the treatment of Alzheimer's disease to enhance working memory and attention. Its investigation as a drug for the treatment of AD was supported by reports that the α7 nAChR system, not

α4β2 nAChR, is intact in the cortex in AD brain.[9, 10] In clinical phase I trial for AD, GTS-21 enhanced cognition in a dose dependent manner without the side effects seen with nicotine itself.[11]

Because of its ability to normalize auditory gating deficit in the rodent model[12], GTS-21 is also under investigation for the treatment of schizophrenia where it was recently reported to enhance cognitive function in a human study [13]. However, the utility of GTS21 as a drug has been challenged by Tatsumi et al. who comments that GTS-21 "fails to show a satisfactory pharmacokinetics profiles (PK) in the areas of bioavailability and brain permeability." [14]

In view of metabolism, the phase I metabolism of GTS-21 is known to involve O-demethylation to give three metabolites, 2-OH-GTS-21, 4-OH-GTS-21 and 2,4-diOH-GTS-21 (Figure 2.2). Interestingly, the major metabolite, 4-OH-GTS-21 shows active partial agonistic activity for α7 nAChR which is 10 times greater than GTS-21 itself (Ki= 0.45 ± 0.02 μmol and 23 ± 2 μmol for human SK-N-SH cells, respectively)[15]. However, even though the metabolites of GTS-21 are more potent at the alpha-7 nAChR than the parent compound, their brain penetration is not known and consequently the relevance of these metabolites to the therapeutic effects of GTS-21 in humans is not known[16].

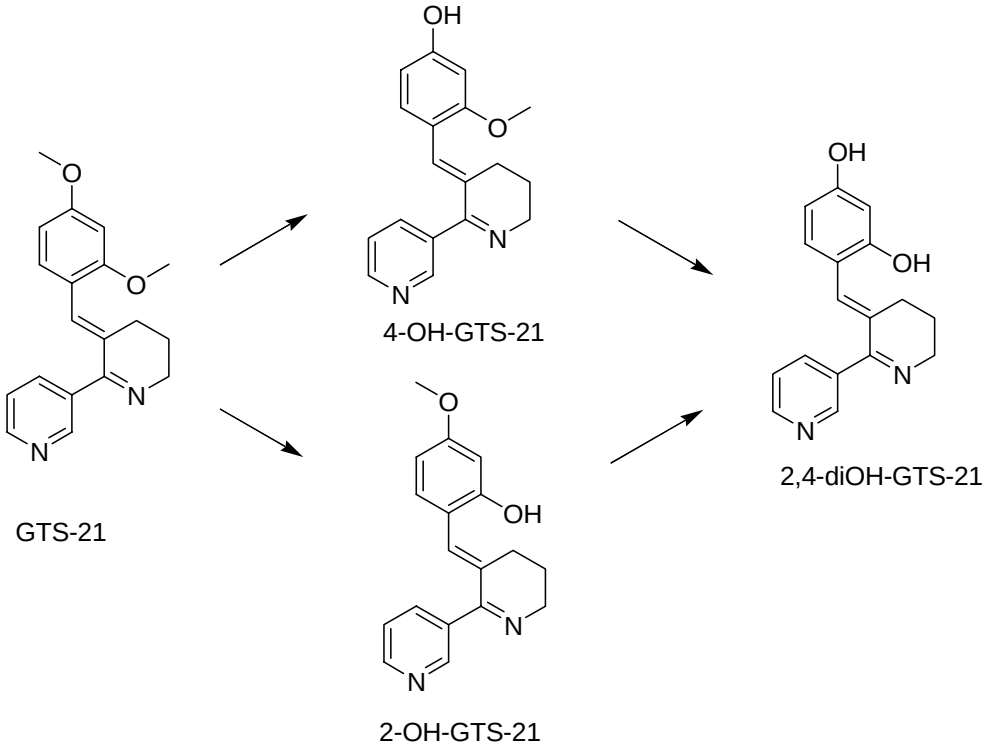

Figure 2.2 The metabolic route of GTS-21

2.2 Objectives

We developed and compared two regiospecifically labeled [^{11}C]GTS-21 radiotracers as a tool to measure GTS-21 distribution and pharmacokinetics in brain and peripheral organs in the baboon and in the mouse using PET and microPET, respectively. We labeled in two different positions because the profile of labeled metabolites would differ for the two isotopomers and we reasoned that this would provide insight on possible bioavailability of labeled metabolites in the brain. We also assessed the effect of a therapeutic dose of GTS-21 on the brain pharmacokinetics of **2-^{11}C-2**. Finally, we measured the chemical form of C-11 in the brain and plasma after the administration of 2-[^{11}C]GTS-21 in the mouse and measured the distribution in peripheral organs using microPET.

2.3 Synthesis

GTS-21 (**2-2**), 4-OH-GTS-21(**2-3**), and 2-OH-GTS-21 (**2-4**), 2,4-diOH-GTS-21 (**2-5**) were synthesized by known methods (Figure 2.3).[17]

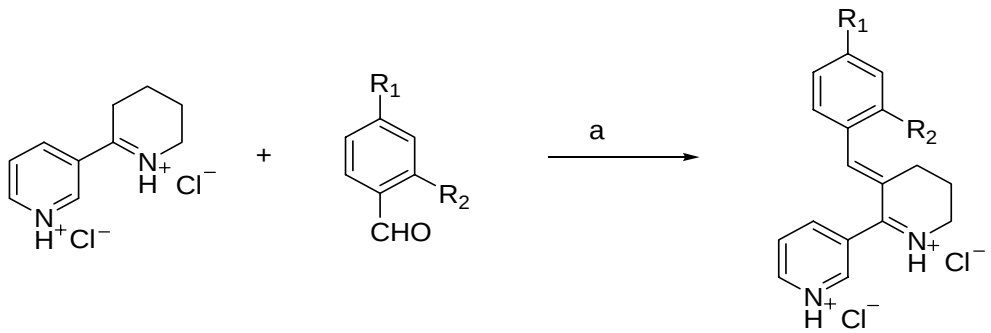

R_1, R_2= OCH_3
R_1=OH, R_2=OCH_3
R_1=OCH_3, R_2=OH
R_1, R_2=OH

R_1, R_2= OCH_3, (**2-2**)
R_1=OH, R_2=OCH_3, (**2-3**)
R_1=OCH_3, R_2=OH, (**2-4**)
R_1, R_2=OH, (**2-5**)

Scheme 2.1 The synthetic scheme for GTS-21 and its metabolites. a, ethanol, reflux

2.4 Radiolabeling, log D and free fraction in plasma

A moderate radiochemical yield was obtained for both **2-^{11}C-2** and **4-^{11}C-2,** ranging from 20-43% corrected to the end of cyclotron bombardment (EOB). Specific activities ranged from 0.8-5.1 Ci/μmol at EOB and radiochemical purities were > 98% for the two labeled compounds. The total synthesis time, from the end of the cyclotron bombardment to delivery for PET studies, was approximately 50 min. The radiochemical yield was not improved by using longer reaction times or higher temperatures. Initial attempts to separate the product from the precursor and side products using 20 mM phosphate buffer (pH = 2.8)/ acetonitrile (77.2/22.8) at a flow rate 4 ml/min on a semi-preparative Luna C18 (Phenomenex, 250 mm X 10 mm, 5 μ) were not successful. However, when the pH was adjusted to 12 with triethylamine on a Phenomenex Gemini column, a satisfactory and reproducible separation was achieved (Figure 2.3). Labeled

demethylated metabolites, **^{11}C-3** and **^{11}C-4** were synthesized in 12-15% yield with >99% radiochemical purity and specific activity 5.1-6.0 Ci/μmol.

The log D at pH = 7.4 (n= 4) of [^{11}C]GTS-21 was 2.82 which is, in principle, suitable for blood-brain barrier (BBB) penetration [18]. As expected, two labeled metabolites have lower log D (2.10 for **^{11}C-4**, 2.07 for **^{11}C-3**) than [^{11}C]GTS-21. We note that the free fractions in the plasma were 4.47%, 9.32%, 15.47% for [^{11}C]GTS-21, **^{11}C-4**, **^{11}C-3**, respectively, which are similar to values reported elsewhere.[16]

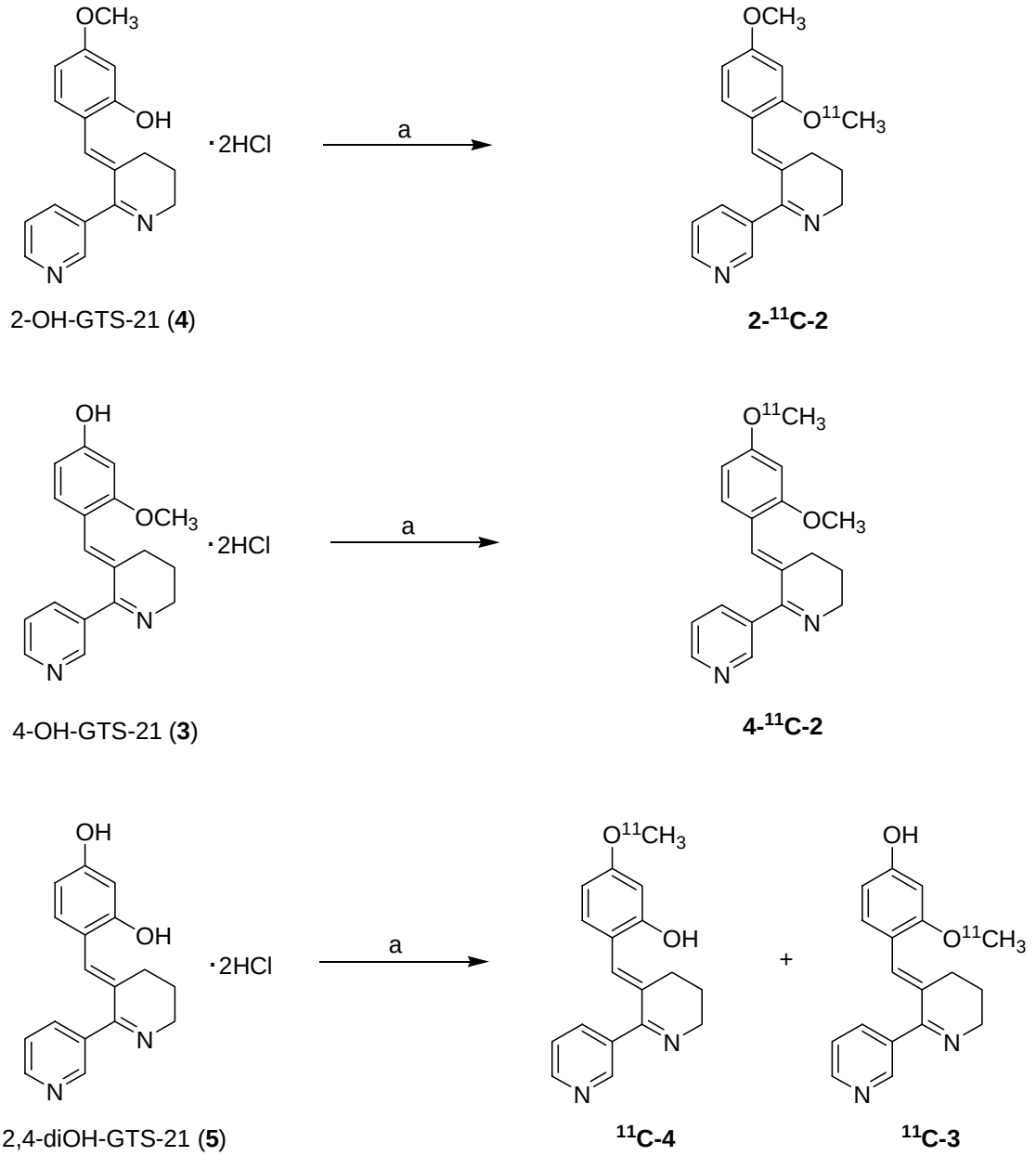

Scheme 2.2 The radiosynthesis of C-11 labeled GTS-21 and its metabolites. Reagent and condition: i) [^{11}C]CH_3I , aqueous sodium hydroxide in DMF, 100 ^{o}C, 3 min.

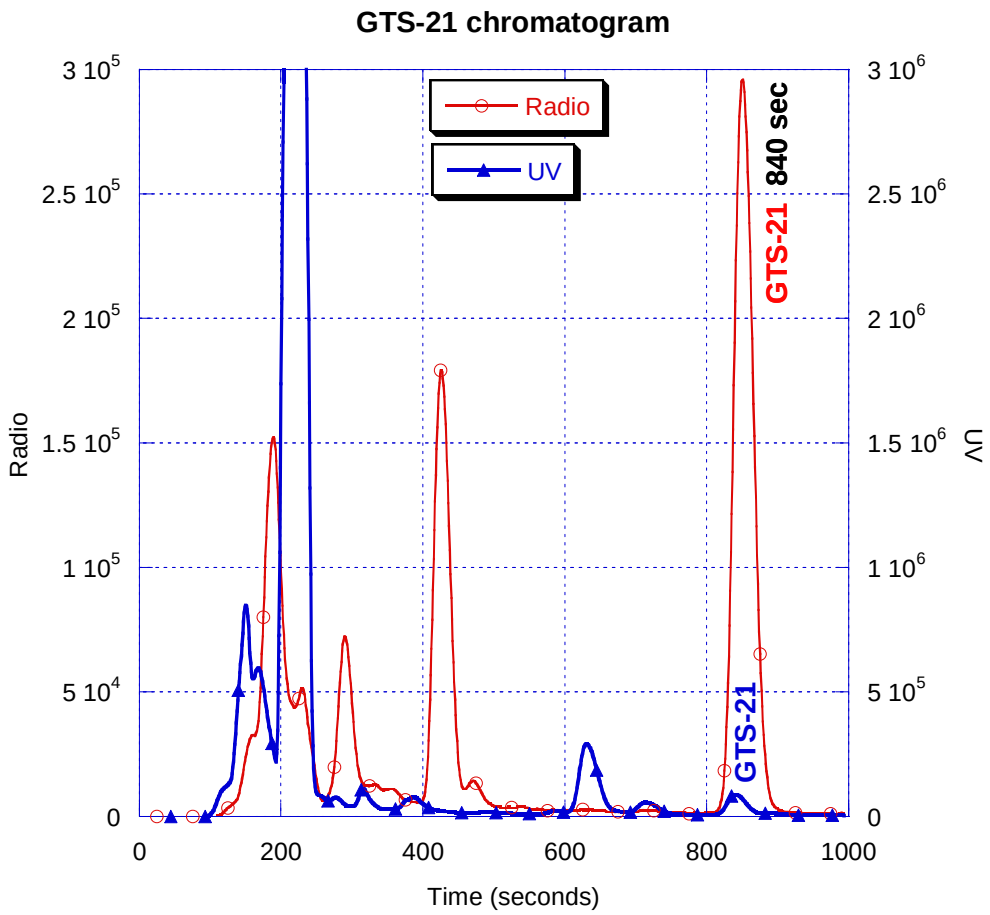

Figure 2.3 The HPLC profiles of [^{11}C] GTS-21.

2.5 Biological study

PET studies in baboons were performed by C-11 labeled GTS-21 isotopomers and its labeled metabolites as table 2.1. To investigate chemical form of C-11 labeled GTS-21 in rat brain and biodistribution in the peripheral organ, we performed *ex vivo* mouse study with **2-^{11}C-2**.

Table 2.1 Summary of baboon PET studies.

Study #	Baboon	Radiotracer/drug	Brain/Torso
Test-retest in the brain			
BEJ330dy1	Pearl	**2-^{11}C-2**	brain
BEJ330dy2	Pearl	**2-^{11}C-2**	brain
Comparison of two isotopomers of [^{11}C]GTS-21			
BEJ319 dy1	April	**2-^{11}C-2**	brain
BEJ319 dy2	April	**4-^{11}C-2**	brain
BEH154dy1	April	**4-^{11}C-2**	brain
BEH154dy2	April	**2-^{11}C-2**	brain
BEJ324dy1	April	**4-^{11}C-2**	brain
Comparison of two labeled metabolites			
BEJ335dy1	Daisy	**^{11}C-4**	brain
BEJ335dy2	Daisy	**^{11}C-3**	brain
Co-injection with therapeutic dose of GTS-21 (0.031 mg/kg)			
BEJ323dy1	Missy	**2-^{11}C-2**	brain
BEJ323dy2	Missy	**2-^{11}C-2/**GTS-21	brain
Distribution of peripheral organ			
BEJ327dy1	Daisy	**2-^{11}C-2**	torso

2.5.1. Brain and torso imaging of 2-^{11}C-GTS-21(2-^{11}C-2) in baboon

In the baboon brain, the global uptake was high (0.027-0.038 ID%/cc) and rapid (peaking at 1-3.5 min after injection), followed by rapid clearance to 0.01-0.005 ID%/cc at 22.5 min with the high reproducibility in the test-retest (Figure 2.4). Carbon-11 is widely distributed in the cortical and subcortical regions, showing higher uptake in thalamus, putamen, and cerebellum compared to the frontal cortex and similar uptakes at later times. The low affinity if GTS-21 for the α4β2 nAChR and α7 nAChR subtypes as well as their relatively low density preclude the observation of specific binding if GTS-21 in the brain [19]. For example, the density (B_{max}) of the α4β2 nAChR in thalamus of the squirrel monkey ranged 17.1-40.7 fmol/mg protein [20] and the density of α7 nAChR in thalamic nuclei of the macaque monkey is 1.5-12.7 fmol/mg protein,[21] while the K_i's for

the α4β2 and α7 nAChR for rat brain membrane are 84 and 211 nM, respectively. If we use K_i in the rat as an estimate of K_d in the monkey, then B_{max}/K_d which is an estmate of the signal to noise is 0.20-0.48 for α4β2 nAChR and 0.007- 0.06 for α7 nAChR. In contrast, 6-[^{18}F]fluoro-A85830 which has a K_i of 0.12 nM against (-)-cytisine in the rat brain membrane [22] has a B_{max}/K_i of 142.5-339.1 based on similar condition and the PET image shows a good signal to noise ratio in the thalamus and other brain regions [23, 24]. For another reference, [^{123} I] and [^{125} I]ADAM, which are known as a serotonin transporter tracer, has relatively high binding potential value (149)[19, 25]. Thus our observation of high uptake and rapid clearance is consistent with the low affinity of GTS-21 for nAChR subtypes and the relatively low concentration of brain nAChR.

The distribution of C-11 in peripheral organs after the injection of 2-^{11}C-GTS-21 (**2-^{11}C-2**) showed that the main excretion route was through the biliary tract (Figure 2.5). The liver uptake increased to 0.08 %dose/cc at 22 min and decreased gradually while the gall bladder steadily accumulated C-11 reaching a dose of 1.7 %dose/cc at 49 min. This is consistent with the previous report that GTS-21 (**2**) is cleared mainly by the in liver [26].

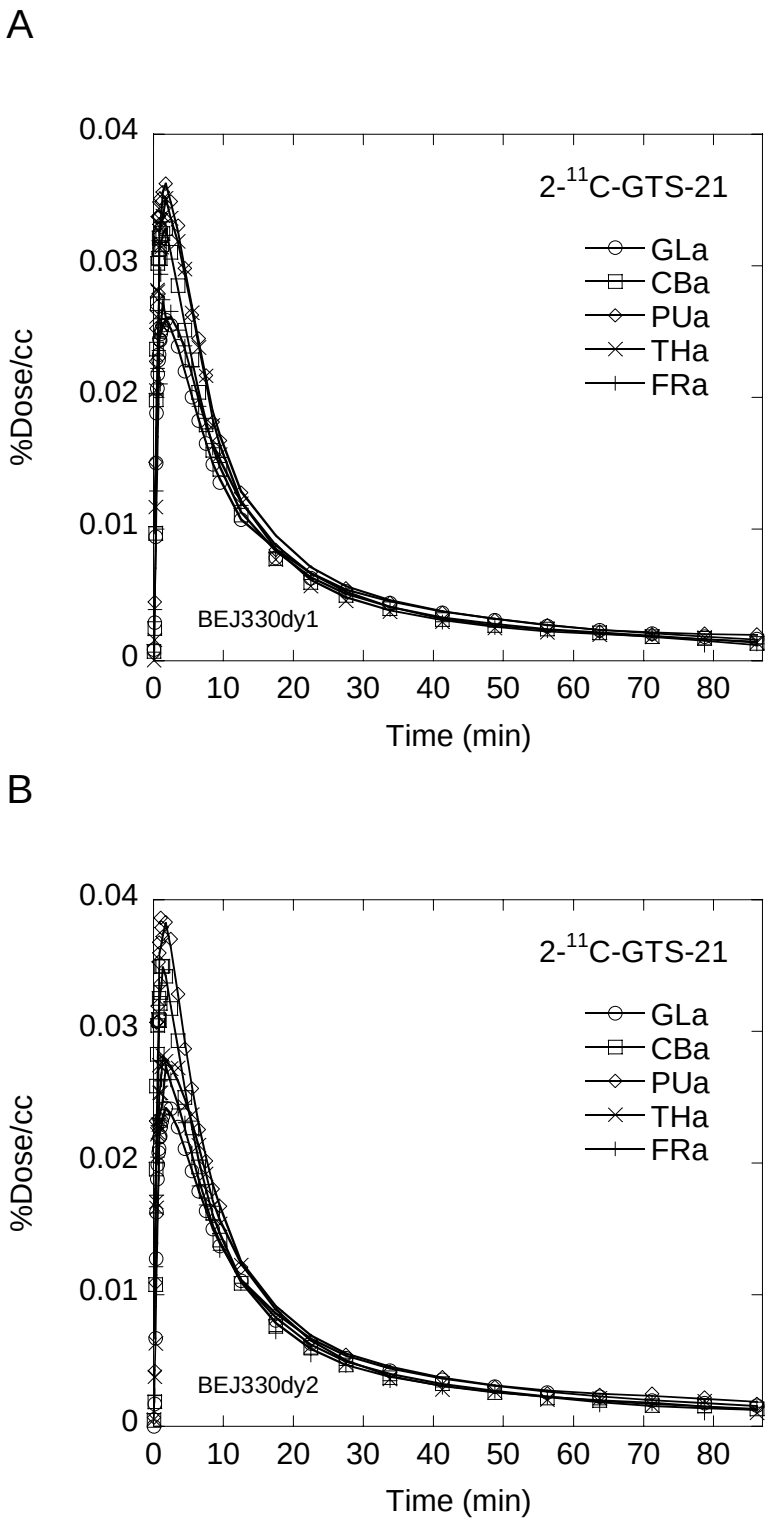

Figure 2.4 Time-activity curves for selected regions of interest of **2-^{11}C-2**. A, B are test, retest, respectively. FR, frontal cortex; CB, cerebellum; PU, putamen; TH, thalamus; GL, global. The most of brain regions are reproducible.

Table 2.2 The reproducibility of **2-^{11}C-2** PET study in the baboon brain.

Region of interest	Test (a)		Retest (b)		|a-b|/a·100 (%)	
	K_1	DV	K_1	DV	K_1	DV
Cerebellum	0.68	3.02	0.67	2.91	1.5	3.6
Frontal cortex	0.52	2.89	0.48	2.67	7.7	7.6
global	0.49	2.98	0.41	2.87	16.3	3.7
Putamen	0.74	3.41	0.71	3.36	4.1	1.5
Thalamus	0.72	3.10	0.48	2.87	33.3	7.4

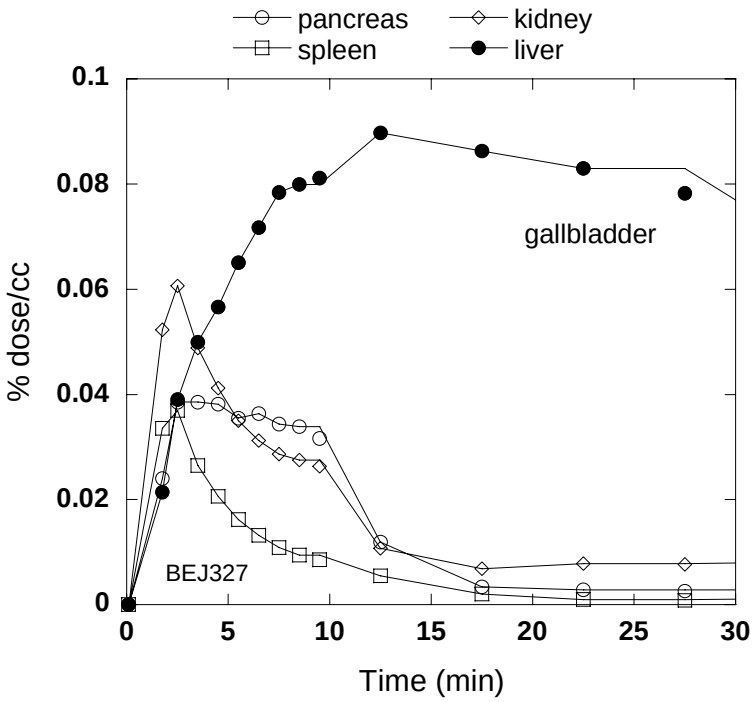

Figure 2.5 Time-activity curves for baboon torso after administration of **2-^{11}C-2**.

2.5.2 Plasma analysis for radiotracer in baboon

We measured the total C-11 concentration in the plasma over the time course of each study and performed HPLC analysis of selected samples to determine the fraction present as parent labeled compound. The recoveries of C-11 from HPLC effluent based on injected plasma sample were ≥ 75% (decay corrected). The total C-11 and the fraction

of C-11 present as GTS-21 in baboon plasma differed for 2-^{11}C-GTS-21 (**2-^{11}C-2**) and 4-^{11}C-GTS-21 (**4-^{11}C-2**) (Figure 2.6). The total radioactivity concentration in plasma was consistently higher for the 4-isotopomer (**4-^{11}C-2**) than for the 2-isotopomer (**2-^{11}C-2**) from 15 min to the end of the study as assessed by the area under the time-activity curve (P=0.004). The % radioactivity of the fraction of unchanged parent compound by HPLC is also clearly different, being lower for **4-^{11}C-2** than for **2-^{11}C-2** consistent with more rapid demethylation of the 4-methoxy group (Fig. 6) [16]. After the total C-11 for each isotopomer was corrected for the fraction that is present as the parent isotopomer, there was no significant difference between the areas under the curves for **2-^{11}C-2 and 4-^{11}C-2** at 90 min (Figure 2.6).

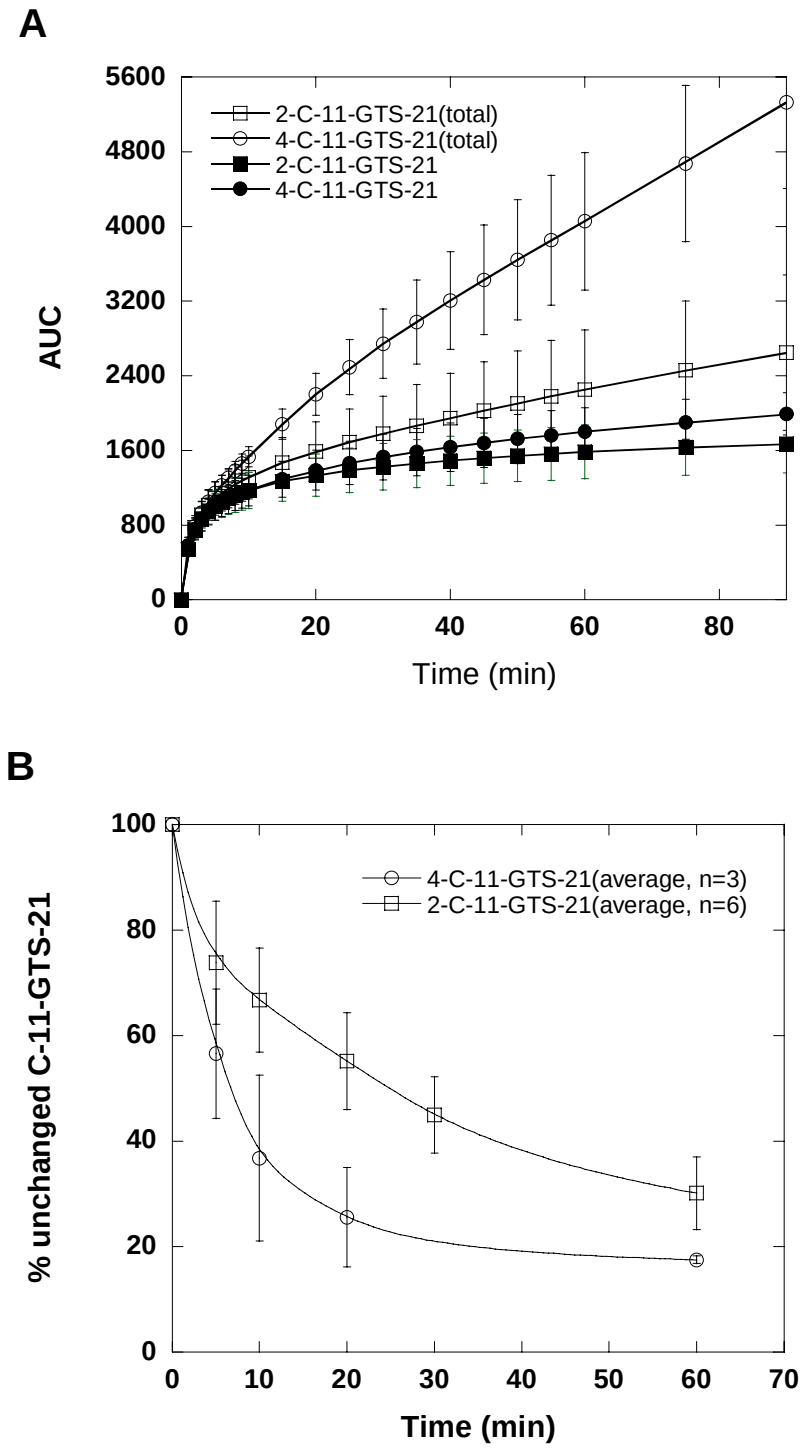

Figure 2.6 (A) The time-AUC(the area under the curve) curve of averaged total radioactivity in baboon plasma. (B) The percent (%) of unchanged C-11 labeled GTS-21 for two isotopomers in baboon plasma. These data were the averaged values obtained after **4-^{11}C-2** (n= 3) and **2-^{11}C-2** (n= 6) administration in three baboons.

2.5.3 Comparison of dynamic PET images of two isotopomers

Comparison of the two isopotomers in the brain showed slight differences in pharmacokinetics with **2-^{11}C-2** being higher until 22.5 min. However, the AUC for the plasma was also 11.5% higher for **2-^{11}C-2** at 10 min so that when the brain time-activity curves are normalized for the plasma, they parallel each other showing that difference are driven by plasma input. After 27 min, it is higher for **4-^{11}C-2** than **2-^{11}C-2** to end of experiment. The distribution volumes (DV) for each compound until 27 min were consistently similar, while there are then clearly higher DV for **4-^{11}C-2** (Fig. 7). Therefore, the brain image after 27 min is affected by C-11 labeled GTS-21 metabolite, presumably **4-^{11}C-4**.

A

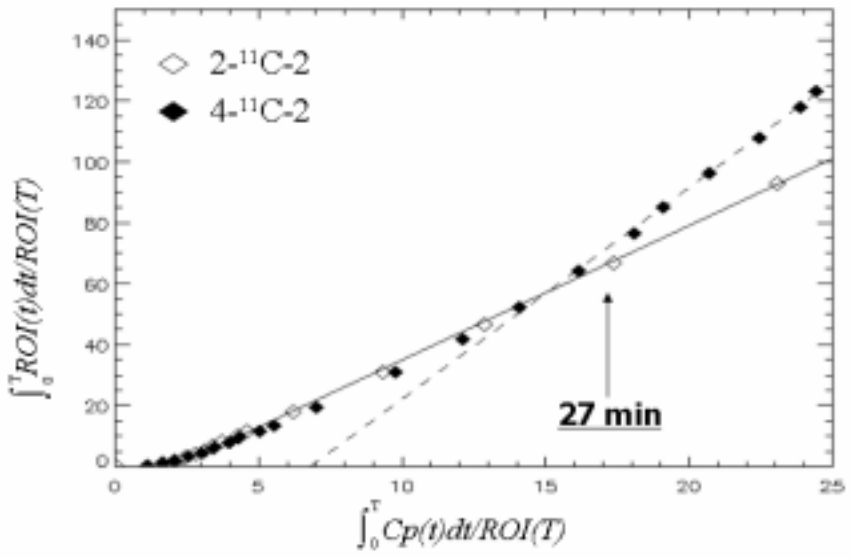

B

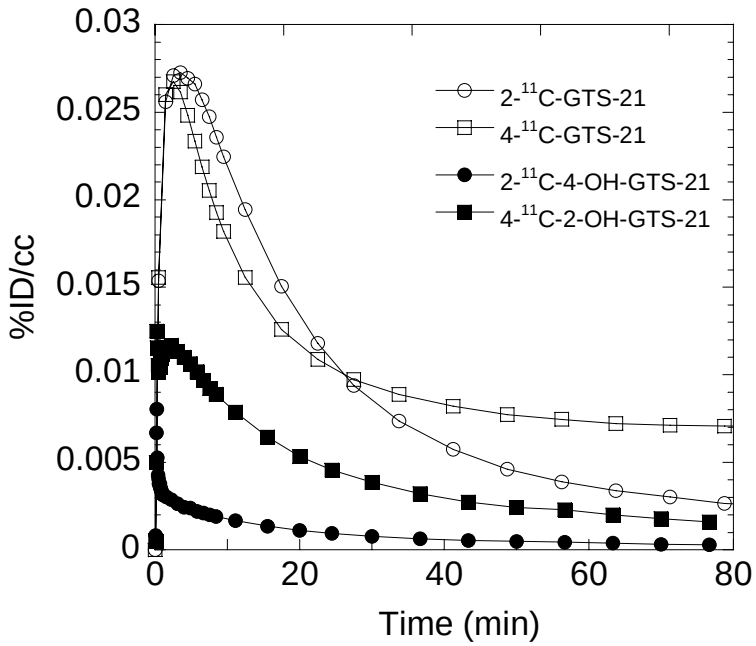

Figure 2.7 (A) Distribution volumes of two isotopomers of [^{11}C]GTS-21. (B) Time activity-curves of two isotopomers of [^{11}C]GTS-21 and their labeled metabolites

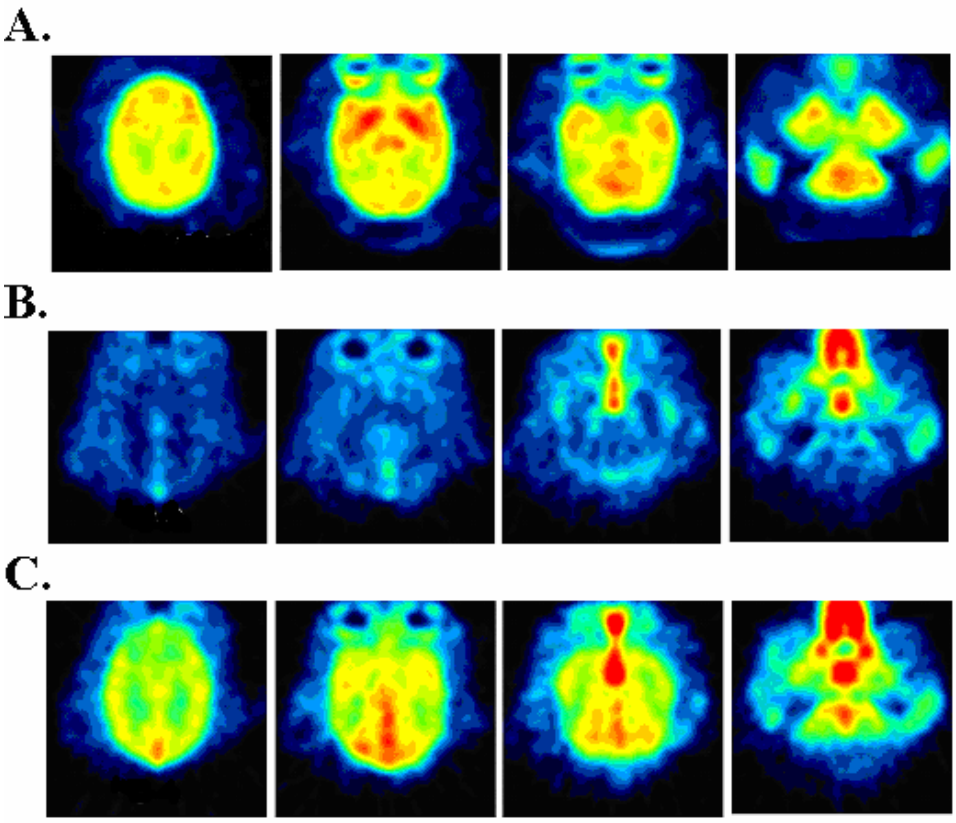

Figure 2.8 The PET image in baboon summed from time of injection through 90 min for (A) **2-^{11}C-2** (injected dose = 2.96 mCi)**,** (B) **^{11}C-3** (injected dose = 3.42 mCi), and (C) **^{11}C-4** (injected dose = 3.27 mCi). Ketamine hydrochloride (10 mg/kg) was used as an anesthesia by an intramuscular injection. We note that the distribution of **4-^{11}C-2** is not shown as the images do not differ between **4-^{11}C-2** and **2-^{11}C-2**.

2.5.4 Comparison of dynamic PET images of two C-11 labeled metabolites

In the comparative study in the same baboon, the global uptake of **^{11}C-4** was moderate (0.012%ID/cc at 2.5 min). The C-11 brain uptake of **^{11}C-4** was 4 times greater than 4-OH-[methoxy-^{11}C]GTS-21 and 2 times lower than [^{11}C]GTS-21 at 2.5 min post IV injection. Even though **^{11}C-4** has similar lipophilicity and less free fraction in plasma compared with the other major metabolite, **^{11}C-3**, its blood brain barrier penetrability is comparably high. This result seems to be different from the reported data in the rat brain, which demonstrated the better BBB penetrability of 4-OH-GTS-21 (**3**) than 2-OH-GTS-

21 (**4**) [16]. Based on our result and its known pharmacological activity at α7 nAChR, 2-OH-GTS-21(**4**) might be considered as a therapeutically active metabolite in the primate brain.

2.5.5 Effect of co-administration of a therapeutic dose of GTS-21

The co-administration of a therapeutic dose of GTS-21 (**2**) with **2-^{11}C-2** noticeably reduced brain uptake in initial 5-10 minutes (Figure 2.9). The AUC for the plasma after co-administration was 17-23% higher than baseline possible due to drug occupancy of peripheral binding [27]. The blood to tissue transfer terms (K_1) for thalamus, putamen and cerebellum were decreased by 20-40%, indicating a decrease in blood flow in each ROI (Table 1). Even though the heterogeneous distribution of nAChR in the brain is known in many literatures [20, 21], the distribution volumes decreased by 15-20% in all these regions indicating a non-specific effect consistent with the low binding affinity of GTS-21.

On the basis of this study in which we co-administered 0.031 mg/kg of GTS-21 along with **2-^{11}C-2**, we estimated that the global brain concentration of GTS-21 after iv administration is 0.5 μM at peak and 0.1 μM at 20 minutes post injection which Machu et al. have considered to be a pharmacologically effective drug concentration [2]. Based on these concentrations and the Ki's and Bmax's of the α4β2 and α7 nAChR's, we estimated that the receptor occupancies of α4β2 and α7 nAChR by GTS-21 would be 85 and 70% at peak and 60 and 36% at 20 min, respectively.

A

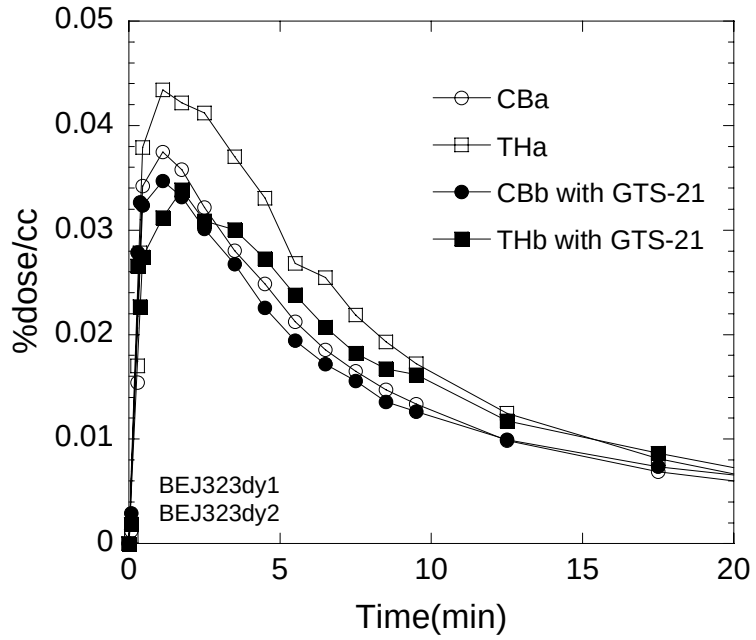

B

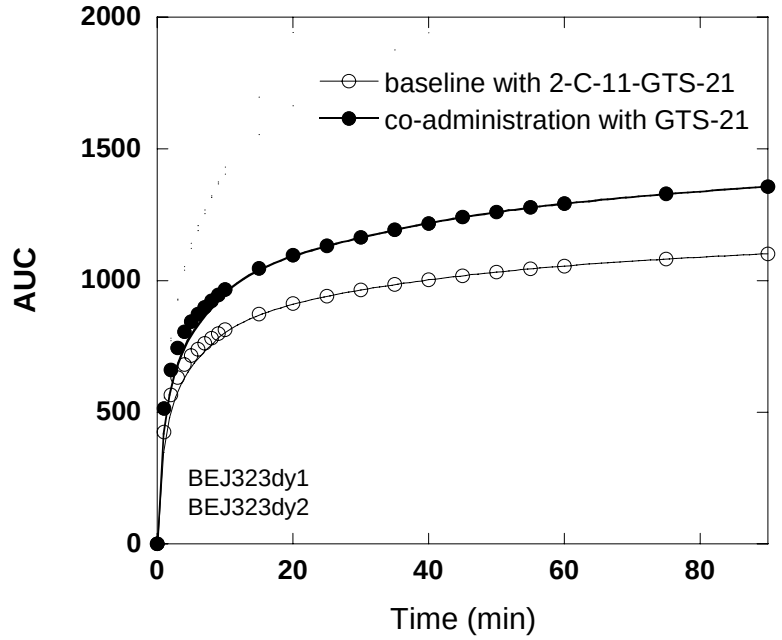

Figure 2.9 (A). The time-activity curves for selected ROIs of baseline (a) and co-administration with GTS-21 (b). **2-^{11}C-2** was co-injected with GTS-21(0.032 mg/kg). CB, cerebellum; TH, thalamus. (B) The area under the curves of **2-^{11}C-2** of baseline and co-administration of GTS-21.

Table 2.3 Effect of therapeutic dose of GTS-21 (0.031 mg/kg)* in the baboon brain.

Region of interest	Baseline		Co-injection with GTS-21	
	K_1	DV	K_1	DV
Cerebellum	1.12	3.86	0.88	3.19
Caudate	1.03	4.42	0.74	3.57
Putamen	1.18	4.70	0.85	3.90
Thalamus	1.21	4.83	0.72	3.75

* 2-^{11}C-GTS-21 was co-injected with GTS-21

2.5.6 Micropet and ex vivo studies in mouse

MicroPET study in mice Similar to the baboon study, the uptake of [^{11}C]GTS-21 in the brain was rapid with 2.4 - 5.0%dose/cc at 32-53 sec after tail vein injection. Clearance from the brain was also rapid with a half-time of maximum uptake (5.7 min - 9 min). In peripheral organs, the liver showed a gradual increase and the gallbladder showed a more pronounced increase over a 20 minute observation time, indicating that radioactivity are excreted primarily through the biliary tract.

A

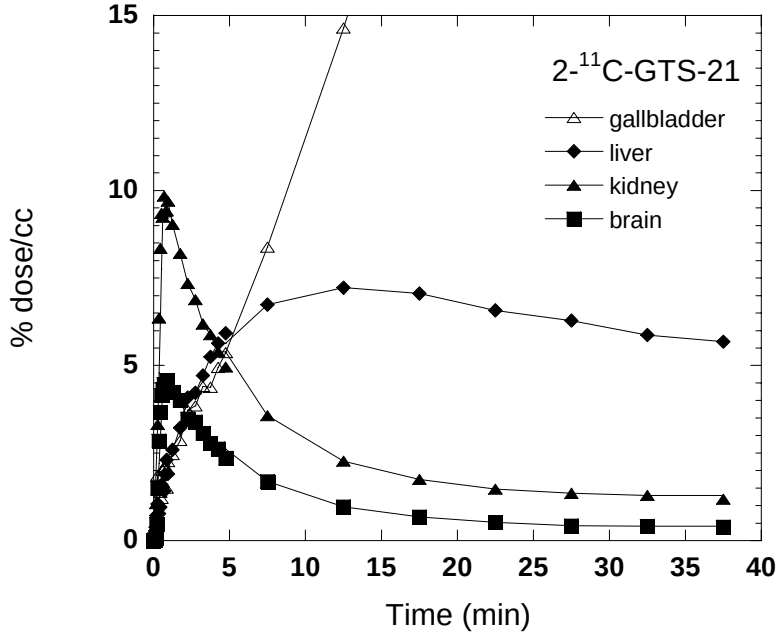
2-11C-GTS-21
gallbladder
liver
kidney
brain
% dose/cc
Time (min)
0
5
10
15
0
5
10
15
20
25
30
35
40

B

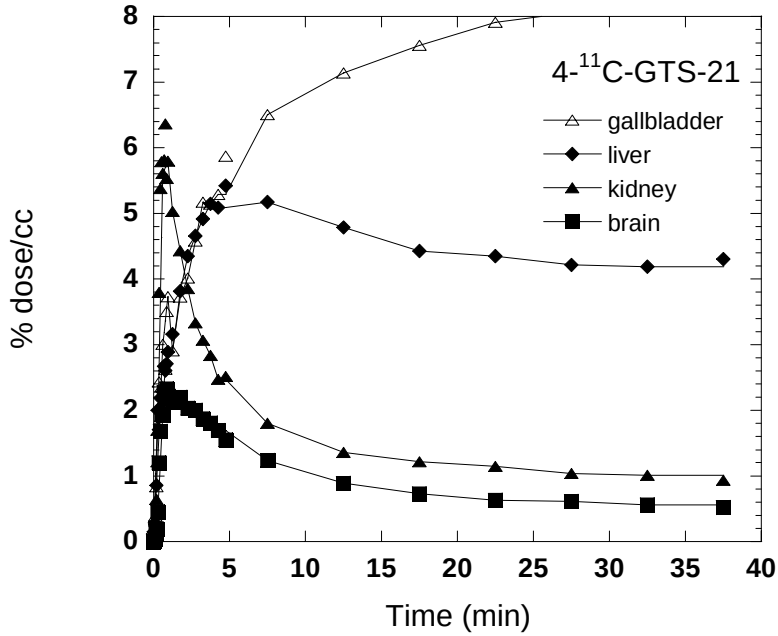
4-11C-GTS-21
gallbladder
liver
kidney
brain
% dose/cc
Time (min)
0
1
2
3
4
5
6
7
8
0
5
10
15
20
25
30
35
40

Figure 2.10 Time-activity curves of each organ in mouse with A**2-^{11}C-2**, B) **4-^{11}C-2**. C-11 uptake of gallbladder and liver shows high over 40 min.

Ex vivo study in the mouse (n=2) HPLC analysis of mouse brain homogenate at 17.5 min post injection showed 0.3 %Dose/cc which is consistent with microPET study (0.25 %dose/cc, figure 12). The major fraction of the total C-11 in the mouse brain was **2-^{11}C-2** (86%) and its metabolite, **^{11}C-3** was less than 3 %. However, **2-^{11}C-2**, **^{11}C-3** were 23% and 42% of the total C-11 in the plasma, respectively. Based on these HPLC analyses, the **^{11}C-3** which we found in the brain may be due to the presence of blood in the brain, suggesting that blood brain barrier penetration of the demethylated metabolites is poor. The ratio of the concentration of **2-^{11}C-2** in brain to that in the plasma was 2.3, which is similar in the literature [10].

In the peripheral organs, the radioactivity concentration in the gallbladder and liver were high (Table 2). Consistent with baboon study, liver uptake and gallbladder accumulation of C-11 probably reflects the accumulation and excretion of labeled metabolites. This is also consistent with known report where 67% of radioactivity excreted in the feces after oral administration of [^{14}C]GTS-21 in rat study [28].

Table 2.4 Whole body biodistribution of [2-methoxy-^{11}C]GTS-21 and [4-methoxy-^{11}C]GTS-21 in mouse.

	2-^{11}C-GTS-21 (%dose/cc)*	4-^{11}C-GTS-21 (%dose/cc)*	2-^{11}C-GTS-21 (%dose/cc)**	4-^{11}C-GTS-21 (%dose/cc)**
Heart	0.46	1.54	0.47	0.84
Lung	0.72	1.95	0.67	1.01
Gallbladder	-	6.46	-	8.56
Spleen	0.76	2.27	0.67	0.78
Kidneys	1.12	3.37	1.04	1.49
Small Intestine	-	4.9	11.43	3.85
Liver	3.50	6.7	5.64	4.62

Stomach	-	3.5	4.90	7.01
Large Intestine	-	1.5	0.52	1.04
Brain	0.32	1.39	0.24	0.66
Muscle	-	0.8	0.41	0.56
Trunk blood	-	1.2	0.36	0.74

* These values were obtained 20 min after injection of each [^{11}C]GTS-21

** These values were obtained 40 min after injection of each [^{11}C]GTS-21

- not determined

2.6 Conclusion

Labeled drugs are of intrinsic interest in that they allow the direct assessment of drug pharmacokinetics. Of particular relevance for CNS drugs are BBB penetration, drug concentration over time, and the identification of target organs as well as the potential brain penetration of pharmacologically active metabolites. This PET study illustrates the value of comparing different label positions and labeled metabolites to gain insight on the behavior of a CNS drug and its metabolites in the brain. GTS-21 is of interest because it is already being evaluated in humans for its efficacy in improving cognition in schizophrenia [13]. Our main findings from this PET study in baboons are that (1) GTS-21 has a very high initial uptake in both cortical and subcortical brain regions followed by rapid clearance; (2) 2-OH-GTS-21, one of the pharmacologically active metabolites of GTS-21, penetrates the BBB; (3) the binding in brain of C-11 labeled GTS-21 (**2-^{11}C-2**) was only transiently affected by the co-administration of a therapeutic dose of GTS-21 with little specificity, consistent with the relatively low affinity of GTS-21 for nAChR and indicating that its distribution and kinetics is dominated by non-specific binding; (4) GTS-21 and its labeled metabolites are excreted via the hepatobiliary pathway. This study also showed that GTS-21 labeled in the 2-methoxy position is more suitable for the brain pharmacokinetic study of GTS-21 itself than GTS-21 labeled in the 4-methoxy

group as this latter isotopomer reflects the distribution for both the parent drug and the labeled metabolite. It is clear that carbon-11 labeled GTS, while providing valuable information on the pharmacokinetics of GTS-21 and its metabolites, is not suitable for imaging the nicotinic receptor. This is consistent with its low affinity and specificity. However, based on the results of this PET study, we suggest that this new information on the rapid clearance of GTS-21 from the brain may need to be considered in future applications of this drug in the treatment of neurocognitive disorders. Furthermore, the moderate BBB penetration of the GTS-21 metabolite, 2-OH-GTS-21, suggests that it may contribute to the therapeutic effects of GTS-21.

2.7 Experimental

2.7.1. General

Anabaseine was purchased from Toronto Research Chemicals Inc. (North York, Ontario, Canada). GTS-21 (2), 4-OH-GTS-21(3), and 2-OH-GTS-21 (4), 2,4-diOH-GTS-21 (5) were synthesized by known methods [29]. All other chemicals were purchased from Aldrich Chemical Company (Milwaukee, WI, USA) and were used without further purification. NMR spectra were recorded using a Bruker Avance 400 MHz NMR spectrometer (Bruker Instruments Inc. Billerica, MA, USA). During the radiosynthesis, carbon-11 was measured by a Capintec CRC-712MV radioisotope calibrator (Capintec Inc., Ramsey, NJ, USA). [^{11}C]Methyl iodide was synthesized using PETtrace MeI Microlab (GE Medical Systems, Milwaukee, WI, USA) from [^{11}C]carbon dioxide which is produced by an EBCO cyclotron. [^{11}C]Carbon dioxide was generated by the nuclear reaction, ^{14}N(p,α)^{11}C, using a nitrogen/oxygen (1000 ppm) target. Semi-preparative high

performance liquid chromatography (HPLC) was performed by a Knauer HPLC system (Sonntek Inc., Woodcliff Lake, NJ, USA) with a model K-5000 pump, a model 87 variable wavelength monitor, and NaI radioactivity detector. Specific activity was determined by measuring the radioactivity and mass; the latter is derived from a standard curve at UV (254 nm) using different concentrations of the authentic reference compounds. Radiochemical purity was also determined by thin layer chromatography (TLC) using and measuring radioactivity distribution on Macherey–Nagel polygram sil G/UV_{254} plastic-back TLC plate with Bioscan system 200 imaging scanner (Bioscan Inc., Washington, DC). ^{11}C radioactivity was measured by a Packard MINAXI γ 5000 automated gamma counter (Packard Instrument, Meriden, CT). All measurements were decay-corrected. All experiments with animals were approved by the Brookhaven Institutional Animal Care and Use Committee.

2.7.2 Synthesis

(3E)-3-[[2,4-dimethoxyphenyl]methylene]-3,4,5,6-tetrahydro-2,3'-bipyridine (GTS-21, **2**) To absolute ethanol (0.7 ml) was added anabaseine dihydrochloride (24 mg, 0.1 mmol) and 2,4-dimethoxybenzaldehyde (20.8 mg, 0.12 mmol). The mixture was heated under reflux for 6 hrs. After ethyl acetate was added, the precipitate was filtered and washed with ethyl acetate. The solid was dried under reduced pressure to give yellow solid (19.7 mg, 52%). ^{1}H-NMR (DMSO-d_6) δ 8.9 (d, 1 H), 8.8 (s, 1 H), 8.1 (d, 1 H), 7.7 (dd, 1 H), 7.6 (d, 1 H), 7.3 (s, 1 H), 6.7 (dd, 1 H), 6.6 (s, 1 H), 3.9 (s, 3 H), 3.8 (t, 2 H), 3.7 (t, 3 H), 2.9 (t, 2 H), 2.0 (t, 2 H).

(3E)-3-[[2-hydroxy-4-methoxyphenyl]methylene]-3,4,5,6-tetrahydro-2,3'-bipyridine (**4**) The same procedure as GTS-21 synthesis was applied. Yield (68%) ^{1}H-NMR (DMSO-d_6) δ 8.9 (d, 1 H), 8.8 (s, 1 H), 8.1 (dd, 1 H), 7.7 (dd, 1 H), 7.6 (d, 1 H), 7.4 (s, 1 H), 6.6 (d, 1 H), 6.5 (s, 1 H), 3.8 (s, 3 H), 3.7 (t, 2 H), 2.9 (t, 2 H), 2.0 (t, 2 H).

(3E)-3-[[4-hydroxy-2-methoxyphenyl]methylene]-3,4,5,6-tetrahydro-2,3'-bipyridine (**3**) The same procedure as GTS-21 synthesis was applied. Yield (30%) ^{1}H-NMR (DMSO-d_6) δ 8.9 (dd, 1 H), 8.8 (d, 1 H), 8.0 (dd, 1 H), 7.7 (dd, 1 H), 7.5 (d, 1 H), 7.4 (s, 1 H), 6.4 (d, 1 H), 6.3 (s, 1 H), 3.8 (t, 2 H), 3.6 (s, 3 H), 2.9 (t, 2 H), 2.0 (t, 1 H).

(3E)-3-[[4-hydroxy-2-methoxyphenyl]methylene]-3,4,5,6-tetrahydro-2,3'-bipyridine (**5**) The same procedure as GTS-21 synthesis was applied. Yield (42%) ^{1}H-NMR (DMSO-d_6) δ 8.9 (d, 1 H), 8.8 (s, 1 H), 8.1 (d, 1 H), 7.7 (dd, 1 H), 7.5 (d, 1 H), 7.4 (s, 1 H), 6.4 (d, 1 H), 6.3 (s, 1 H), 3.8 (t, 2 H), 2.9 (t, 2 H), 2.0 (t, 1 H).

Radiosynthesis of (3E)-3-[[2-(methoxy-^{11}C)-4-methoxyphenyl]methylene]-3,4,5,6-tetrahydro-2,3'-bipyridine (**2-^{11}C-2**) and (3E)-3-[[2-methoxy-4-(methoxy-^{11}C)phenyl]methylene]-3,4,5,6-tetrahydro-2,3'-bipyridine (**4-^{11}C-2**) A solution of (*E*)-3-(2-hydroxy-4-methoxybenzylidene)anabaseine (4) dihydrochloride (or (*E*)-3-(4-hydroxy-2-methoxybenzylidene)anabaseine (3) dihydrochloride) (1 mg, 2.7 μmol) in 0.3 ml of N,N-dimethylformamide and 5.8 μL of NaOH (6 N) was stirred until the color changed to yellow (Fig. 3). The solution was cooled in a dry ice/acetonitrile bath and [^{11}C]methyl iodide was purged into the solution and trapped. When measured ^{11}C peaked, the reaction vessel was sealed and heated at 100 ^{o}C for 3 minutes in an oil bath, then cooled for five seconds in a cooling bath (dry ice/acetonitrile). The reaction mixture was diluted with 1 ml of HPLC eluent, then purified with HPLC using water/acetonitrile (60/40)

including triethylamine (0.4%(v/v)) at a flow rate 5 ml/min on a semi-preparative Gemini C18 (Phenomenex, 250 mm X 10 mm, 5 μ). The product was collected at the expected retention time (RT= 14 min) and solvent was removed by azeotropic evaporation with acetonitrile. After dilution with saline (4 mL, baboon; 2 mL, mouse), the solution was filtered through a Acrodisc® 13 mm Syringe Filter with 0.2 μm HT Tuffryn® Membrane (Pall cooperation, Ann Arbor, MI) into a sterile vial for delivery. For quality control, thin-layer chromatography (TLC) was performed with eluent (chloroform:methanol:ammonia solution= 9:1:0.06); R_f value of 0.7 for carbon-11 which was congruent with an authentic standard of GTS-21 (**2**) co-spotted with the sample and detected by UV (λ= 254 nm).

Radiosynthesis of (3E)-3-[[2-hydroxy-4-(methoxy-^{11}C)phenyl]methylene] -3,4,5,6-tetrahydro-2,3'-bipyridine (**^{11}C-4**) and (3E)-3-[[4-hydroxy-2-(methoxy-^{11}C)phenyl]methylene] -3,4,5,6-tetrahydro-2,3'-bipyridine (**^{11}C-3**) A solution of (*E*)-3-(2,4-dihydroxybenzylidene)anabaseine (**5**) dihydrochloride was used as a starting material in the same procedure described in 2.2. **^{11}C-3** was purified with HPLC using 0.1 M ammonium formate solution (water/acetonitrile= 80/20) at a flow rate 5 ml/min on a semi-preparative Gemini C18 (Phenomenex, 250 mm X 10 mm, 5 μ), eluting at 18.8 min. The same column and conditions were used for purification of **^{11}C-4** with 0.1 M ammonium formate solution (water/acetonitrile=75/25) and collected at 17 min. Two labeled compounds were analyzed by TLC with eluent (chloroform:methanol:ammonia solution= 8:2:0.4). R_f's were 0.77 and 0.74 for **^{11}C-4** and **^{11}C-3**, respectively.

2.7.3 Measurement of free fraction in plasma and log D

A modification of a literature procedure for measurement of the free fraction of [^{11}C]GTS-21 in baboon plasma was used [30]. An aliquot of [^{11}C]GTS-21 was measured for radioactivity and added to 500 µl of baboon plasma, and this mixture was incubated for 10 min at room temperature. Aliquots (20-40 µL) of the incubated spike plasma were assayed for radioactivity. A portion of the incubation mixture (200-400 µL) was placed in the upper level of a Centrifree tube (Amicon Inc, Beverly, MA, USA) and this was centrifuged for 10 minutes. After centrifuging, the top portion of the Centrifree tube containing the bound portion was removed and discarded, and precisely measured aliquots (20-40 µL) of the liquid in the cup (unbound fraction) were counted. The free fraction is the ratio of the decay-corrected counts of the unbound aliquots to the decay-corrected counts of the unspun aliquots.

Log D (an index for lipophilicity) at pH= 7.4 was also measured using a previous method [30, 31]. Briefly, an aliquot (50 µL) of [^{11}C]GTS-21 solution was added to a mixture of 1-octanol (2.5 mL) and phosphate buffered saline (PBS, pH 7.4; 2.5 ml). The mixture was vortexed at room temperature for 2 min and then centrifuged at 7000 rpm for 2 min. An aliquot (0.1 mL) of the octanol layer and 1.0 ml of the buffer layer were sampled separately into two empty vials and counted. Two mL of the octanol layer was transferred into a test tube containing 0.5 ml of fresh octanol and 2.5 ml of buffer and the process of vortexing and centrifuging was repeated. The aliquots from each layer were extracted and counted until 6 measures of the ratio of counts in the octanol to counts in the buffer were obtained. Log D is as the $\log_{10}$ of the average of the ratios of the decay corrected counts in the octanol:buffer.

2.7.4 PET studies in baboon

Four adult female *Papio Anubis* baboons were anesthetized by an intramuscular injection of ketamine hydrochloride (10 mg/kg), and then maintained with oxygen (800 ml/min), nitrous oxide (1500 ml/min), and isoflurane (Forane, 1-4%) during the scanning. Either **2-^{11}C-2** or **4-^{11}C-2** (2-4 mCi in saline) was injected through a catheter placed in a radial arm vein and arterial blood was sampled through a catheter in popliteal artery with the following time intervals; every 5 sec for 2 min, then 2, 5, 10, 20, 30, 60, 90 min. Heart rate, respiration rate, PO2, and body temperature were checked during the PET scanning. Dynamic PET Imaging was performed by Siemens HR + (Siemen's high-resolution, whole-body PET scanner with 4.5 x 4.5 x 4.8 mm at center of field of view) for a total of 90 min with the following time frames in 3D mode (10 x 60 sec; 4 x 300 sec; 8 x 450 sec). Either the brain or the torso was placed in the field of view. Prior to the study, a transmission scan was obtained by rotating a ^{68}Ge rod source to correct for attenuation. Each animal was scanned with either **2-^{11}C-2** or **4-^{11}C-2** for the baseline followed by a 2 hour interval after which the other isotopomer was administered (Table 1). To evaluate reproducibility, **2-^{11}C-2** was injected twice with a 2 hr interval between injections. To assess the effect of a therapeutic dose of GTS-21, a baboon was scanned at baseline with **2-^{11}C-2**. Two hours later, an intravenous dose of GTS-21 (**2**) dihydrochloride (0.031 mg/kg; 81.3 nmol/kg based on the literature [8]) was co-administered with **2-^{11}C-2** and the baboon was scanned following the same scanning protocol described above.

To compare the pharmacokinetics of the demethylated GTS metabolites (**3** and **4)**, PET studies in baboons were carried out using **^{11}C-3** and **^{11}C-4** with a 2 hour interval between injections. Arterial plasma samples were obtained over the 90 min time course of the study.

2.7.5 Image Analysis

All image data were reconstructed using filtered back-projection (FBP). For image analysis, we constructed a region of interest (ROI) file with the published MR template and $H_2{}^{15}O$ template images [32] by PMOD (PMOD Technologies, Ltd.). The ROI for the global uptake was obtained by selecting four representative transaxial planes. After ECAT7 files were converted to ANALYZE format and all time frames were summed for each file, they were co-registered with $H_2{}^{15}O$ template images without normalization. ROI's were applied to the summed images and adjusted manually for each region and projected onto the dynamic frames to provide time-activity curves for each brain region. Time activity curves were normalized with injected dose to give % injected dose/cc. Model terms K_1 and distribution volume (DV) were determined by Logan graphical analysis to evaluate the effect of a therapeutic dose of GTS-21 (**2**) [33]. ROI's for peripheral organs were drawn manually in the dynamic images.

2.7.6 Plasma Analysis of [^{11}C]GTS-21 (2-^{11}C-2 and 4-^{11}C-2)

All arterial blood samples were centrifuged and the resulting plasma samples were assayed for radioactivity in a well counter to give the total carbon-11 concentration at each sampling time point. Selected plasma samples (1, 5, 10, 30, 60 min) were further analyzed for unchanged radiotracer using the following procedure. Each sample (0.1-0.4

mL) was added to acetonitrile (0.3 mL), spiked with unlabeled GTS-21 and demethylated metabolites **3** and **4**, then sonicated (Polytron, Brinkmann Instruments, Westbury, NY, USA) to disrupt cells. After centrifugation for 3 min, the pellet and supernatant solution were counted and the supernatant was subjected to HPLC analysis (Phenomenex Ultremex 5 C18, 250 mm X 4.60 mm eluting with 100 mM phosphate buffer (pH = 4.5)/methanol (60/40) analysis with UV detector (λ= 254 nm)). The retention time (Rt) of [^{11}C]GTS-21 was 13.8 min at a flow rate of 0.7 mL/min (Rt = 9 min for **^{11}C-3** and **^{11}C-4)**. Fractions were collected and counted, noting the fractions containing the standards. The ratio of the C-11 in the fraction containing the GTS-21 to the C-11 in the sum of all fractions was used to correct the arterial plasma time-activity curve to give the input function for [^{11}C]GTS-21.

2.7.7 Plasma Analysis of ^{11}C-3 and ^{11}C-4

Arterial plasma samples were analyzed by solid phase extraction [34] after the baboon was injected with the labeled demethylated metabolites **^{11}C-3** and **^{11}C-4.** Briefly, the Sep-Pak was conditioned by rinsing with 5 mL of methanol followed by 5 mL of water. A sample of plasma (50-600 μL) was diluted with water (3 mL), then poured onto Bond Elut LRC-C18-500 mg (Varian, Harbor City, CA) pre-loaded with deionized water (2 mL). The combined water fractions (3 mL + 2 mL) were pushed through the Sep-Pak with nitrogen and collected. The Sep-Pak was then rinsed sequentially with water (5 mL x 2) and 50% aqueous methanol (5 mL x 2). Each fraction of eluent was collected separately and counted. Finally, the radioactivity remaining on the Sep-Pak was assayed. The Sep-Pak and the last fraction of eluent contained **^{11}C-3** and **^{11}C-4**.

2.7.8 Mouse Studies

Micro PET study Four male mice (Swiss-Webster, 30-40 g) were imaged with small animal PET (MicroPET R4 ™, Siemens) after the injection of **2-^{11}C-2** or **4-^{11}C-2**; two were scanned for 20 min and sacrificed for HPLC analysis of brain and plasma and the other two mice were scanned for 40 min to get the whole body distribution and kinetics after injection of **2-^{11}C-2** and **4-^{11}C-2**, respectively. Mice were anesthetized using ketamine/xylazine (90/10, 100mg/kg) and positioned prone in the scanner. Radiotracers were administered by intravenous injection in the tail vein (300-438 μCi, specific activity = 1.8-2.9 Ci/μmole at EOB). Data acquisition was started simultaneously with tracer injection and continued for 20-40 min. List mode data was binned into a maximum of 22 frames (5 x 2 sec, 10 x 5 sec, 7 x 300 sec) using microPET Manager (v. 2.3.3.0) software. The resulting sinograms were scatter-corrected using a custom tail-fit method and reconstructed by two dimensional filtered-back projection (FBP) after Fourier rebinning using a filter cutoff at the Nyquist criteria (default parameters of software) [35]. Time-activity curves for the brain, liver, kidney, and gall bladder were determined using ASIPro VM software by drawing regions of interest directly on the summed frame PET image and projected onto the individual dynamic frames.

Ex vivo biodistribution studies (n=3) Following 20 min or 40 min PET scans with **2-^{11}C-2** or **4-^{11}C-2**, two mice were sacrificed and decapitated. Trunk blood, brain, heart, kidney, spleen, lung, liver, gallbladder, and stomach were harvested consecutively. Each organ was weighed and counted to determine the % injected dose/g. Arterial blood was

centrifuged for 3 min to give a plasma sample. To determine the ratio of the brain to plasma of GTS-21 and its labeled metabolites, one mouse was sacrificed and decapitated at 20 min after injection of **2-^{11}C-2**. The whole brain was homogenized in methanol (1 ml) using a Tissue Tearor (Biospec Producs, Bartlesville, OK) with medium speed for 1 min, centrifuged and the homogenate was filtered to give the supernatant solution. This brain extract was subjected to HPLC analysis using the same conditions which were used to analyze the baboon plasma.

2.8 References

1. Kim, S. W.; Ding, Y.-S.; Alexoff, D.; Patel, V.; Logan, J.; Lin, K.-S.; Shea, C.; Muench, L.; Xu, Y.; Carter, P.; King, P.; Constanzo, J. R.; Ciaccio, J. A.; Fowler, J. S. Synthesis and positron emission tomography studies of C-11-labeled isotopomers and metabolites of GTS-21, a partial [alpha]7 nicotinic cholinergic agonist drug. *Nuclear Medicine and Biology* **2007,** 34, 541-551.

2. Machu, T. K.; Hamilton, M. E.; Frye, T. F.; Shanklin, C. L.; Harris, M. C.; Sun, H. W.; Tenner, J. E.; Soti, F. S.; Kem, W. R. Benzylidene analogs of anabaseine display partial agonist and antagonist properties at the mouse 5-hydroxytryptamine(3A) receptor. *Journal of Pharmacology and Experimental Therapeutics* **2001,** 299, 1112-1119.

3. Kitagawa, H.; Takenouchi, T.; Azuma, R.; Wesnes, K. A.; Kramer, W. G.; Clody, D. E.; Burnett, A. L. Safety, pharmacokinetics, and effects on cognitive function of multiple doses of GTS-21 in healthy, male volunteers. *Neuropsychopharmacology* **2003,** 28, 542-51.

4. de Fiebre, C. M.; Meyer, E. M.; Henry, J. C.; Muraskin, S. I.; Kem, W. R.; Papke, R. L. Characterization of a series of anabaseine-derived compounds reveals that the 3-(4)-dimethylaminocinnamylidine derivative is a selective agonist at neuronal nicotinic alpha 7/125I-alpha-bungarotoxin receptor subtypes. *Mol Pharmacol* **1995,** 47, 164-71.

5. Zoltewicz, J. A.; Prokaitatrai, K.; Bloom, L. B.; Kem, W. R. Long-Range-Transmission of Polar Effects in Cholinergic 3-Arylideneanabaseines - Conformations Calculated by Molecular Modeling. *Heterocycles* **1993,** 35, 171-180.

6. Kem, W. R. Study of Occurrence of Anabaseine in Paranemertes and Other Nemertines. *Toxicon* **1971,** 9, 23-&.

7. de Fiebre, N. C.; de Fiebre, C. M. Alpha 7 nicotinic acetylcholine receptor-mediated protection against ethanol-induced neurotoxicity. *Alcohol* **2003,** 31, 149-53.

8. Briggs, C. A.; Anderson, D. J.; Brioni, J. D.; Buccafusco, J. J.; Buckley, M. J.; Campbell, J. E.; Decker, M. W.; Donnelly-Roberts, D.; Elliott, R. L.; Gopalakrishnan, M.; Holladay, M. W.; Hui, Y. H.; Jackson, W. J.; Kim, D. J.; Marsh, K. C.; O'Neill, A.; Prendergast, M. A.; Ryther, K. B.; Sullivan, J. P.; Arneric, S. P. Functional characterization of the novel neuronal nicotinic acetylcholine receptor ligand GTS-21 in vitro and in vivo. *Pharmacol Biochem Behav* **1997,** 57, 231-41.

9. Martin-Ruiz, C. M.; Court, J. A.; Molnar, E.; Lee, M.; Gotti, C.; Mamalaki, A.; Tsouloufis, T.; Tzartos, S.; Ballard, C.; Perry, R. H.; Perry, E. K. Alpha4 but not alpha3 and alpha7 nicotinic acetylcholine receptor subunits are lost from the temporal cortex in Alzheimer's disease. *J Neurochem* **1999,** 73, 1635-40.

10. Kem, W. R. The brain alpha7 nicotinic receptor may be an important therapeutic target for the treatment of Alzheimer's disease: studies with DMXBA (GTS-21). *Behav Brain Res* **2000,** 113, 169-81.

11. Kitagawa, H.; Takenouchi, T.; Azuma, R.; Wesnes, K. A.; Kramer, W. G.; Clody, D. E.; Burnett, A. L. Safety, pharmacokinetics, and effects on cognitive function of multiple doses of GTS-21 in healthy, male volunteers. *Neuropsychopharmacology* **2003,** 28, 542-551.

12. Stevens, K. E.; Kem, W. R.; Mahnir, V. M.; Freedman, R. Selective alpha7-nicotinic agonists normalize inhibition of auditory response in DBA mice. *Psychopharmacology (Berl)* **1998,** 136, 320-7.

13. Olincy, A.; Harris, J. G.; Johnson, L. L.; Pender, V.; Kongs, S.; Allensworth, D.; Ellis, J.; Zerbe, G. O.; Leonard, S.; Stevens, K. E.; Stevens, J. O.; Martin, L.; Adler, L. E.; Soti, F.; Kem, W. R.; Freedman, R. Proof-of-concept trial of an alpha 7 nicotinic agonist in schizophrenia. *Archives of General Psychiatry* **2006,** 63, 630-638.

14. Tatsumi, R.; Fujio, M.; Satoh, H.; Katayama, J.; Takanashi, S.; Hashimoto, K.; Tanaka, H. Discovery of the alpha 7 nicotinic acetylcholine receptor agonists. (R)-3 '-(5-Chlorothiophen-2-yl)spiro-1-azabicyclo[2.2.2]octane-3,5 '-[1 ',3 ']-oxazolidin-2 '-one as a novel, potent, selective, and orally bioavailable ligand. *Journal of Medicinal Chemistry* **2005,** 48, 2678-2686.

15. Meyer, E. M.; Kuryatov, A.; Gerzanich, V.; Lindstrom, J.; Papke, R. L. Analysis of 3-(4-hydroxy, 2-Methoxybenzylidene)anabaseine selectivity and activity at human and rat alpha-7 nicotinic receptors. *J Pharmacol Exp Ther* **1998,** 287, 918-25.

16. Kem, W. R.; Mahnir, V. M.; Prokai, L.; Papke, R. L.; Cao, X. F.; LeFrancois, S.; Wildeboer, K.; Prokai-Tatrai, K.; Porter-Papke, J.; Soti, F. Hydroxy metabolites of the Alzheimer's drug candidate 3-[(2,4-dimethoxy)benzylidene]-anabaseine dihydrochloride (GTS-21): Their molecular properties, interactions with brain nicotinic receptors, and brain penetration. *Molecular Pharmacology* **2004,** 65, 56-67.

17. Kem, W. R.; Zoltewicz, J. A.; Meyer, E. M.; Prokai-tatrai, K. Anabaseine derivatives useful in the treatment of degenerative diseases of the nervous system. 96-392763
5741802, 19960105., 1998.

18. Dischino, D. D.; Welch, M. J.; Kilbourn, M. R.; Raichle, M. E. Relationship between Lipophilicity and Brain Extraction of C-11-Labeled Radiopharmaceuticals. *Journal of Nuclear Medicine* **1983,** 24, 1030-1038.

19. Eckelman, W. C.; Mathis, C. A. Targeting proteins in vivo: in vitro guidelines. *Nuclear Medicine and Biology* **2006,** 33, 161-164.

20. Kulak, J. M.; Musachio, J. L.; McIntosh, J. M.; Quik, M. Declines in different beta 2*nicotinic receptor populations in monkey striatum after nigrostriatal damage. *Journal of Pharmacology and Experimental Therapeutics* **2002,** 303, 633-639.

21. Kulak, J. M.; Schneider, J. S. Differences in [alpha]7 nicotinic acetylcholine receptor binding in motor symptomatic and asymptomatic MPTP-treated monkeys. *Brain Research* **2004,** 999, 193-202.

22. Gundisch, D.; Koren, A. O.; Horti, A. G.; Pavlova, O. A.; Kimes, A. S.; Mukhin, A. G.; London, E. D. In vitro characterization of 6-[F-18]fluoro-A85380, a high-affinity ligand for alpha 4 beta 2*nicotinic acetylcholine receptors. *Synapse* **2005,** 55, 89-97.

23. Horti, A. G.; Chefer, S. I.; Mukhin, A. G.; Koren, A. O.; Gundisch, D.; Links, J. M.; Kurian, V.; Dannals, R. F.; London, E. D. 6-[18F]fluoro-A-85380, a novel radioligand for in vivo imaging of central nicotinic acetylcholine receptors. *Life Sciences* **2000,** 67, 463-469.

24. Ding, Y. S.; Liu, N.; Wang, T.; Marecek, J.; Garza, V.; Ojima, I.; Fowler, J. S. Synthesis and evaluation of 6-[F-18]fluoro-3-(2(S)azetidinylmethoxy)pyridine as a PET tracer for nicotinic acetylcholine receptors. *Nuclear Medicine and Biology* **2000,** 27, 381-389.

25. Acton, P. D.; Choi, S. R.; Hou, C.; Plossl, K.; Kung, H. F. Quantification of serotonin transporters in nonhuman primates using [I-123]ADAM and SPECT. *Journal of Nuclear Medicine* **2001,** 42, 1556-1562.

26. Azuma, R.; Hirota, T.; Manabe, H.; Komuro, M.; Kiwada, H. First-pass of GTS-21 on canine gut wall and liver determined by portal-systemic concentration difference. *European Journal of Pharmaceutical Sciences* **2001,** 14, 159-165.

27. Kem, W.; Soti, F.; Wildeboer, K.; LeFrancois, S.; MacDougall, K.; Wei, D. Q.; Chou, K. C.; Arias, H. R. The nemertine toxin anabaseine and its derivative DMXBA (GTS21): Chemical and pharmacological properties. *Marine Drugs* **2006,** 4, 255-273.

28. Azuma, R.; Komuro, M.; Korsch, B. H.; Andre, J. C.; Onnagawa, O.; Black, S. R.; Mathews, J. M. Metabolism and disposition of GTS-21, a novel drug for Alzheimer's disease. *Xenobiotica* **1999,** 29, 747-762.

29. Kem, R. W.; Zoltewicz, A. J.; Meyer, M. e.; Prokai-tatrai, K. Anabaseine derivatives useful in the treatment of degenerative diseases of the nervous system. 1998.

30. Ding, Y. S.; Lin, K. S.; Logan, J.; Benveniste, H.; Carter, P. Comparative evaluation of positron emission tomography radiotracers for imaging the norepinephrine transporter: (S,S) and (R,R) enantiomers of reboxetine analogs ([C-11]methylreboxetine, 3-Cl-[C-11]methylreboxetine and [F-18]fluororeboxetine), (R)-[C-11]nisoxetine, [C-11]oxaprotiline and [C-11]lortalamine. *Journal of Neurochemistry* **2005,** 94, 337-351.

31. Delrosario, R. B.; Jung, Y. W.; Baidoo, K. E.; Lever, S. Z.; Wieland, D. M. Synthesis and in-Vivo Evaluation of a Tc-99m/99-Dadt-Benzovesamicol - a Potential Marker for Cholinergic Neurons. *Nuclear Medicine and Biology* **1994,** 21, 197-203.

32. Black, K. J.; Snyder, A. Z.; Koller, J. M.; Gado, M. H.; Perlmutter, J. S. Template images for nonhuman primate neuroimaging: 1. Baboon. *Neuroimage* **2001,** 14, 736-743.

33. Logan, J.; Fowler, J. S.; Volkow, N. D.; Wolf, A. P.; Dewey, S. L.; Schlyer, D. J.; MacGregor, R. R.; Hitzemann, R.; Bendriem, B.; Gatley, S. J.; et al. Graphical analysis of reversible radioligand binding from time-activity measurements applied to [N-11C-methyl]-(-)-cocaine PET studies in human subjects. *J Cereb Blood Flow Metab* **1990,** 10, 740-7.

34. Alexoff, D. L.; Shea, C.; Fowler, J. S.; King, P.; Gatley, S. J.; Schlyer, D. J.; Wolf, A. P. Plasma input function determination for PET using a commercial laboratory robot. *Nuclear Medicine and Biology* **1995,** 22, 893-904.

35. Alexoff, D. L.; Vaska, P.; Marsteller, D.; Gerasimov, T.; Li, J.; Logan, J.; Fowler, J. S.; Taintor, N. B.; Thanos, P. K.; Volkow, N. D. Reproducibility of C-11-raclopride binding in the rat brain measured with the MicroPET R4: Effects of scatter correction and tracer specific activity. *Journal of Nuclear Medicine* **2003,** 44, 815-822.

3. The development of quinuclidine-based α7 nAChR PET tracers

3.1 Background

The pharmacological effects of the first functionally selective α7 nAChR agonist, GTS-21, stimulated medicinal chemist60

ry research directed to the development of α7 nAChR selective ligands.[1] In order to achieve therapeutically favorable effects as well as reduce side effects such as nicotinic addiction, the discovery of lead compounds and optimization of binding affinity and selectivity for α7 nAChR have been of particular interest and need for drug development.[2]

Pharmacophore and SAR The endogenous neurotransmitter, acetylcholine has a distinctive quaternary ammonium cation, ester, and space between two functional groups (Figure 3.1). Two representative natural products, muscarine and nicotine share these similar structural characteristics. Based on this pharmacophore, most of nAChR ligands possess a cationic center and hydrogen bond acceptor, and hydrophobic group. In particular, the cationic center is essential for the binding, while the other pharmacophoric elements are amenable to chemical modification (Figure 3.2). Ayers's et al. reported that even simple quaternary ammonium salts showed micro or submicromolar range affinity for the α7 nAChR.[3-5]

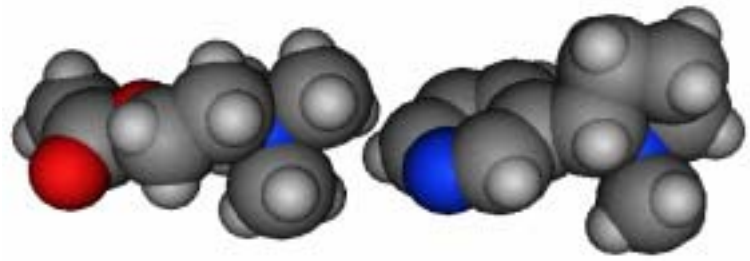

acetylcholine **nicotine**

Figure 3.1 The three dimensional structures of acetylcholine and nicotine. The model was generated by MOE flexible alignment. Blue, nitrogen; red, oxygen; gray, carbon and hydrogen.

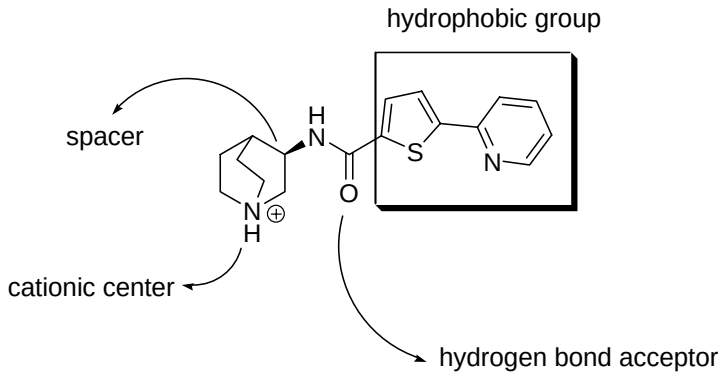

Figure 3.2 The strategy for SAR study.

Initially, since the rigid azabicyclic system was applied as a isostere for the quaternary ammonium center in the development of α4β2 nAChR and mAChR ligands for the (ex. epibatidine, varenicline), quinclidine scaffold has been used for the α7 nAChR.[6] Due to its high basicity (pKa= ~11, pK_{BH}^{+}= 20 in acetonitrile) and well-defined rigid ring structure, quinuclidine system has proved to be a suitable structural component for α7 nAChR. Compared with other azacylic systems such as N-methylpyrrolidine and N-methylpiperidine, the quinulidine-based ligands showed superior binding properties (Figure 3.3).[7]

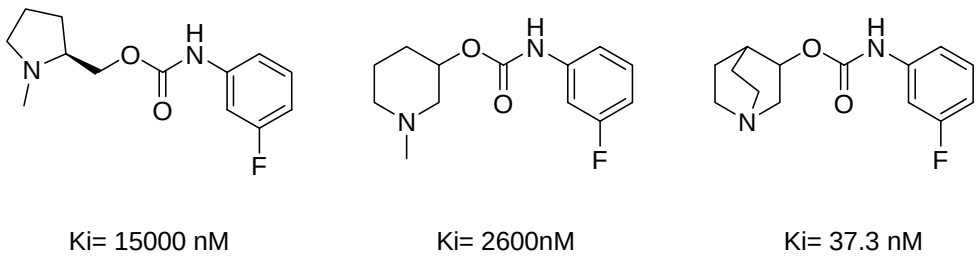

Figure 3.3 Comparison of azacylic systems for cationic center for α7 nAChR[7]

Secondly, spacers between cationic center and hydrogen bonding acceptor usually consist of two or three atoms as acetylcholine and nicotine. In the previous literature, many ligands chemically-modified at 3-position on quinuclidine ring have been reported, where R configuration showed dramatic improvement in binding affinity (Figure 3.4).[8] It was suggested that two carbons as the length of spacer was favorable.[9]

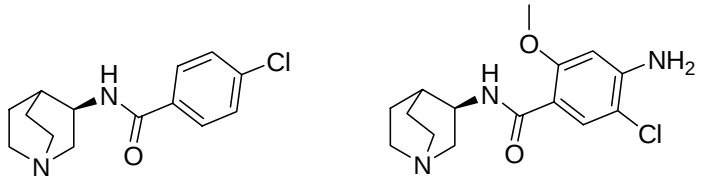

PNU 282987, R, Ki=25 nM
S, Ki=200 nM

zacopride, R, Ki= 1000 nM
S, Ki> 13000 nM

Figure 3.4 Stereochemistry at 3-postion of quinuclidine ring for α7 nAChR binding

Thirdly, a hydrogen acceptor, such as an amide, ether, ester, carbamate, and urea were tested.[10] It is generally accepted that carbonyl oxygen functions as a hydrogen bonding acceptor. Binding affinity is not sensitive to these functional groups though exceptionally bulky groups like sulfonamide seem disruptive to receptor binding.

Finally, as a hydrophobic group, aromatic rings such as benzene, thiophene, and furan are favorable. The bulky substituent on benzene of quinuclidinyl carboxamide derivatives improved binding affinity (Figure 3.5). The orientation of these substituents and heteroatoms in aromatic ring is often critical for binding.[2]

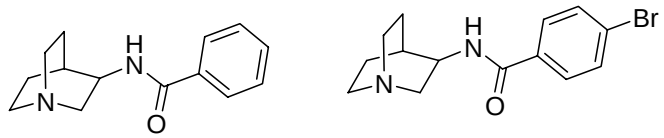

Ki= 68 nM Ki= 18 nM

Figure 3.5 Effect of substituent of the hydrophobic group of quinuclidine carboxamide on affinity for α7 nAChR.

Representative templates Quinuclidine-based lead compounds have been investigated based on three variables; position of modification of the quinuclidine scaffold, hydrophobic groups, and structural change in the hydrogen bond acceptor part. Mazurov et al. report that structural modification at 2-position of quinuclidine ring with the 3-pyridinylmethylene group improved binding affinity and selectivity consistently.[11] The presence and position of nitrogen were also very crucial for the binding affinity (Figure 3.6).

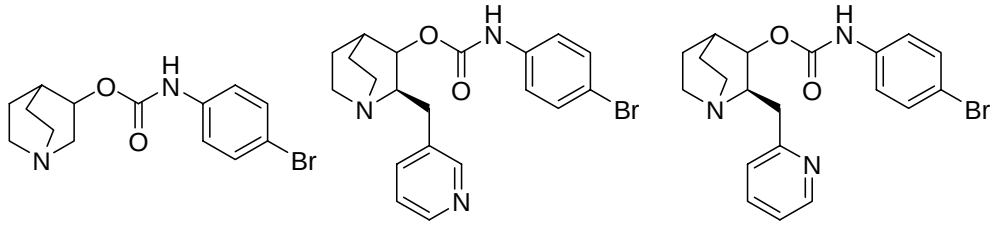

Ki= 40 nM Ki= 5 nM Ki >10000 nM

Figure 3.6 Effect of substituents at 2-positon of quinuclidine ring on α7 nAChR binding affinity.

With respect to hydrogen bond acceptors, AR-R17779, the first selective full agonist for α7 nAChR, has carbonyl group in structurally rigid spirocyclic carbamate ring.[12] Interestingly, binding selectivity and affinity seemed to be very sensitive to small

structural modifications of carbamate ring. For example, the positional exchange of nitrogen and oxygen abolished α7 nAChR binding, a methyl group of carbamate nitrogen reduced the selectivity.[12] The enantiomer of AR-R17779 also showed reduced activity for α7 nAChR. Even though there seemed little room for structural modification of this template, Ogawa et al. reported that I-TSA showed subnanomolar binding activity for α7 nAChR.[13] In our view, the hydrophobic interaction of 5-iodothiophenyl group seemed to overwhelm the loss of interaction by altering hydrogen bond acceptor properties (**Table 3.1**).

Table 3.1 SAR study of AR-R17779 derivatives for nAChR subtype binding.

	Ki for α7 nAChR	Ki for α4β2 nAChR
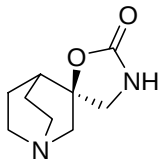 **AR-R17779**	92 nM	16000 nM
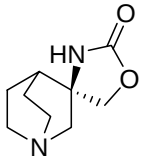	4300 nM	-
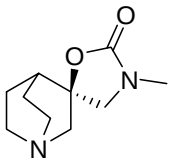	220 nM	200 nM
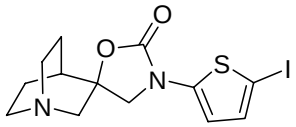	0.54	-

Another example of a rigid structure at 3-position of quinuclidine ring is spiroazabicylcodihydrofuropyridinyl template which possess high structural similarity to

AR-R17779. Binding affinity also improved significantly with the addition of a hydrophobic moiety to the pyridine ring (Figure. 3.7).[14]

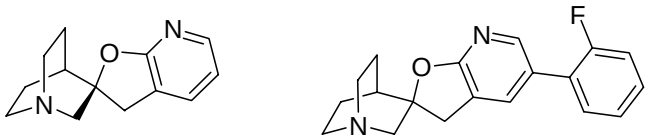

Ki= 14 nM Ki= 0.35nM

Figure 3.7 Spirodihydrofuropyridine derivatives for α7 nAChR

Cross reactivity with 5-HT$_3$R In addition to selectivity against other nAChR, the α7 nAChR ligands must be validated for the selectivity against a homologous protein target. One of the highly homologous receptors with the α7 nAChR in the CNS is serotonin type 3 receptor 5-HT$_3$, which is the same type of LGIC and has 30% homology in its protein sequence. Some 5-HT$_3$R ligands were known to bind α7 nAChR as an agonist or antagonist.[15] For example, Tropisetron, a 5-HT$_3$R antagonist drug, showed partial agonism toward α7 nAChR. Tropisetron has similar structural characteristics with α7 nAChR ligands mentioned above. Thus, its Ki toward α7 nAChR is low. However, Ondansertron, which has much less basic nitrogen in the imidazole ring, failed to show the cross activity (Table 3.2).

Table 3.2 Comparison of cross binding activity (Ki) of 5-HT_3R drugs

	Tropisetron	Ondansetron
	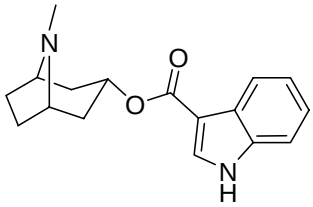	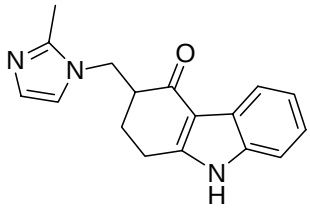
α7 nAChR	6.9 nM	> 3000 nM
5-HT_3R	5.3 nM	12 nM

To our knowledge, the α7 nAChR ligands with highest affinity is spirodihydrofuropyridine derivative, **3-2**. However, these ligands may not be selective (Table 3).

Table 3.3 Binding profile (Ki) of spirodihydrofuropyridine derivatives

	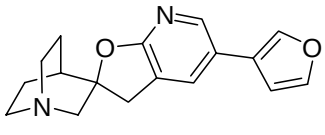 **3-2**	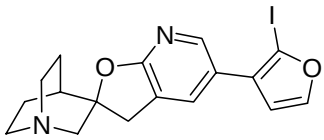
α7 nAChR	0.033 nM	0.26 nM
α4β2 nAChR	83000 nM	-
5-HT_3R	-	0.57 nM

For the selectivity between the α7 nAChR and the 5-HT_3R, Baker et al. reported quinuclidine-based carboxamide derivatives which avoided the cross binding. The hydrophobic component seemed to modulate the cross reactivity with 5-HT_3R. Even though the quinuclidine carboxamide with different aryl-aryl substituent were investigated, the rational explanation for the selectivity still remains elusive (Figure 3.8).[16]

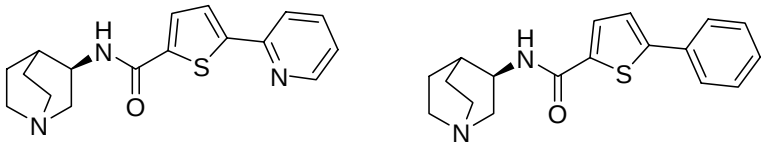

Compoud A

Ki = 1.3 nM for alpha7

Ki= 15.5% at 10uM 5-HT_3

Ki = 1.8 nM for alpha7

Ki= 24% 10 uM for 5-HT_3

Figure 3.8 The selective α7 nAChR ligands

With respect to functional activity, Pfizer reported that PNU-282987 showed high selectivity for the α7 nAChR relative to the 5-HT_3R.[8]

In summary, due to the high protein sequence homology and similar structural characteristics between the α7 nAChR and the 5-HT_3R, they share similar binding properties for the quinuclidine-based ligands. One of the most promising selective templates is quinuclidinyl 2-arylthiophene-5-carboxamide.

3.2 Objectives

We synthesized a spiroquinuclidinyl dihydrofuropyridine compound, **3-1**, which is based on the structure of compound (**3-2**, Ki= 33 pM), with a view to the eventual synthesis of C-11 labeled **3-1** (Figure 3.9). Considering the cross reactivity between α7 nAChR and 5HT_3R, we also synthesized quinuclidinyl carboxamide compound, **3-21,** and tested its potential for a selective PET tracer. In this procedure, we would develop reliable and facile synthetic methodologies for heteroaryl-heteroaryl carboxylic acid, which might facilitate the parallel synthesis of a diverse array of α7 nAChR ligands.

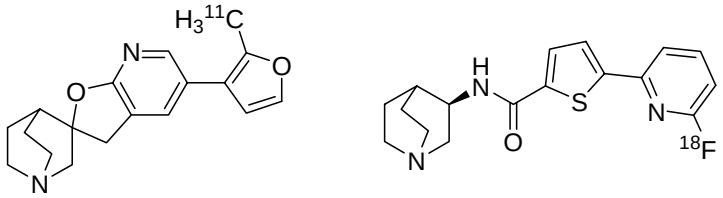

3-1 **3-21**

Figure 3.9 Target compounds

Since lead structures from the medicinal chemistry literature frequently did not have a functional group which can be labeled with C-11 or F-18, we investigated quantitative structure-activity relationship (QSAR) and homology modeling, in order to help to determine the optimal position for labeling as well as reveal how small structural changes required for PET chemistry might affect binding affinity of the parent structure.

3.3 The synthesis of quinuclidine-based dihydrofuropyridine

3.3.1 Initial design

To date, a compound with the greatest binding affinity for α7 nAChR is a quinuclidine-based dihydrofuropyridine derivative, **3-2** (Ki= 33 pm) (Scheme 3.1). Our starting point is to design a putative structure which maintains the binding characteristics of **3-2**. Initially, due to lack of suitable position for C-11 labeling, we planned to label on furan ring with C-11 methyl iodide. We reasoned the chemical modification of furan would be valuable for labeling to minimize the decline of binding affinity.

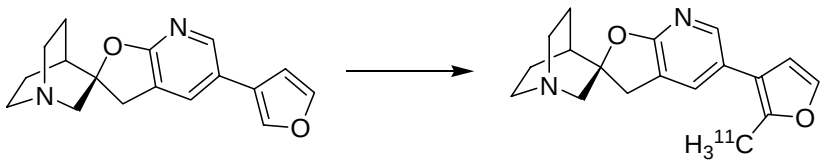

Scheme 3.1 The synthesis of precursor **3.2** and unlabeled labeled target compound **3.1**

3.3.2 Synthesis of precursor 3-2

Using a modification of synthetic procedure in the patent,[17] we synthesized **3-2**, as a precursor (Scheme 3.1 (**3.2**)). The quinuclidinyl oxirane compound (**3-4**) was prepared by Corey-Chaykovsky reaction in anhydrous dimethylsulfoxide. Instead of 3-quinuclidinone, which is not commercially available and hard to handle, its hydrocholoric salt form was used and treated with an excess amount sodium hydride. When the temperature was elevated, the side reaction occurred. Compound **3-4** was also volatile and decomposed easily under our conditions. We, therefore, decided that it needed to be protected by borane within one hour after its synthesis. After protection with borane as solid form, it was treated with lithiated 2-chloropyridine under the dry ice/acetone bath and the temperature was elevated to -35 ^{o}C to complete the reaction. Many side reactions occurred, requiring purification by silica gel and subsequent recrystallization. As a protecting group, amine-borane complex was stable at room temperature. Intramolecular cyclization was performed to give spiroazabicyclodihydrofuropyridine, **3-7**. Initially, this step was problematic because of the tendency toward ring reopening (Scheme 3.2). The temperature was critical for this step to prevent the ring opening. When care was not taken, the ring-opened product (**3-30)** was obtained almost quantitatively, producing a double bond with a *trans* configuration (Scheme 3.3). After the removal of borane, bromination was carried out under reflux in fairly good yield. In the final step,

Pd(dppf)CH_2Cl_2/DMF system provided the best yield. This reaction seemed to be sensitive to air when tetrakistriphenylphosphine palladium(0) was used.

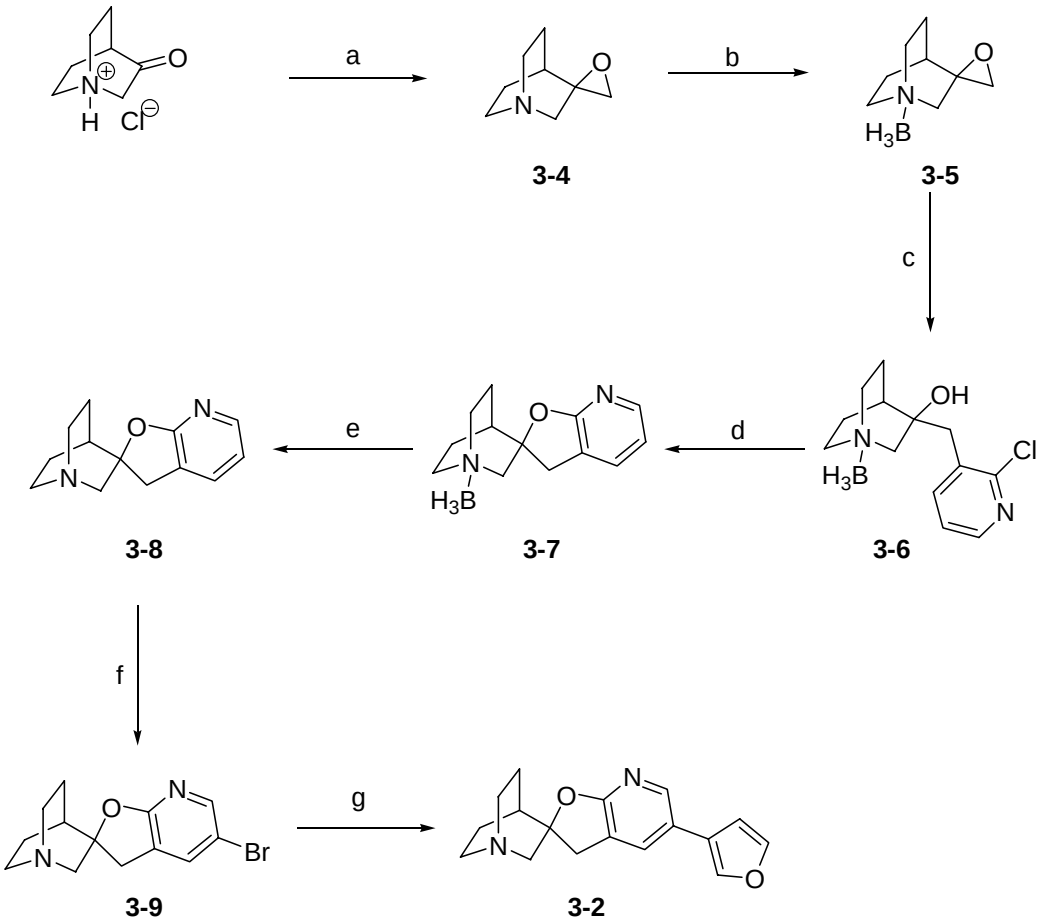

Scheme 3.2 (a) trimethylsulfoxonium iodide, sodium hydride, DMSO; (b) borane, THF; (c) phenyllithium, 2-chloropyridine, THF; (d) sodium hydride, DMF, 95.5%; (e) aqueous hydrobromic acid, acetone, 16 hrs, 99.5%; (f) bromine, sodium acetate, aqueous acetic acid; 88% (g) 3-furanboronic acid, Pd(dppf)$Cl_2 \cdot CH_2Cl_2$, 2 M sodium carbonate, DMF, 75.5%.

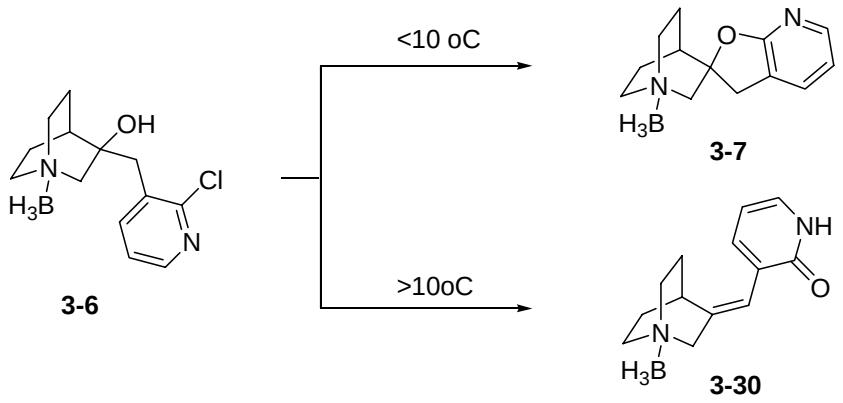

Scheme 3.3 The ring closure to a dihydrofuropyridine ring using sodium hydride/DMF

3.3.2.1 Alternative synthetic approaches via selective lithiation

Initially, we designed another route for the preparation (Scheme 3.4). This strategy was advantageous in that one can avoid the last problematic coupling reaction and reduce several steps in our original plan as shown in Scheme 3.4. Compound **3-10** was synthesized by simple Suzuki-Myaura coupling reaction in water with palladium(II) acetate and potassium carbonate, resulting in high yield with simple purification. In our preliminary attempts, when sodium carbonate as a base was used, the reaction conversion was only 33% by nmr analysis, indicating that choice of base is critical. $PdCl_2$(dppf)$CHCl_2$/diisopropylamine/DMF system gave a three component mixture including 2,5-di(furan-3-yl)pyridine, which was non-regioselective. In the next step, the synthesis of **3-9** failed possibly due to lithiation at α position of the furan ring. Chlorine-induced orhto-lithiation of 2-chloro-5-(furan-3-yl)pyridine seemed to compete with furan α lithiation.

In an attempt to optimize reactivity and protection for lithiation, we tried direct trimethylsilylation via α lithiation on furan ring. As a result, though the α position of

furan seemed more reactive, a mixture of trimethylsilylated products was obtained. In detail, as shown Table 3.3, whereas buthyllithium in ether did not work, LDA in THF showed trimethylsilylated products unquestionably via lithiation. Even though regioselectivity for 2-position of furan ring was observed by slightly excess amount of LDA in THF, excess LDA produced a mixture by both direct *ortho*-metallation and α lithiation on furan ring (Table 3.4).

Based on this observation, we performed bromination for selective lithiation and protection on furan ring since halide-lithium exchange using heteroaryl bromide and iodide usually is likely to be more favorable than α lithiation of heterocyles and halide induced ortho-lithiation of pyridine (Figure 3.4).

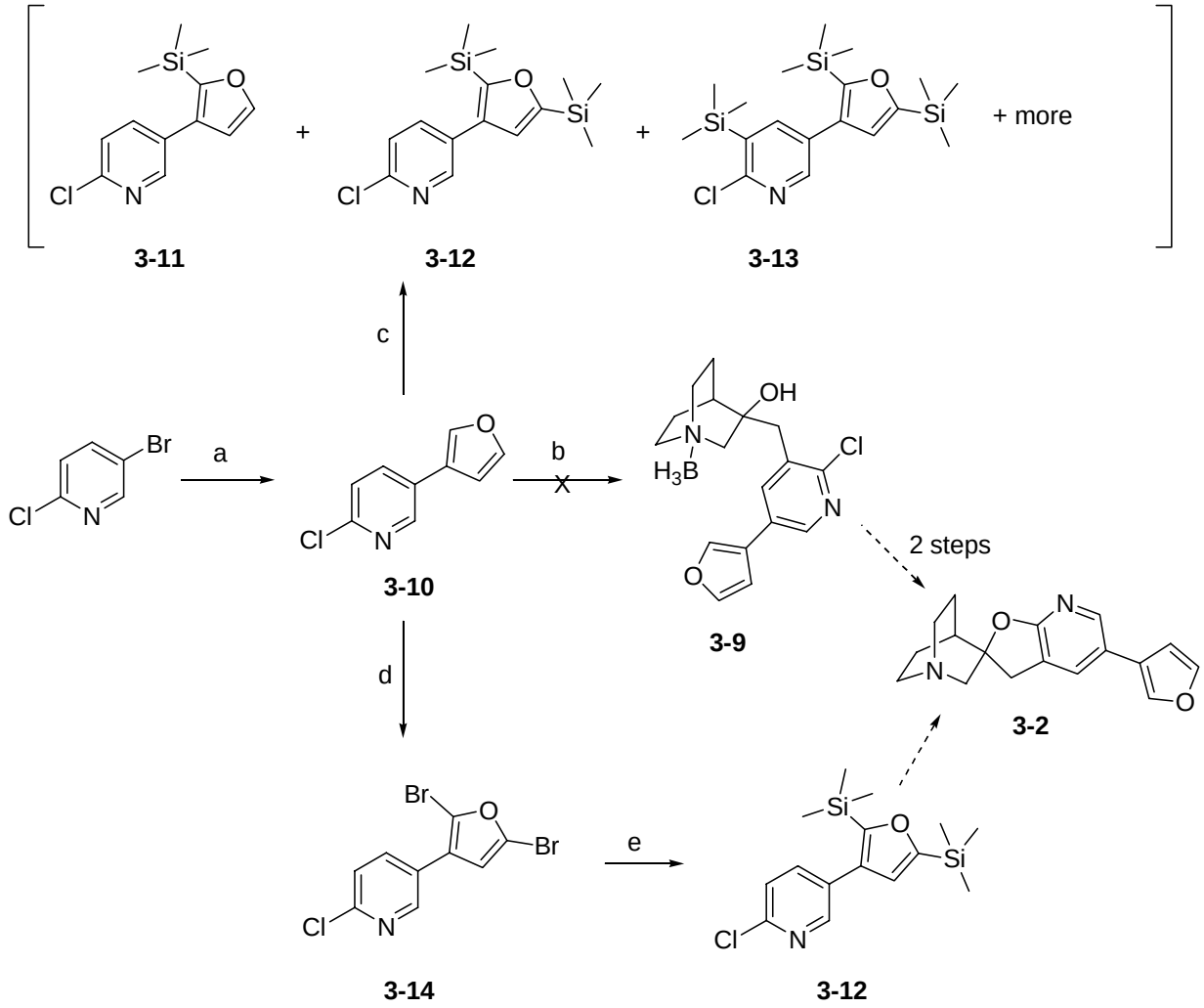

Scheme 3.4 The synthetic route via lithiation of pyridine derivatives: a, palladium acetate, potassium carbonate, TBAB, water, 87%; b, phenyllithium, compound number, THF; c.phenyllithium, THF, then, TMSCl; d, bromine, carbon tetrachloride; e, LDA, TMSCl.

Table 3.4 Conditions for selective lithiation of 2-chloro-5-(furan-3-yl)pyridine

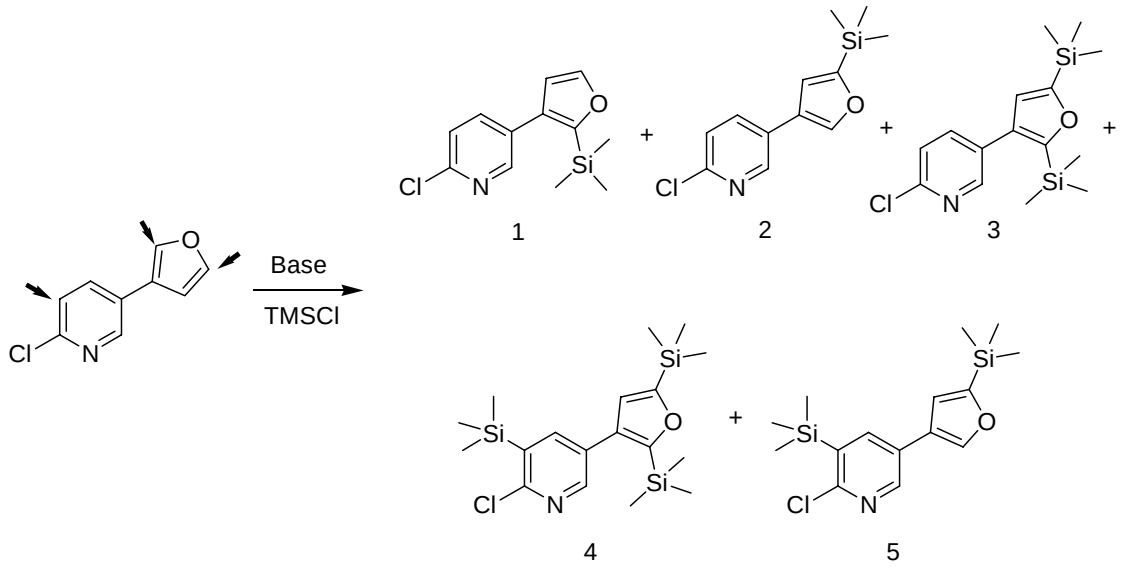

Temperature(oC)	Solvent	Base	Equivalency	Product (%) in NMR				
				1	2	3	4	5
-78 ~ -60	THF	LDA	3.8			20	80	
-78 ~ -60	THF	LDA	1.3*	40	t*			
-78 ~ -60	THF	LDA	2.8		21	20	26	34
-78	Ether	n-BuLi	1	-				
-78	Ether	n-BuLi	2	-				
-78	Ether	n-BuLi	4	-				

* trace
** starting material is 60%

For the F-18 version of this compound, synthesis of F-18 labeled analogues of compound (**3-2**) is under the way (scheme 3.5).

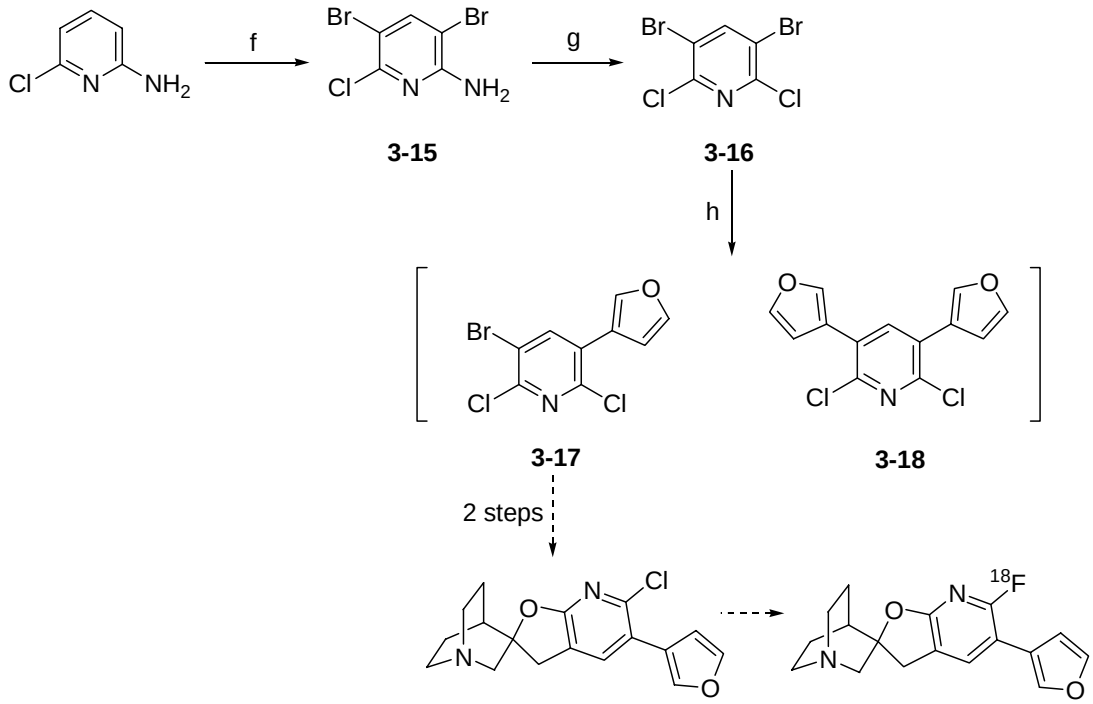

Scheme 3.5 The synthetic pathway of F-18 labeled **3-2.** f, NBS, acetonitrile, 95.3%; g, sodium nitrite, CuCl, hydrochloric acid, 48.5%; h, $Pd(OAc)_2$, potassium carbonate, TBAB, water.

3.3.3 The synthesis of reference compound **3-1**

The reference compound **3-1** was synthesized by a conventional Suzuki coupling reaction conditions. To prepare a boronate counterpart (**3-20**), the 3-bromo-2-methylfuran (**3-19**) was synthesized by regioselective lithiation and subsequent methylation at 2-position of furan ring. Due to its volatility, we used it as a crude form for the next Miyaura reaction (Scheme 3.6).

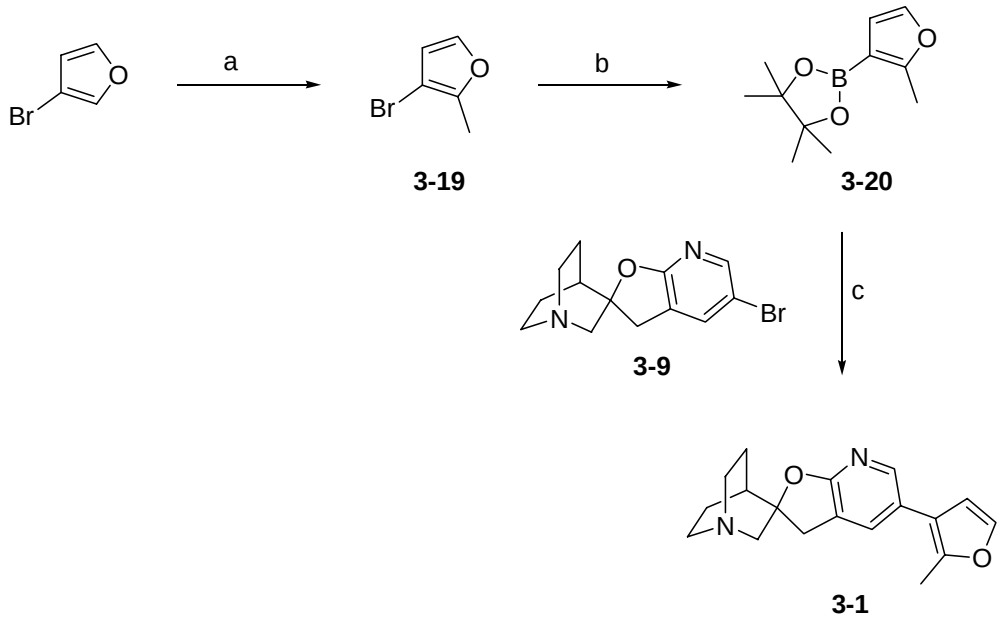

Scheme 3.6 The synthesis of 5'-(2-Methyl-3-furanyl)spiro[1-azabicyclo[2.2.2]octane-3,2'(3'H)-furo[2,3-b]pyridine]. a, LDA, THF, then dimethylsulfate; b, (pinacolato)diboron, potassium acetate, DMSO; c. tetrakis(triphenlyphosphine)palladium(0), sodium carbonate, DMF.

3.4 The synthesis of quinuclidinyl carboxamide derivatives

3.4.1 Initial design of the PET tracer

High selectivity and binding affinity for α7 nAChR are important criteria when deciding on a target compound for PET tracer development. In general, the mAChR, α4β2 nAChR and 5-HT_3R were considered to be the cross binding sites for α7 nAChR ligands in the CNS. Quinuclidine-based ligands with bulky aromatic rings as a hydrophobic pharmacophore showed acceptable selectivity against α4β2 and mAChR. However, an α7 ligand lacking of 5-HT_3R binding is still under development. One of possible candidate published is a quinuclidine compound with thiophenyl pyridine or benzene group as hydrophobic group.[16] The substitution on 3- or 4-position of thiophene ring reduces binding affinity. We reasoned that F-18 labeling on the pyridine ring of **3-21**, is feasible and would not change the binding characteristics of the parent compound

shown in Figure 3.8 (Scheme 3.8). We also planned to use a parallel synthesis for producing this series of compounds using various heteroaryl-heteroarylcarboxylic acids.

3.4.2 The synthesis of precursor and reference compound

Reference compound and precursor were synthesized as shown Scheme 3.7. Compound, **3-22**, was synthesized by Suzuki coupling using tetrakis(triphenylphosphine)palladium(0) in acetonitrile (Scheme 3.7). This method is the efficient and reliable method that we have found after extensive investigation. The final amidation was performed using HOBT, TBTU in DMF to give moderate yield. 2-Amino-6-bromopyridine was oxidized by hydrogen peroxide in acidic condition to give corresponding nitro compound (**3.23**). This reaction has not been optimized.

A)

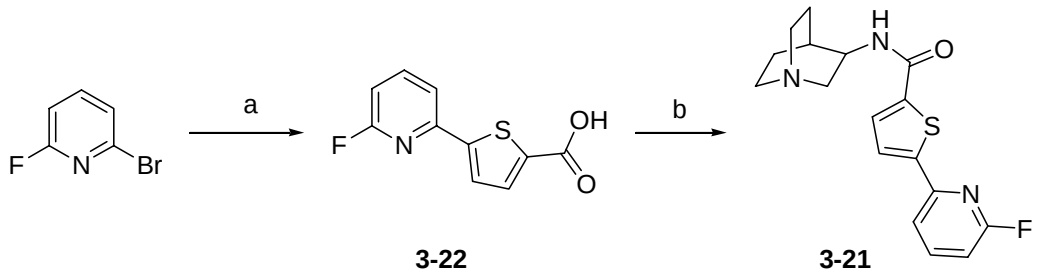

B)

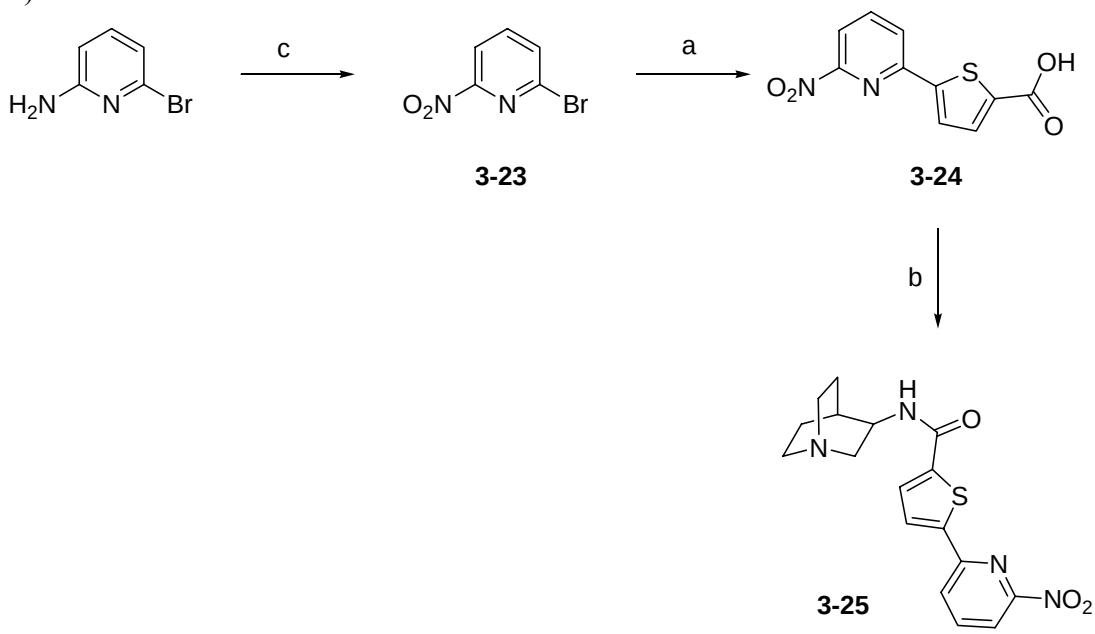

Scheme 3.7 The synthetic route for (A) the reference compound (**3-21)** and (B) precursor (**3-25**). a, 5-(dihydroxyboryl)-2-thiophene carboxylic acid, tetrakis(triphenylphosphine)palladium(0), acetonitrile; b, HOBT, TBTU, hunig's base, DMF; c, hydrogen peroxide, con. sulfuric acid, 21%.

3.4.3 Radiosynthesis

Compound (**3-21**) was labeled with F-18 via aromatic nucleophilic substitution with $^{18}F^-$ in the presence of phase transfer catalyst, K_{222} in DMSO (yield = 10-15%) (Scheme 3.8). When, cesium carbonate was used instead of K_{222}, the yield was lower (7.3%). The initial purification using general reverse-phase HPLC systems such as C_{12} (Phenomenex, Polar-RP), C_{18} (Phenomenex, Gemini, C_{18}) was not successful due to poor separation of the desired product. Normal phase HPLC was also not acceptable because the high basic nitrogen on quinuclidine ring. We tested another type of column (Phenomenex, Prodigy, PH-3), which shows aromatic selectivity by π-π interaction. Even though conditions were not optimized, this system was used for the purification step in the radiosynthesis. Radiochemical purity was >97%.

3-25 **3-21**

Scheme 3.8 The radiosynthesis of quinuclidinyl 2-(6-^{18}F-fluoropyridinyl)tihiophene-5-carboxamide (**3-21**)

3.4.4 PET studies

A PET study in a baboon was performed by quinuclidinyl 2-(6-^{18}F-fluoropyridinyl)thiophene-5-carboxamide (**3-21**). Surprisingly, brain uptake was negligible and bone uptake was high (Figure 3.10). The lipophilicity (1.0, n=2) and plasma protein binding (free fraction = 23%, n=2) were acceptable for BBB penetration,

compared with conventional radiotracers. One of the explanations for the lack of brain uptake is fast metabolism of **3-21** such as defluorination. There is an example in the older PET literature, where the inactive enantiomer of cocaine ((+)-[N-^{11}C-methyl-]cocaine) failed to penetrate the brain due to extremely fast metabolism by plasma butyrylcholinesterase within just 30 sec. Therefore, this labeled product was not detected in the brain or in the blood.[18 19, 20] Unfortunately, the plasma analysis for the baboon study with 3-21 was not successful.

While compound A (Figure 3.8), which is an identical compound except for F-18, demonstrate its efficacy for animal model, the concern of its bioavailability in the brain remains.

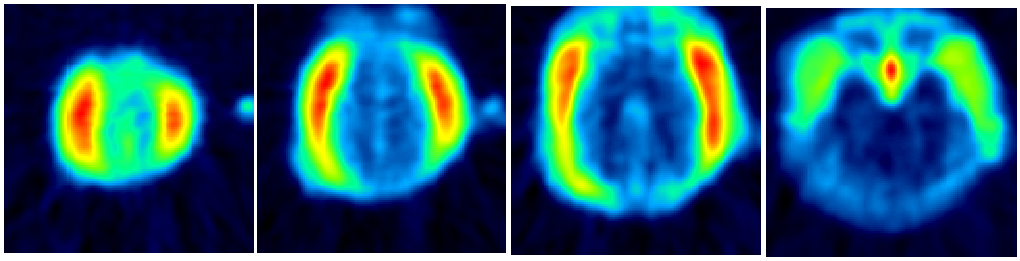

Figure 3.10 Distribution of quinuclidinyl 2-(6-^{18}F-fluoropyridinyl)thiophene-5-carboxamide (**3-21**) in the baboon showing lack of brain uptake.

3.4.5 Strategy for parallel synthesis

The synthesis of the quinuclidine 3-arylthiophenyl carboxamide derivatives can be devised in three different pathways (Scheme 3.9). In the beginning of synthesis, since the 5-dihydroxyborylthiophene carboxylic acid was not commercially available, route a or c were mainly investigated.

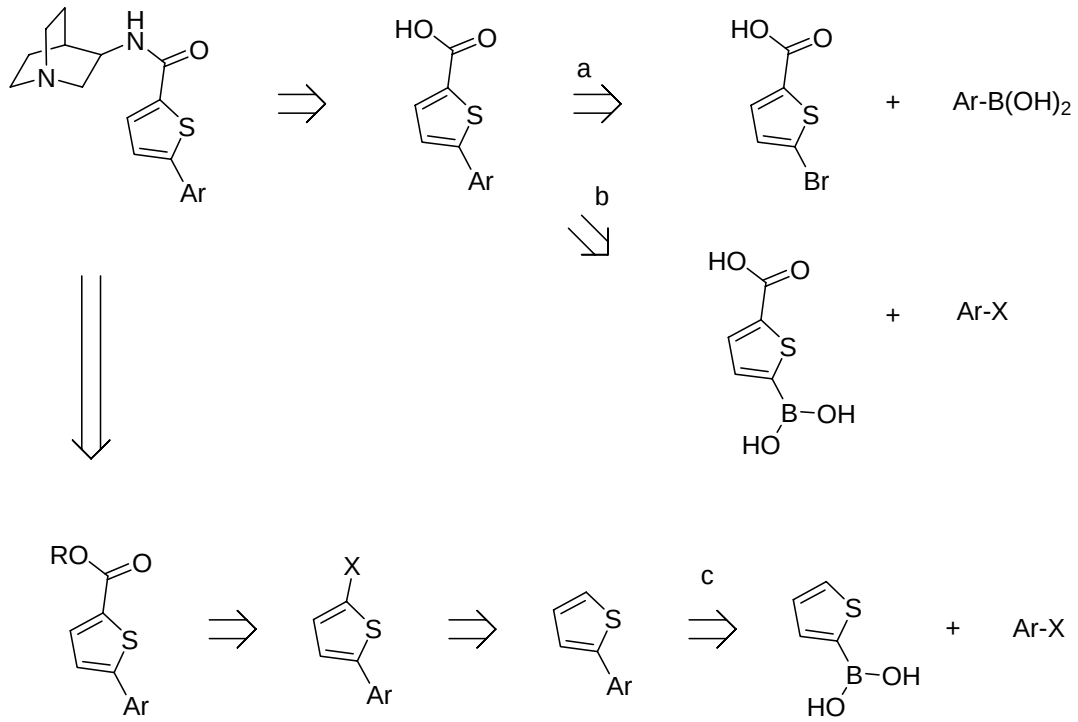

Scheme 3.9 Strategy for parallel synthesis of quinuclindin-3-yl heteroarylthiophenyl carboxamide derivatives.

3.4.6 Suzuki reaction of heteroarylthiophenecarboxylic acids

The metal catalyzed cross-coupling reaction for C-C bond formation has been used as a general synthetic methodology. Compared with other coupling reactions, the Suzuki-Miyaura coupling reaction has the following advantages: 1) relatively non toxic and stable organoboronic acid, 2) functional group tolerance, 3) facile purification. However, it is also problematic for commercial scale reactions due to the use of expensive phosphine ligands and toxic solvents like diglyme or DMF which are not easily removable in the work-up process. Currently, varieties of methodologies have been developed for a wide scope of aryl halides and boronic acids.

One type of Suzuki reaction that has not been fully explored is the heteroaryl-heteroaryl carboxylic acid coupling reaction. Heteroaryl-heteroaryl carboxylic acids have

been reported in the previous literature on a case-by-case basis.[21, 22] Heteroaryl halides with carboxylic acid may be less reactive due to electronic effects and heteroaryl boronic acids are also prone to protodeboration, particularly at the α position of hetero atom.[23] In general, protodeboration is catalyzed by acids and bases in aqueous media or metal bromide even without a palladium ligand.[24] It is also known that aryl boronic acids with electron donating substituents protodeborate at a faster rate. Fast protodeboration is only problematic if the rate of cross-coupling reaction is not fast enough to compete. In addition, homocoupling of arylboronic acid was reported to be faster in the presence of electron donating substituents.[23]

Route A Initial attempts to synthesize heteroaryl thiophene-2-carboxylic acids focused on searching for a reliable methodology. A palladium acetate (II)/TBAB/water system was used as a test condition, due to our previous success using pyridine and furan boronic acid to synthesize 2-chloro-5-(furan-3-yl)pyridine. Even if it showed the protodeboration of 3-furan-boronic acid, the yield was high at room temperature (Scheme 3.10).

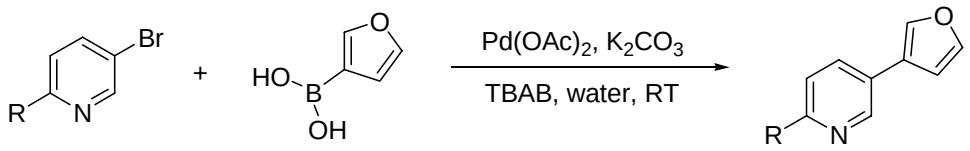

R= F **3-26** 88%

Cl **3-10** 87%

Scheme 3.10 Suzuki coupling of furan-3-boronic acid using 3-bromopyridine derivatives

Unlike activated pyridine, the 2-bromothiophene-5-carboxylic acid with pyridine boronic acids did not give the desired coupling product under the same reaction

conditions, possibly due to the electron rich thiophene and unreactive pyridine. In case of two pyridine boronic acids (Table 3.5, entry 1-7), the major product was 2-thiophene carboxylic acid produced by dehalogenation. In the case of electron rich 3-furanboronic acid, protodeboration was observed. However, the coupling reaction was successful, possibly due to the fast coupling reaction rate (Scheme 3.10).

We also examined the reactivity of non-heterocyclic boronic acids. Interestingly, while 4- or 3-fluorophenylboronic acid gave underwent coupling (Table 3.5, entry 8, 9, 13), phenylboronic acid generated the homocoupling product under similar reaction conditions (Table 3.5, entry 11), which showed electronic effect for homocoupling.

To investigate possible interference by the carboxylic acid on the heteroaryl compound, we synthesized the methyl ester of 2-bromothiophene carboxylic acid and tested the coupling reaction with pyridine-4-boronic acid (Scheme 3.11). The major product was 4,4'-bipyridyl which is the homocoupling product. In case of an activated arene, when an electron deficient aryl halide used, the desired coupling product was obtained in moderate yield. As the next step, we screened catalysts such as tetrakis(triphenylphostphine)palladium(0) and the other conventional catalysts (Table 3.6). However, conversion was poor.

Table 3.5 Palladium catalyzed cross coupling reactions with 5-bromothiophene-2-carboxylic acid and palladium acetate

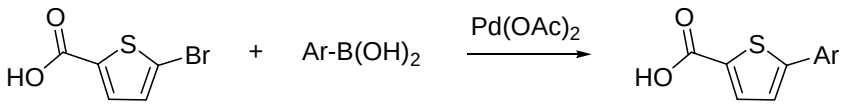

	Arylboronic acid	Base and additives	condition	Yield (%)
1	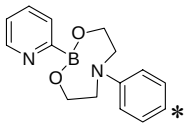 *	K_2CO_3/TBAB**	water, 90°C	-
2		KF/ PEG(2000)	water, RT	-
3		K_2CO_3	methanol, 24hrs, reflux	dehalogenation
4	Pyridine-4-	K_2CO_3/TBAB	Water, reflux	-
5		KF/PEG(2000)	water, RT	-
6		K_2CO_3	methanol, RT	-
7		K_2CO_3	methanol, 24 hrs, reflux	dehalogenation
8	4-fluorobenzene-	KF/PEG(20000)	water, RT	product
9		K_2CO_3	Acetone/water(2/1), reflux, overnight.	product
10	2, 4,5-trifluorophenyl	K_2CO_3/TBAB**	water, 70 °C, overnight	-
11	benzene	K_2CO_3/TBAB**	water, RT	Conve.65.8% homocoupling
12		K_2CO_3	methanol, 24 hrs, reflux	-
13	3-fluorophenyl	K_2CO_3	methanol, 12 hrs, 50 °C	product

* 2-pyridineboronic acid N-phenyldiethanolamine ester
** TBAB, tetrabutylammonium bromide

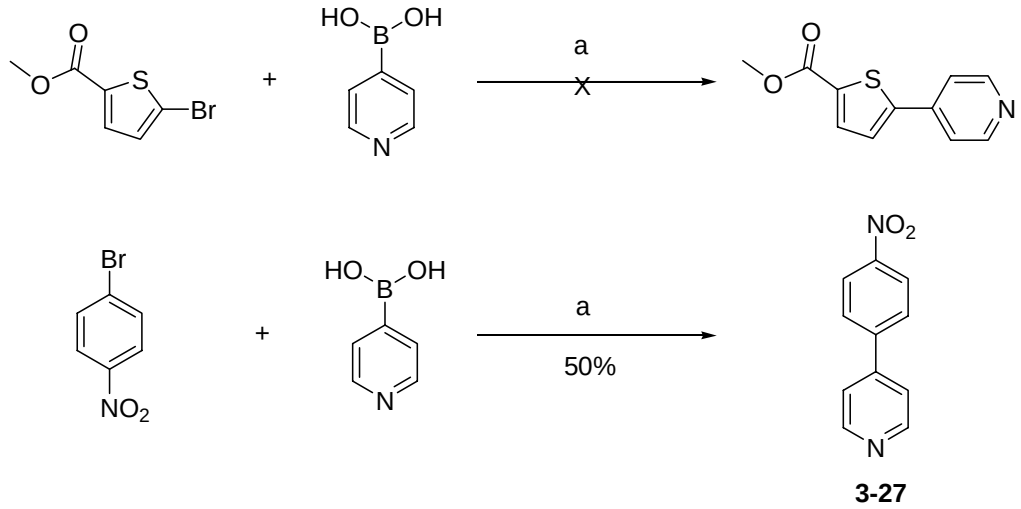

Scheme 3.11 Palladium-catalyzed cross-coupling reaction of pyridine-4-boronic acid. a, palladium(II) acetate, potassium carbonate, methanol, reflux, overnight.

Table 3.6 Palladium catalyzed cross coupling reaction with 5-bromothiophene-2-carboxylic acid and various palladium catalysts and bases

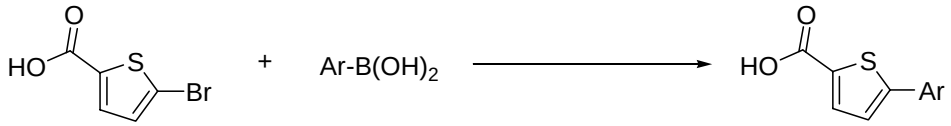

Arylboronic acid	Base and additives	condition	Yield (%)
Pyridine-4-	Bisphenylphosphine palladium(II) dichloride	Cesium carbonate/1,4-dioxane, 90oC,12hrs	-
	$(PPh_3)_4Pd(0)$	Potassium t-butoxide/diglyme, 90 ^oC, 3hrs	dehalogenation
Furan-3-	$Pd(II)Cl_2(dppf)(CH_2Cl_2)$	Potassium carbonate/TABA/water, RT	10.8% by nmr
benzene	$Pd(II)Cl_2(dppf)(CH_2Cl_2)$	Hunig's base/1-propanol, 12 hrs, RT	

<u>*Routes B and C*</u> Since 5-(dihydroxyboryl)thiophene-2-carboxylic acid recently became commercially available, path B in the scheme 3.8 was tested using different pyridines. Though protodeboration was observed, the reaction was successful with

palladium acetate/potassium carbonate/TBAB/water system except for the 2 position of pyridine (Table 3.7). We failed to get desired coupling product using a strong phosphine ligand, SPhos with palladium acetate.

Table 3.7 Palladium catalyzed cross coupling reaction with 5-(dihydroxyboryl)thiophene-2- carboxylic acid and 2-bromopyridine derivatives

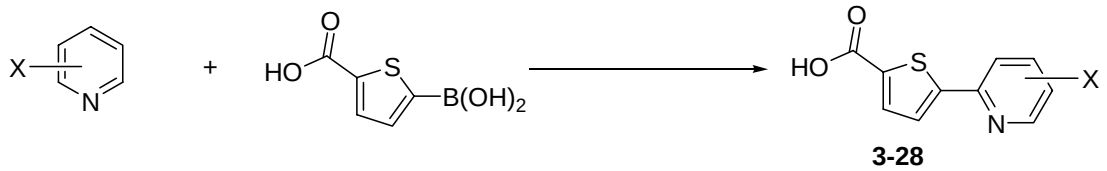

	Pyridine	Catalyst/ligand	condition	Conversion (%)
1	2-bromo	$Pd(OAc)_2$/SPhos*	K_2CO_3/acetnitrile, water, 4hrs, 100 ^oC	-
2	3-bromo	$Pd(OAc)_2$	K_2CO_3/TBAB/water, RT later 90^oC	-
3	4-bromo	$Pd(OAc)_2$	K_2CO_3/TBAB/water, RT later 90^oC	product
		$Pd(OAc)_2$/SPhos*	K_2CO_3/acetnitrile, water, RT, 24hrs	deboration
4	2-bromo-6-fluoro	$Pd(OAc)_2$/SPhos*	KF/acetnitrile, water, RT, 24hrs	-
		$Pd(PPh_3)_4$	Na_2CO_3/acetonitrile, water, 90^oC, 12 hrs	65%
5	2-bromo-6-nitro	$Pd(PPh_3)_4$	Na_2CO_3/acetonitrile, water, 90^oC, 12 hrs	40%

*2-(2',6'-dimethoxybiphenyl)dicyclohexylphosphine (SPhos)

The reactivity of 2-bromopyridine was further investigated with other aryl boronic acids which have no carboxylic acid moiety (Table 3.8). While 5-(dihydroxyboryl)thiophene-2- carboxylic acid did not react at all, the electron rich thiophene-2-boronic acid showed fairly high yields under the same conditions. Carboxylic acids under basic conditions may reduce the reactivity (table 3.7). These products can be used for Route C.

Table 3.8 Palladium catalyzed cross coupling reaction with 2-bromopyridine and non-carboxyl aryl boronic acid

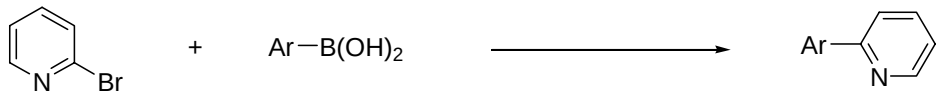

	Ar	Catalyst/ligand	condition	Conversion (%)
1	Furan-2-	$(PPh_3)_4Pd(0)$	K(t-BuO)/diglyme, 90oC,12hrs	product
2	4-fluorobenzene-	$Pd(OAc)_2$	K_3PO_4/THF	-
3	2-thiophene-	$Pd(bpy)Cl_2$	K_2CO_3/acetnitrile, water, relux	homocoupling
4	2-thiophene	$Pd(OAc)_2$/SPhos*	K_2CO_3/acetnitrile, water, reflux, 4 hrs	**3-29**, 93%

For route C, we also investigated 2-bromo-6-fluoropyridine which is less basic and more hydrophobic than 2-bromopydrine. Palladium catalyst chelated pyridine-based ligand in methanol or acetonitrile showed no homocoupling product of phenylboronic acid. Therefore, this system may be useful for general application for nitrogen containing heteroaryl halide and arylboronic acids without carboxylic acids. Further investigations for N-H containing azaheteroaryl halides will be valuable.

Table 3.9 Palladium catalyzed cross coupling reaction with 2-bromo-6-fluoropyridine and non-carboxyl aryl boronic acid

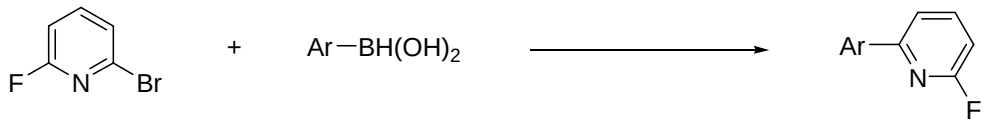

	Ar	Catalyst/ligand	condition	product
1	3,5-difluorobenzene	$Pd(OAc)_2$	K_3PO_4/TBAB/ H_2O, RT	product
2	benzene	$Pd(bpy)Cl_2$	K_3PO_4/MeOH, 24hrs, 90 ^oC	product*
4	benzene	$Pd(bpy)Cl_2$	K_3PO_4/acetonitrile, 24hrs, 90 oC	product
5	benzene	$Pd(bpy)Cl_2$	KF/DMF/H_2O/K_3PO_4, 90 oC	product**
6	2-thiophene	$Pd(OAc)_2$/SPhos*	K_3PO_4/acetnitrile/ H_2O, RT, 24 hrs	product

* 2-methoxy-6-phenylpyrididine was also observed.
** Only desired product was observed by GC-MS

In summary, though there have recently been reported several methods for heteroaryl-heteroaryl cross coupling reaction[25-27], it is often substrate specific or needs sophisticated ligands and catalysts. The development of universal synthetic methodology for heteroaryl-heteroaryl compound remains elusive. In case of heteroaryl coupling partner with carboxylic acid, the reports for successful cases are even more rare.[28] Our study of reactivity in the various Pd catalysts and reaction media would be valuable basis for the development of synthetic methology for heteroaryl-heteroaryl cross coupling reaction.

3.6 Homology modeling of α7 nAChR

3.6.1 background

The human α7 nAChR is an ionophore assembled by five identical subunits, one of which consists of 502 amino acids. To date, there is no the crystal structure of mammalian α7 nAChR. However, the protein structures of several acetylcholine binding proteins of the other species have been reported to elucidate that of the mammalian α7 nAChR (Figure 3.11). In particular, the binding mode of the ligand binding domain is important for discovery of a drug lead and the study of functional activity.

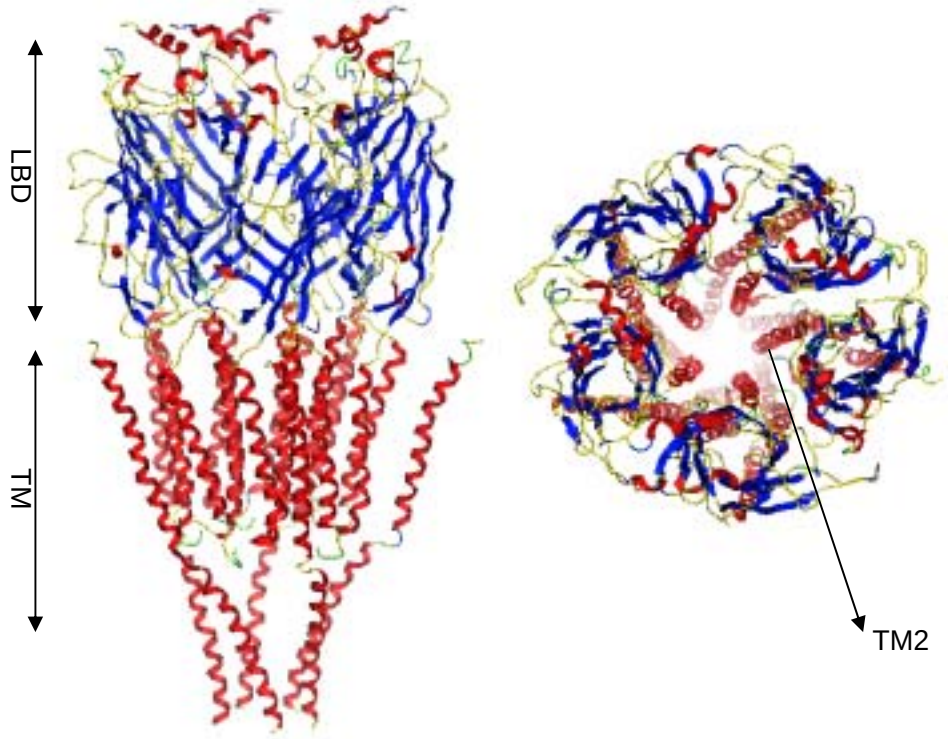

Figure 3.11 The nicotinic acetylcholine receptor of *Torpedo marmorata* (PDB ID: 2BG9) generated by MOE (Moleculer Operation Environment).

<u>*Structure*</u> Based on the crystal structure of AChBP of *Torpedo marmorata* (PDB ID: 2BG9), the ion channel consists of five subunits (Figure 11). Each subunit has a ligand binding domain (LBD) in the extracellular space from N-terminal and five transmembrane domains to the C-terminal. The aqueous lumen in the ion channel pore is formed by the lining of the second transmembrane domains (TM2) from each subunits. Methyllycaconitine (MLA) bound AChBP crystal structure (PDB ID: 2BYR) showed that MLA binds to the pocket between adjacent ligand binding domains of each subunit. These binding sites are similar to that of epibatidine bound AChBP (PDB ID: 2BYQ) and 2-(4-(hydroxymethyl)piperazin-1-yl)ethanesulfonic acid(HEPES) (PDB ID: 2BR7). Interestingly, while the orientation of the hydrophobic pharmacophore of epibatidine was deep inside of pocket, the benzoylester group of MLA showed opposite orientation, which might explain why the 3-iodo substitution of MLA did not affect binding affinity (Chapter 1.1).

3.6.2 Homology modeling

Hanson et al. reported several AChBP crystal structures which are bound with agonists and antagonists. Most of all, since most of the quinuclidine-based ligands showed agonistic activity, we chose the epibatidine bound AChBP to build up our homology model for mouse α7 nAChR. The sequence alignment was repeatedly performed by several different algorithms which are packaged in MOE (homology= 28%), and showed no significant difference between species and between algorithms.

After sequence alignment processing by MOE, we observed the conserved residues of binding pocket.

Based on its sequence alignment on epibatidine bound AChBP, we generated the mouse homology model. After energy minimization, similar interaction for the binding was observed with epibatidine (Table 3.10). In the binding pocket, the vicinal disulfide bridge (C190(C212)-C191(C213)) was well-matched between a generated mouse model structure and AChBP. The other critical residues in the binding site are well conserved as shown Table 3.10.

Table 3.10 Comparison of ligand interactions between sea hare AChBP (PDB ID: 2BYQ) and homology model of mouse α7 nicotinic acetylcholine receptor

Binding Pocket interaction	sea hareAChBP (mouse AChBP)
Hydrophilic interactions	W147 (W171), Y93(Y115), Y55(W77)
Hydrophobic interactions	Y188 (Y210), Y195(Y217),V108(131L) I118(L141),V148(S172)
Close contacts*	I106(N129), A107(V130), M116(Q139), C191(C213), C190(C212)
π-cation interactions	W147 (W171)

* within 2.5-3.9 nm

Five identical subunits of the sea hare AChBP were aligned in the three dimensional coordination, showing that the loop regions are distinguished from the structurally rigid secondary structures. During homology modeling, we found the naturally uncommon structure as *cis* conformation of amide bond. However, all *cis* amide bonds were not close to the epibatidine binding pocket. We assumed that these regions were not significant contributors to the ligand binding properties.

As figure 3.12 shows, W147 of the epibatidine-bound AChBP contacts closely with with the hydrophilic carbonyl oxygen and shows π-cation interaction with the indole moiety.

(A)

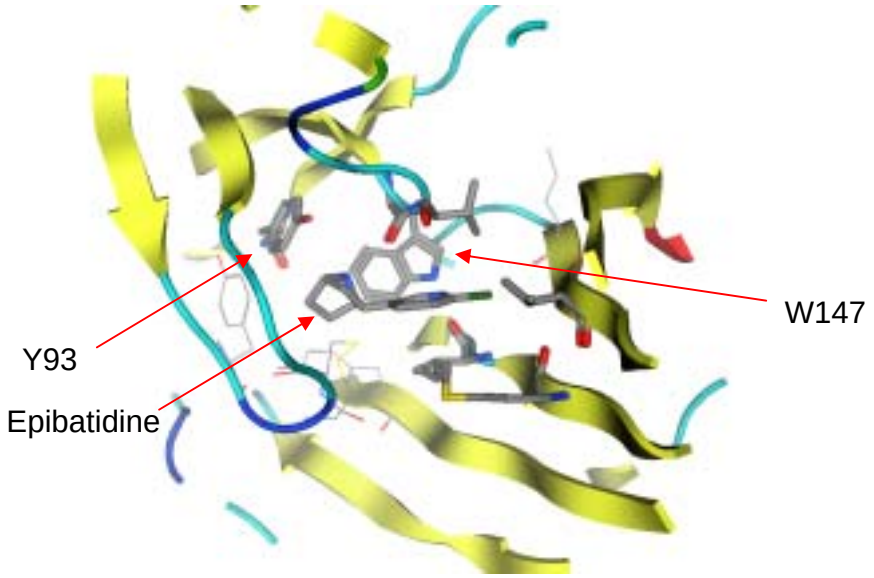

(B)

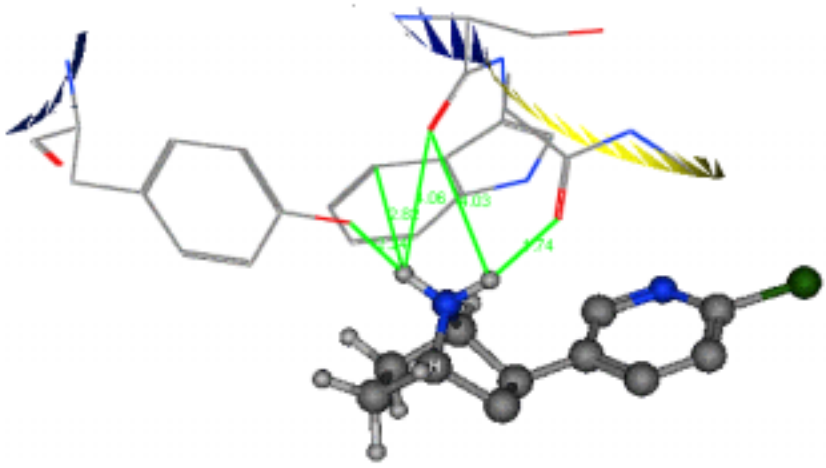

Figure 3.12 The binding pocket of sea hare AChBP with epibatidine (PDB ID: 2BYQ)

Our homology model also demonstrates the similar interaction pattern (Figure 3.13). Both Y93 and W171 was coordinated to interact cationic center of epibatidine. The chloropyridine group of epibatidine resides the hydrophobic binding regions, indicating that the hydrophobic pharmacophore of qunuclidine derivatives is critical for α7 nAChR binding.

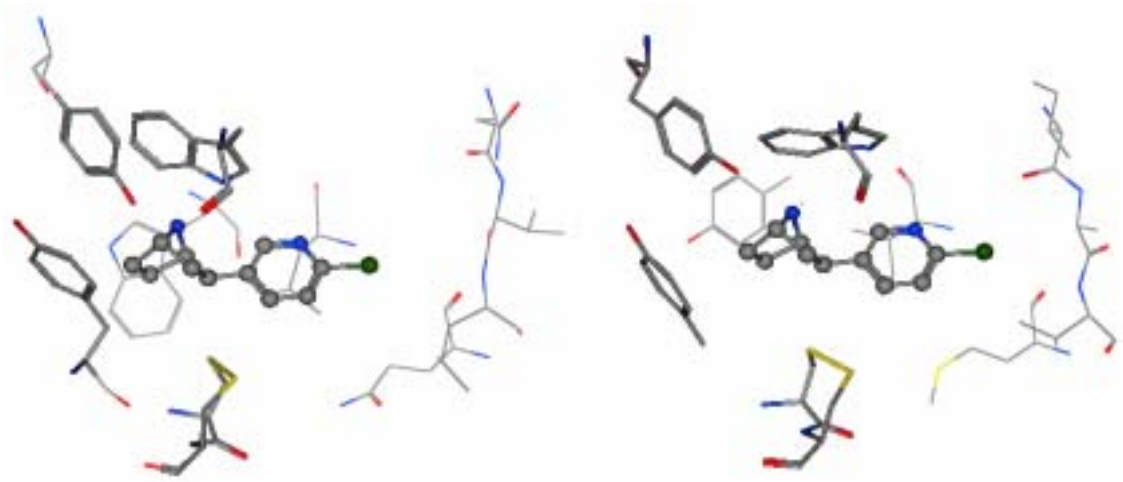

(A) (B)

Figure 3.13.Comparison of epibatidine binding pockets between sea hare AChBP (A, PDB ID: 2BYQ) and the homology model of mouse nAChR (B).

3.6.3 Docking

The docking model with the compound, **3-2**, on the homology model was tested by MOE. The initial rigid docking simulation showed that 3-2 resided in the binding pocket in only 1 out of 100 hits. This procedure is still underway.

3.7 Quantitative Structure-Activity Relationship (QSAR) study

As part of our research for the design of the α7 nAChR PET tracer, the correlation between ligand structure and binding properties was investigated. In particular, our

major purpose is the quantitative calculation for the degree of binding affinity change produced by modification of hydrophobic group.

Owing to published ligands and their activities[9, 11], we collected only quinuclidine-based ligands with diverse modification of hydrophobic group as well as hydrogen bond acceptors. All compounds have a hydrogen bonding acceptor at 3 position of quinuclidine ring. QSAR simplified by these structural similarities would be quantifiable for the difference of hydrophobic group, which is expected to be modified by PET chemistry in order to introduce the label. Furthermore, based on QSAR database of diverse hydrophobic groups, our QSAR was expected to be sensitive enough to describe a change in molecular binding properties by the hydrophobic group.

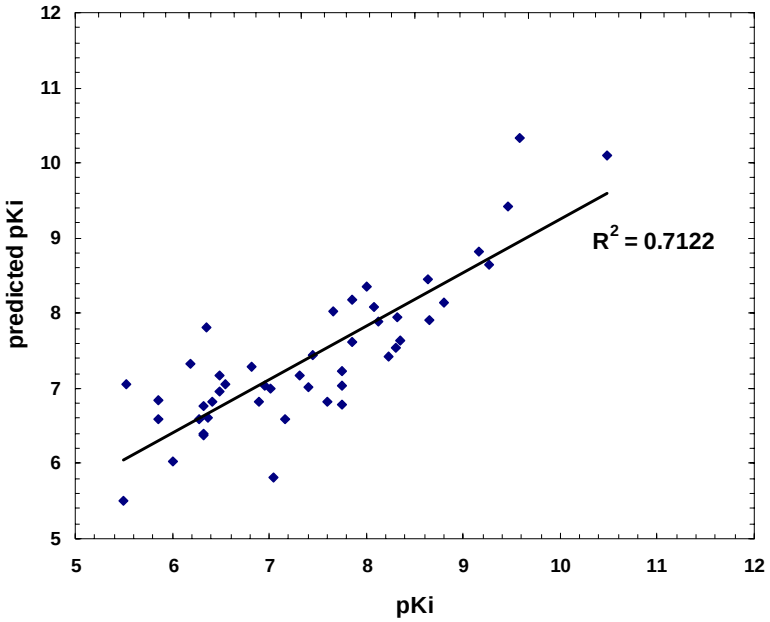

Figure 3.14 Correlation plot of QSAR model and training set.

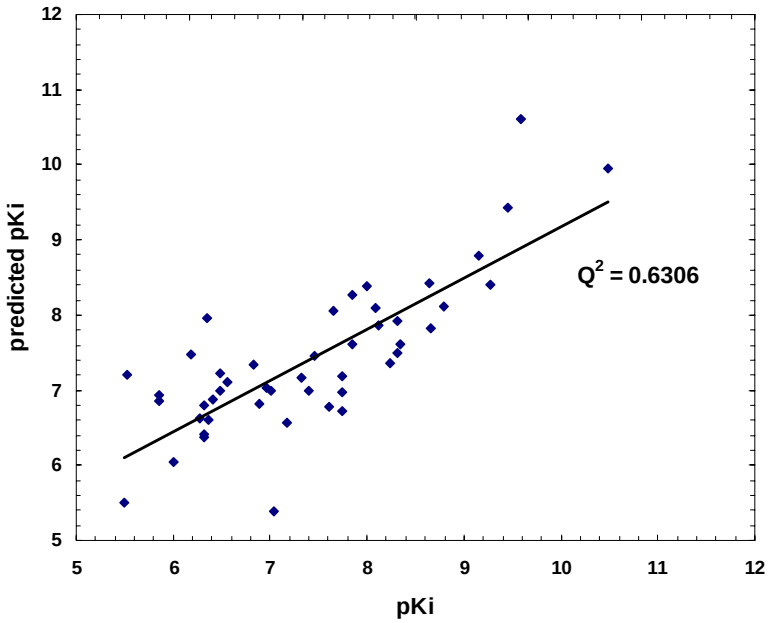

Figure 3.15 Cross-validation plot of QSAR model.

Through the several steps of refinement for descriptors packaged on MOE, we derived four distinctive descriptor (Figure 3.15, R^2= 0.71), which is generally acceptable as follows.

$$pKi = 5.68 + (0.06*Zagreb) + (0.02*ASA) – (3.40*PC+) – (0.81*\log P(o/w))$$

Where Zagreb is Zagreb index (the sum of d_i^2 over all heavy atoms i), ASA is water accessible surface area, PC+ is partial charge, log P(o/w) is log of the octanol/water partition coefficient. Relative importance of each descriptor are 0.79 for Zagreb, 0.89 for ASA, 1 for PC+ and 0.63 for log P(o/w), respectively. Because we used database with structural similarity of quinuclidine parts in our database, the high relative importance of partial charge was due to hydrophobic group and hydrogen acceptor.

As another validation tool, our QSAR model was evaluated by test compounds which were reported in the previous literature. Except for two outliers, QSAR showed high correlation between calculated value and observed value (Figure 3.16).

A)

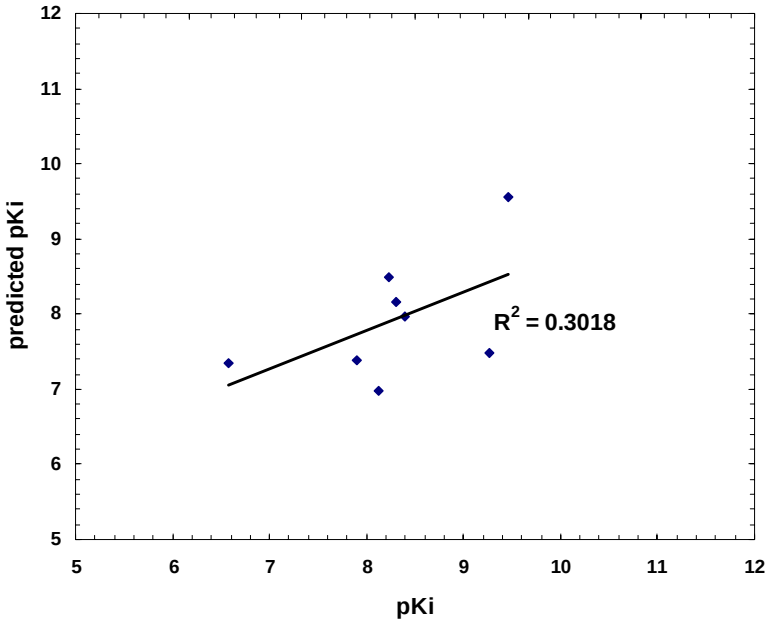

B)

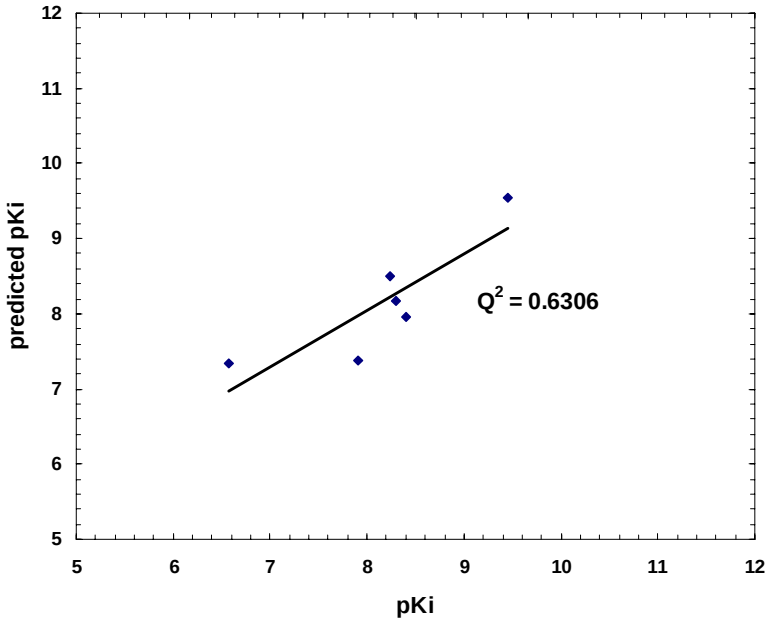

Figure 3.16 The validation of QSAR model by a test set. A, all test compounds; B, 6 test compounds except for 2 outliers of test compounds.

3.7.1 PET tracer candidates

Based on our QSAR model, we generate the putative PET ligands using the virtual library generation tool. The refinement of the QSAR model is still underway, where our own real dataset of biological assays will feed back into the QSAR model.

Table 3.11 The PET ligand candidates calculated by QSAR model.

Ligands	Calculated pKi
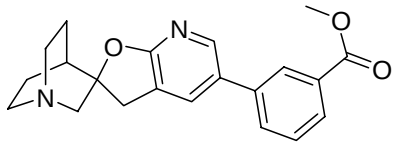	14.8
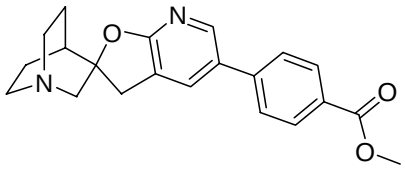	14.5
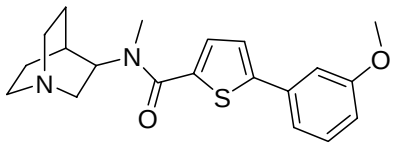	13.2

3.8 Experimental

General

Both ^{1}H-NMR and ^{13}C-NMR spectra were taken using a 400 MHz Bruker NMR. GC-MS analysis was performed using a GC-6890N and 5973N Mass detector (Agilent). LC-MS analysis was performed using LCQ Advantage Mass Spectrometer System (Thermo Finningan).

Spiro[1-azabicyclo[2.2.2]octane-3,2'-oxirane] **(3-4)**[17]

3-quinuclidinone hydrogen chloride (8 g, 49.5 mmol) and trimethylsulfoxonium iodide (14.2 g, 64.5 mmol) were dissolved in anhydrous DMSO (135 ml). Sodium hydride (95 %, 3.2 g , 126 mmol) was slowly added for 1 hour and hydrogen gas evolved. After stirring overnight, cold water (800 ml) was added cautiously. The reaction mixture was extracted with chloroform (320 ml X 5). The combined chloroform layer was washed with water (400 ml X 2) and brine (200 ml), and then dried over anhydrous magnesium sulfate. Filtration and concentration under reduced pressure gives the desired crude oil product. The crude product was used in the next step without further purification. ^{1}H NMR ($CDCl_3$, δ) 3.1 (d, 1 H) 2.9 (d, 1 H), 3.1-2.8 (m, 4 H), 2.7 (dd, 2 H), 2.0 (m, 1 H), 1.8 (m, 2 H), 1.6 (m, 1 H), 1.4 (bt, 1 H). ^{13}C NMR ($CDCl_3$) δ 23.03, 25.28, 29.58, 47.12, 47.39, 53.85, 55.90, 60.11. MS-EI: *m/z* calculated 139.10; found 139$(M)^+$.

Trihydro(spiro[1-azabicyclo[2.2.2]octane-3,2'-oxirane]-N1)boron **(3-5)**[17]

Anhydrous THF (120 ml) was added into a crude compound **3-4**. Into this solution was added borane (1 M in THF, 42 ml, 42 mmol) dropwise at 0 ^{o}C for 30 min. The mixture was stirred stirred for 1 hour and THF was evaporated under reduced pressure. The white solid crude product (7.07 g, 93.3 % from 3-quinuclidinone

dihydrochloride) was used without any further purification. ^{1}H NMR ($CDCl_3$, δ) 3.3 (dd, 1 H), 3.2-2.9 (m, 5 H), 2.8 (dd, 2 H), 2.1 (m, 1 H), 1.9 (m, 2H), 1.8 (m, 1H), 1.6 (m, 1 H), 2.0-1.0 (b, 3H).

[3-[(2-Chloro-3-pyridinyl)methyl]-1-azabicyclo[2.2.2]octan-3-ol-κN1]trihydroboron **(3-6)**[17]

To a solution of phenyllithium (1.8 M in cyclohexane-ether, 51.1 ml, 90.2 mmol) in anhydrous THF (105 ml) was added 2-chloropyridine dropwise at. After the reaction mixture was warmed to 40 ^{o}C and stirred for 2 hours, it was cooled back to –78 ^{o}C. After **3-5** (7.07 g, 46.2 mmol) in anhydrous THF (22.5 ml) was added for 30 min., the reaction mixture was warmed to –40 ^{o}C and kept stirring for 3 hours. The reaction mixture was quenched by saturated sodium bicarbonate solution (45 ml), and then temperature was naturally elevated to 20 ^{o}C. The reaction mixture diluted with water (45 mL) and extracted with ethyl acetate (3 X 30 ml). The combined organic fractions were dried with magnesium sulfate. After evaporation, the residual crude oil was purified by column chromatography (silica, ethyl acetate: hexane = 1:1) to give a light pink solid **3** (5.68 g, 43.1% from 3-quinuclidinone dihydrochloride). ^{1}H NMR ($CDCl_3$, δ) 8.3 (dd, 1 H), 7.7 (dd, 1 H), 7.2 (dd, 1 H), 3.1 (s, 2H), 3.1-2.9 (m, 6 H), 2.2-2.0 (m, 2 H), 2.0-1.8 (m, 2 H), 1.7 (bs, 1 H), 2.0-1.0 (b, 3H). ^{13}C NMR ($CDCl_3$, δ) 152.0, 148.3, 141.7, 130.8, 122.7, 72.1, 67.1, 53.0, 52.8, 40.8, 30.9, 22.9, 21.1.

Trihydro(spiro[1-azabicyclo[2.2.2]octane-3,2'(3'H)-furo[2,3-b]pyridine]-κN1)boron **(3-7)**[17]

To a solution of **3-6** (5.23 g, 19.7 mmol) in DMF (140 ml) was added NaH (95 %, 1.26 g, 49.9 mmol) at 0 – 9 ^{o}C for 3 hrs. Reaction progress was observed by ^{1}H-NMR.

After adding saturated ammonium chloride (17.64 ml) and water (176 ml), the reaction mixture was extracted with ethyl acetate (40 ml X 5). The combined organic layer was dried over magnesium sulfate, filtered and evaporated under reduced pressure to give an oil containing residual DMF. The residual DMF was removed under high vacuum to give an orange solid. This solid was purified by short column chromatography (silica, chloroform:ethyl acetate = 96 : 4) to give orange solid (4.32 g, 95.5 %). ^{1}H NMR ($CDCl_3$, δ) 8.0 (d, 1 H), 7.5 (dd, 1 H), 6.8 (dd, 1 H), 3.5 (dd, 1 H), 3.4 (d, 1 H), 3.2 (m, 1 H), 3.1-2.9 (m, 5 H), 2.4 (m, 1 H), 2.2 (b, 1 H), 1.9 (m, 2 H), 1.7 (m, 1 H), 2.0-1.0 (b, 3H). ^{13}C NMR ($CDCl_3$, δ) 166.6, 147.5, 134.1, 118.2, 117.4, 84.8, 67.8, 53.2, 52.7, 39.3, 31.3, 21.8, 21.0

[(E)-3-(quinuclidin-8-ylidenemethyl)pyridin-2(1H)-one-κN1]trihydrobrane (**3-24**)

To a solution of **3-6** (412 mg, 1.55 mmol) in anhydrous DMF (11 ml) was added sodium hydride (95%, 110 mg, 4.35 mmol) at 0 ^{o}C for 1 hr. After 30 min stirring, temperature was elevated to 17 ^{o}C for 2 hrs. After reaction vessel was cooled down to 0 ^{o}C, the water added slowly and resultant solid was filtered, washed, and dried under reduced pressure to give **3-8** (256 mg, 72%). ^{1}H NMR ($CDCl_3$, δ) 7.36 (dd, 1 H), 7.33 (dd, 1 H), 6.3 (dd, 1 H), 6.27 (s, 1 H), 3.8 (s, 2 H), 3.1 (m, 4 H), 3.0 (m, 1 H), 1.9 (m, 4 H), 2.1-1.0 (b, 3 H). ^{13}C NMR ($CDCl_3$, δ) 164.3, 140.2, 139.3, 133.5, 127.7, 117.0, 107.0, 61.9, 54.0, 25.91, 25.85.

Spiro[1-azabicyclo[2.2.2]octane-3,2'(3'H)-furo[2,3-b]pyridine] **(3-8)**[17]

To a solution of **3-7** (3.75g, 16.3 mmol) in acetone (66 ml) was added hydrobromic acid (24%, 15.4 ml) at 0 ^{o}C. After stirring for16 hr, acetone was evaporated

under reduced pressure and the pH of the reaction mixture was adjusted by sodium hydroxide solution (50%) to pH = 11. The reaction mixture was diluted with saturated sodium bicarbonate solution (15.4 ml) and extracted with chloroform (30 ml X 4). The combined organic layer was dried by magnesium sulfate, filtered and evaporated to give a white solid (3.51 g, 99.5 %). ^{1}H NMR was measured with a hydrochloride salt form of **3-8** by treating with excess hydrochloric acid. (DMSO-d_6 ,δ) 2.2 (m, 2 H), 3.1 (t, 2 H), 3.8 (s, 3 H), 3.9 (t, 2 H), 3.9 (s, 3 H), 6.7 (d, 1 H), 6.8 (dd, 1 H), 7.6 (s, 1 H), 3.4 (d, 1 H), 3.5 (dd, 1 H), 6.8(dd, 1 H), 7.5 (dd, 1 H), 8.0 (d, 1 H). ^{13}C NMR was measured with a free base form of **3-8.** ^{13}C NMR ($CDCl_3$, δ) 167.3, 147.1, 133.8, 119.5, 116.7, 86.8, 64.0, 47.0, 46.7, 39.4, 31.8, 23.0, 21.7.

5'-Bromospiro[1-azabicyclo[2.2.2]octane-3,2'(3'H)-furo[2,3-b]pyridine] (**3-9**)[17]

3-8 (1 g, 4.62 mmol) was dissolved in 50 % aqueous acetic acid (40 ml) and sodium acetate (4.10 g, 50 mmol). The reaction mixture was warmed to 60 ^{o}C and bromine (1 ml, 19.4 mmol) was added slowly for 15 min. The mixture was refluxed for 1 hour and cooled down to room temperature. Saturated sodium carbonate solution (17 g) was added and pH was adjusted to 11.8 by aqueous sodium hydroxide solution (50%). The reaction mixture was extracted by chloroform (100 ml X 4). The combined organic layer was dried by magnesium sulfate, filtrated, and evaporated to give white solid (1.2 g, 88 %). ^{1}H NMR ($CDCl_3$) δ 8.0 (bt, 1 H), 7.46 (bt, 1 H), 3.3 (m, 2 H), 3.0-2.8 (m, 6 H), 2.1 (m, 1 H), 1.94 (m, 1 H), 1.6 (m, 2 H) 1.4 (m, 1 H). ^{13}C NMR ($CDCl_3$, δ) 166.0, 147.4, 136.3, 121.9, 11.3, 88.1, 63.5, 46.7, 46.4, 39.1, 31.6, 22.7, 21.4.

5'-(3-Furanyl)spiro[1-azabicyclo[2.2.2]octane-3,2'(3'H)-furo[2,3-b]pyridine] (**3-2**)

To a solution of **3-9** (70 mg, 0.23 mmol) and tetrakistriphenylphosphine palladium(0) (30 mg, 0.025 mmol) in DMF (2 ml) was added sodium carbonate (370 mg, 3.5 mmol) and furan-3-boronic acid (110 mg, 1 mmol). After stirring at 60 ^{o}C for 36 hrs, a reaction mixture was filtered. Ethyl acetate and sodium hydroxide solution (1%) were added into the mixture. The organic layer was washed with distilled water and dried with anhydrous magnesium sulfate. After column chromatography (silica, diisopropylamine : methanol = 1.5 : 98.5) to give a white solid (**3-2**, 50.6 mg, 75.5%). ^{1}H NMR ($CDCl_3$, δ) 8.1 (bt, 1 H), 7.6 (bt, 1 H), 7.52 (bt, 1 H), 7.48 (bt, 1 H), 6.6 (dd, 1 H), 3.4 (m, 2H), 3.1-2.8 (m, 6 H), 2.2 (m, 1 H), 2.0 (m, 1), 1.68 (m, 2 H), 1.5 (m, 1 H). ^{13}C NMR ($CDCl_3$, δ) 166.6, 144.4, 144.0, 138.0, 131.7, 123.7, 122.0, 119.8, 100.1, 87.4, 63.9, 46.9, 46.6, 39.4, 31.8, 23.0, 21.7.

3-Bromo-2-methylfuran (**3-19**)

n-Butyllithium (1.6 M in hexane, 3.75 ml, 6 mmol) was added to a solution of diisopropylamine (0.95 ml, 6.57 mmol) in tetrahydrofuran (6.5 ml) at -78 ^{o}C for 10 min. The reaction mixture was warmed to 0 ^{o}C and cooled back to -78 ^{o}C. 3-Bromofuran (606.8 mg, 4.1 mmol) was added slowly and stirred for 1hr. After dimethylsulfate (1.13 ml, 12 mmol) was added, the reaction mixture was warmed to room temperature and stirred overnight. To the reaction mixture was added saturated ammonium hydroxide solution and product was extracted with diethyl ether. The ether layer was dried with anhydrous magnesium sulfate and removed under reduced pressure to give 3-bromo-2-methylfuran which was identified by GC-MS and used for Myaura reaction without further purification.

2-(2-Methyl-3-furanyl)-4,4,5,5-tetramethyl-1,3,2-Dioxaborolane (**3-20**)

Crude 3-bromo-2-methylfuran (4.1 mmol) was added to DMSO solution (6 ml) containing $PdCl_2(dppf)\cdot CH_2Cl_2$ (99.4 mg, 0.12mmol), potassium acetate (1.2 g, 12.3 mmol) and bis (pinacolato)diboron (1.15 g, 4.51 mmol). The reaction mixture was heated to 70 ^oC and stirred overnight. The reaction progress was monitored by GC. After cooling, ethyl acetate (30 ml) and water (30 ml) were added. The organic layer was separated and washed with water (30 ml). The resulting organic layer was dried with anhydrous magnesium sulfate. The ethyl acetate was removed under reduced pressure. The crude product was purified by column chromatography (silica gel, ether:hexane=1:20) to give a desired product. ^1H NMR ($CDCl_3$, δ) 7.29 (d, 1 H), 6.5 (bs, 1 H), 2.5 (s, 3 H), 1.3 (s, 12 H). GC-EI: *m/z* calculated 208.13; found 208 $(M)^+$.

5'-(2-Methyl-3-furanyl)spiro[1-azabicyclo[2.2.2]octane-3,2'(3'H)-furo[2,3-b]pyridine] (**3-1**)

To a solution of DMF (0.2 ml) and water (0.18 ml) containing **3-9** (7 mg, 0.023 mmol), sodium carbonate (37 mg, 0.35 mmol) was added tetrakistriphenylphosphine palladium (0) (3 mg, 2.5 μmol). A mixture was stirred at 60~70 ^oC for 24 hrs. After completion of the reaction was monitored by NMR, ethyl acetate (1 ml) was added and the reaction mixture was filtered. The ethyl acetate layer was treated with dilute sodium hydroxide solution (0.1 N), washed with water, and evaporated under the reduced pressure. The residue was purified by column chromatography (silica gel, methanol containing isopropylamine (1.5%)) to a desired product. ^1H NMR ($CDCl_3$, δ) 8.0 (bt, 1 H), 7.44 (bt, 1 H), 7.33 (d, 1 H), 6.43 (d, 1 H), 3.4 (m, 2H), 3.1-2.8 (m, 6 H), 2.4 (s, 3 H), 2.2 (m, 1 H), 2.0 (m, 1), 1.71 (m, 2 H). LC-ESI: *m/z* calculated 295.15; found 297.3 $(M+H)^+$.

5-(2,5-bis(trimethylsilyl)furan-3-yl)-2-chloropyridine (**3-12**)

To anhydrous tetrahydrofuran (0.8 ml) containing **3-14** (10 mg, 0.03 mmol) was added n-butyllithium (1.3 M in hexane, 0.4 ml) at -78 ^{o}C. After stirring for 1 hr at -78 ^{o}C, the reaction mixture was quenched by trimethylsilyl chloride (0.26 ml, 0.05 mmol). The brown color changed into yellow as the temperature was elevated to -40 ^{o}C. After stirring for 1hr, the reaction mixture was treated with dilute sodium bicarbonate solution (3 %) and was extracted with chloroform. The chloroform layer was washed with water and brine, and dried with anhydrous magnesium sulfate. After evaporation of chloroform under reduced pressure, crude residue was purified by column chromatography (silica gel, hexane) to give a desired disilylated compound, **3-12** (white crystal, 5.27 mg, 55%, mp= 77 ^{o}C). ^{1}H NMR (CDCl3, δ) 8.4 (d, 1 H), 7.6 (dd, 1 H), 7.3 (d, 1 H), 6.7 (s, 1 H), 0.3 (s, 3 H), 0.2 (s, 3 H) ^{13}C NMR ($CDCl_3$, δ) 165.51, 161.08, 149.96, 149.29, 138.70, 132.18, 130.35, 123.87, 120.96. -0.70, -1.40.

5-(2,5-bis(trimethylsilyl)furan-3-yl)-2-chloro-3-(trimethylsilyl)pyridine (**3-13**)

To anhydrous tetrahydrofuran (1 ml) were added diisopropylamine (0.1 ml, 0.71 mmol) and butyllithium (1.3 M in hexane, 0.480 ml, 0.636 mmol) at 0 ^{o}C. After stirring for 1 hr and cooling down to -78 ^{o}C, 2-chloro-5-(furan-3-yl)pyridine (30 mg, 0.167 mmol) was added. A reaction mixture was stirred for 1hr. Trimethylsilyl chloride (0.3 ml) in anhydrous tetrahydrofuran (1 ml) was added slowly into the reaction mixture. After stirring at -60 ^{o}C for 2hrs, water was added into the reaction mixture. The reaction mixture was extracted with chloroform, washed with aqueous sodium hydroxide solution (1%). The chloroform layer was separated with brine and dried with anhydrous

magnesium sulfate. After removal of chloroform under reduced pressure, the residue was purified by column chromatography (silica gel, hexane) to give a **3-13** (45 mg, 70%). ^{1}H NMR (CDCl3, δ) 8.4 (d, 1 H), 7.7 (d, 1 H), 6.7 (s, 1 H), 0.4 (s, 3 H), 0.3 (s, 3 H), 0.2 (s, 3 H). ^{13}C NMR ($CDCl_3$, δ) 166.46, 161.95, 156.47, 150.60, 146.05, 135.37, 133.58, 130.73, 121.98, 1.21, 0.3, -0.4.

2-chloro-5-(2,5-dibromofuran-3-yl)pyridine (**3-14**)

To carbon tetrachloride (5.5 ml) was added **3-10** (98.4 mg, 0.55 mmol) at room temperature. Bromine (263.3 mg, 1.64 mmol) was slowly added into the reaction mixture. After this reaction mixture was vortexed for 2 min, saturated sodium carbonate solution (5 ml) was added cautiously. The crude product was extracted by diethyl ether (10 ml X 2) and dried with anhydrous magnesium sulfate. The organic layer was concentrated under reduced pressure. The purification by flash column chromatography (silica gel, hexane) gives the desired product, **3-14** (120 mg, 64%). ^{1}H NMR (CDCl3, δ) 8.6 (d, 1 H), 7.9 (dd, 1 H), 7.4 (d, 1 H), 6.6 (s, 1 H).

2-amino-3,5-dibromo-6-chloropyridine (**3-15**)

2-amino-6-chloropyridine (642.8 mg, 5 mmol) was dissolved into acetonitrile (15 ml). N-bromosuccinimide (1779.9 mg, 10 mmol) was added over the 30 minutes. After stirring for 1.5 hrs, the starting compound was disappeared in the thin-layer chromatography analysis (silica gel, ether). The reaction mixture was added into water (50 ml) and resulting reddish solid product was filtered and washed with distilled water thoroughly. This solid product was dried under high vacuum to give 3-15 (1.36g, 95.3%). ^{1}H NMR ($CDCl_3$, δ) 7.8 (s, 1 H), 5.1 (bs, 2 H).

3,5-dibromo-2,6-dichloropyridine (**3-16**)

2-amino-3,5-dibromo-6-chloropyridine (**3-15**, 1.3 g, 4.53 mmol) was dissolved to conc. hydrochloric acid (37%, 6.9 ml) at room temperature. After a reaction mixture was cooled down to -7-0 ^{o}C, sodium nitrite (861.3 mg, 12.48 mmol) was added slowly, and then copper(I) chloride (646 mg, 6.53 mmol) was also added. After stirring for 1hr at 0 ^{o}C, the reaction mixture was warmed to room temperature and stirred for 2 hrs more. Ice and water added to reaction mixture to get yellow precipitation, which was then filtered and dried under air. The crude compound was dissolved into ethyl acetate and dried by anhydrous magnesium sulfate. After evaporation of ethyl acetate, the crude residue was purified by column chromatography (silica gel, cyclopentane) to give a desired product, **3-16** (670 mg, 50%) ^{1}H NMR (CDCl3, δ) 8.2 (s, 1 H). ^{13}C NMR ($CDCl_3$, δ) 148.7, 146.7, 119.1.

<u>2-chloro-5-(furan-3-yl)pyridine</u> (**3-10**)

Tetrabutylammonium bromide (696 mg, 2.2 mmol) and potassium carbonate (1488 mg, 10.8 mmol) was dissolved in water (7 ml). 2-chloro-5-bromopyridine (414.5 mg, 2.15 mmol), 3-furanboronic acid (414 mg, 3.7 mmol), and palladium acetate (12.3 mg, 0.06 mmol) were added at one time under argon. The black coagulated mixture was stirred overnight. The resulting solution was extracted with ether in several portions. The ether layers were combined and dried with anhydrous magnesium sulfate and filtered. The product was purified by column chromatography on silica (ethyl acetate:hexane=1:6) to give 2-chloro-5-(furan-3-yl)pyridine (340 mg, 88.3%). ^{1}H-NMR (DMSO-d_6, δ) 8.72 (d, 1 H), 8.4 (dd, 1 H) 8.1 (dd, 1 H), 7.8(dd, 1 H), 7.5 (d, 1 H), 7.1(dd, 1 H). ^{1}H-NMR ($CDCl_3$, δ) 8.5 (d, 1 H), 7.8 (bs, 1 H), 7.7 (dd, 1 H) 7.5 (bt, 1 H), 7.3 (d, 1 H), 6.7 (bt, 1 H). ^{13}C NMR ($CDCl_3$, δ) 149.9, 147.0, 144.6, 139.4, 136.0, 127.7, 124.5, 122.4.

2-fluoro-5-(furan-3-yl)pyridine (**3-26**)

Tetrabutylammonium bromide (355 mg, 1.1 mmol) and potassium carbonate (456 mg, 3.3 mmol), 2-fluoro-5-bromopyridine (193 mg, 1.1 mmol), 3-furanboronic acid (111.9 mg, 184.6 mmol), and palladium acetate (12.3 mg, 0.06 mmol) were added to water (3.5 mL). The coagulated mixture was stirred overnight. The resulting solution was extracted with ether with several portions. The ether layer was combined and dried with anhydrous magnesium sulfate and filtered. The product was purified by column chromatography on silica (ethylacetate:hexane=1:6) to give colorless liquid, 2-fluoro-5-(furan-3-yl)pyridine (157.5 mg, 88%). ^{1}H NMR (CDCl3, δ) 8.4 (d, 1 H), 7.9 (dt, 1 H), 7.7 (bs, 1 H), 7.5 (bt, 1 H), 7.0 (dd, 1 H), 6.7 (t, 1 H). ^{19}F NMR (CDCl3, δ) -70.726.

2-bromo-6-nitropyridine (**3-23**)

To the reaction vessel containing con. sulfuric acid (13.3 ml) was added 2-amino-6-bromopyridine (2.45 g, 14.1 mmol) at 0 ^{o}C. A mixture of hydrogen peroxide (35%, 17.2 ml) and conc. sulfuric acid (40 ml) was added dropwise. This mixture was stirred overnight and was then basified with aqueous potassium hydroxide solution (3 M, 200 ml) at 0 ^{o}C to give a precipitation. The solid was filtered and washed with water and dried under the reduced pressure to give a desired product (0.6 g, 0.3 mmol, 21.2%). ^{1}H NMR (CDCl3, δ) 7.89 (dd, 1H), 7.91 (dd, 1H), 8.24 (dd, 1H). ^{13}C NMR ($CDCl_3$, δ) 116.79, 134.03, 140.99, 141.57, 155.89. GC-EI: *m/z* calculated 201.9, 203.9; found 202, 204 $(M)^{+}$.

5-(6-nitropyridin-2-yl)thiophene-2-carboxylic acid (**3-24**)

Sodium carbonate (37.2 mg, 0.3 mmol) was dissolved in water/acetonitrile (560 µl/580 µl). 5-(dihydroxyboryl)thiophene-2- carboxylic acid (17.2 mg, 0.1 mmol), 2-

bromo-6-nitropyridine, and tetrakis(triphenyl)palladium(0) were added. The reaction mixture was heated to reflux for 3 hrs. After cooling, the reaction mixture was filtered. After dichloroethane was added, the water layer was separated, acidified by hydrochloric acid to pH= 4. The resultant solid was filtered and washed with cold water to give desired coupling product (10.2 mg, 40%)

(R)-5-(6-nitropyridin-2-yl)-N-(quinuclidin-3-yl)thiophene-2-carboxamide (**3-25**)

5-(6-nitropyridin-2-yl)thiophene-2-carboxylic acid (**3-24**, 10.2 mg, 0.04 mmol) and (R)-azabicyclo[2,2,2]oct-3-ylamine dihydrochloride (7mg, 0.035 mmol) were added to the DMF solution containing N,N-diisopropylethylamine (27.8 mg, 0.2 mmol). To a reaction mixture were added 1-hydroxybenzotriazole hydrate (5.5 mg, 0.04 mmol) and TBTU (13 mg, 0.04 mmol). After stirring for 2 days, DMF was evaporated under high vacuum. The resultant residue was extracted by chloroform and washed with aqueous sodium hydroxide solution (1%). After drying with anhydrous magnesium sulfate and evaporation of chloroform under reduced pressure, the crude residue was purified by column chromatography (silica gel, methanol containing isopropylamine(1.5%)) to give the desired product, **3-25** (8.5 mg, 68%). ^{1}H NMR (CDCl3, δ) 8.12 (d, 1), 8.05 (t, 1), 8.00 (dd, 1 H), 7.73 (d, 1 H), 7.62 (d, 1 H), 6.12 (bt, 1 H), 4.16 (m, 1 H), 3.5 (m, 1 H), 3.0-2.8 (m, 4 H), 2.6 (m, 1 H), 2.06 (m, 1 H), 1.7 (m, 3 H).

5-(6-fluoropyridin-2-yl)thiophene-2-carboxylic acid (**3-22**)

To the reaction vial containing degassed water (0.5 ml) and acetonitrile (0.7 ml) was added sodium carbonate (43.2 mg, 0.35 mmol), 5-(dihydroxyboryl)thiophene-2-carboxylic acid (23.7 mg, 0.14 mmol). After stirring 5 min. under the argon, 2-bromo-5-fluoropyridine (19.6 mg, 0.11 mmol) and tetrakis(triphenylphosphine)palladium(0) were

added. The mixture was heated to reflux overnight. After cooling, 1,2-dicholoroethane was added. The water layer was collected and was acidified with hydrochloric acid (1 N) to pH= 6 to give a precipitate. The solid was filtered, washed with water, and dried under reduce pressure to give the desired product (16 mg, 65%). ^{1}H NMR (CD_3OD, δ) 7.74 (d, 1 H), 7.40-.7.55 (m, 3 H), 7.46 (d, 1 H), 7.10(ddt, 1 H). ^{13}C NMR (CD_3OD, δ) 165.97, 165.18, 163.54, 150.81, 137.23, 137.14, 135.72, 135.23, 132.31, 132.22, 126.06, 123.23, 123.20, 116.68, 116.47, 114.0, 113.75.

(R)-5-(6-fluoropyridin-2-yl)-N-(quinuclidin-3-yl)thiophene-2-carboxamide (**3-21**)

5-(6-fluoropyridin-2-yl)thiophene-2-carboxylic acid (**3-22**, 8.9 mg, 0.04 mmol) and (R)-azabicyclo[2,2,2]oct-3-ylamine dihydrochloride (7mg, 0.035 mmol) were added to the DMF (0.5 ml) solution containing N,N-diisopropylethylamine (26 mg, 0.2 mmol). To a reaction mixture were added 1-hydroxybenzotriazole hydrate (11 mg) and TBTU (17 mg, 0.05 mmol). After stirring for 2 days, DMF was evaporated under high vacuum. The resultant residue was extracted with chloroform and washed with aqueous sodium hydroxide solution (1%). After drying with anhydrous magnesium sulfate and evaporation of chloroform under reduced pressure, the crude residue was purified by column chromatography (silica gel, methanol containing isopropylamine(1.5%)) to give the desired product, **3-25** (5.2 mg, 45%). ^{1}H NMR (CDCl3, δ) 7.5 (d, 1), 7.4 (m, 1), 7.3 (m, 1 H), 7.27 (d, 1 H), 7.0 (m, 1 H), 6.2 (bd, 1 H), 4.1 (m, 1 H), 3.4 (m, 1 H), 3.0-2.8 (m, 4 H), 2.6 (m, 1 H), 2.06 (m, 1 H), 1.7 (m, 3 H), 1.5 (m, 1 H).

Homology modeling

Sequence alignment for α7 nAChRs of human, mouse, cow, and AChBP of California sea hare, *Aplysia californica* (PDB ID: 2BYQ) (**Figure 3.17**). This alignment was tested in several different algorithms that are packaged in MOE. The residues in the binding pocket were highly conserved in all species. According to the procedure of homology modeling procedure of MOE, we constructed the mouse homology model. The region of epibatidine binding pocket was energy minimized with AMBER 99.

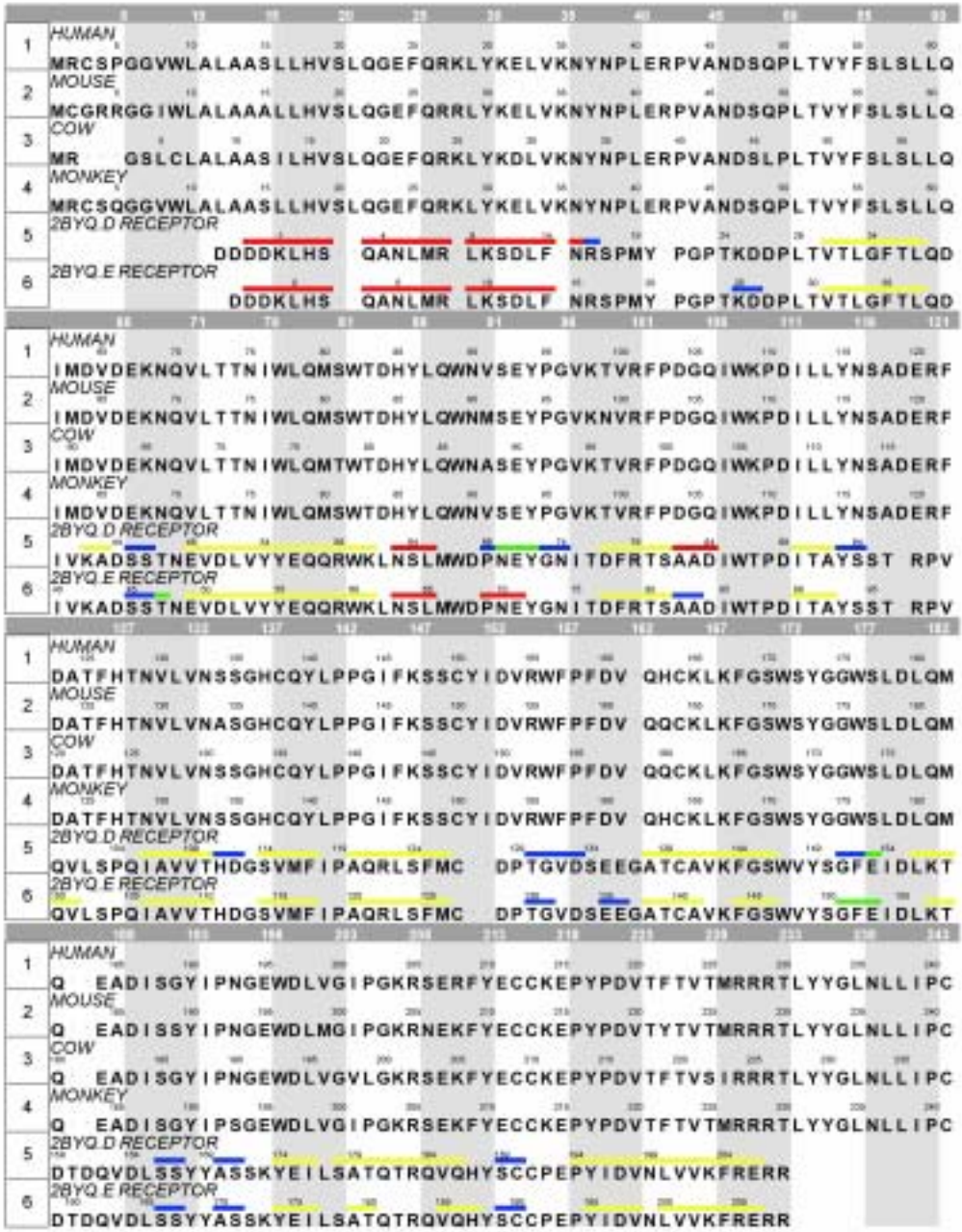

Figure 3.17 The sequence alignment of human, mouse, cow, and monkey nAChR with acetylcholine binding protein of *Aplysia Californica* (PDB ID: 2BYQ).

Quantitative Structure-Activity Relationship Study

Each structure was minimized by MMFF94x force field in the MOE environment. Initial QSAR study was performed using whole descriptors to select correlation between binding affinity and descriptors. 150 descriptors were chosen by considering the contingency coefficient and Cramer's V and linear correlation. Some improper descriptors were removed. After QSAR modeling with selected 150 descriptors, 25 descriptors were selected by removing descriptors having less than 35% correlation with binding affinity. The distribution of correlation between each descriptor and activity was also investigated in the correlation matrix and similar terms were removed.

For nine descriptors obtained by these refinements, the contribution of each descriptor was tested one by one by removing descriptor of interest. We chose four descriptors which showed high correlation and wide distribution and performed QSAR modeling (R^2=0.71). This final model was evaluated by cross-validation (Q^2=0.63). We also used the test known set to validate our QSAR model (R^2 = 0.30 with two outliers, R^2=0.74 without 2 outliers).

Table 11. The validation of QSAR model using test set

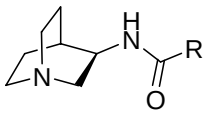

R	Experimental pKi	Predicted pKi
5-(2-nitrophenyl)thienyl-2-	8.12	6.8
5-(3-fluoro-4-hydroxyphenyl)thienyl-2-	8.4	8.1
2-thienyl	7.9	7.8
5-cyanothienyl-2-	6.6	7.3
5-methylsufanylthineyl-2-	9.3	7.4
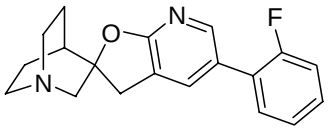	9.5	9.6

3.8 References

1. Kem, W. R. The brain alpha7 nicotinic receptor may be an important therapeutic target for the treatment of Alzheimer's disease: studies with DMXBA (GTS-21). *Behav Brain Res* **2000,** 113, 169-81.

2. Mazurov, A.; Hauser, T.; Miller, C. H. Selective alpha 7 nicotinic acetylcholine receptor ligands. *Current Medicinal Chemistry* **2006,** 13, 1567-1584.

3. Ayers, J. T.; Dwoskin, L. P.; Deaciuc, A. G.; Grinevich, V. P.; Zhu, J.; Crooks, P. A. bis-azaaromatic quaternary ammonium analogues: Ligands for alpha 4 beta 2* and alpha 7* subtypes of neuronal nicotinic receptors. *Bioorganic & Medicinal Chemistry Letters* **2002,** 12, 3067-3071.

4. Wilkins, L. H.; Grinevich, V. P.; Ayers, J. T.; Crooks, P. A.; Dwoskin, L. P. N-n-alkylnicotinium analogs, a novel class of nicotinic receptor antagonists: Interaction with alpha 4 beta 2*and alpha 7*neuronal nicotinic receptors. *Journal of Pharmacology and Experimental Therapeutics* **2003,** 304, 400-410.

5. Ragab, H. M.; Kim, J. S.; Dukat, M.; Navarro, H.; Glennon, R. A. Aryloxyethylamines: binding at alpha7 nicotinic acetylcholine receptors. *Bioorg Med Chem Lett* **2006,** 16, 4283-6.

6. Bunnelle, W. H.; Dart, M. J.; Schrimpf, M. R. Design of Ligands for the nicotinic acetylcholine receptors: The quest for selectivity. *Current Topics in Medicinal Chemistry* **2004,** 4, 299-334.

7. Gundisch, D.; Andra, M.; Munoz, L.; Tilotta, M. C. Synthesis and evaluation of phenylcarbamate derivatives as ligands for nicotinic acetylcholine receptors. *Bioorganic & Medicinal Chemistry* **2004,** 12, 4953-4962.

8. Bodnar, A. L.; Cortes-Burgos, L. A.; Cook, K. K.; Dinh, D. M.; Groppi, V. E.; Hajos, M.; Higdon, N. R.; Hoffmann, W. E.; Hurst, R. S.; Myers, J. K.; Rogers, B. N.; Wall, T. M.; Wolfe, M. L.; Wong, E. Discovery and structure - Activity relationship of quinuclidine benzamides as agonists of alpha 7 nicotinic acetylcholine receptors. *Journal of Medicinal Chemistry* **2005,** 48, 905-908.

9. Phillips, E. a alpha 7-selective compounds as novel potential therapeutics for CNS diseases. *Abstracts of Papers of the American Chemical Society* **2004,** 228, U911-U911.

10. Gundisch, D.; Andra, M.; Munoz, L.; Cristina Tilotta, M. Synthesis and evaluation of phenylcarbamate derivatives as ligands for nicotinic acetylcholine receptors. *Bioorganic & Medicinal Chemistry* **2004,** 12, 4953-4962.

11. Mazurov, A.; Klucik, J.; Miao, L.; Phillips, T. Y.; Seamans, A.; Schmitt, J. D.; Hauser, T. A.; Johnson, R. T., Jr.; Miller, C. 2-(Arylmethyl)-3-substituted quinuclidines as selective alpha 7 nicotinic receptor ligands. *Bioorg Med Chem Lett* **2005,** 15, 2073-7.

12. Mullen, G.; Napier, J.; Balestra, M.; DeCory, T.; Hale, G.; Macor, J.; Mack, R.; Loch, J.; Wu, E.; Kover, A.; Verhoest, P.; Sampognaro, A.; Phillips, E.; Zhu, Y. Y.; Murray, R.; Griffith, R.; Blosser, J.; Gurley, D.; Machulskis, A.; Zongrone, J.; Rosen, A.; Gordon, J. (-)-spiro[1-azabicyclo[2.2.2]octane-3,5 '-oxazolidin-2 '-one], a conformationally restricted analogue of acetylcholine, is a highly selective full agonist at the alpha 7 nicotinic acetylcholine receptor. *Journal of Medicinal Chemistry* **2000,** 43, 4045-4050.

13. Ogawa, M.; Tatsumi, R.; Fujio, M.; Katayama, J.; Magata, Y. Synthesis and evaluation of [125I]I-TSA as a brain nicotinic acetylcholine receptor [alpha]7 subtype imaging agent. *Nuclear Medicine and Biology* **2006,** 33, 311-316.

14. Ravert H.T., D. P., Foss C.A., Fan H., Holmquist C.R., Phillips E.,; McCarthy D.J., H. R., Holt D., Dannals R.F., Pomper M.G. Synthesis of 5'-(2-[18F]fluorophenyl)-spiro[1-azabicyclo[2.2.2.]octane]-3,2'(3'H)-furo[2,3-b]pyridine ([18F]FPS), an agonist at the α7 nicotinic acetylcholine receptor. *Journal of Labelled Compounds and Radiopharmaceuticals* **2005,** 48, S168.

15. Macor, J. E.; Gurley, D.; Lanthorn, T.; Loch, J.; Mack, R. A.; Mullen, G.; Tran, O.; Wright, N.; Gordon, J. C. The 5-HT3 antagonist tropisetron (ICS 205-930) is a potent and selective alpha 7 nicotinic receptor partial agonist. *Bioorganic & Medicinal Chemistry Letters* **2001,** 11, 319-321.

16. Baker, S. R.; Boot, J.; Brunavs, M.; Dobson, D.; Green, R.; Hayhurst, L.; Keenan, M.; Wallace, L. High affinity ligands for the [alpha]7 nicotinic receptor that show no cross-reactivity with the 5-HT3 receptor. *Bioorganic & Medicinal Chemistry Letters* **2005,** 15, 4727-4730.

17. Philips, E.; Mack, R.; Macor, J.; Semus, S. Spiroazo bicyclic heterocyclic. *US Patent 6703502* **2004**.

18. Fowler, J. S.; Volkow, N. D.; Wang, G. J.; Gatley, S. J.; Logan, J. [(11)]Cocaine: PET studies of cocaine pharmacokinetics, dopamine transporter availability and dopamine transporter occupancy. *Nuclear Medicine and Biology* **2001,** 28, 561-572.

19. Gatley, S. J.; Macgregor, R. R.; Fowler, J. S.; Wolf, A. P.; Dewey, S. L.; Schlyer, D. J. Rapid stereoselective hydrolysis of (+)-cocaine in baboon plasma prevents its uptake in the brain - implications for behavioral-studies. *Journal of Neurochemistry* **1990,** 54, 720-723.

20. Gatley, S. J. Activities of the enantiomers of cocaine and some related-compounds as substrates and inhibitors of plasma butyrylcholinesterase. *Biochemical Pharmacology* **1991,** 41, 1249-1254.

21. Price, S.; Bordogna, W.; Braganza, R.; Bull, R. J.; Dyke, H. J.; Gardan, S.; Gill, M.; Harris, N. V.; Heald, R. A.; van den Heuvel, M.; Lockey, P. M.; Lloyd, J.; Molina, A. G.; Roach, A. G.; Roussel, F.; Sutton, J. M.; White, A. B. Identification and optimisation of a series of substituted 5-pyridin-2-yl-thiophene-2-hydroxamic acids as potent histone deacetylase (HDAC) inhibitors. *Bioorg Med Chem Lett* **2007,** 17, 363-9.

22. Anderson, K. W.; Buchwald, S. L. General catalysts for the Suzuki-Miyaura and Sonogashira coupling reactions of aryl chlorides and for the coupling of challenging substrate combinations in water. *Angew Chem Int Ed Engl* **2005,** 44, 6173-7.

23. Kuivila, H. G.; Nahabedian, K. V. Electrophilic Displacement Reactions. X. General Acid Catalysis in the Protodeboronation of Areneboronic Acids1-3. *J. Am. Chem. Soc.* **1961,** 83, 2159-2163.

24. Moreno-Manas, M.; Perez, M.; Pleixats, R. Palladium-Catalyzed Suzuki-Type Self-Coupling of Arylboronic Acids. A Mechanistic Study. *J. Org. Chem.* **1996,** 61, 2346-2351.

25. Kudo, N.; Perseghini, M.; Fu, G. C. A versatile method for Suzuki cross-coupling reactions of nitrogen heterocycles. *Angewandte Chemie-International Edition* **2006,** 45, 1282-1284.

26. Kondolff, I.; Doucet, H.; Santelli, M. Synthesis of biheteroaryl derivatives by tetraphosphine/palladium-catalysed Suzuki coupling of heteroaryl bromides with heteroarylboronic acids. *Journal of Molecular Catalysis a-Chemical* **2007,** 269, 110-118.

27. Molander, G. A.; Ellis, N. Organotrifluoroborates: Protected boronic acids that expand the versatility of the Suzuki coupling reaction. *Accounts of Chemical Research* **2007,** 40, 275-286.

28. Liu, G.; Zhao, H.; Liu, B.; Xin, Z.; Liu, M.; Kosogof, C.; Szczepankiewicz, B. G.; Wang, S.; Clampit, J. E.; Gum, R. J.; Haasch, D. L.; Trevillyan, J. M.; Sham, H. L. Aminopyridine carboxamides as c-Jun N-terminal kinase inhibitors: Targeting the gatekeeper residue and beyond. *Bioorganic & Medicinal Chemistry Letters* **2006,** 16, 5723-5730.

Chapter 4. The PET study and synthesis of des-N-ethyl-^{11}C-methylMLA

4.1 Background

Methyllycaconitine (MLA, also known as mellictine, delsemidine, delartine), an insecticidal[1] norditerpenoid which is rich in larkspur species (*Delphinium nuttallianum, Delphinium brownii*),[2] was known to be the major toxin for larkspur poisoning of livestock in the western US in 1979.[3, 4] Since it was first reported by Manske as a crude form[5] in 1938, Goodson isolated from the seeds of *Delphinium elatum*, showing that hydrolysis of MLA by alkaline solution produced methylsuccinic acid, anthranilic acid, and lycoctonine.[6] In 1981, Pelletier et al. reported its isolation from *Delphinium glaucescens* Rybd. and reported its NMR spectrum.[7] The S-configuration of chiral center of succinimide group was confirmed by Coates et al. in 1994.[8] The total synthesis of MLA has been a challenge due to its complicate ring structure and many chiral centers.

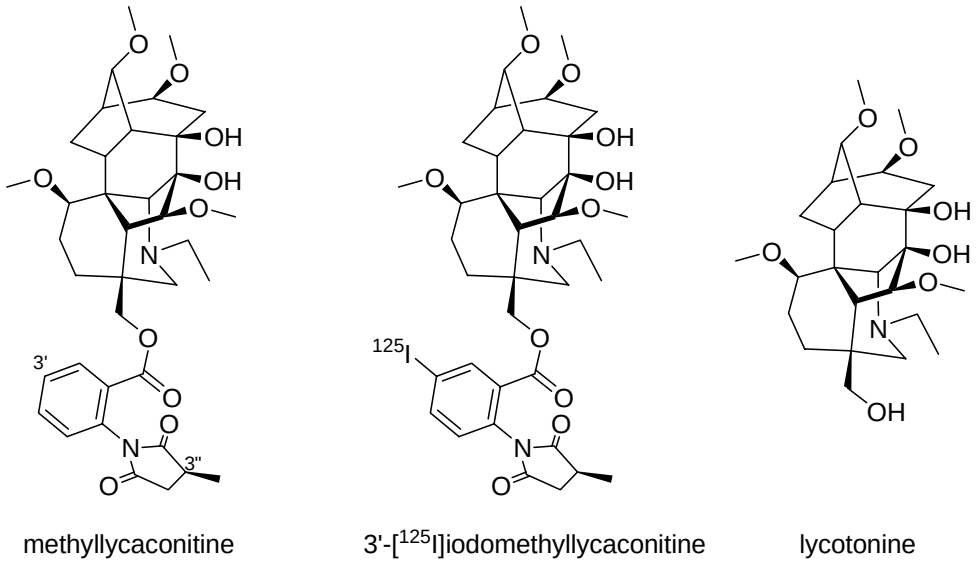

Figure 4.1 The structure of methyllycaconitine derivatives

Pharmacology Currently, MLA is the most potent small molecule antagonist for mammalian α7 nAChR and insect neuronal nAChR. Due to its toxicity against livestock, MLA is not appropriate as an insecticide. MLA administration to calf also induced paralysis by blocking the muscular neurotransmission.[9] Turek et al. demonstrated the pharmacokinetic profile of MLA, where the plasma half-life was short (19 min) in rat after intravenous injection.[10] Possibly due to its antagonism, MLA (dose= 3.9 and 7.8 mg/kg[11], LD_{50}= 4.8 mg/kg in mice[12]) ameliorated nicotine self-administration and withdrawal symptoms in rat study.[11, 13]

Binding characterization The neurotoxicity of MLA as an insecticide was due to antagonism for insect nicotinic receptor, showing inhibition within nanomolar range for [^{125}I]α-BTX binding in various insect experiments.[1, 14, 15] For the mammalian nAChR, the Wonnacott[12] group reported that MLA also inhibited [^{125}I]α-BTX binding with high affinity (Ki= 1.4 nM) in rat brain membranes, discriminating it from the neuromuscular [^{125}I]α-BTX binding.[14, 16] Later, [^{3}H]MLA binding displayed identical pattern with [^{125}I]α-BTX binding in the rat brain autoradiography.[12, 17] Therefore, radiolabeled MLA became an alternative standard compound as an α7 nAhCR probe and even better than [^{125}I]α-BTX (Figure 1.2, MW= 7800~8000 kD, 74 amino acids) which showed high nonspecific binding and was unlikely to penetrate the blood brain barrier (BBB). In contrast to [^{125}I]α-BTX, MLA (MW=682.35) showed lack of neuromuscular binding. In 2000, Carroll et al. synthesized[18] and characterized[19] an ^{125}I-labeled version of MLA (Ki= 3.2 nM for MLA). It showed poor BBB penetration in an *ex vivo* study, and its distribution pattern was consistent with an in vitro autoradiography study.

Recently, it was reported that MLA also binds to α6 and α9α10 nAChR[20, 21]

Structure and activity MLA has a basic tertiary amine (calculated pKa = 12.2) in aconitane ring similar to nicotine, epibatidine. MLA and epibatidine share the same binding pockets of acetylcholine binding protein (AChBP) in the X-ray crystal structures (PDB ID: 2BYQ, 2BYR). According to Wonnacott's publication, a structural change in the lycoctonine part affects subtype selectivity, while 2-(methylsuccinimido)benzoyl group is critical for α7 nAChR binding.[22] Due to the high binding profile of 3'-iodomethyllycaconitine (Ki= 2.0 nM for [^{125}I]α-BTX), potency and selectivity seems to be tolerant for the para position relative to succinimide ring.[18] Interestingly, lycaconitine, which has no methyl group at 3" position in succinimide ring, showed about 20 times lower binding affinity than MLA.[23]

4.2 Objectives

Owing to its high binding affinity for α7 nAChR and selectivity, radiolabel MLA has been developed as a standard compound for binding essay for α7 nAChR. In continuing our effort to pursue the selective a α7 nAChR PET tracer, we developed the C-11 labeled MLA analogue, **4-2**, which might be useful as a α7 nAChR probe for imaging and quantification of α7 nAChR in peripheral organs as well as central nervous system. Since the N-ethyl group resides in the deep binding pocket in AChBP, perhaps hydrophobic interaction may be present. However, we reasoned that the little change ethyl to methyl may not disrupt seriously binding property of MLA and this structure could potentially be labeled rapidly using C-11 methyl iodide. In addition, des(N-ethyl)-N-^{11}C-methylMLA ([^{11}C]**4-2**) would show whether MLA penetrate BBB in a tracer-dose

level. This information might be critical for further MLA based PET tracer development because its high molecular weight and low lipophilicity which would be predicted to be unfavorable for BBB penetration.

4.3 Synthesis

The synthesis of des(N-ethyl)-N-methylmethyllycaconitine performed by Carroll et al (Chemistry and Life Science, Research Triangle Institute, NC). N-deethylation of MLA using mercuric(II) acetate/aqueous acetic acid was reported by Sun et al.[24]

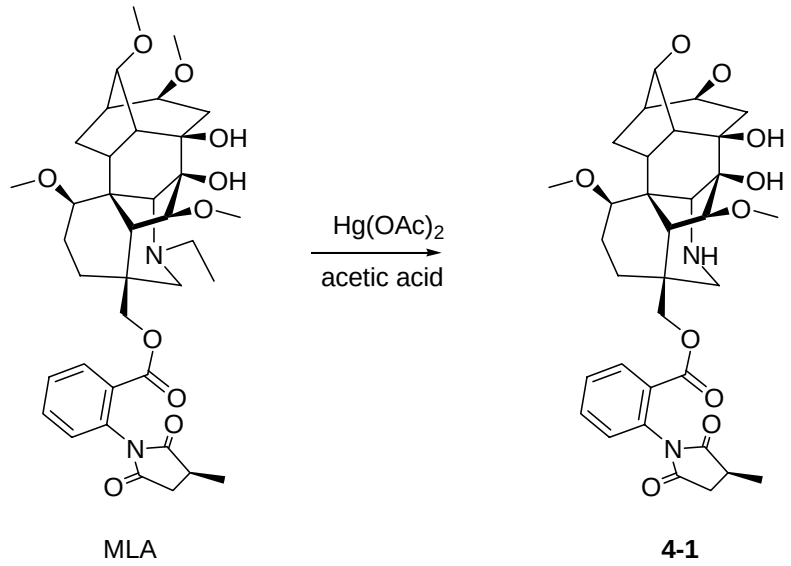

Scheme 4.1 Synthesis of Des(N-ethyl)-N-methylMLA.

Des(N-ethyl-N-methyl MLA Des(N-ethyl-N-methyl MLA was synthesized through reduction by sodium cyanoborohydride without further methylation. After preparative TLC, this compound was identified by nmr and mass spectrometer (ES).

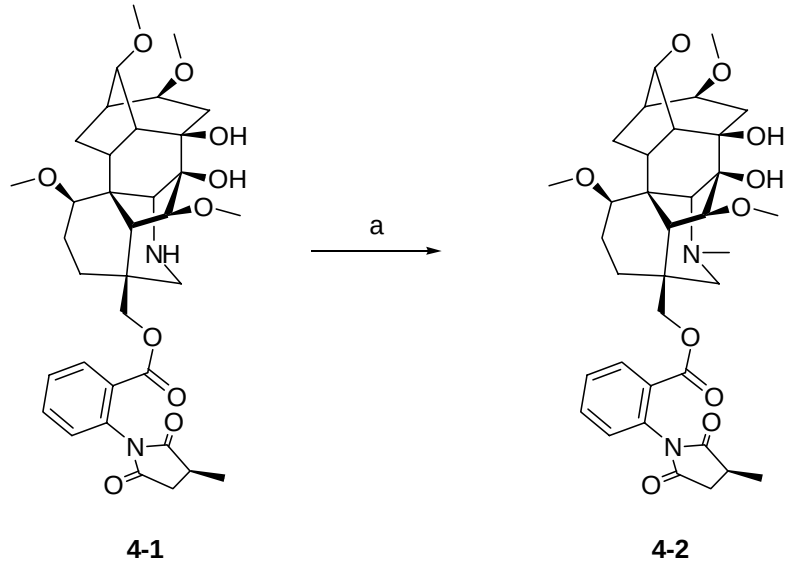

Scheme 4.2 Synthesis of Des-N-ethylmethylMLA, a, formaldehyde, sodium cyanoborohydride, acetic acid, acetonitrile.

Radiosynthesis C-11 labeling was performed under the basic condition (potassium carbonate) in DMF. Radiochemical yield was low (4-9%) and was changed little in the range between 80 and 120 ^{o}C. However, C-11 labeled product could often not removed from round bottom flask or filter after solvent evaporation. Therefore, ethanol (5%) in saline was used.

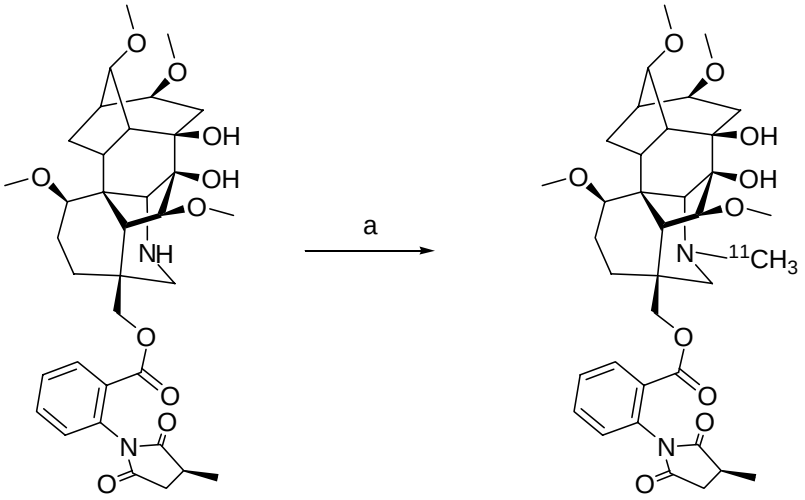

Scheme 4.3 Radiosynthesis of Des-N-ethyl-^{11}C-methylMLA. a, [^{11}C]methyl iodide, potassium carbonate, DMF

log P and Plasma protein binding The log $D_{7.4}$ was 0.57 which is close to calculated lipophilicity of methyllycaconitine (log $D_{7.4}$= 0.7). The observed unbound fraction in plasma was 24%.

4.4 Baboon study

Two baboon brain PET studies were performed in the same day and same baboon. The radioactivity in the brain was negligible. The high molecular weight and low lipophilicity (log $D_{7.4}$= 0.57, calculated log P= 0.7) may limit brain entry.

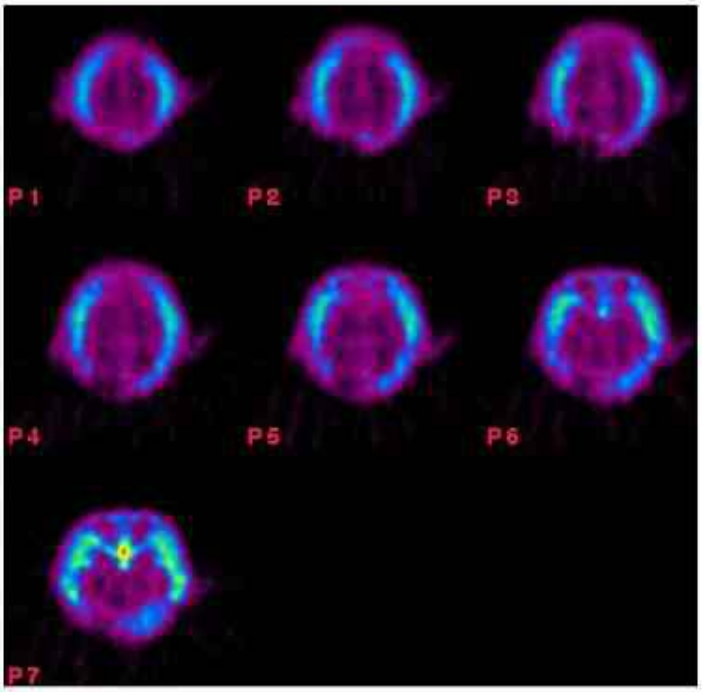

Figure 4.2 The PET image in baboon summed from time of injection through 90 min for (A) **2-^{11}C-2** (injected dose = 1.8 mCi). Ketamine hydrochloride (10 mg/kg) was used as an anesthetic by an intramuscular injection.

4.5 Experimental

General The precursor des-N-ethylmethylMLA (**4-1**)was generously given by Dr. Carroll (Chemistry and Life Science, Research Triangle Institute, NC)

(1α,6β,14α,16β)-20-Methyl-1,6,14,16-tetramethoxy-4-[[[2-[(3S)-3-methyl-2,5-dioxo-1-pyrrolidinyl]benzoyl]oxy]methyl]-aconitane-7,8-diol

To des-N-ethylmethyllycaconitine ($C_{35}H_{46}N_2O_{10}\cdot 0.75H_2O$, 1.3 mg, 1.95 μmol) in anhydrous acetonitrile (200 μL), was added 37% formaldehyde (3.37 μL) with stirring.

After 3 hrs at room temperature, sodium cyanoborohydride (1 mg) was added. After stirring for 3 hr at room temperature, and glacial acetic acid (15 μL) was added. The reaction mixture was analyzed by TLC (chloroform: methanol: 28% ammonium hydroxide solution = 90:10:1). Aqueous saturated sodium bicarbonate solution (2 ml) was poured into the reaction mixture and extracted with chloroform (2 × 2 mL). The combined chloroform layers were washed with brine, dried ($MgSO_4$), filtered, and then evaporated in vacuum to give a white solid. The crude product was purified by preparative TLC (chloroform: methanol: 28% ammonium hydroxide solution = 90:10:1) to give a methylated product. ^{1}H NMR ($CDCl_3$, δ) 1.47 (br d, 3H), 1.6-2.1 (m, 5H), 2.1 (b, 1H), 2.51 and 3.17 (br, 2H), 2.63 (s, 3H), 3.06 (t, J = 5.1Hz, 1H), 3.09 (s, 1H), 3.23 (t, J = 7.93 Hz, 1H), 3.28 (s, 3H), 3.35 (s, 3H), 3.39 (s, 3H), 3.42 (s, 3H), 3.89 (s, 1H), 4.17 and 4.20 (each d, J = 9.0 Hz, 2H), 7.29 (d, J = 7.6 Hz, 1H), 7.55 (dd, J = 7.6, 7.6, 1H), 7.70 (dd, J = 7.6, 7.6 Hz, 1H), 8.06 (d, J = 7.4 Hz, 1H). ^{13}C NMR ($CDCl_3$, δ) 16.38, 26.08, 28.71, 32.08, 33.57, 35.25, 37.03, 37.76, 38.05, 43.17, 44.45, 46.06, 49.14, 49.96, 54.94, 56.31, 56.37, 57.88, 58.18, 65.84, 69.53, 77.42, 82.52, 83.84, 84.43, 89.07, 90.60, 127.03, 129.41, 130.08, 131.05, 133.06, 133.71, 164.16, 175.81, 179.87. MS-ESI: *m/z* calculated 668.33; found 667.5, 669.4 $(M+H)^+$,

Radiolabeling of (1α,6β,14α,16β)-20-[^{11}C]Methyl-1,6,14,16-tetramethoxy-4-[[[2-[(3S)-3-methyl-2,5-dioxo-1-pyrrolidinyl]benzoyl]oxy]methyl]-aconitane-7,8-diol *(7)*

[^{11}C]Methyl iodide was transferred into long neck V-shaped vessel containing des-N-ethylmethylmethyllycaconitine (**4-1,** 1 mg) and 1 M potassium carbonate solution (1.2 μl) in dimethylformamide (300 μl) which was cooled in a dry ice/acetonitrile bath. [^{11}C]Methyl iodide was transferred into the reaction mixture and when ^{11}C peaked, the

inlet and outlet of the reaction vessel were closed. The reaction mixture was heated at 80°C for 10 minutes in an oil bath. It was cool down for five seconds under dry ice/acetonitrile bath and was diluted with 1 ml of HPLC eluent. This diluted solution was injected into Knauer HPLC system with uv detection (give wavelength) and eluted with to collect the desired product (retention time = 17 min.). It was performed with eluent (A: water = 92:8; A, citrate buffer (75 %, pH = 4.33) in ethanol) at a flow rate 5 ml/min on a semi-preparative Luna C18 (Phenomenex, 250 mm X 10 mm, 5 μ). After evaporating the collected eluent under the reduced pressure by azeotropical evaporation acetonitrile (4 ml X 2), the product was diluted with saline (4 ml) containing ethanol(5 %(v/v)) and was filtered by a 0.22 mm Millipore® filter (Millipore Corp., Billerica, MA) into a sterile vial. The radiochemical yield and purity were 4-9 % and >98%, respectively. The total time from end of cyclotron bombardment to delivery was around 1 hr. Quality control was performed by HPLC with at a flow rate 1 ml/min on a Luna C18(2) (Phenomenex, 250 mm X 4.60 mm, retention time congruent with authentic standard). R_f value of TLC analysis was 0.68 in chloroform: methanol: saturated ammonia = 90:10:1 eluent.

4.6 References

1. Jennings, K. R.; Brown, D. G.; Wright, D. P. Methyllycaconitine, a naturally-occurring insecticide with a high-affinity for the insect cholinergic receptor. *Experientia* **1986,** 42, 611-613.

2. Aiyar, V. N.; Benn, M. H.; Hanna, T.; Jacyno, J.; Roth, S. H.; Wilkens, J. L. Principal toxin of delphinium-brownii rydb, and its mode of action. *Experientia* **1979,** 35, 1367-1368.

3. Aiyar, V. N.; Benn, M. H.; Hanna, T.; Jacyno, J.; Roth, S. H.; Wilkens, J. L. The principal toxin ofdelphinium brownii rydb., and its mode of action. *Cellular and Molecular Life Sciences (CMLS)* **1979,** 35, 1367-1368.

4. Nation, P. N.; Benn, M. H.; Roth, S. H.; Wilkens, J. L. Clinical signs and studies of the site of action of purified larkspur alkaloid, methyllycaconitine, administered parenterally to calves. *Canadian Veterinary Journal-Revue Veterinaire Canadienne* **1982,** 23, 264-266.

5. Manske, R. H. An alkaloid from Delphinium brownii Rydb. *Canadian Journal of Research* **1938,** 16, 57-60.

6. Goodson, J. A. The alkaloids of the seeds of Delphinium elatum, L. *Journal of the Chemical Society* **1943**, 139.

7. Pelletier, S. W.; Dailey, O. D.; Mody, N. V.; Olsen, J. D. Isolation and structure elucidation of the alkaloids of delphinium-glaucescens rybd. *Journal of Organic Chemistry* **1981,** 46, 3284-3293.

8. Coates, P. A.; Blagbrough, I. S.; Hardick, D. J.; Rowan, M. G.; Wonnacott, S.; Potter, B. V. L. Rapid and efficient isolation of the nicotinic receptor antagonist methyllycaconitine from delphinium - assignment of the methylsuccinimide absolute stereochemistry as S. *Tetrahedron Letters* **1994,** 35, 8701-8704.

9. Gubanow, I. A. Delphinium als quelle curareahnlicher praparate. *Planta Medica* **1965,** 13, 200-&.

10. Turek, J. W.; Kang, C. H.; Campbell, J. E.; Arneric, S. P.; Sullivan, J. P. A sensitive technique for the detection of the alpha 7 neuronal nicotinic acetylcholine receptor antagonist, methyllycaconitine, in rat plasma and brain. *J Neurosci Methods* **1995,** 61, 113-8.

11. Athina, M.; Neil, E. P. The nicotinic antagonist methyllycaconitine has differential effects on nicotine self-administration and nicotine withdrawal in the rat. *Nicotine & Tobacco Research* **2001,** 3, 361-373.

12. Panter, K. E.; Manners, G. D.; Stegelmeier, B. L.; Lee, S.; Gardner, D. R.; Ralphs, M. H.; Pfister, J. A.; James, L. F. Larkspur poisoning: toxicology and alkaloid structure-activity relationships. *Biochemical Systematics and Ecology* **2002,** 30, 113-128.

13. Tucci, S.; Genn, R. F.; Marco, E.; File, S. E. Do different mechanisms underlie two anxiogenic effects of systemic nicotine? *Behavioural Pharmacology* **2003,** 14, 323-329.

14. Macallan, D. R. E.; Lunt, G. G.; Wonnacott, S.; Swanson, K. L.; Rapoport, H.; Albuquerque, E. X. Methyllycaconitine and (+)-anatoxin-a differentiate between nicotinic receptors in vertebrate and invertebrate nervous systems. *Febs Letters* **1988,** 226, 357-363.

15. Sattelle, D. B.; Pinnock, R. D.; Lummis, S. C. R. Voltage-independent block of a neuronal nicotinic acetylcholine-receptor by n-methyl lycaconitine. *Journal of Experimental Biology* **1989,** 142, 215-224.

16. Ward, J. M.; Cockcroft, V. B.; Lunt, G. G.; Smillie, F. S.; Wonnacott, S. Methyllycaconitine - a selective probe for neuronal alpha-bungarotoxin binding-sites. *Febs Letters* **1990,** 270, 45-48.

17. Whiteaker, P.; Davies, A. R. L.; Marks, M. J.; Blagbrough, I. S.; Potter, B. V. L.; Wolstenholme, A. J.; Collins, A. C.; Wonnacott, S. An autoradiographic study of the distribution of binding sites for the novel α7-selective nicotinic radioligand [3H]-methyllycaconitine in the mouse brain. *European Journal of Neuroscience* **1999,** 11, 2689-2696.

18. Navarro, H. A.; Zhong, D. S.; Abraham, P.; Xu, H.; Carroll, F. I. Synthesis and pharmacological characterization of [I-125]iodomethyllycaconitine ([I-125]iodo-MLA). A new ligand. *Journal of Medicinal Chemistry* **2000,** 43, 142-145.

19. Navarro, H. A.; Xu, H.; Zhong, D.; Abraham, P.; Carroll, F. I. In vitro and in vivo characterization of [I-125]iodomethyllycaconitine in the rat. *Synapse* **2002,** 44, 117-123.

20. Klink, R.; d'Exaerde, A. D.; Zoli, M.; Changeux, J. P. Molecular and physiological diversity of nicotinic acetylcholine receptors in the midbrain dopaminergic nuclei. *Journal of Neuroscience* **2001,** 21, 1452-1463.

21. Mogg, A. J.; Whiteaker, P.; McIntosh, J. M.; Marks, M.; Collins, A. C.; Wonnacott, S. Methyllycaconitine is a potent antagonist of alpha-conotoxin-MII-sensitive presynaptic nicotinic acetylcholine receptors in rat striatum. *Journal of Pharmacology and Experimental Therapeutics* **2002,** 302, 197-204.

22. Hardick, D. J.; Cooper, G.; Scott-Ward, T.; Blagbrough, I. S.; Potter, B. V.; Wonnacott, S. Conversion of the sodium channel activator aconitine into a potent alpha 7-selective nicotinic ligand. *FEBS Lett* **1995,** 365, 79-82.

23. Jacyno, J. M.; Harwood, J. S.; Lin, N. H.; Campbell, J. E.; Sullivan, J. P.; Holladay, M. W. Lycaconitine revisited: Partial synthesis and neuronal nicotinic acetylcholine receptor affinities. *Journal of Natural Products* **1996,** 59, 707-709.

24. Sun, F.; Bai, Y.; Benn, M. The Natural Occurrence and Partial Synthesis of 1-Alpha-4(S),6-Beta,14-Alpha-16-Beta-19,20-Didehydro-1,6,14,16-Tetramethoxy-4-[[[2-(3-Methyl-2,5-Dioxopyrrolidinyl)Benzoyl]Oxy]Methyl]Aconitane-7,8-Diol Concerning Anhweidelphinine. *Heterocycles* **1991,** 32, 1137-1141.

Chapter 5. PET study of C-11 labeled nicotine

5.1 Background

History and Chemistry: Nicotine, is a simple natural alkaloid abundant (0.3-5% in dry leaf) in the tobacco plant, *Nicotiana tabacum*. Jean Nicot de Villemain, the French ambassador, was the first to report the therapeutically favorable effects of tobacco plant in his medical publication to Europe.[1] Nicotine, one of the active ingredients in tobacco, was first isolated from tobacco plant by Posselt and Reimann[2] of Heidelberg University in 1828 and its empirical formula and molecular weight were determined by Mesens, Barral, Schlösing in the mid 19th century. The chemical structure of nicotine was proposed by Pinner in 1893[3] and the first total synthesis was achieved as the racemate by Pictet and Rotschy in 1904.[4] After structural analysis of the salt using X-ray crystallography,[5, 6] optically pure S-nicotine was synthesized from L-proline[7]. Asymmetric synthesis of the other unnatural enantiomer of nicotine was recently published.[8, 9]

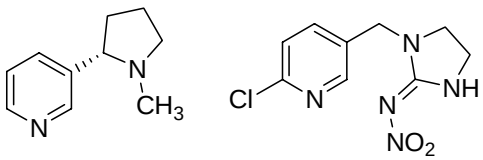

Figure 5.1 Nicotine and imidacloprid

The de novo synthesis in tobacco root followed by transportation to the leaf is a plant protective action against attack from insects and forms the basis for the use of nicotine and imidacloprid (structurally modified from nicotine) as an insecticide.

Tobacco related diseases: It is well-known from epidemiological studies that tobacco smoking causes heart disease, stroke, vascular disease, cataracts, and lung

cancer, resulting in 4 million deaths in every year. According to 2005 National Surveys of Drug Use and Health, 34.9% of Americans aged over 12 had a smoking experience in the previous year. The economic cost for healthcare and other losses from tobacco use reached 180 billion US dollar/year. Moreover, 17.3% of pregnant women smoked during pregnancy, which may affect prenatal development of the fetus. In fact, prenatal nicotine exposure in a monkey study significantly altered neuronal and lung development in offspring.[10] Though nicotine itself is not suspected to be carcinogenic[11], it contributes significantly to carcinogenesis indirectly by reinforcing chronic cigarette smoking which introduces about 60 other known carcinogenic compounds.

Peripherally, nicotine is also associated with etiology of non-small cell lung cancer (SCLC) through tobacco smoking. One of metabolite of nicotine, 4-(methylamino)-1-(3-pyridyl)-1-butanone, has been suggested as a precursor of the potent carcinogen, 4-(methylnitrosamino)-1-(3-pyridyl)-1-butanone.[11] Also, nicotine showed antiapoptotic effects in lung cancer cells treated by anticancer drugs, possibly resulting in reduction of therapeutic effect.[12] This result underscores the importantance of tobacco smoking cessation therapy using nicotine.

Pharmacology of nicotine: Due to chronic nicotine exposure, the upregulation and desensitization of β2 subunit-containing nAChR has been observed and its knock-out mice showed lack of addictive effect. α7 nAChR is also known to partake in nicotine action, for example, showing restorative effect under nicotine exposure against behavioral and electrophysiological alterations caused by lack of β2 subunit-containing nAChR. Additionally, blood brain barrier permeability of MLA was

altered by chronic nicotine[13], indicating BBB alteration and drug bioavailability in the brain.

Nicontine pharmacokinetics and addiction: Nicotine is considered to be a main component responsible for addiction through its binding neuronal nicotinic receptors in the CNS. When smoked, nicotine rapidly enters the arterial blood stream and is delivered to the brain where it binds to nicotinic receptors. Pharmacologically, the addictive action of nicotine is due to striatal dopamine release in nucleus accumbens resulting from both glutamate release and GABA inhibition by nicotine, which simultaneously reinforce the reward (pleasure or high) function of brain dopamine system[14], which is crucial for its reinforcement. Interestingly, in chronic smokers the arterial concentration of nicotine is far lower than would be predicted, leading to the hypothesis that delivery of nicotine to the brain would be lower in the smoker.

Nicotinic receptors as drug target: Although cigarette smoking causes serious diseases, nicotine has been the center of attention because its action induced favorable pharmacological effects such as enhancement of working memory, attention, anxilolysis, neuroprotection, and analgesia in many animal studies.[15] To optimize these favorable effects and reduce its toxicity, nicotine has been an effective lead chemical structure for neurocognitive drug research to treat the symptom of Alzheimer's disease, Parkinson's disease, Schizophrenia.

The change of the nAChR system or nicotine binding sites in the CNS has been investigated in relation to many diseases and developmental stages. For example, Breese et al. reported that there was an increase of nicotine binding sites in the

hippocampus and thalamus in subjects that have a history of chronic tobacco smoking.[16] This might be due to upregulation of nictotinic receptors by nicotine. Since profound alterations of cortical [^{3}H]acetylcholine and [^{3}H]nicotine binding in postmortem brains with AD have been observed [17-20], the development of a reliable tool for in vivo imaging and diagnosis through nAChR is now underway.

Nicotine PET imaging: C-11 labeled S-nicotine was first synthesized by Nordberg et al.[21] and human PET studies were performed by Halldin et al. with some minor synthetic modifications[22] to test its potential as a nicotinic receptor tracer and diagnostic tool for AD[23]. Due to fast uptake and clearance in all brain regions, [^{11}C] nicotine has not been considered as a suitable tracer for the nicotinic binding sites. However, Kadir et al. indicated the correlation between [^{11}C] nicotine binding in the cortical regions and the extent of attention deficit of the AD patients[24]. In 2007, [^{11}C] nicotine PET studies also showed sufficient sensitivity to detect alteration of nicotine binding sites by rivastigmine treatment in a group of mild AD patients.[22, 25] Based on in vitro studies, nicotine showed higher binding affinity for α4β2 nAChR compared with α7 nAChR.

5.2 Objectives

Based on the unexpectedly low arterial nicotine concentrations reported by Rose et al. and his hypothesis that this was due to lung retention[26] as well as anecdotal literature reports of long radiotracer retention in smokers' lungs [27], and our ongoing studies of drug transfer from mother to fetus, we set out to implement the

synthesis of [^{11}C]nicotine which had been reported by Nordberg et al.[21] We have the following specific aims:

1. Reliable synthesis and purification of [^{11}C] nicotine
2. Baboon studies to determine [^{11}C] nicotine and labeled metabolite distribution in brain and peripheral organs for radiation dosimetry for future human studies.
3. Monkey study for maternal and fetal kinetics.
4. Comparison of brain and lung uptake of [^{11}C] nicotine in a group of smokers and non-smokers.

Here, preliminarily, we optimized synthesis and purification of [^{11}C] nicotine and performed the dosimetry for future human studies using baboons. We also observed the transfer of [^{11}C] nicotine from mother to fetus in baboon studies. In 1999, Rose et al. observed a relatively low arterial concentration of nicotine after a puff of smoke and therefore, postulated that lung uptake of nicotine hampered the entry of nicotine into the arterial circulation.[26] Because a change in receptor occupancy for a short time is critical for resultant reward (high) in the brain, the level of nicotine in blood after a puff of smoke is critical for addictive behavior. The extent of lung uptake of nicotine will be compared between a chronic smoker and a non-smoker. It is well-known that the lung can be damaged and topologically changed by chronic tobacco smoking. We postulate higher lung uptake of nicotine in the chronic smokers which would slow nicotine pharmacokinetics in their brain. For quantification, (R)-nicotine PET can be used as a baseline, which means nonspecific

or blood flow measurement, because it has almost identical physical properties compared with (S)-nicotine.

5.3 Radiotracer chemistry

Preliminarily, [^{11}C] nicotine was synthesized using [^{11}C]methyl iodide in acetonitrile[22], followed by normal phase HPLC separation to give a moderate yield (61%). Yield was improved to 84-87% using DMF with the same conditions. However, the [^{11}C] nicotine peak in the preparative normal phase HPLC was very broad and not reproducible likely due to DMF (figure 5.3). As a result, we switched to reverse phase HPLC to improve separation and peak shape. Unfortunately, [^{11}C] nicotine at pH=7 did not elute at the expected retention time in the radiosynthesis. Interestingly, the retention time of a trace amount of nicotine shifted from 9.5 min to 15.1 min with the coinjection of nornicotine (1 mg), PMP (2 μg), while the other reaction components had no effect. This may be due to the interaction between silanol and basic nitrogen. When we use larger amounts of nicotine, this retention time shift was not observed. When the eluent pH was adjusted to 12 with triethylamine, the reproducibility and peak shape of [^{11}C] nicotine were significantly improved.

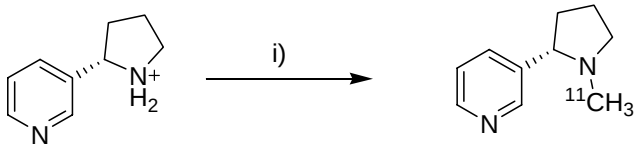

Figure 5.2 Synthesis of [^{11}C] nicotine. i, [^{11}C]methyl iodide, PMP, DMF

a) b)

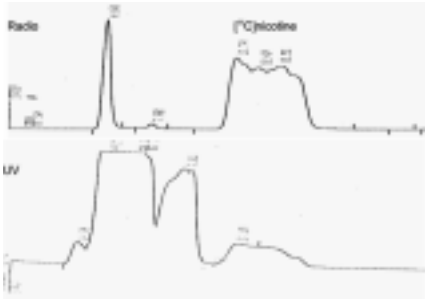

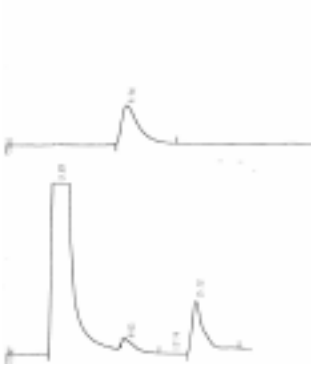

c)

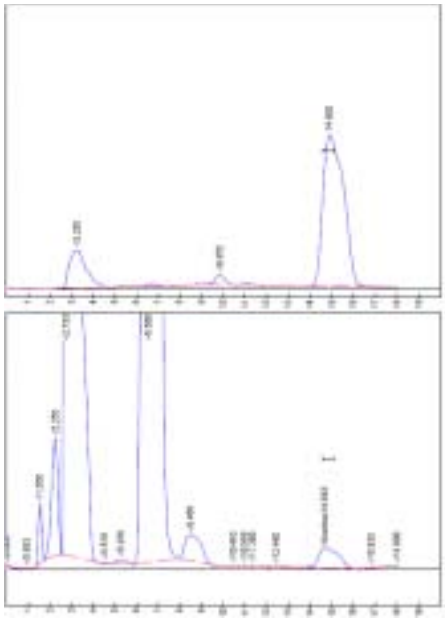

Figure 5.3 HPLC profiles of [^{11}C]nicotine in the different HPLCsystems. a, radiosynthesis (Phenomenex Sphereclone 5µ Sil; eluents, A/Methanol/Hexane(96:4:16), A=methanol/triethylamine(100/1) adjusted to pH=8 with acetic acid; UV, λ=254 nm); b, nicotine (above) and nornicotine including nicotine (below) (Phenomenex Ultremex C18, 5µ; eluent, 100 mM ammonium formate/Acetonirile/methanol = 80:10:10); c, radiosynthesis (Phenomenex Gemini C18, 5µ; eluents,methanol/triethylamine(100/1)

Log D at pH=7.4 of [^{11}C]nicotine was 0.47 (n=2) and free fraction in plasma was 88% (n=2).

Table 5.1 The radiosynthesis and properties of [^{11}C]nicotine

Radiotracer	*RY (%)*	*SA (Ci/μmol)*	*Log $D_{7.4}$*	*PPB (%)*[a]
[^{11}C]nicotine	84-87	1.5-5.2	0.47	22

[a] Free Fraction in plasma

5.4 PET studies

5.4.1 Baboon study

MKY027dy1 was a pregnant monkey which was used the PET study for nicotine transfer from mother to fetus.

Table 5.2 Summary of [^{11}C]nicotine PET studies.

Study #	Baboon	Subject	Brain/Torso
Pharmacokinetics and dosimetry			
BEJ281dy1	Riley	baboon	Torso
BEJ281dy2	Riley	baboon	brain
BEJ283 dy1	Chloe	baboon	brain
BEJ283 dy2	Chloe	baboon	Torso
BEJ344dy1	Chloe	baboon	Torso
BEJ344dy2	Chloe	baboon	Whole body
Prenatal nicotine transfer			
MKY027dy1	Daisy	Macaque	Whole body

5.4.2 Pharmacokinetics

Brain uptake and clearance of [^{11}C]nicotine are fast and high (0.032-0.035 % ID/cc) as reported by Halldin et al. C-11 was widely distributed in the whole brain region. When cerebellum was used as a reference region, distribution volume ratio (DVR) for thalamus calculated by Logan graphical analysis was around 1.1, which means slightly higher binding potential in thalamus. However, according to the baboon study with [^{18}F] NFEP (Figure 1.4) performed by our group, the distribution volume radio (DVR) should be much higher-up to 3-4.[28] Since nicotine is not a substrate for p-glycoprotein[29], a main reason for low signal-to-noise may be due to low affinity to nicotinic binding sites. It was known that the major metabolite, cotinine has negligible BBB permeability.

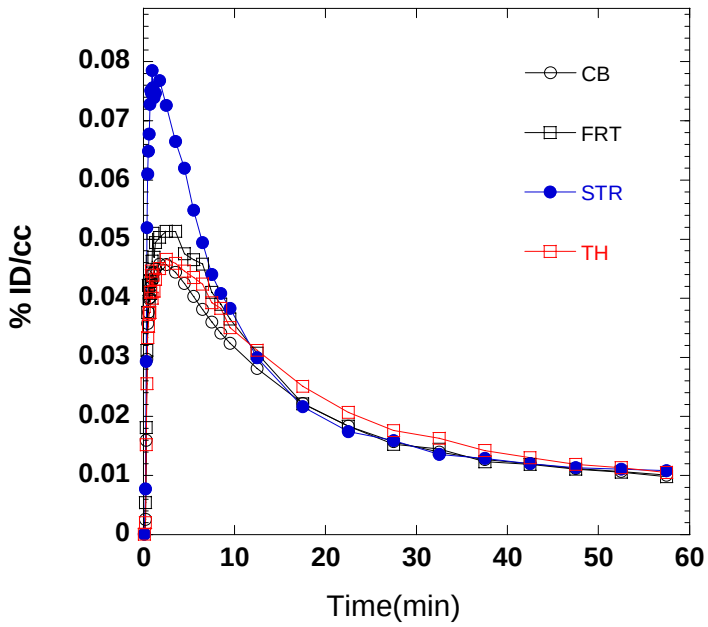

Figure 5.4 The time-activity curves for [^{11}C]nicotine in the baboon brain

Peripherally, kidney uptake for [^{11}C]nicotine peaked high, indicating excretion to the bladder.[30] High C-11 uptake of liver was maintained to the end the study. In a previous report of human smokers' autopsy samples, high nicotine levels were observed in the liver, kidney, spleen, and lung.[31]

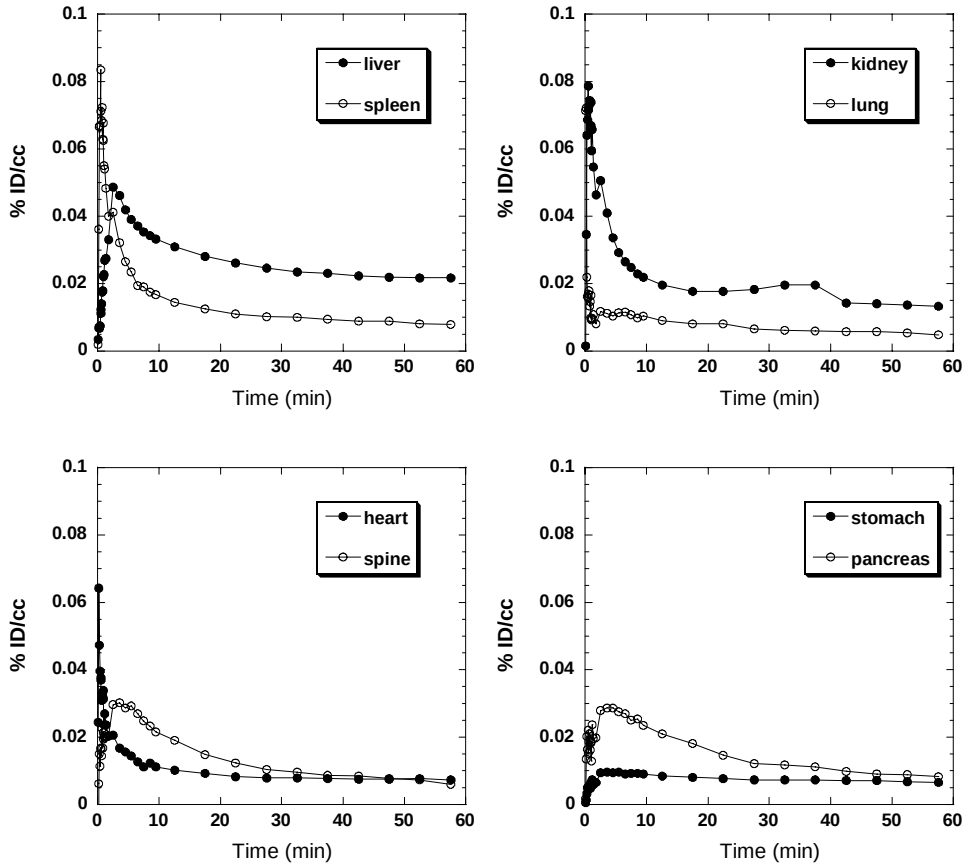

Figure 5.5 The time-activity curve for peripheral organs in the baboon

5.4.3 Dosimetry

The specific objective of this study is to obtain the absorbed radioactivity dose for each organ or tissue in the baboon, which will be applied to dosimetry for human [^{11}C]nicotine PET studies, ensuring human radiation safety. The order of the absorption dose from highest to lowest was kidney, spleen, liver, lung, heart, lung.

Table 5.3 The dosimetry of [^{11}C]nicotine in the baboon

Organs	*Residence Times (hr)*	*Doses (mrem/mCi)*
Brain	0.0137	7.90
Heart Wall	0.0089	22.8
Kidneys	0.0552	152.0
Liver	0.0850	36.5
Lung	0.0256	21.0
Pancreas	0.0010	8.7
Spleen	0.0057	25.4
Remainder	0.2880	-

5.4.4 Pregnant macaque study

A [^{11}C] nicotine PET study was performed in the whole body of a pregnant monkey, *Mecaca radiate*. C-11 transfer from mother to fetus was clearly observed in placenta, liver and brain of fetus. The pharmacokinetics of ^{11}C in fetus had a different distribution. The brain entry and clearance in fetus was slower than in the mother. This experiment proves indirectly that smoking during pregnancy results in transfer of nicotine from the mother to the fetal brain.

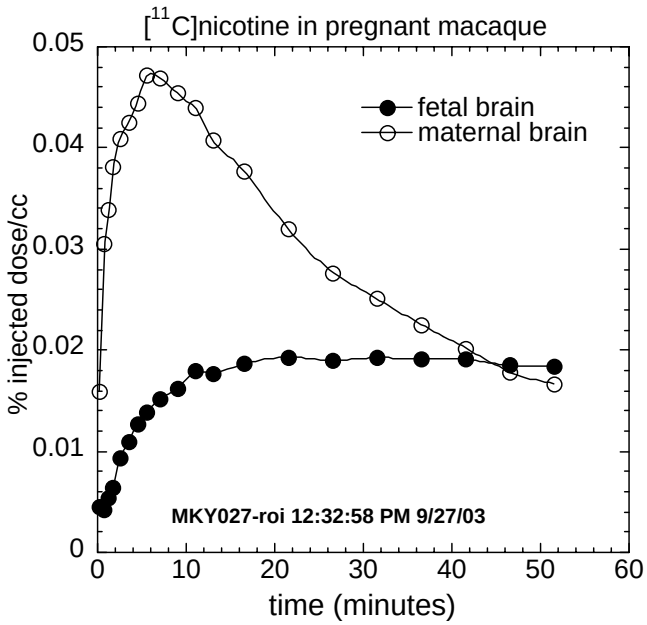

Figure 5.6 The time-activity curve of [^{11}C]nicotine in the pregnant macaque

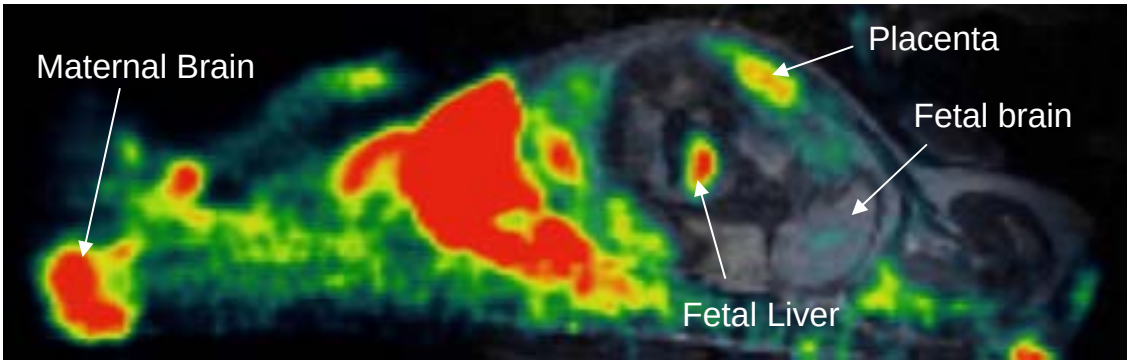

Figure 5.7 The PET image in baboon summed from time of injection.

5.5 Materials and Experimental Methods

The two enantiomeric forms of pure nicotine camsylate were generously given by Dr. N. Castagnoli.

5.5.1 Radiosynthesis

[^{11}C] nicotine :(S)-nornicotine biscamsylate (2.0mg), 1,2,2,6,6-pentamethyl-piperidine (2 μl) was dissolved with DMF (300 μl) in a reaction vessel. The mixture was cooled in a bath (dry ice/acetonitrile, -42 ^{o}C) prior to trapping. After [^{11}C]methyl iodide was transferred and trapped, the reaction vessel was heated at 130 ^{o}C for 5 min. The vessel was cooled in the bath (dry ice/acetonitrile) for 5 sec; the reaction mixture was diluted and injected on a semi-preparative HPLC (Phenomenex Gemini, 250 mm x 10mm, 5 μ). [^{11}C]-nicotine is eluted 14.9 minutes. The collected portion of [^{11}C]-nicotine was transferred to a round bottom flask containing hydrochloric acid (0.1 N, 20 μl). The solvent was removed by azeotropic evaporation with acetonitrile using a rorary evaporator. The residual product was diluted with sterile water (4 ml), and filtered through an Acrodisc 13-mm Syringe Filter with 0.2 μm HT 208 Tuffryn Membrane (Pall Corporation, Ann Arbor, MI) into a sterile vial for delivery. [^{11}C]-S-nicotine was injected to an anesthetized baboon. The purity analysis of product is determined using TLC (alumina-coated plate, ethyl acetate:hexane=1:2, RF=0.64) and HPLC, which was congruent with an authentic standard of nicotine co-spotted with the sample and detected by UV (λ= 254 nm).

5.5.2 Baboon study

Baboon studies were performed by the similar procedure as Chapter 2.6.4. The whole body scan of BEJ344dy2 was performed 4 min after injection of [^{11}C] nicotine from brain. According to the reported protocol[32], MR image of the pregnant macaque study and PET image was coregistered.

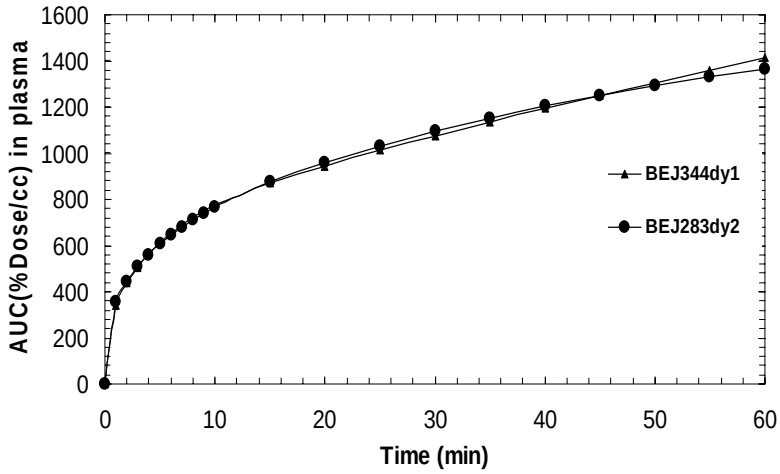

Figure 5.8 The area under the curves (AUC) in the plasma for [^{11}C]nicotine

5.6 References

1. Haas, L. F. Nicot,Jean 1530-1600. *Journal of Neurology Neurosurgery and Psychiatry* **1992,** 55, 430-430.

2. Posselt, W.; Reimann, L. Chemische Untersuchungen des Tabaks und Darstellung des eigenhumlichen wirksamen Principes dieser Pflanze. *Geigers Magazin der Pharmazie* **1828,** 24, 138 -61.

3. Pinner, A. Die Constitution des Alkaloids. *Berichte Der Deutschen Chemischen Gesellschaft* **1893,** 27, 292.

4. Pictet, A.; Rotschy, A. Synthese des nicotins. *Berichte Der Deutschen Chemischen Gesellschaft* **1904,** 37, 1225-1235.

5. Kim, H. S.; Jeffrey, G. A. Crystal Structure of a 1-1 Nicotine-salicylic acid complex (nicotinyl salicylate). *Acta Crystallographica Section B-Structural Crystallography and Crystal Chemistry* **1971,** B 27, 1123-&.

6. Koo, C. H.; Kim, H. S. The Crystal Structure of Nicotine dihydroiodide. *Daehan Hwahak Hwoejee* **1965,** 9, 134.

7. Chavdarian, C. G.; Sanders, E. B.; Bassfield, R. L. Synthesis of Optically-active nicotinoids. *Journal of Organic Chemistry* **1982,** 47, 1069-1073.

8. Girard, S.; Robins, R. J.; Villieras, J.; Lebreton, J. A Short and efficient synthesis of unnatural (r)-nicotine. *Tetrahedron Letters* **2000,** 41, 9245-9249.

9. Welter, C.; Moreno, R. M.; Streiff, S.; Helmchen, G. Enantioselective synthesis of (+)(r)- and (-)(s)-nicotine based on Ir- catalysed allylic amination. *Organic & Biomolecular Chemistry* **2005,** 3, 3266-3268.

10. Sekhon, H. S.; Keller, J. A.; Benowitz, N. L.; Spindel, E. R. Prenatal nicotine exposure alters pulmonary function in newborn Rhesus Monkeys. In 2001; Vol. 164, pp 989-994.

11. Hecht, S. S.; Hochalter, J. B.; Villalta, P. W.; Murphy, S. E. 2'-Hydroxylation of nicotine by cytochrome P450 2A6 and human liver microsomes: formation of a lung carcinogen precursor. *PNAS* **2000,** 97, 12493-12497.

12. Dasgupta, P.; Kinkade, R.; Joshi, B.; DeCook, C.; Haura, E.; Chellappan, S. Nicotine inhibits apoptosis induced by chemotherapeutic drugs by up-regulating xiap and survivin. *PNAS* **2006,** 103, 6332-6337.

13. Lockman, P. R.; Van der Schyf, C. J.; Abbruscato, T. J.; Allen, D. D. Chronic nicotine exposure alters blood-brain barrier permeability and diminishes brain uptake of methyllycaconitine. *Journal of Neurochemistry* **2005,** 94, 37-44.

14. Mansvelder, H. D.; Keath, J. R.; McGehee, D. S. Synaptic mechanisms underlie nicotine-induced excitability of brain reward areas. *Neuron* **2002,** 33, 905-919.

15. Gopalakrishnan, M.; Donnelly-Roberts, D. L. Nicotine: Therapeutic prospects? *Pharmaceutical News* **1998,** 5, 16-20.

16. Breese, C. R.; Marks, M. J.; Logel, J.; Adams, C. E.; Sullivan, B.; Collins, A. C.; Leonard, S. Effect of smoking history on [3h]nicotine binding in human postmortem brain. *J Pharmacol Exp Ther* **1997,** 282, 7-13.

17. Nordberg, A. Correction. *Drug and Alcohol Dependence* **1986,** 16, 383-383.

18. Flynn, D. D.; Mash, D. C. Characterization of l-[h-3]nicotine binding in human cerebral-cortex - comparison between alzheimers-disease and the normal. *Journal of Neurochemistry* **1986,** 47, 1948-1954.

19. Whitehouse, P. J.; Martino, A. M.; Wagster, M. V.; Price, D. L.; Mayeux, R.; Atack, J. R.; Kellar, K. J. Reductions in [h-3] nicotinic acetylcholine binding in alzheimers-disease and parkinsons-disease - an autoradiographic study. *Neurology* **1988,** 38, 720-723.

20. Nordberg, A.; Alafuzoff, I.; Winblad, B. Nicotinic and muscarinic subtypes in the human brain - changes with aging and dementia. *Journal of Neuroscience Research* **1992,** 31, 103-111.

21. Langstrom, B.; Antoni, G.; Halldin, C.; Svard, H.; Bergson, G. Synthesis of some c-11-labeled alkaloids. *Chemica Scripta* **1982,** 20, 46-48.

22. Halldin, C.; Nagren, K.; Swahn, C. G.; Langstrom, B.; Nyback, H. (S)[C-11]Nicotine and (r)-[c-11]nicotine and the metabolite (r/s)-[c-11]cotinine - preparation, metabolite studies and invivo distribution in the human brain using PET. *Nuclear Medicine and Biology* **1992,** 19, 871-880.

23. Nordberg, A.; Hartvig, P.; Lundqvist, H.; Antoni, G.; Ulin, J.; Langstrom, B. Uptake and regional distribution of (+)-(r)-n-[methyl-c-11]-nicotine and (-)-(s)-n-[methyl-c-11]-nicotine in the brains of rhesus-monkey - an attempt to study nicotinic receptors in vivo. *Journal of Neural Transmission-Parkinsons Disease and Dementia Section* **1989,** 1, 195-205.

24. Kadir, A.; Almkvist, O.; Wall, A.; Langstrom, B.; Nordberg, A. PET imaging of cortical C-11-nicotine binding correlates with the cognitive function of attention in Alzheimer's disease. *Psychopharmacology* **2006,** 188, 509-520.

25. Kadir, A.; Darreh-Shori, T.; Almkvist, O.; Wall, A.; Langstrom, B.; Nordberg, A. Changes in brain C-11-nicotine binding sites in patients with mild Alzheimer's disease following rivastigmine treatment as assessed by PET. *Psychopharmacology* **2007,** 191, 1005-1014.

26. Rose, J. E.; Behm, F. M.; Westman, E. C.; Coleman, R. E. Arterial nicotine kinetics during cigarette smoking and intravenous nicotine administration: implications for addiction. *Drug and Alcohol Dependence* **1999,** 56, 99-107.

27. Fowler, J. S.; Logan, J.; Wang, G.-J.; Volkow, N. D.; Telang, F.; Zhu, W.; Franceschi, D.; Shea, C.; Garza, V.; Xu, Y.; Ding, Y.-S.; Alexoff, D.; Warner, D.; Netusil, N.; Carter, P.; Jayne, M.; King, P.; Vaska, P. Comparison of monoamine oxidase a in peripheral organs in nonsmokers and smokers. *J Nucl Med* **2005,** 46, 1414-1420.

28. Ding, Y. S.; Logan, J.; Bermel, R.; Garza, V.; Rice, O.; Fowler, J. S.; Volkow, N. D. Dopamine receptor-mediated regulation of striatal cholinergic activity: positron emission tomography studies with norchloro[18F]fluoroepibatidine. *J Neurochem* **2000,** 74, 1514-21.

29. Wang, J. S.; Markowitz, J. S.; Donovan, J. L.; DeVane, C. L. P-glycoprotein does not actively transport nicotine and cotinine. *Addiction Biology* **2005,** 10, 127-129.

30. Hukkanen, J.; Jacob, P., III; Benowitz, N. L. Metabolism and disposition kinetics of nicotine. *Pharmacol Rev* **2005,** 57, 79-115.

31. Urakawa, N.; Nagata, T.; Kudo, K.; Kimura, K.; Imamura, T. Simultaneous determination of nicotine and cotinine in various human tissues using capillary gas chromatography/mass spectrometry. *International Journal of Legal Medicine* **1994,** 106, 232-236.

32. Benveniste, H.; Fowler, J. S.; Rooney, W.; Ding, Y. S.; Baumann, A. L.; Moller, D. H.; Du, C.; Backus, W.; Logan, J.; Carter, P.; Coplan, J. D.; Biegon, A.;

Rosenblum, L.; Scharf, B.; Gatley, J. S.; Volkow, N. D. Maternal and fetal 11C-cocaine uptake and kinetics measured in vivo by combined PET and MRI in pregnant nonhuman primates. *J Nucl Med* **2005,** 46, 312-20.

Appendix

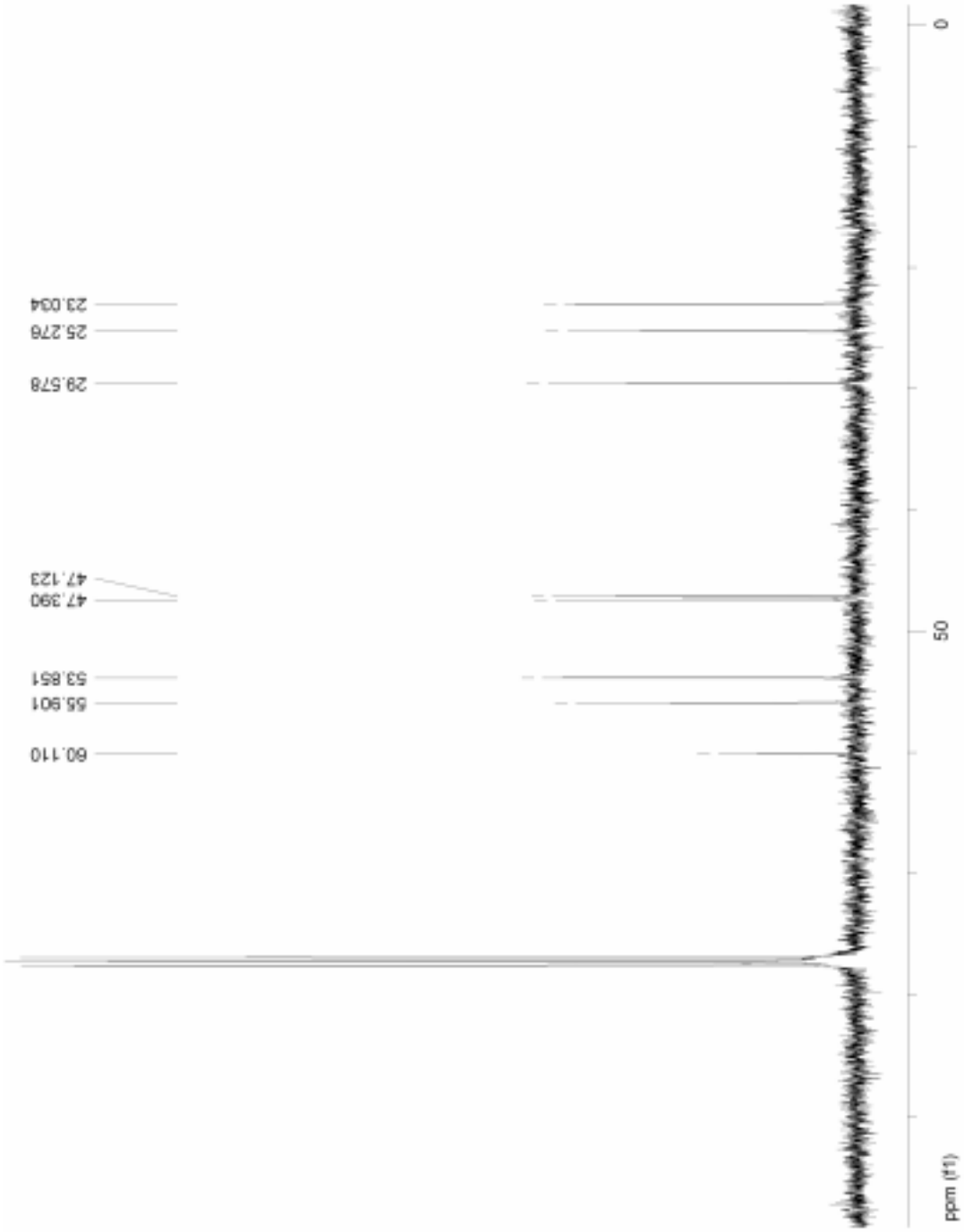

Figure A.1 ^{13}C-NMR spectrum of compound **3-4** in $^{*}CDCl_3$ (400 MHz).

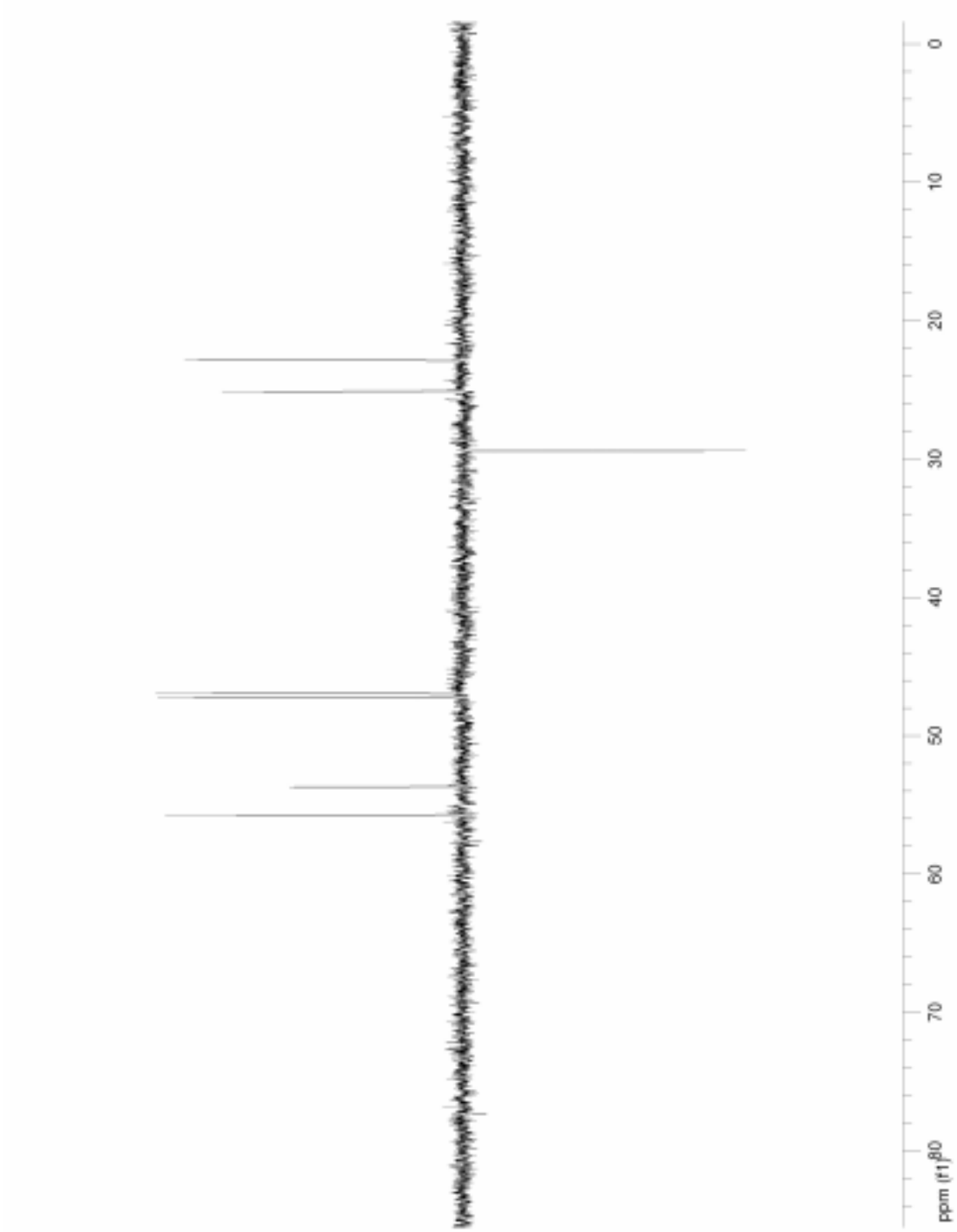

Figure A.2 DEPT spectrum of compound **3-4** in $^{*}CDCl_3$ (400 MHz).

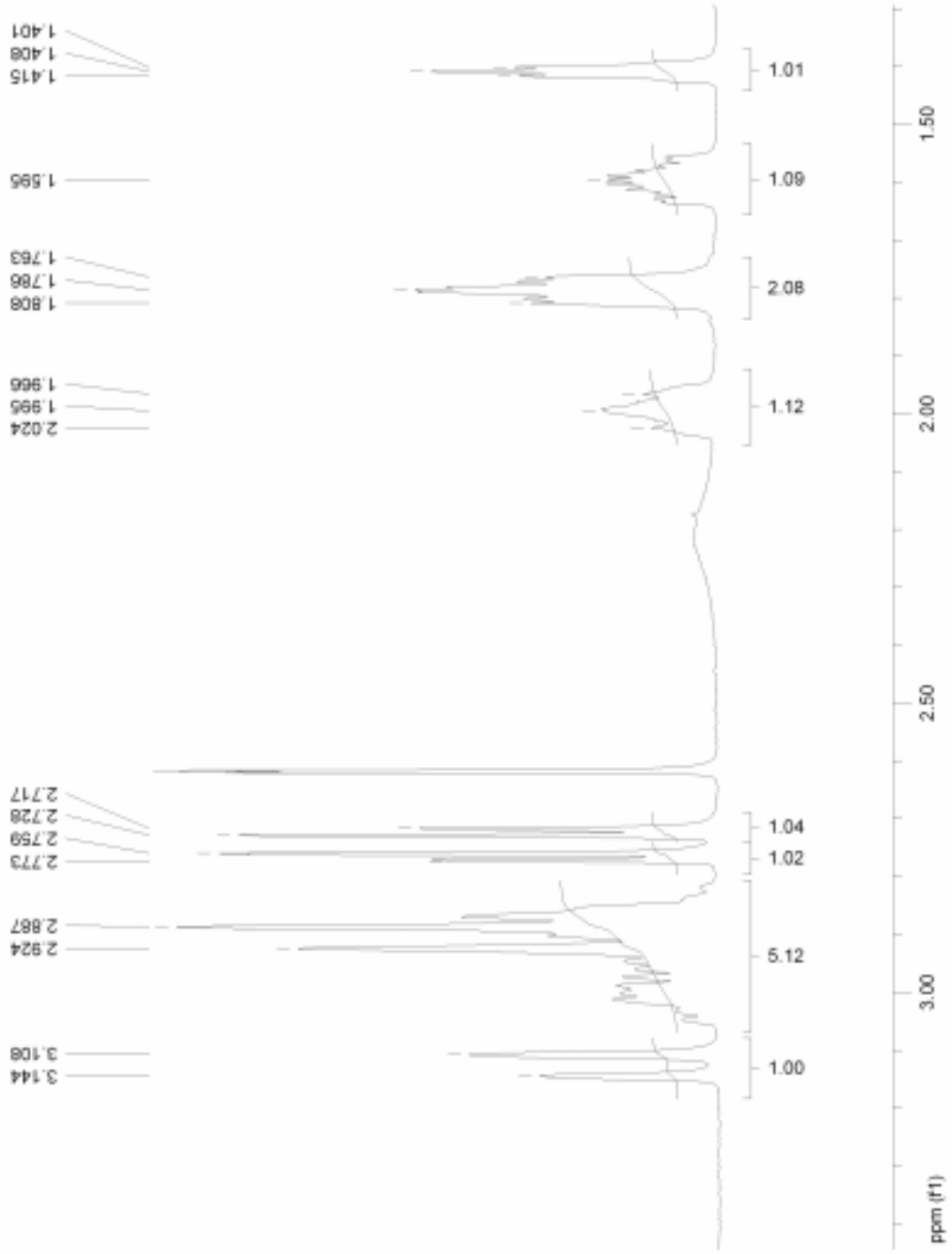

Figure A.3 ^{1}H-NMR spectrum of compound **3-4** in $^{*}CDCl_3$ (400 MHz).

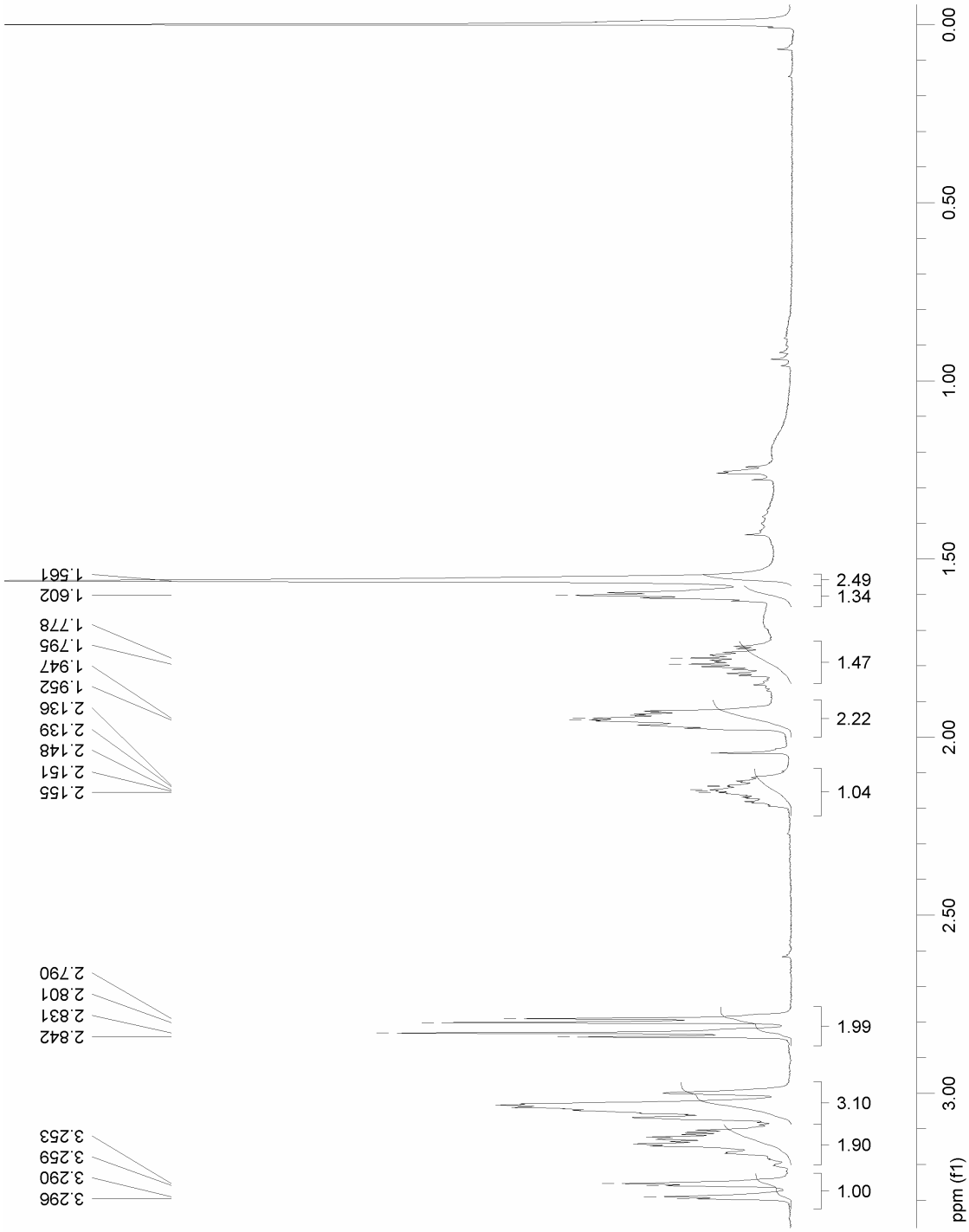

Figure A.4 ^{1}H-NMR spectrum of compound **3-5** in $^{*}CDCl_3$ (400 MHz).

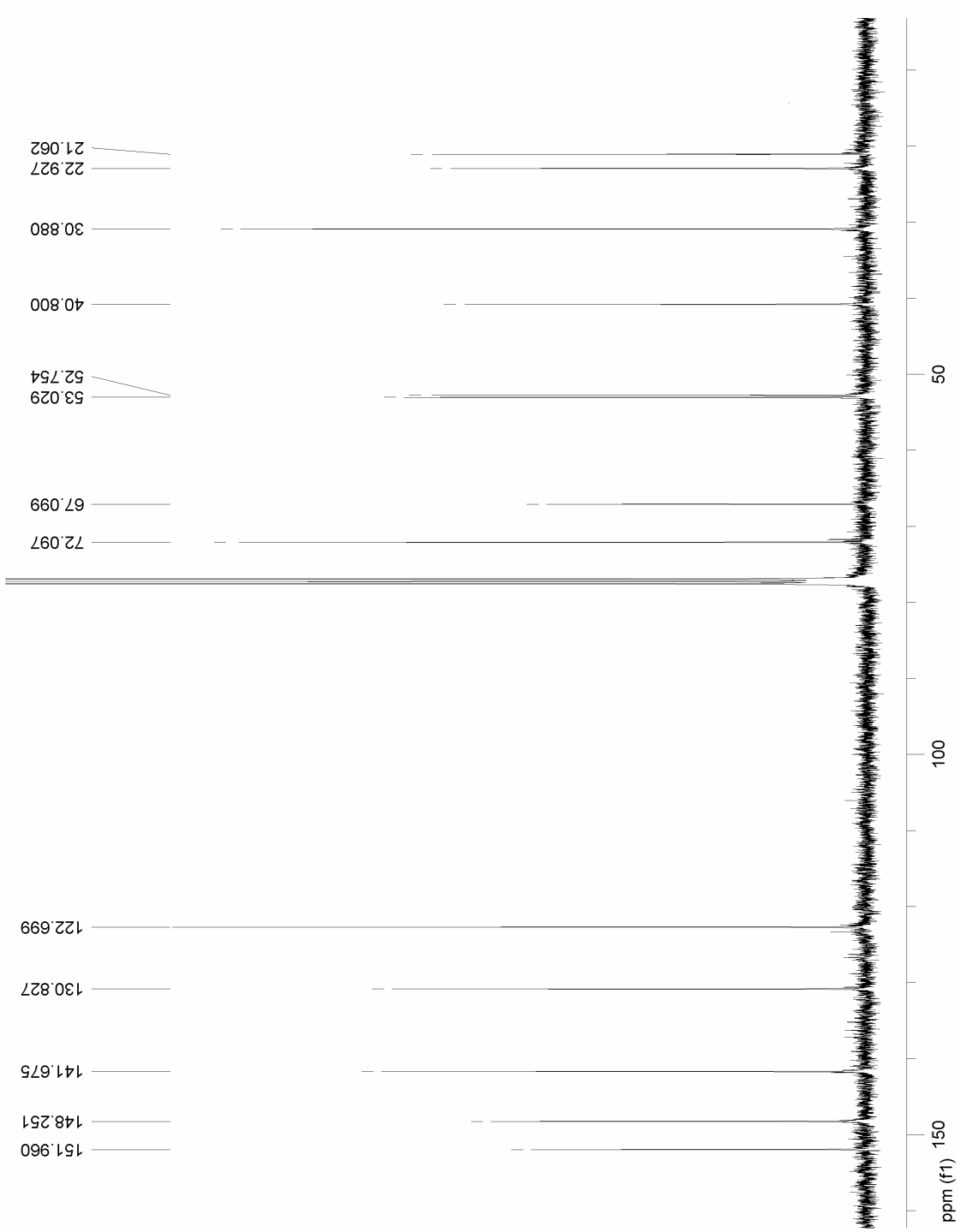

Figure A.5 ^{13}C-NMR spectrum of compound **3-6** in $^{*}CDCl_3$ (400 MHz).

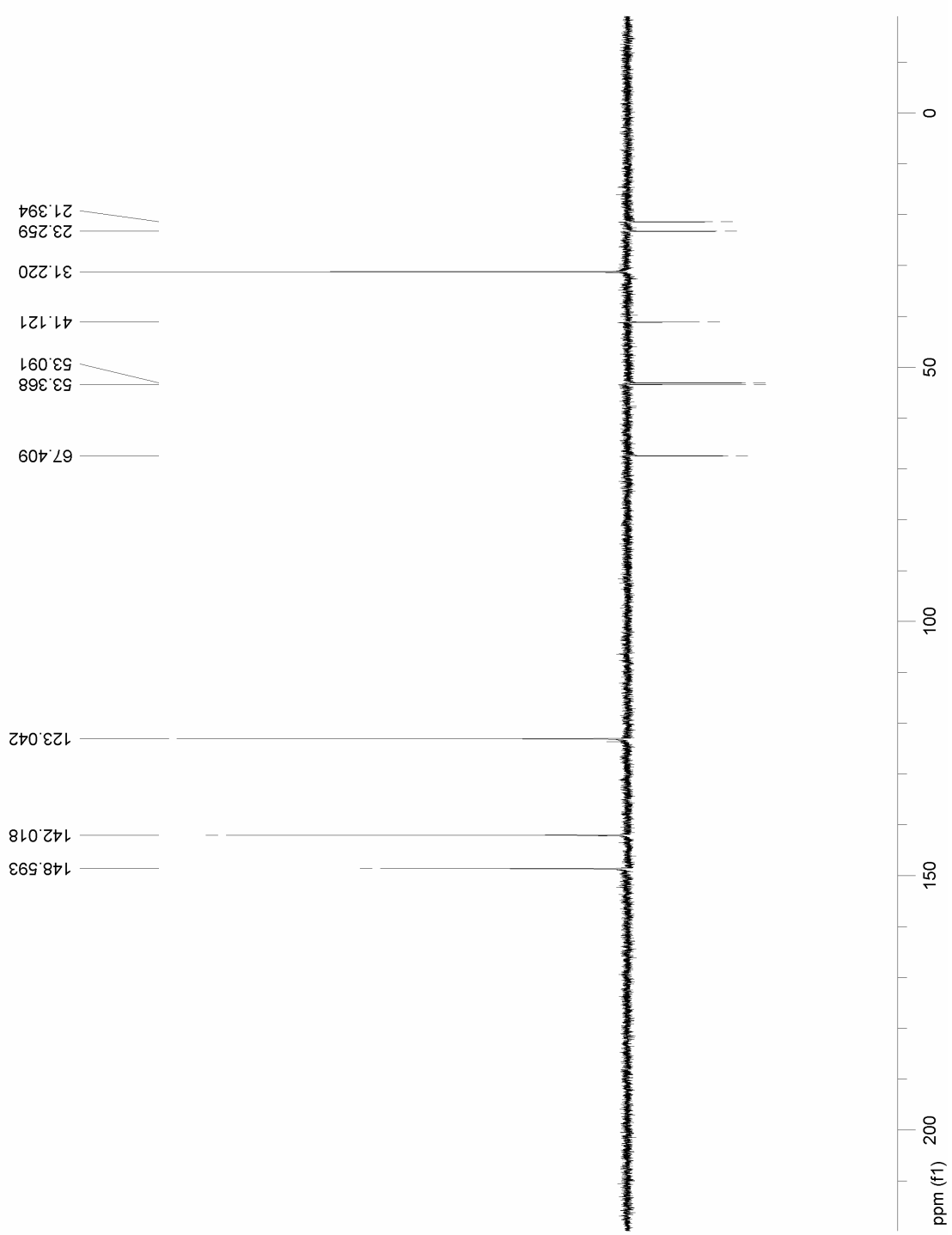

Figure A.6 DEPT spectrum of compound **3-6** in $^{*}CDCl_3$ (400 MHz).

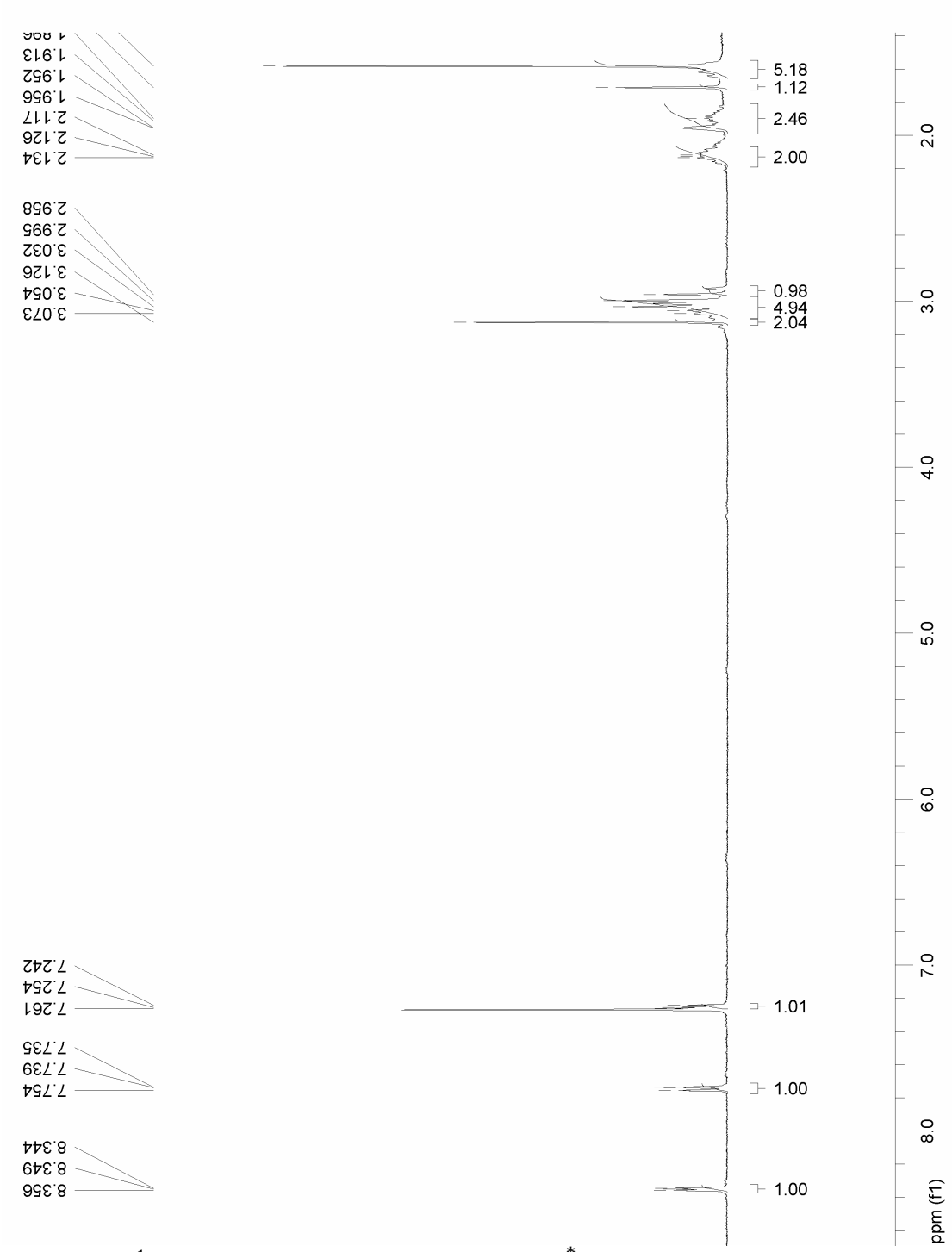

Figure A.7 ^{1}H-NMR spectrum of compound **3-6** in $^{*}CDCl_3$ (400 MHz).

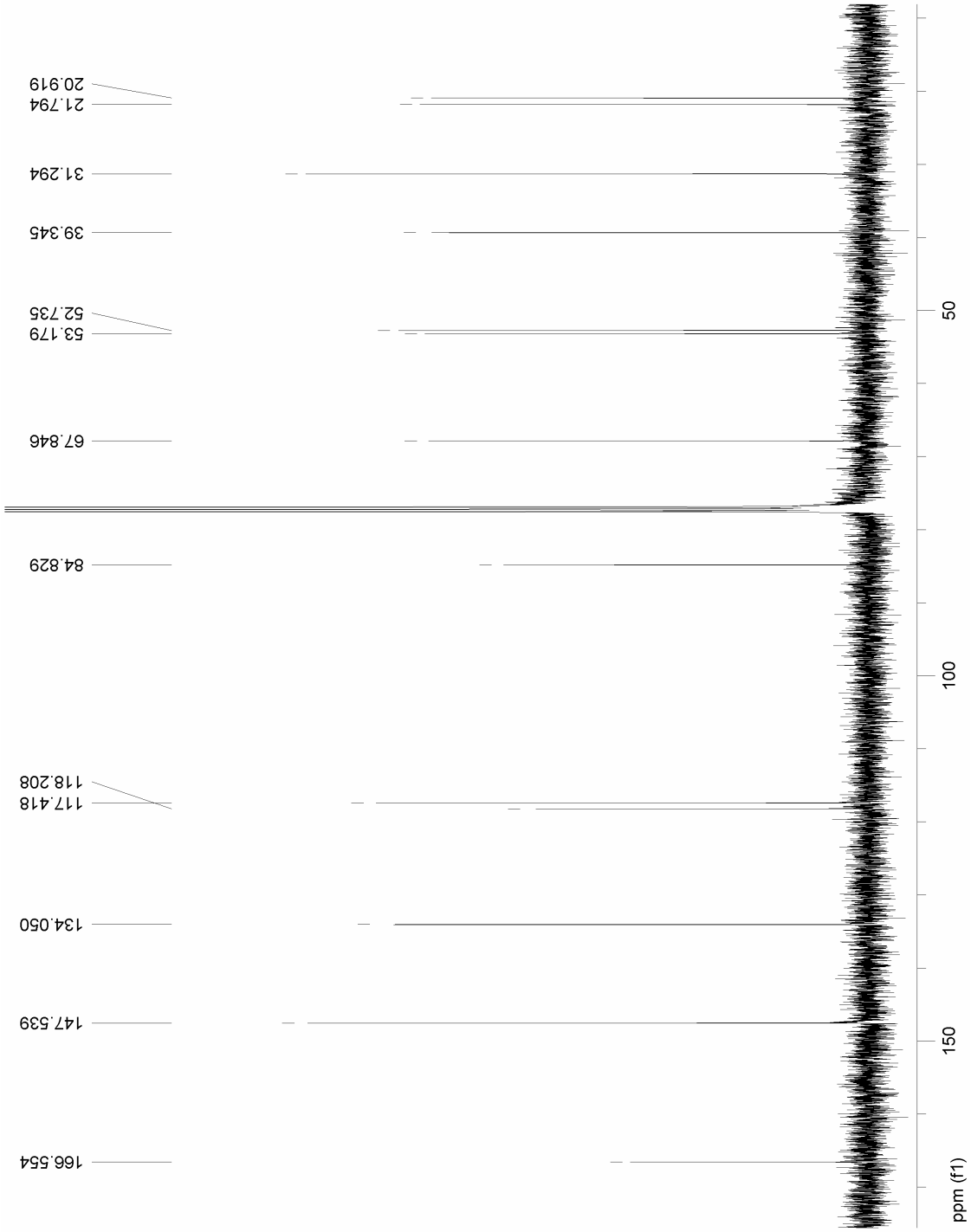

Figure A.8 ^{13}C-NMR spectrum of compound **3-7** in $^{*}CDCl_3$ (400 MHz).

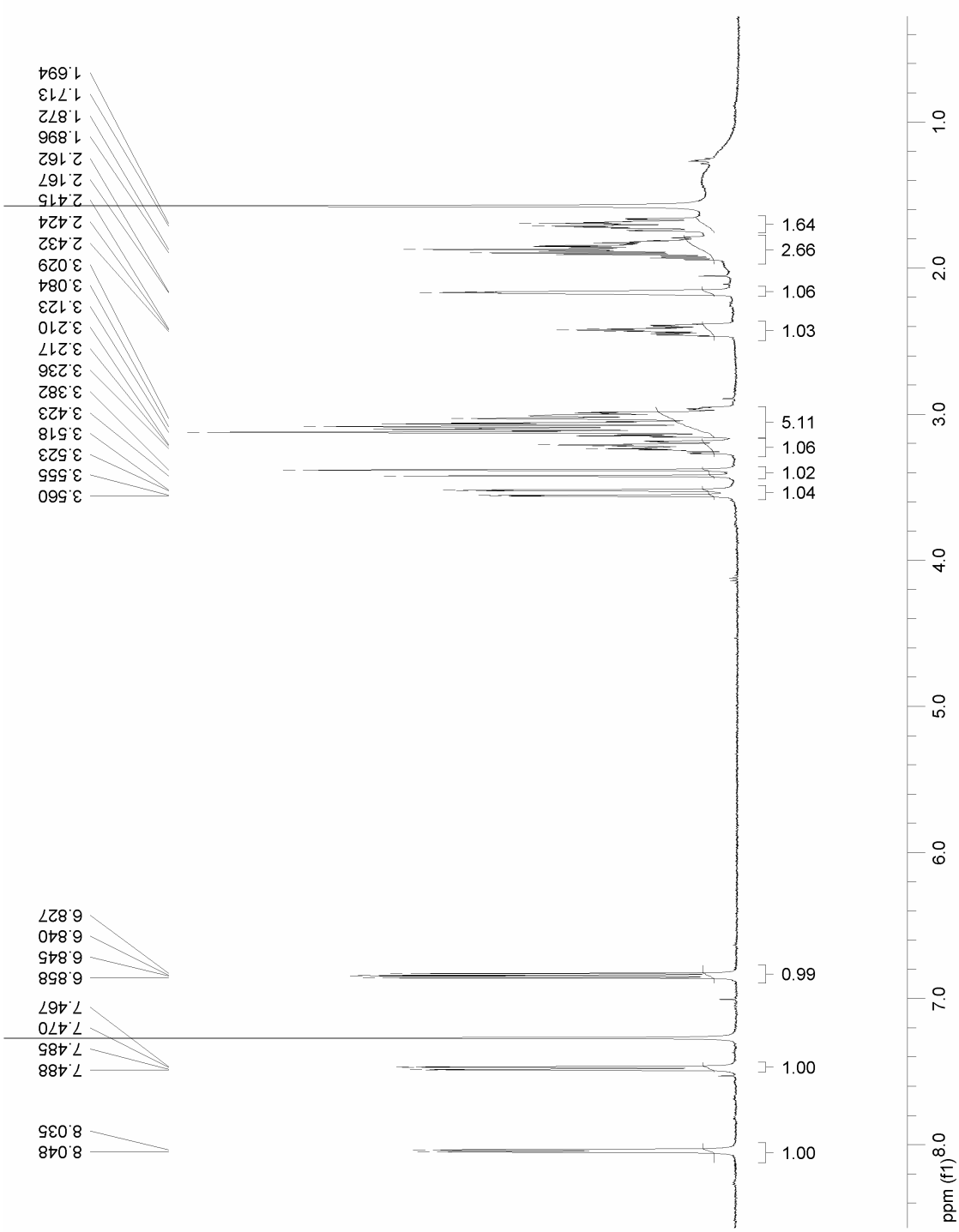

Figure A.9 ^{1}H-NMR spectrum of compound **3-7** in $^{*}CDCl_3$ (400 MHz).

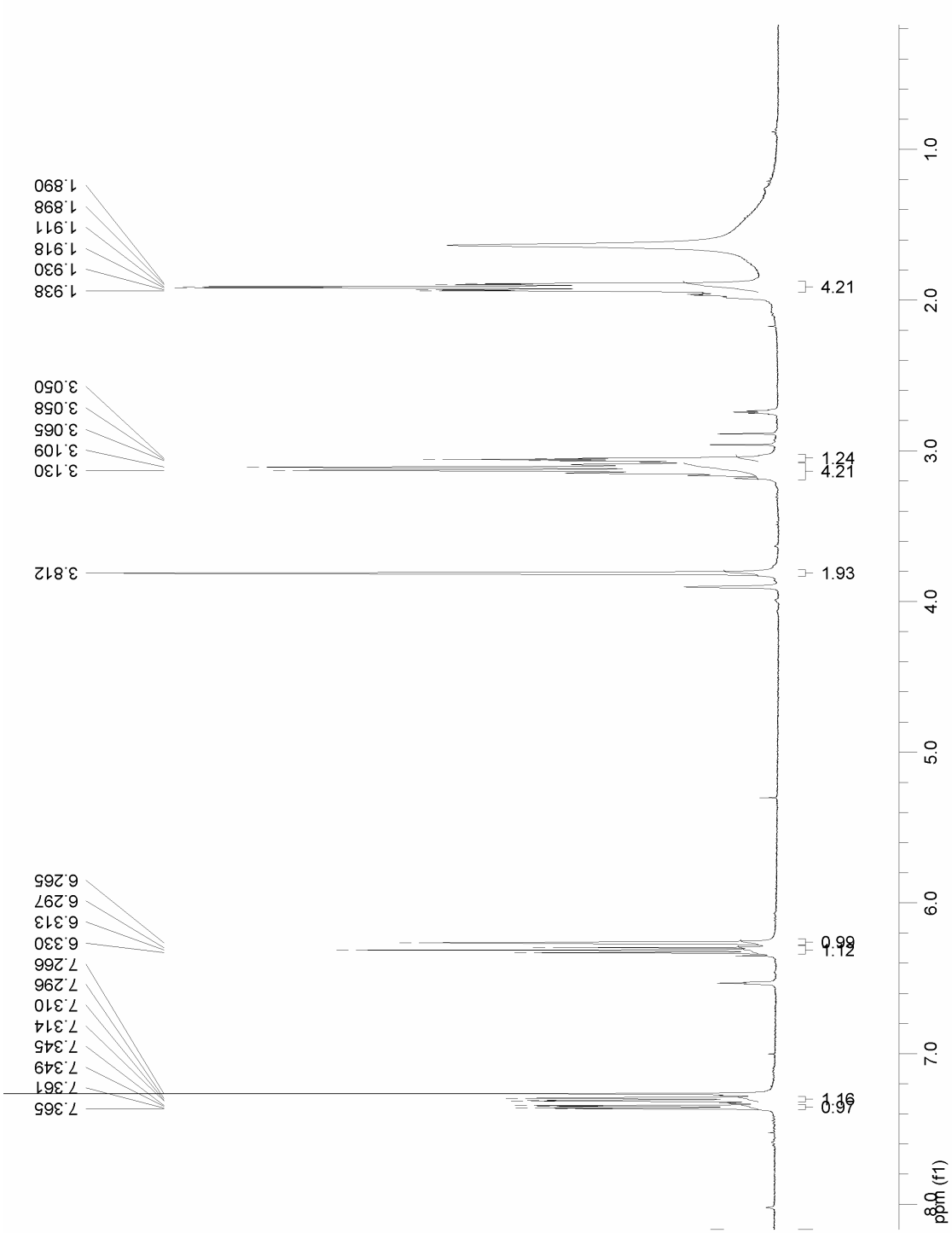

Figure A.10 ^{1}H-NMR spectrum of compound **3-30** in $^{*}CDCl_3$ (400 MHz).

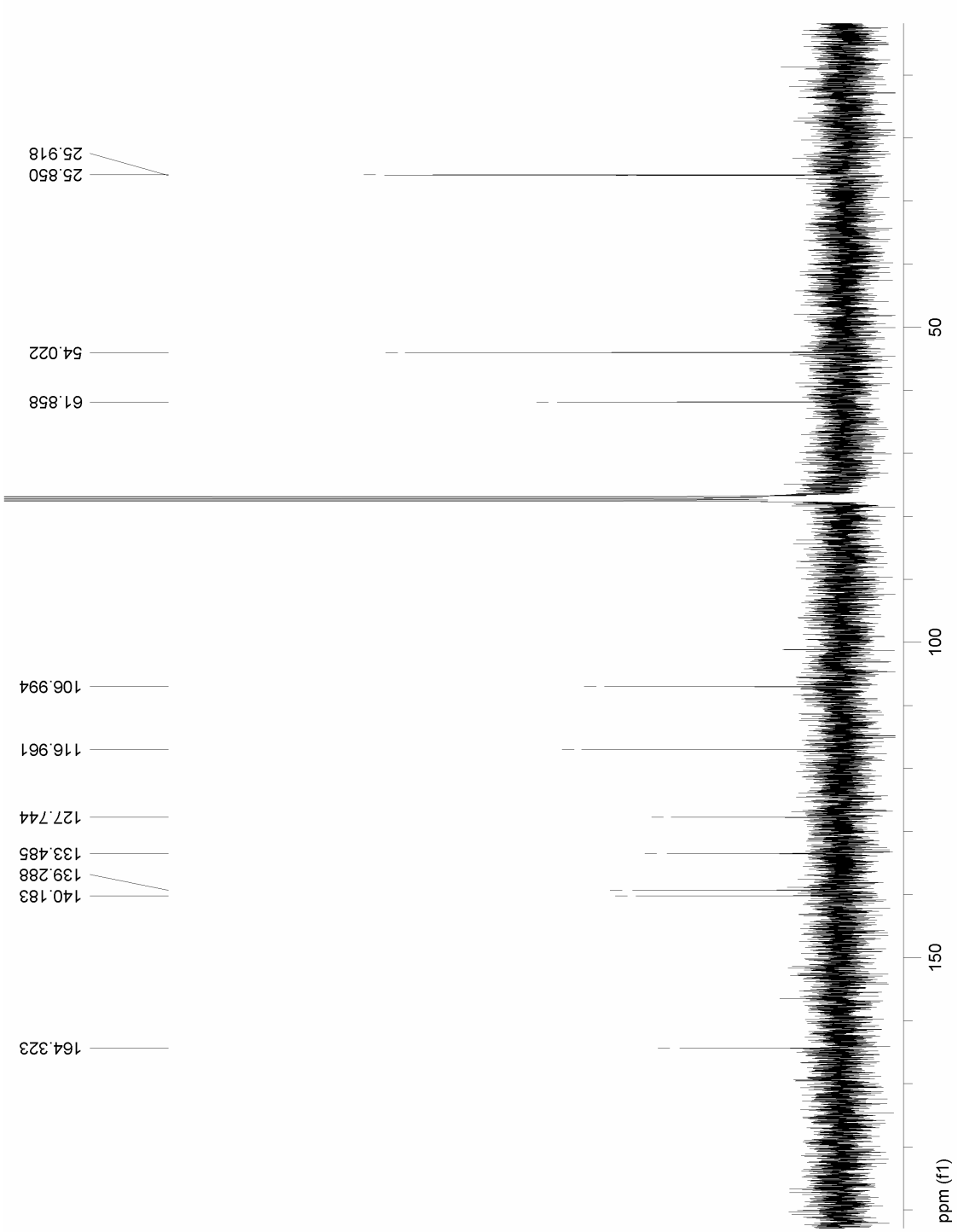

Figure A.11 ^{13}C-NMR spectrum of compound **3-30** in $^{*}CDCl_3$ (400 MHz).

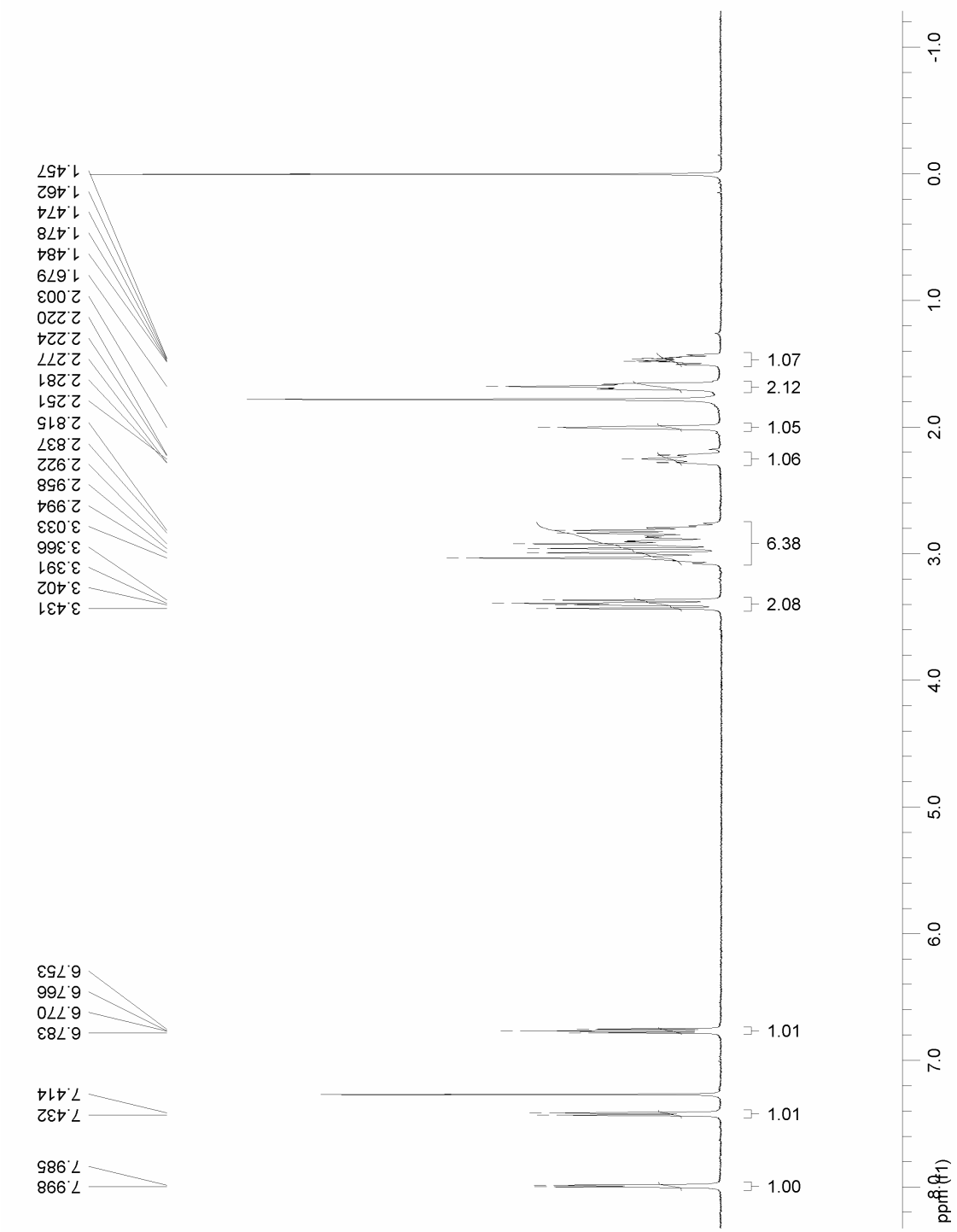

Figure A.12 ^{1}H-NMR spectrum of compound **3-8** in $^{*}CDCl_3$ (400 MHz).

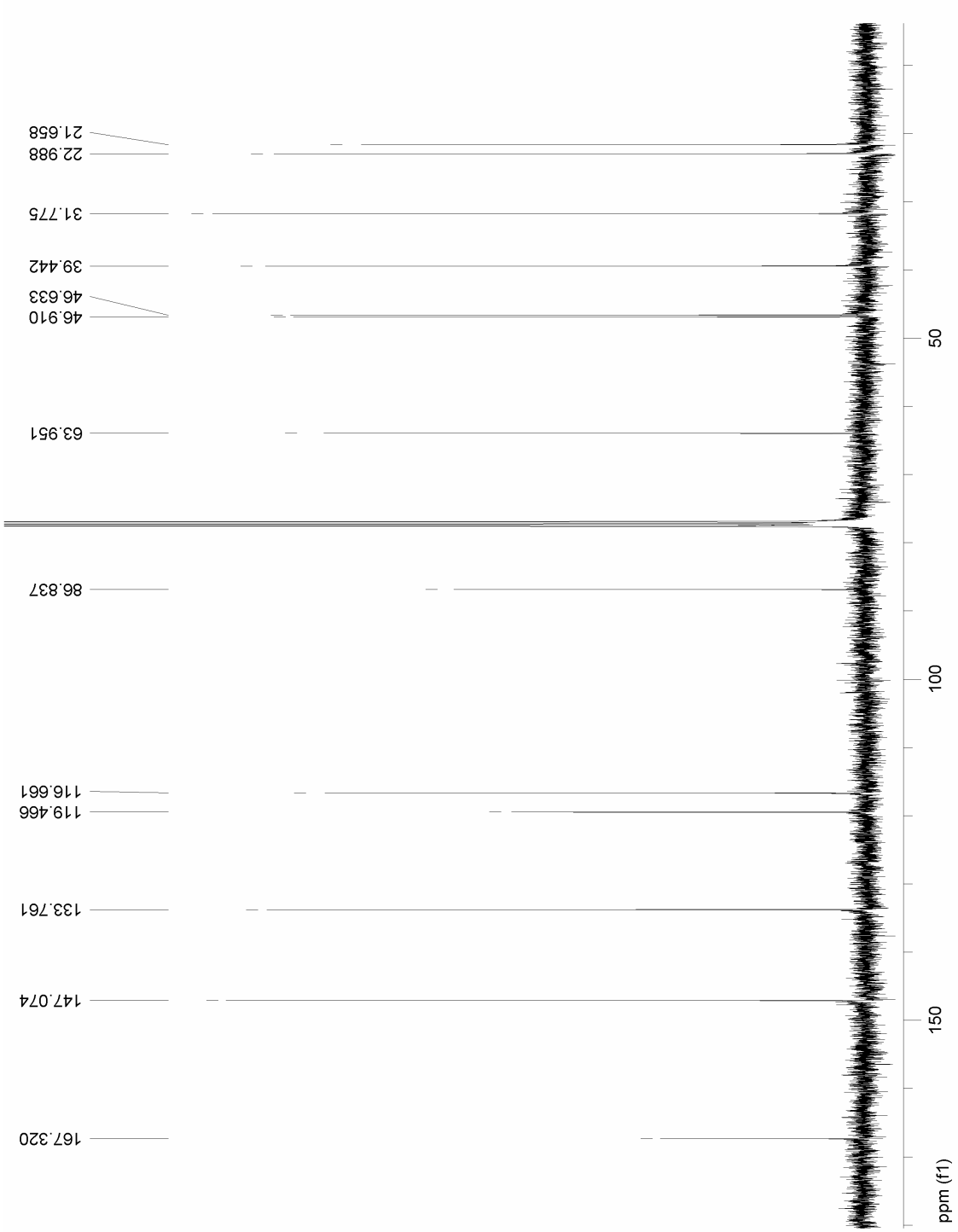

Figure A.13 ^{13}C-NMR spectrum of compound **3-8** in $^{*}CDCl_3$ (400 MHz).

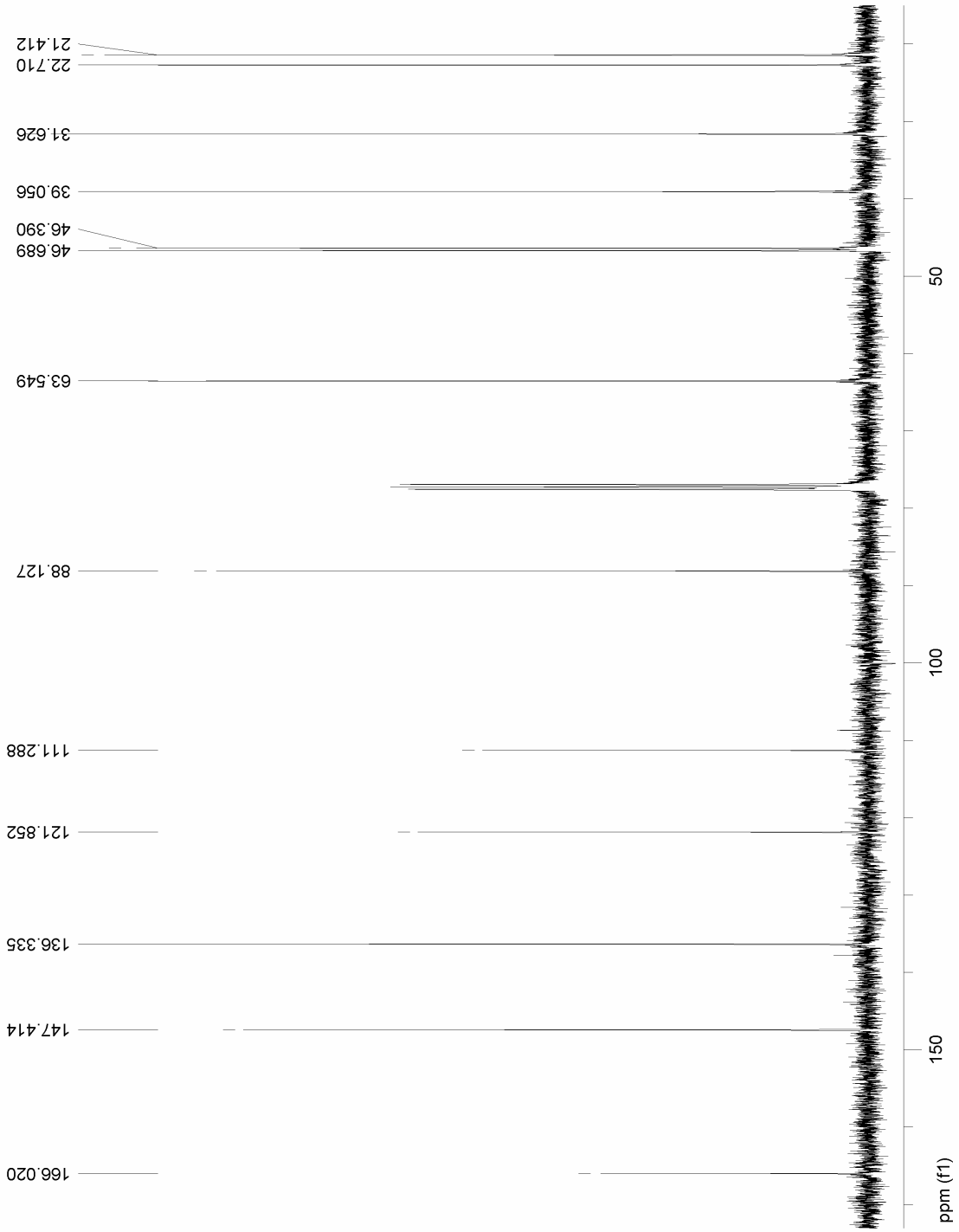

Figure A.14 ^{13}C-NMR spectrum of compound **3-9** in $^{*}CDCl_3$ (400 MHz).

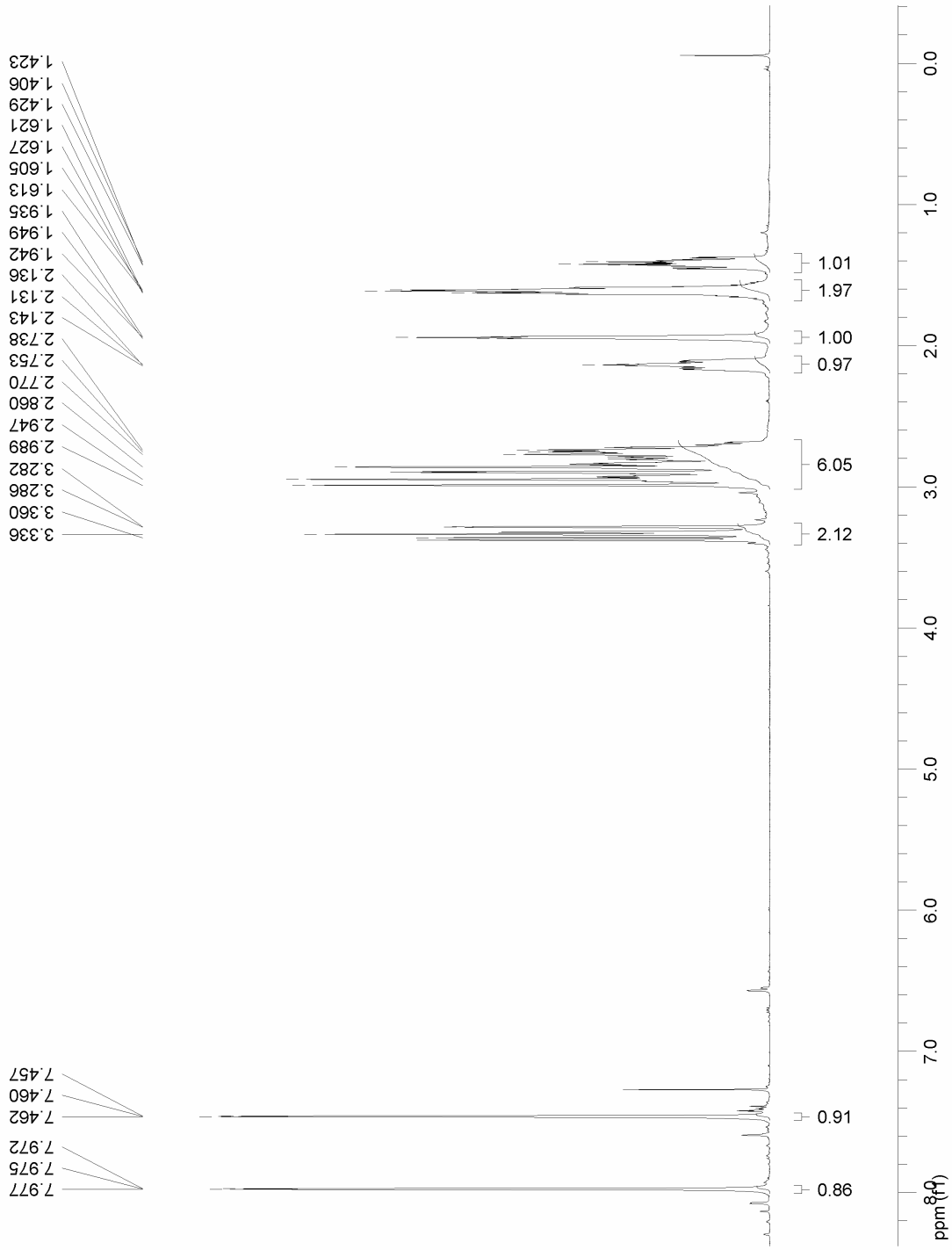

Figure A.15 ^{1}H-NMR spectrum of compound **3-9** in $^{*}CDCl_3$ (400 MHz).
$^{\omega}$ denotes signal from H_2O.

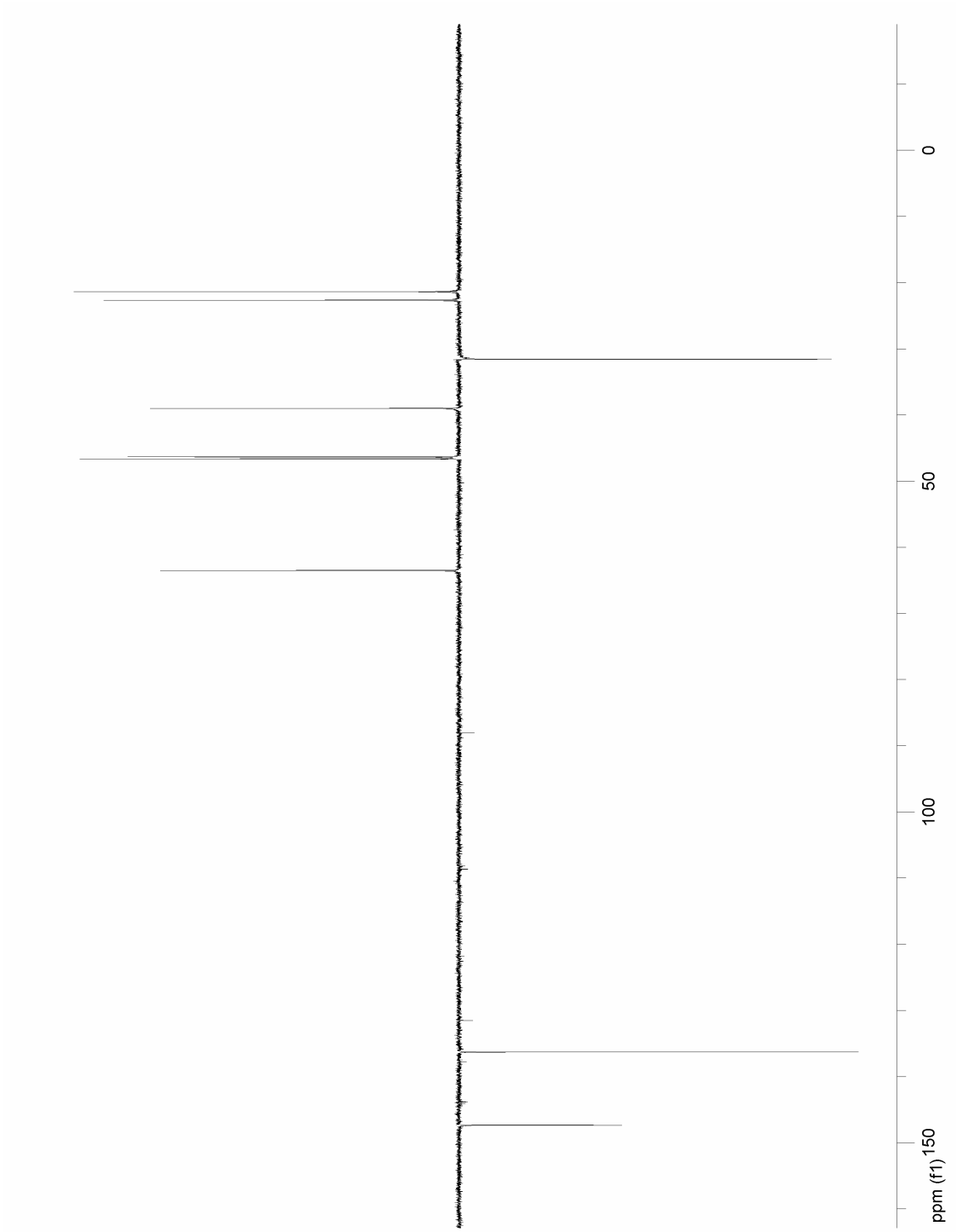

Figure A.16 DEPT spectrum of compound **3-9** in $^{*}CDCl_3$ (400 MHz).
$^{\omega}$ denotes signal from H_2O.

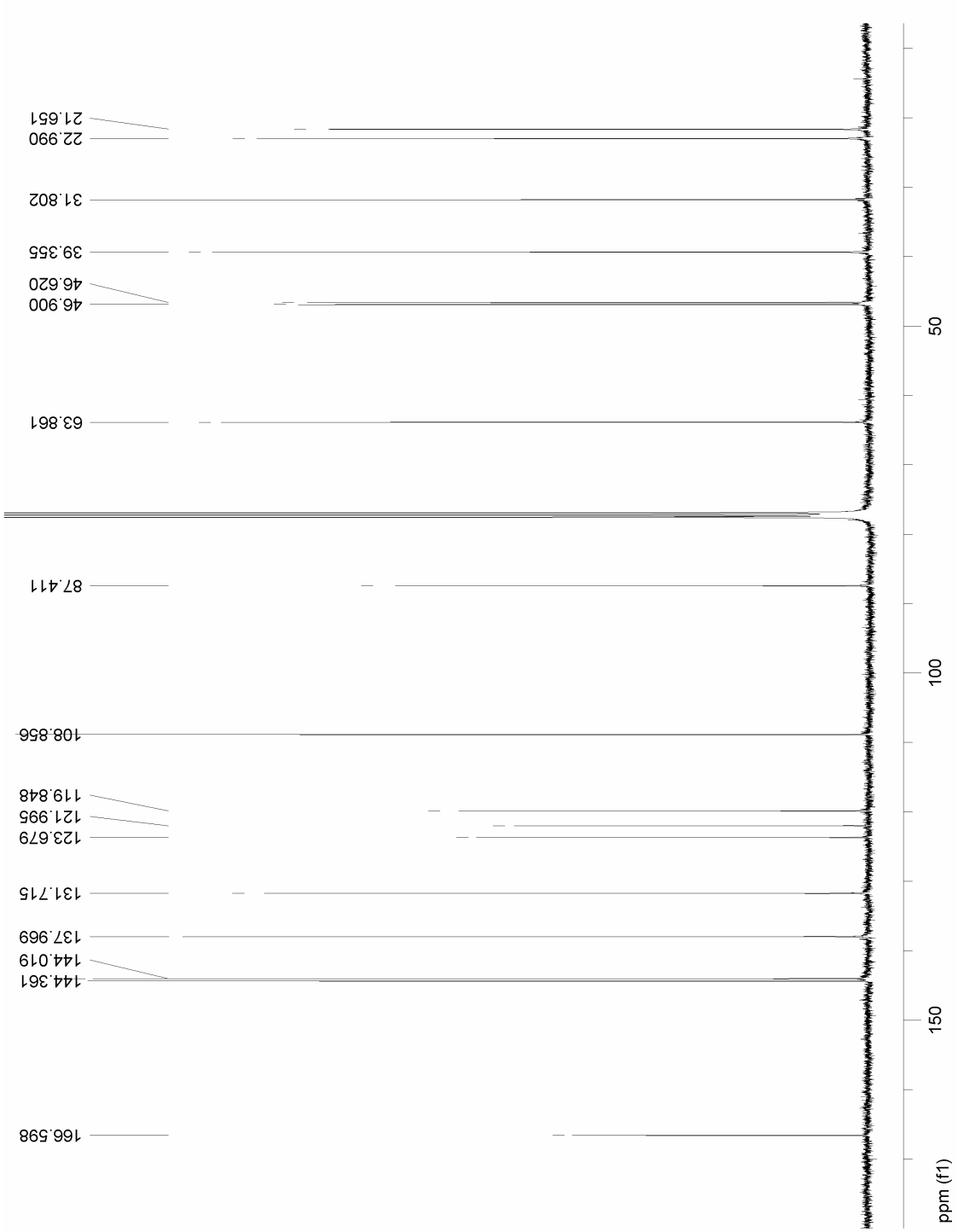

Figure A.17 ^{13}C-NMR spectrum of compound **3-2** in $^{*}CDCl_3$ (400 MHz).

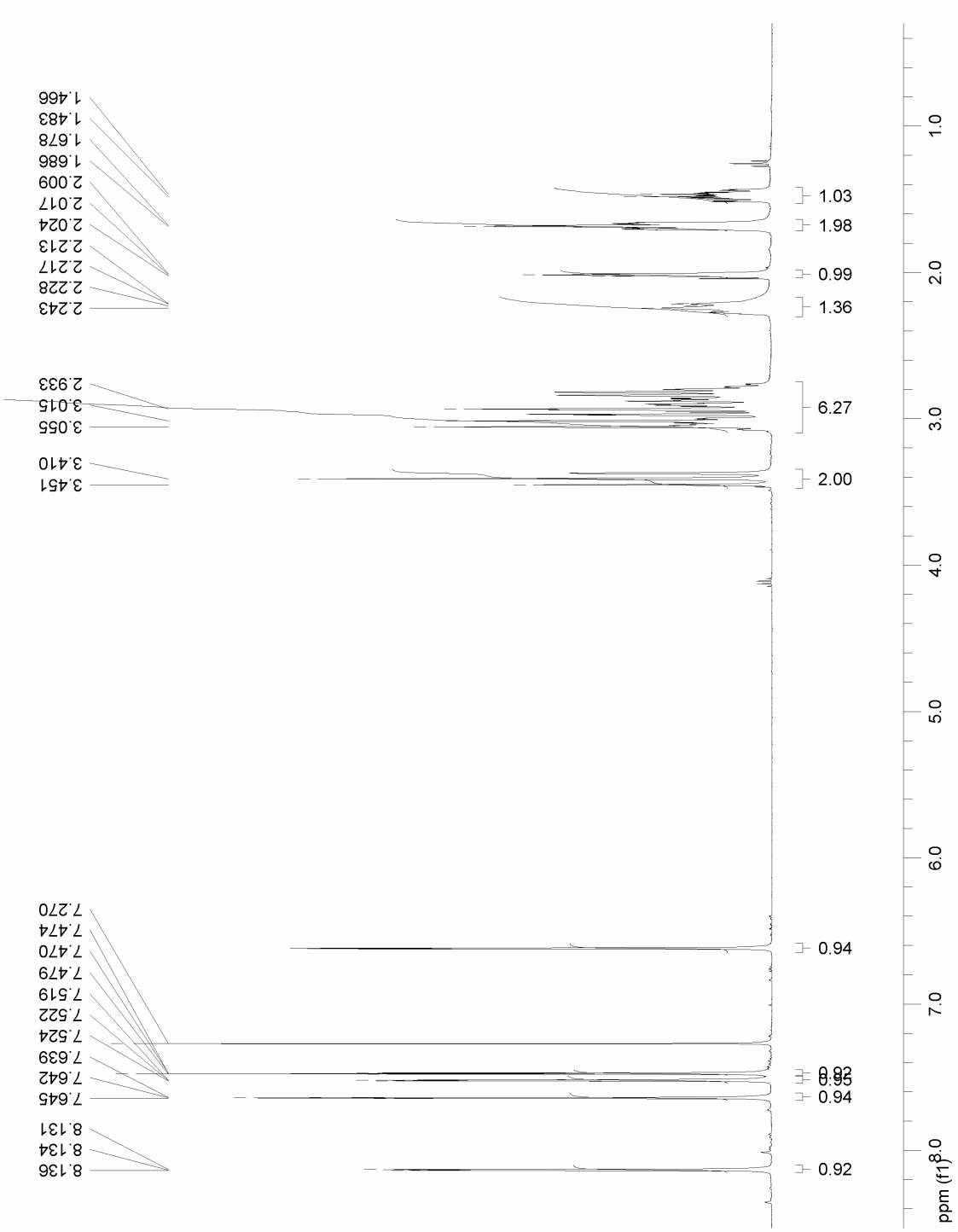

Figure A.18 ^{1}H-NMR spectrum of compound **3-2** in $^{*}CDCl_3$ (400 MHz).

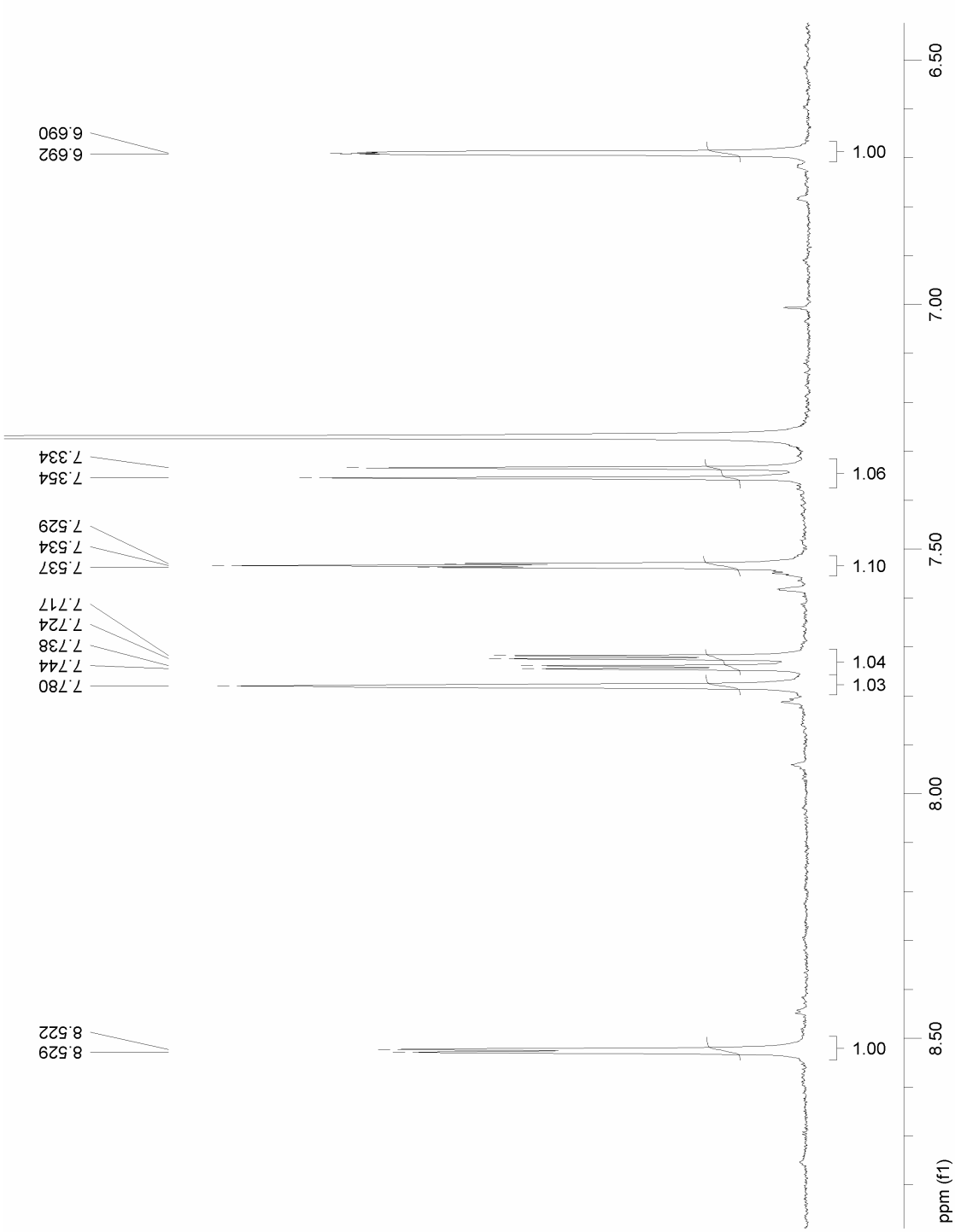

Figure A.19 ^{1}H-NMR spectrum of compound **3-10** in $^{*}CDCl_3$ (400 MHz).

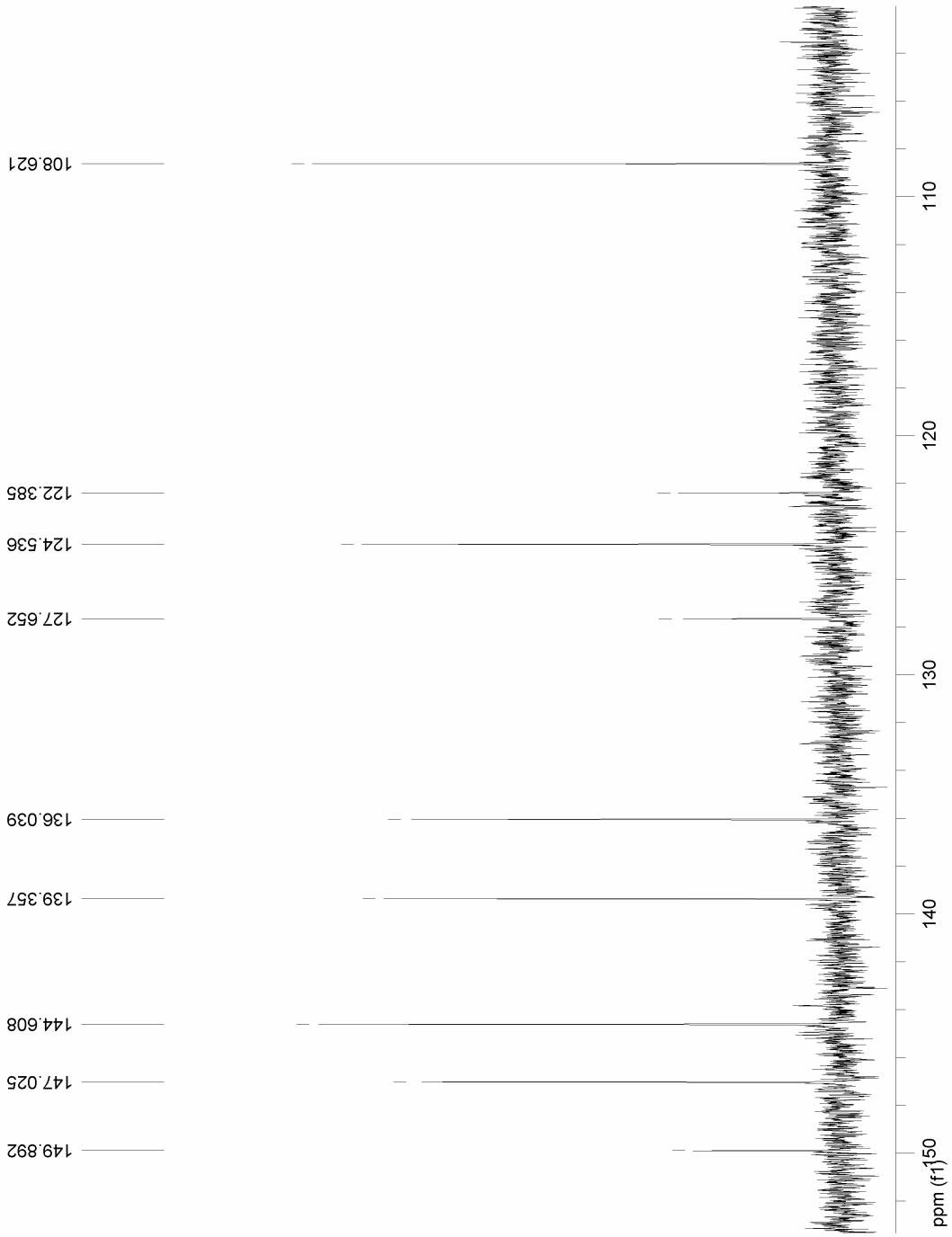

Figure A.20 ^{13}C-NMR spectrum of compound **3-10** in $^{*}CDCl_3$ (400 MHz).

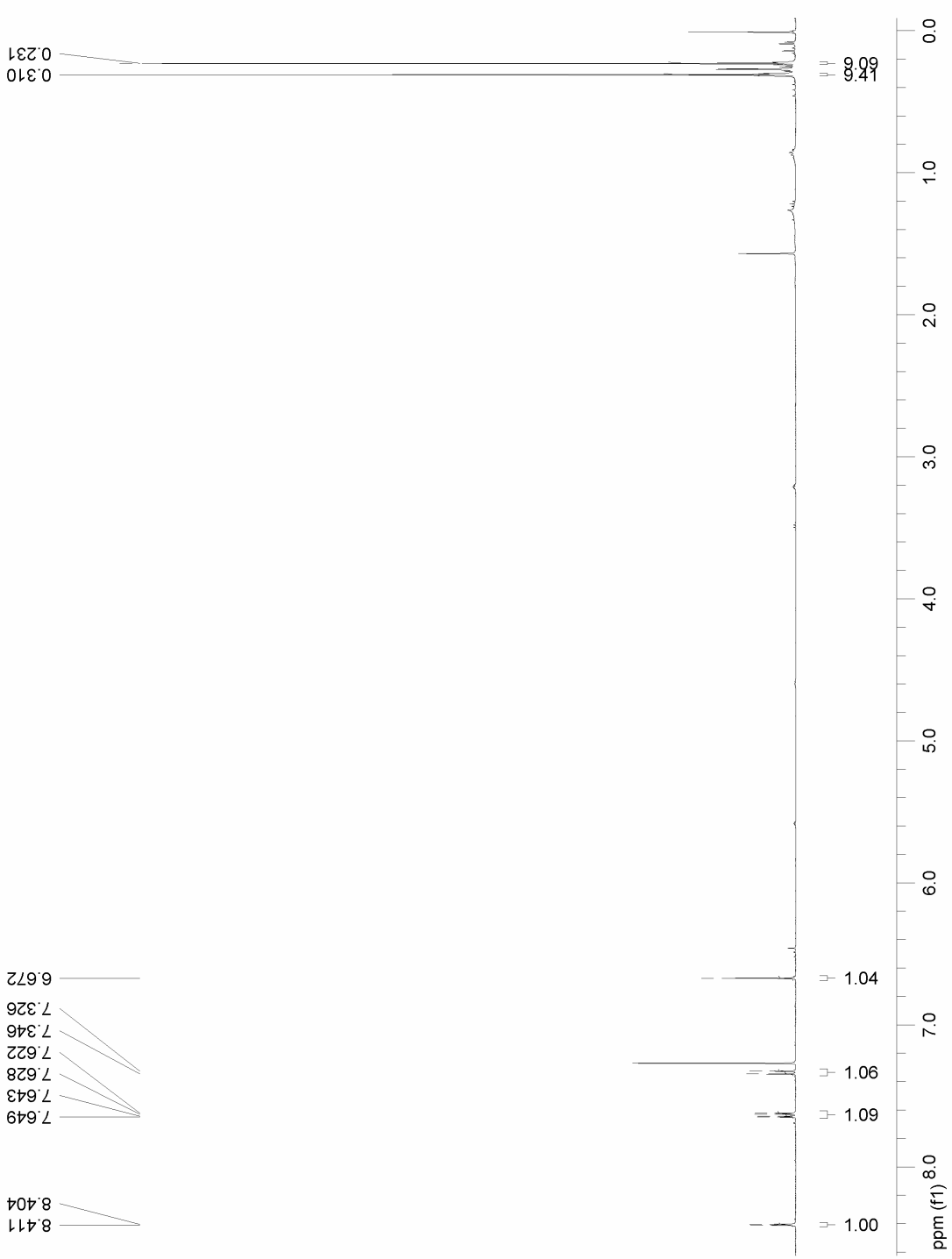

Figure A.21 ^{1}H-NMR spectrum of compound **3-12** in $^{*}CDCl_3$ (400 MHz).

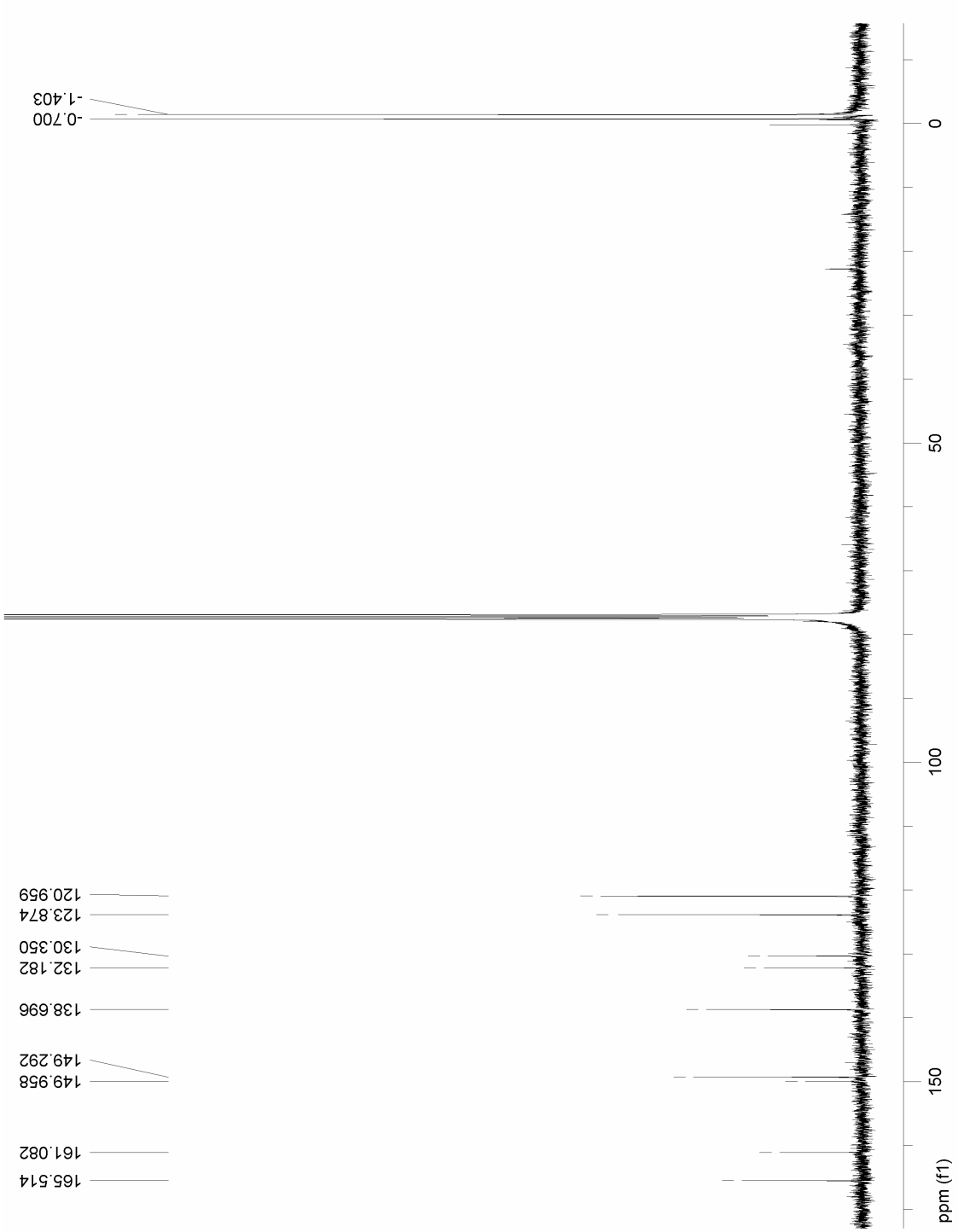

Figure A.22 ^{13}C-NMR spectrum of compound **3-12** in $^{*}CDCl_3$ (400 MHz).

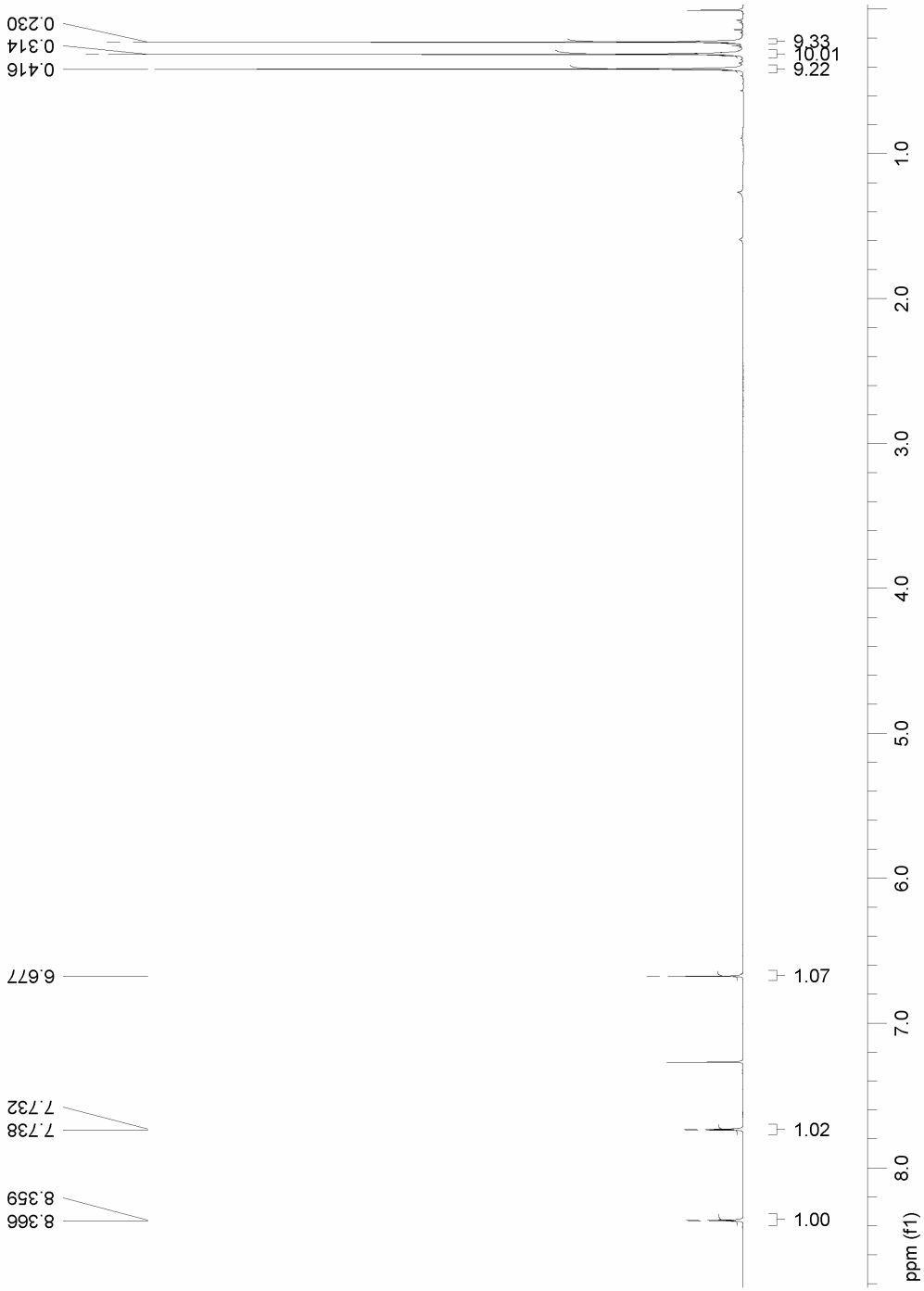

Figure A.23 ^{1}H-NMR spectrum of compound **3-13** in $^{*}CDCl_3$ (400 MHz).

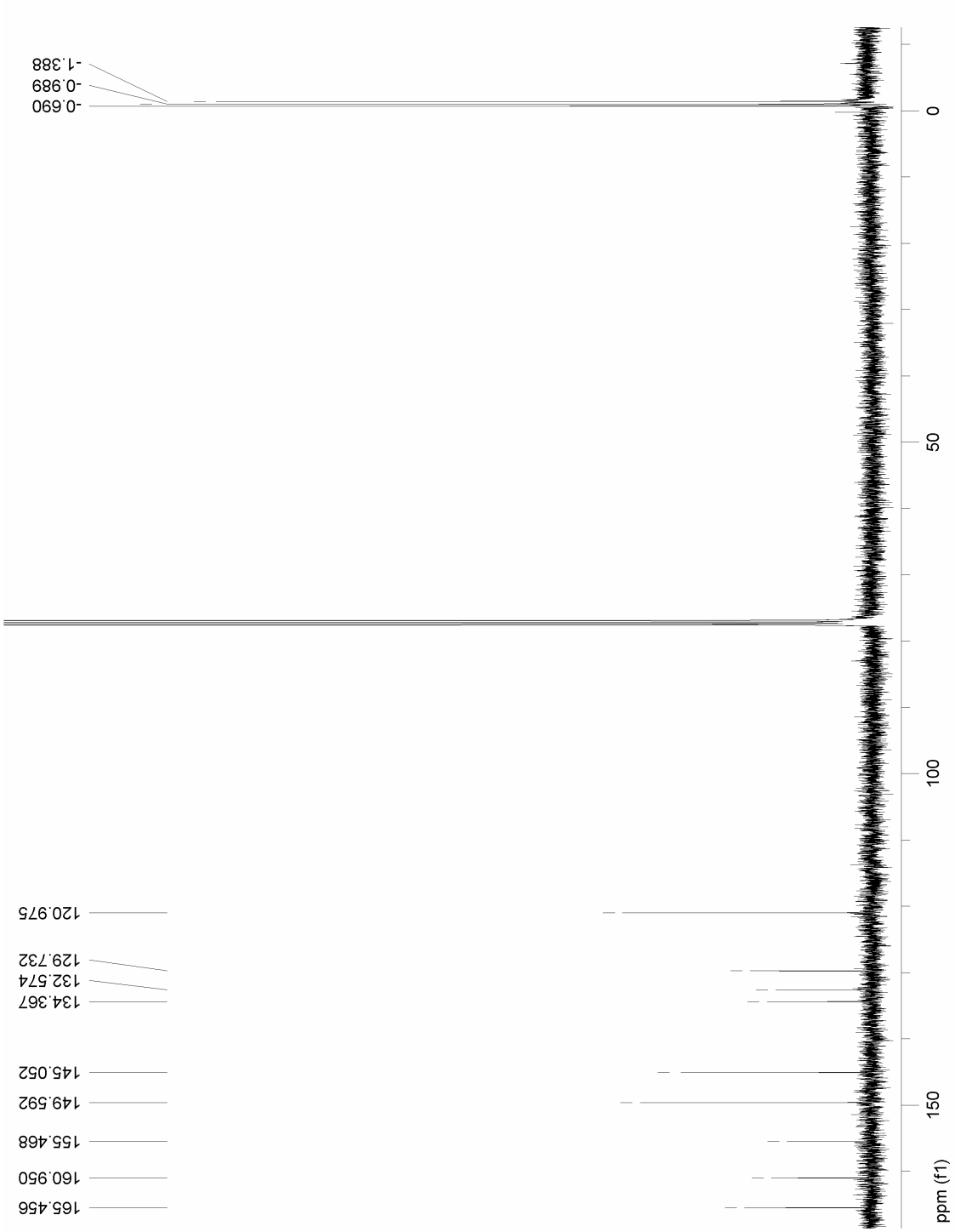

Figure A.24 ^{13}C-NMR spectrum of compound **3-13** in $^{*}CDCl_3$ (400 MHz).

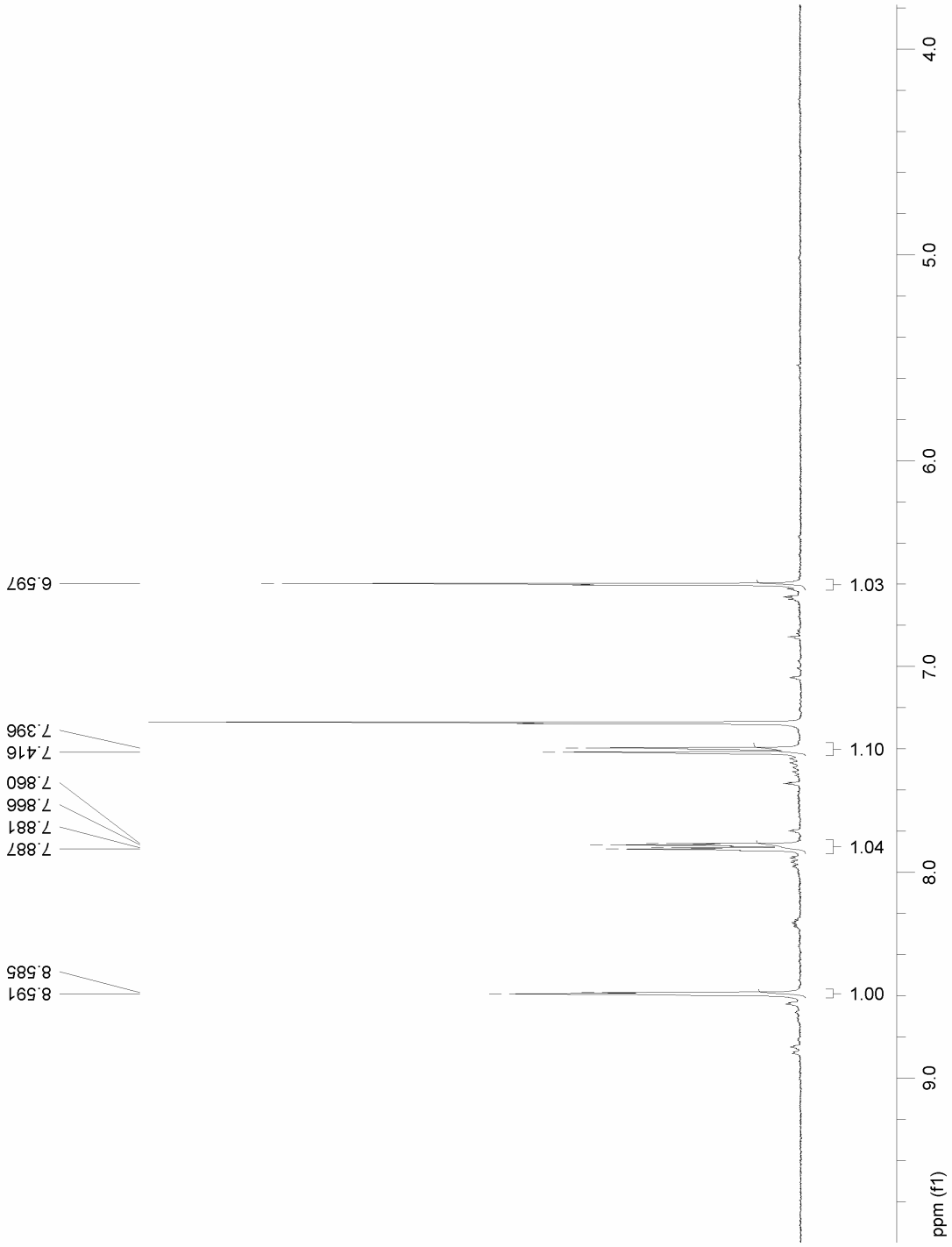

Figure A.25 ^{1}H-NMR spectrum of compound **3-14** in $^{*}CDCl_3$ (400 MHz).

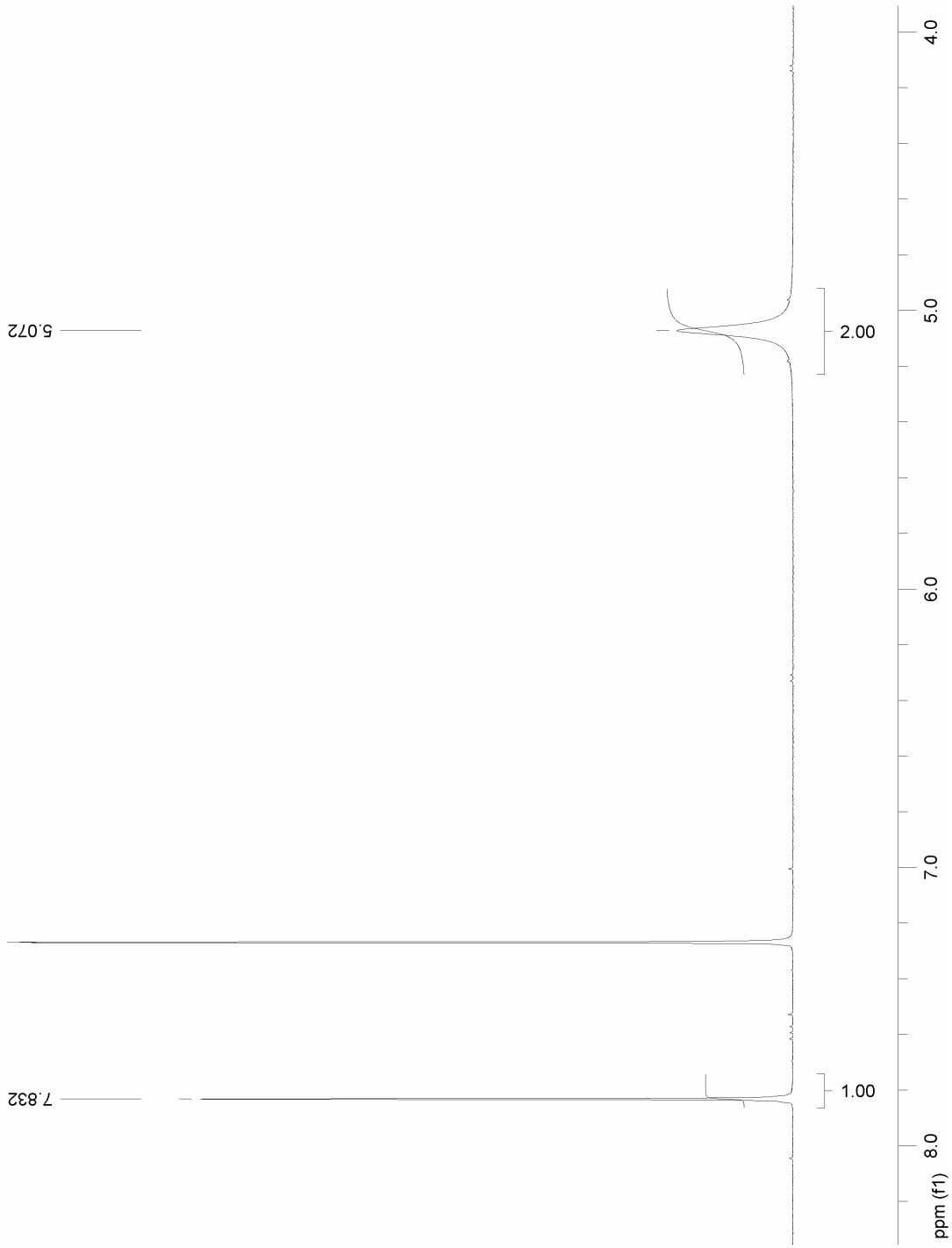

Figure A.26 ^{1}H-NMR spectrum of compound **3-15** in $^{*}CDCl_3$ (400 MHz).

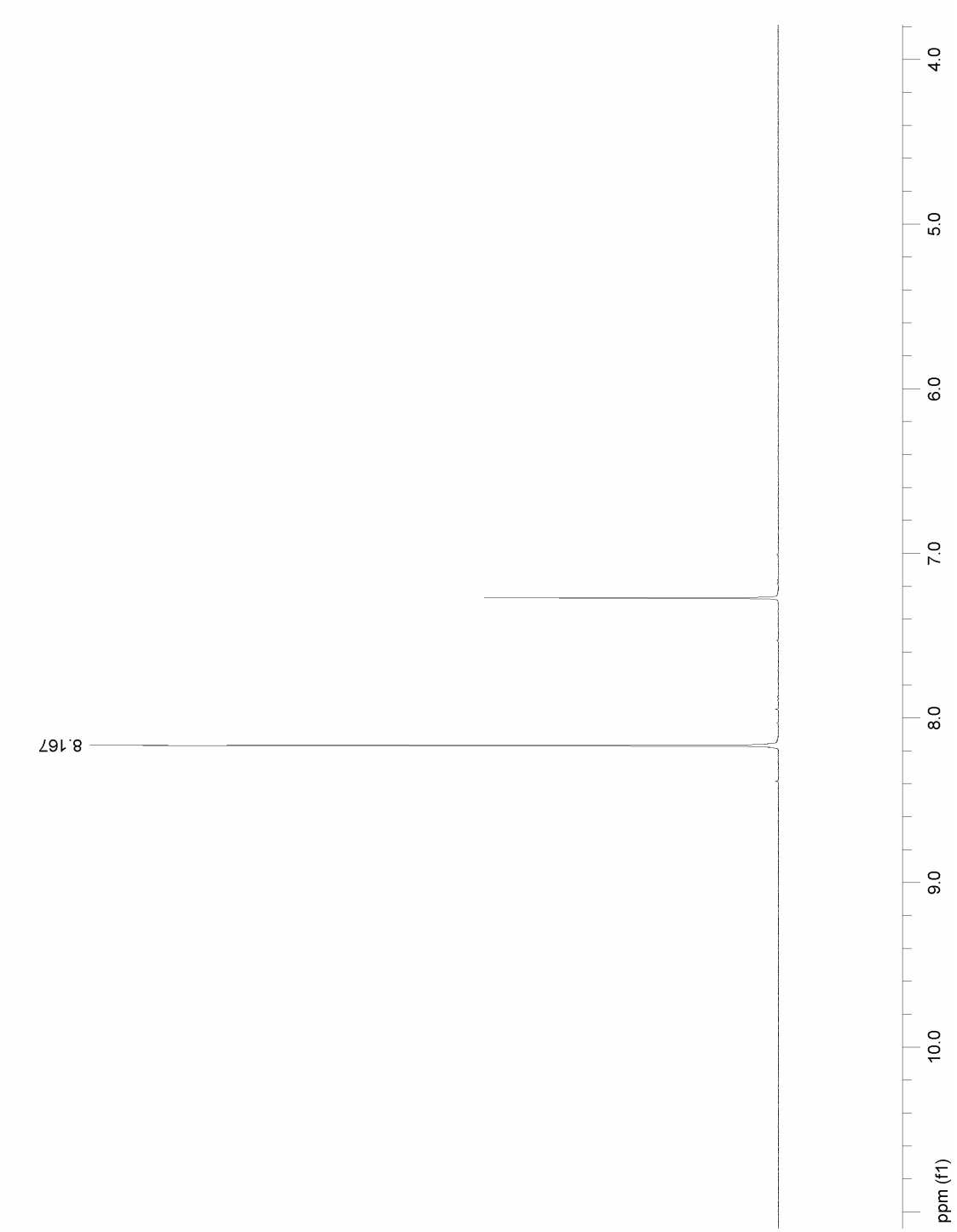

Figure A.27 ^{1}H-NMR spectrum of compound **3-16** in $^{*}CDCl_3$ (400 MHz).

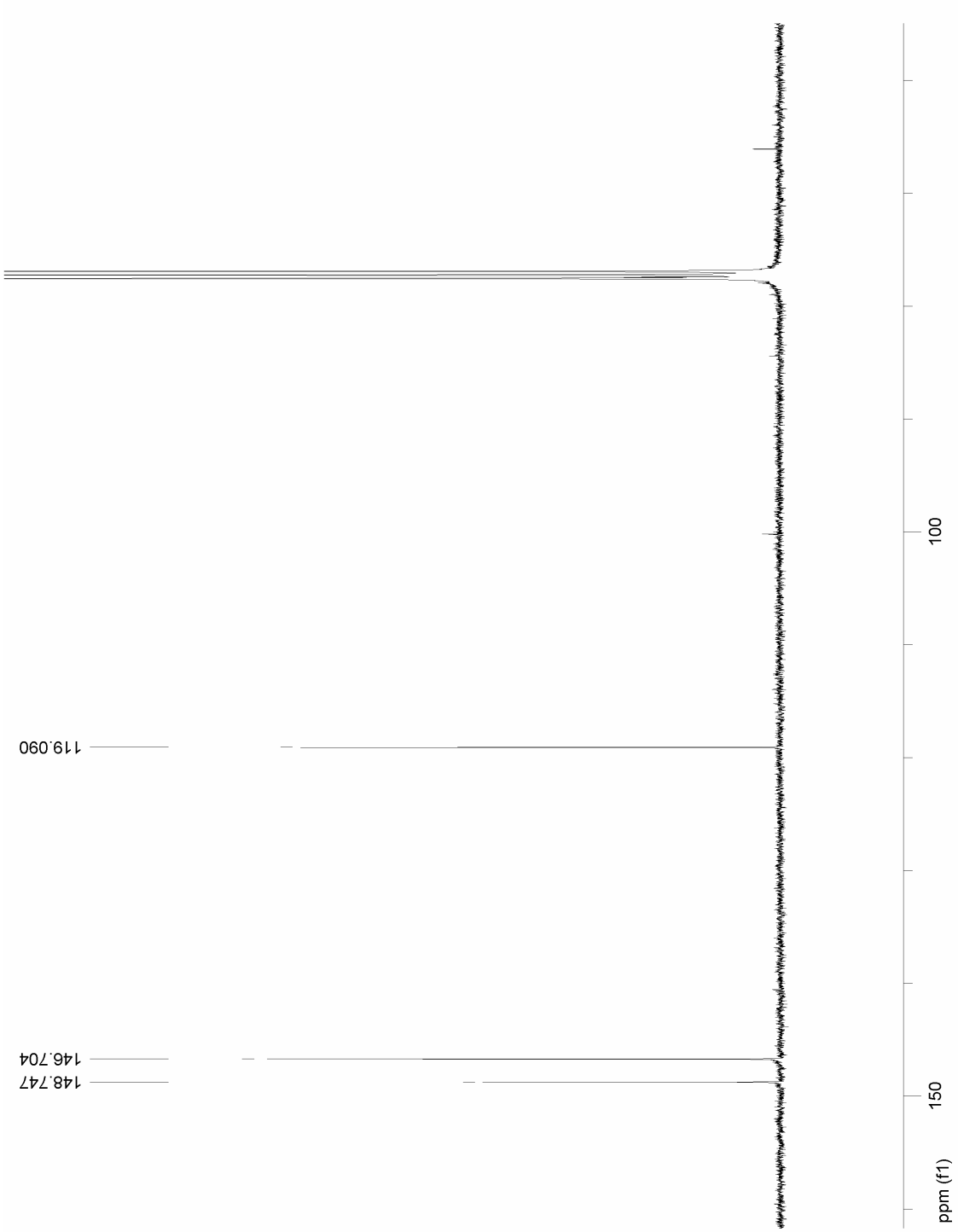

Figure A.28 ^{13}C-NMR spectrum of compound **3-16** in $^{*}CDCl_3$ (400 MHz).

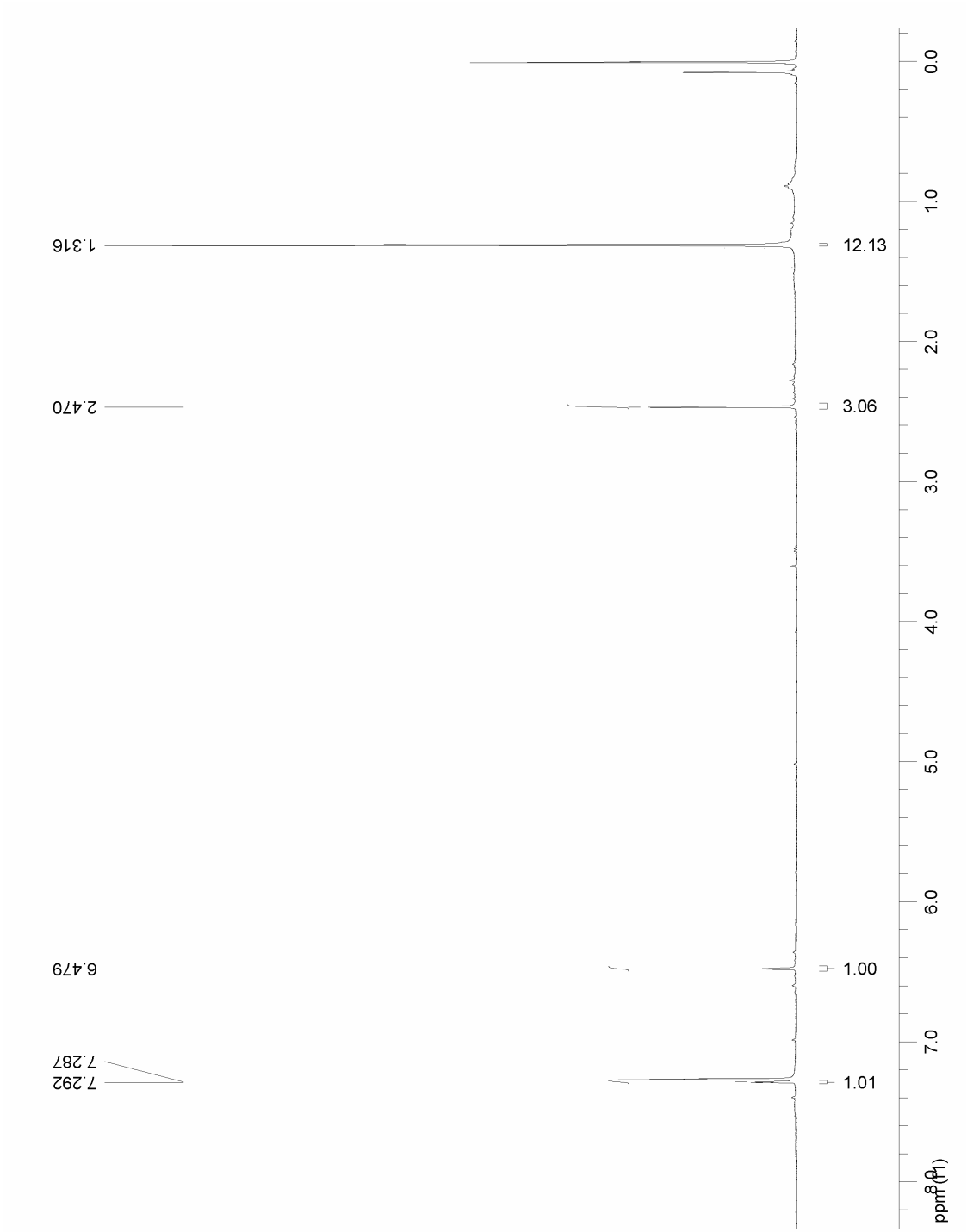

Figure A.29 ^{1}H-NMR spectrum of compound **3-20** in $^{*}CDCl_3$ (400 MHz).

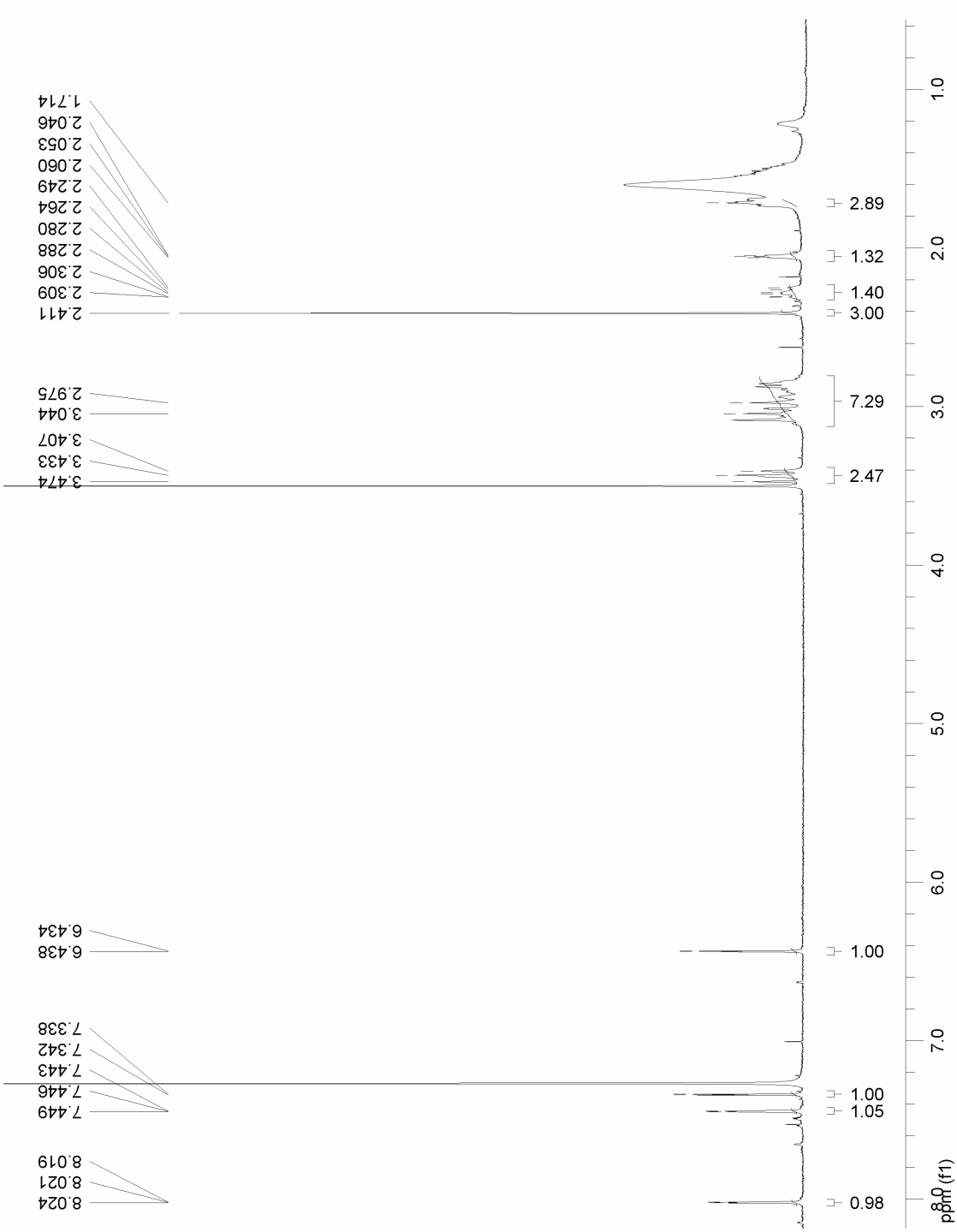

Figure A.30 ^{1}H-NMR spectrum of compound **3-1** in $^{*}CDCl_3$ (400 MHz).

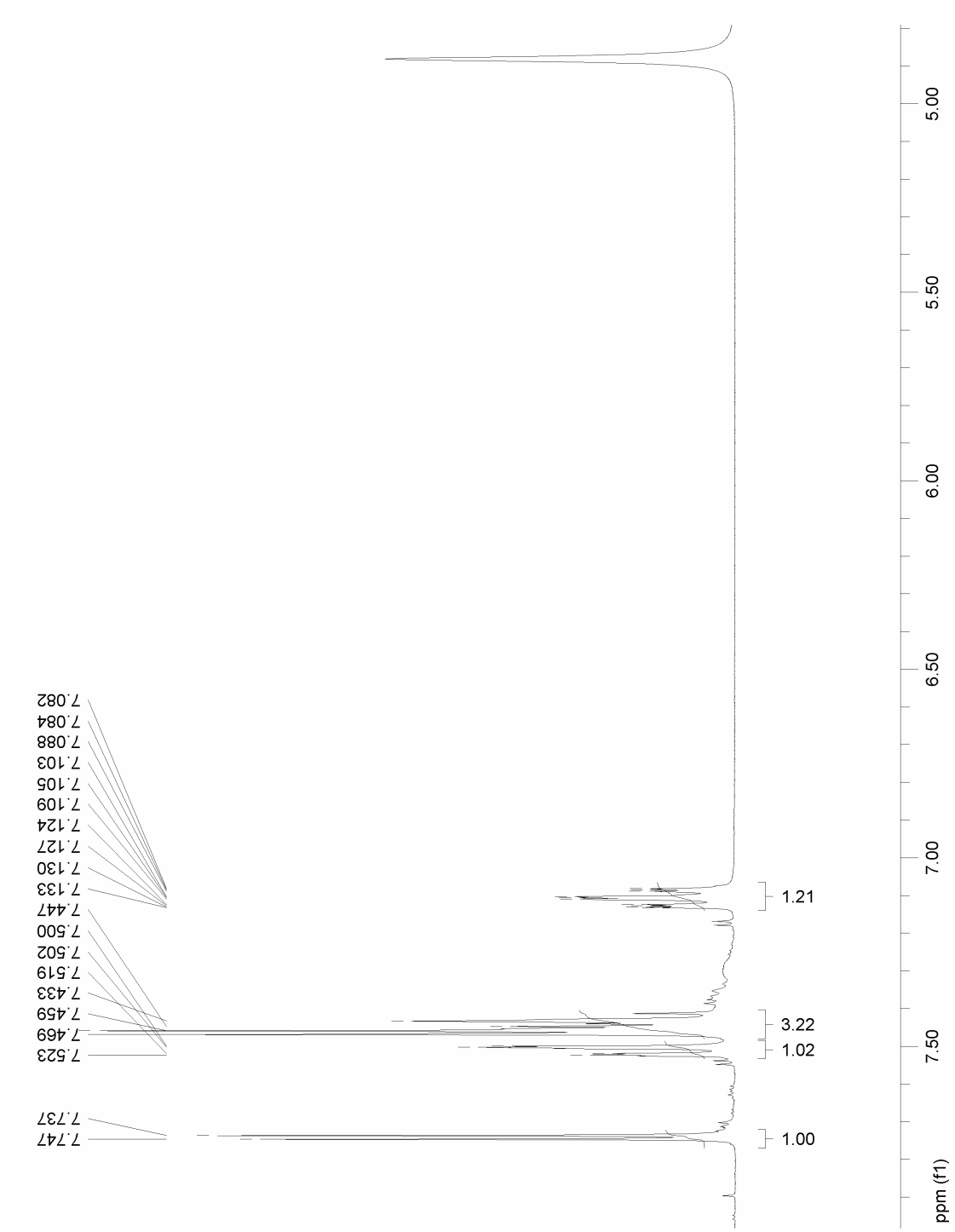

Figure A.31 ^{1}H-NMR spectrum of compound **3-22** in $^{*}CD_3OD$ (400 MHz).

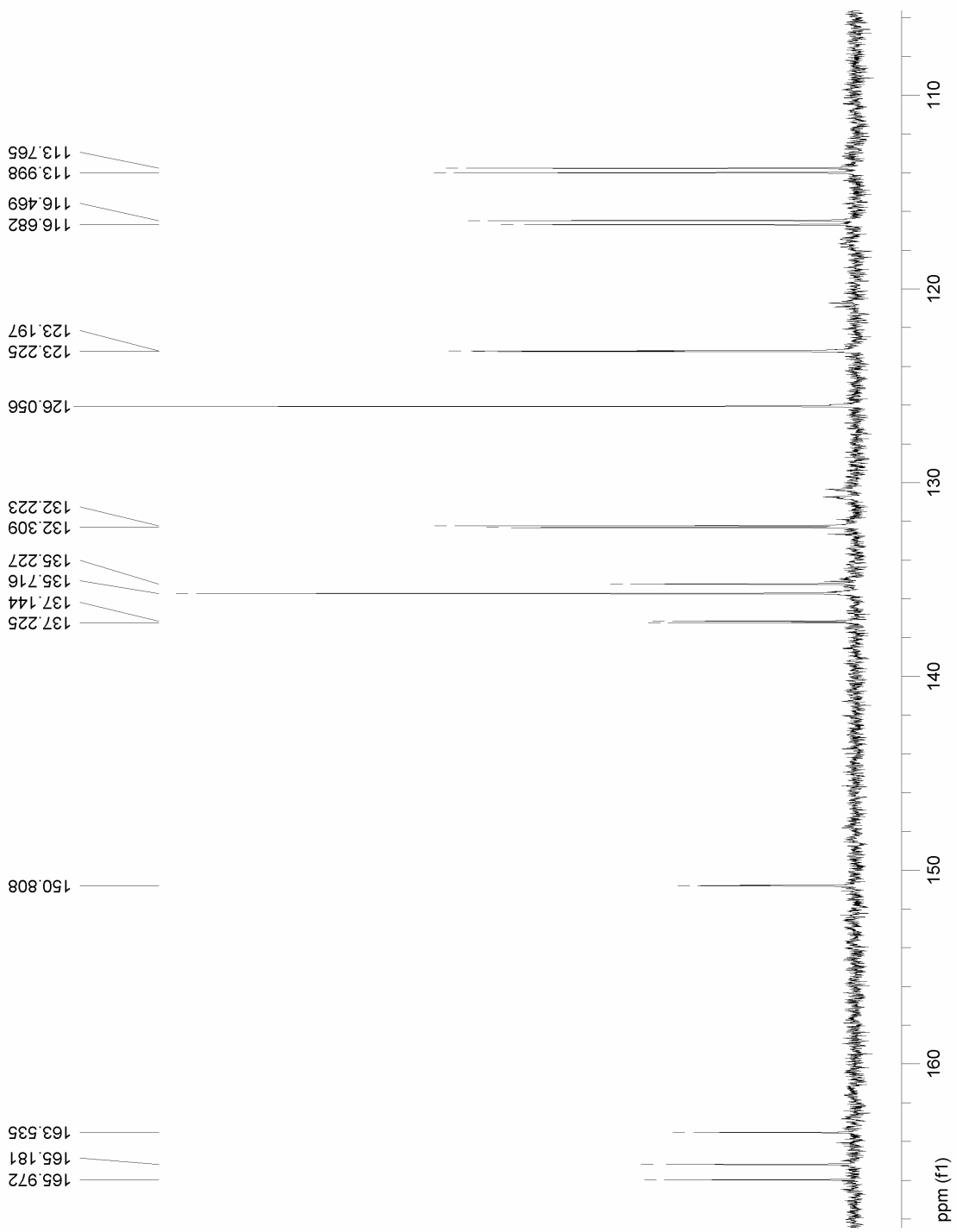

Figure A.32 ^{13}C-NMR spectrum of compound **3-22** in $^{*}CDCl_3$ (400 MHz).

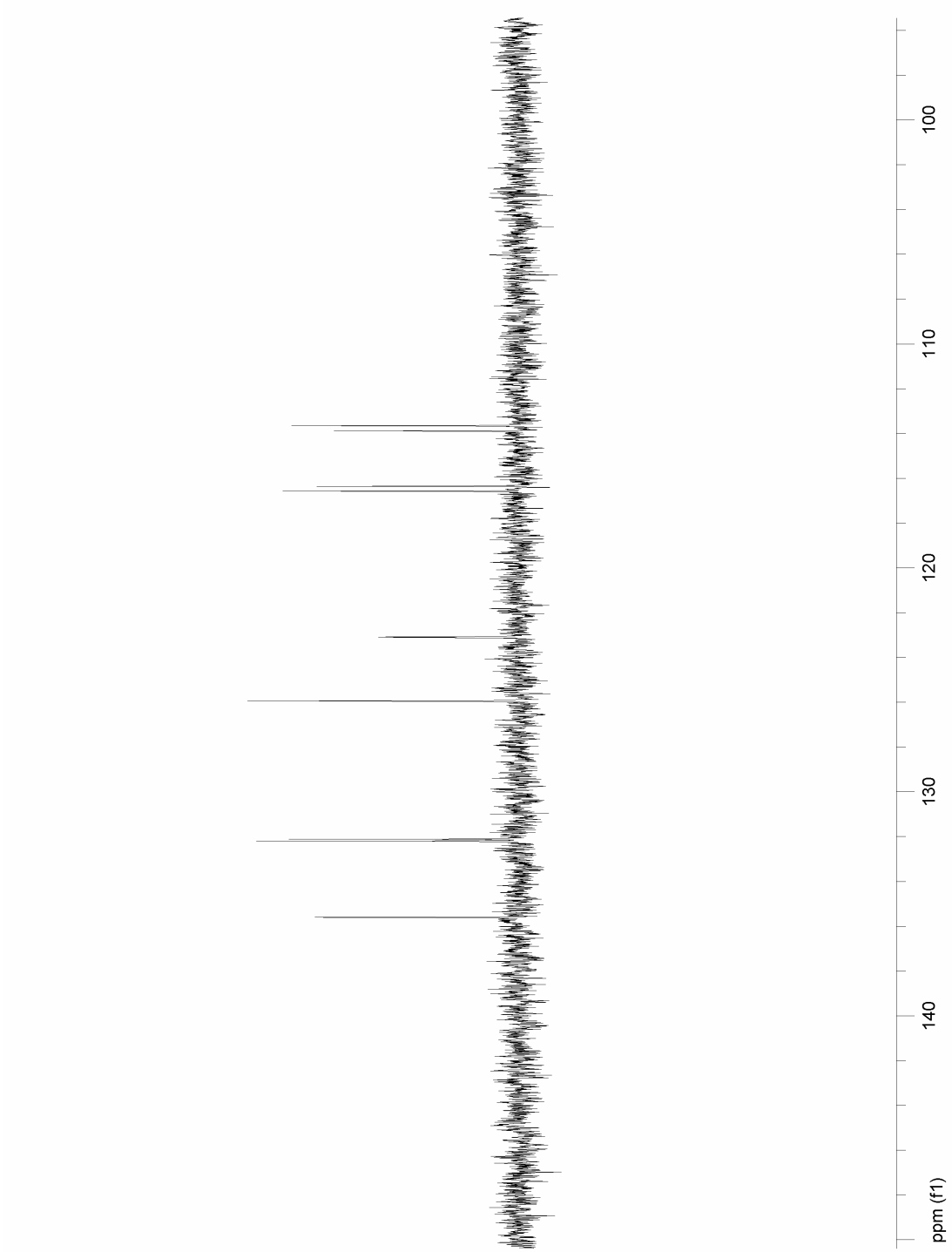

Figure A.33 DEPT spectrum of compound **3-22** in $^{*}CDCl_3$ (400 MHz).

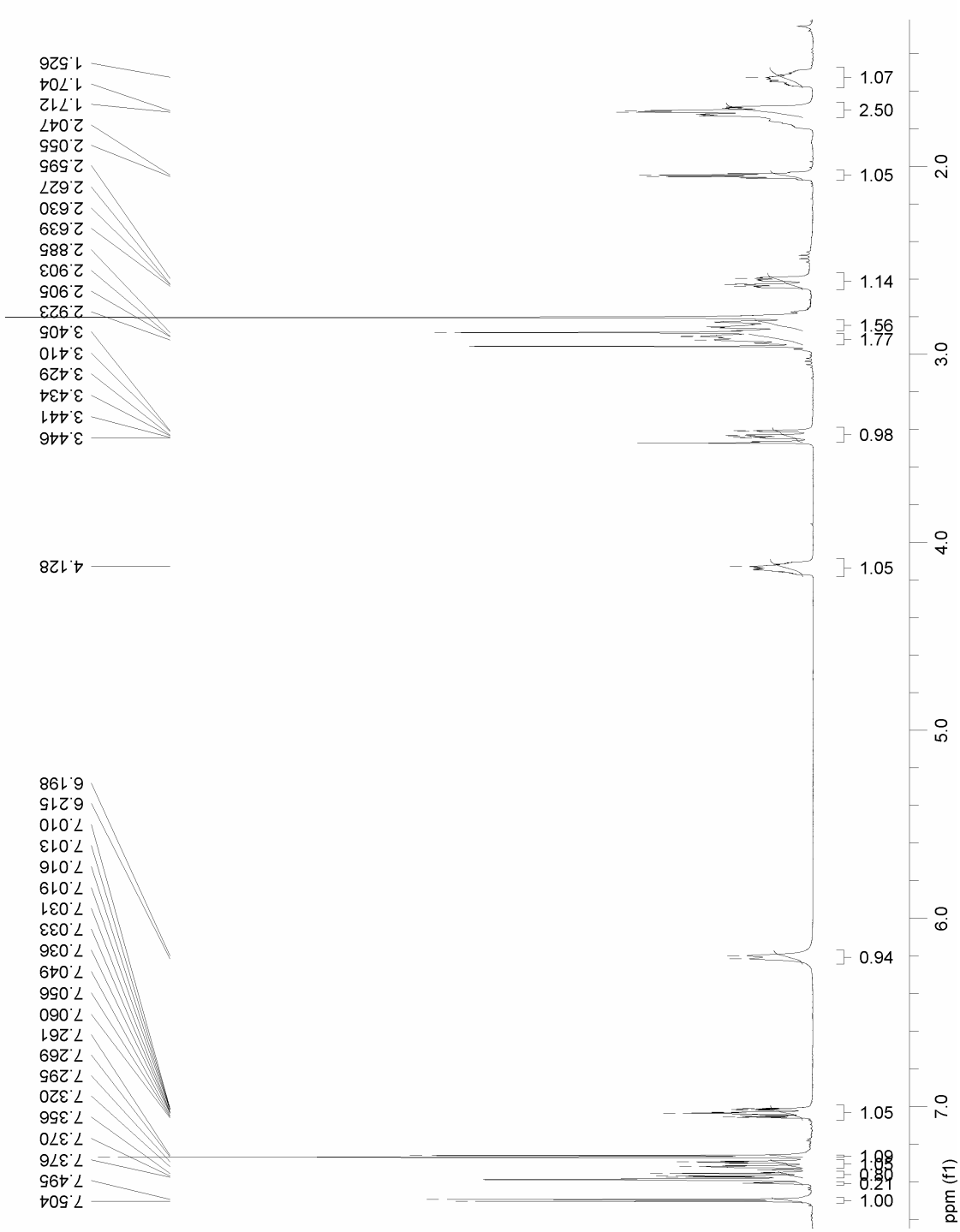

Figure A.34 ^{1}H-NMR spectrum of compound **3-21** in $^{*}CDCl_3$ (400 MHz).

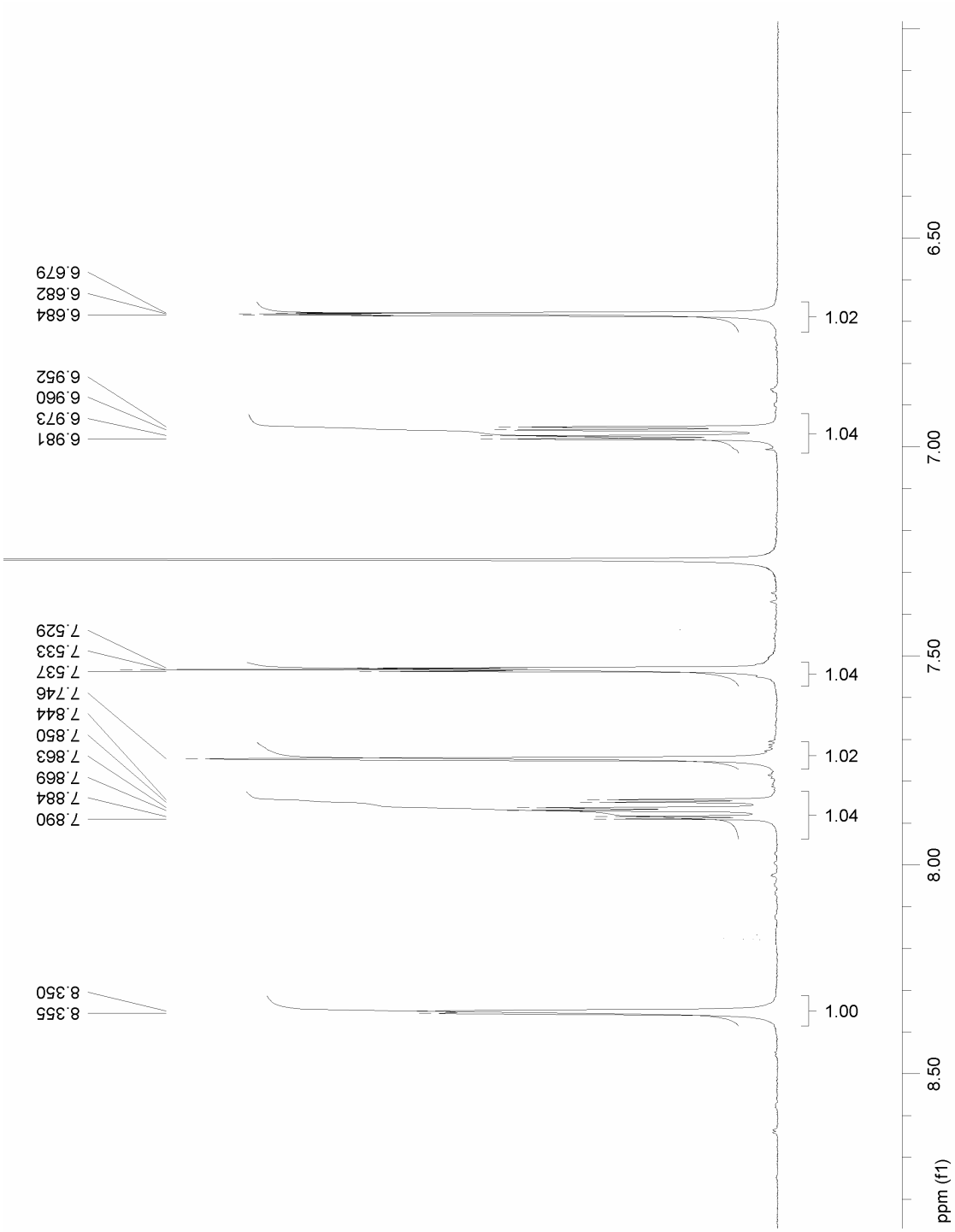

Figure A.35 ^{1}H-NMR spectrum of compound **3-26** in $^{*}CDCl_3$ (400 MHz).

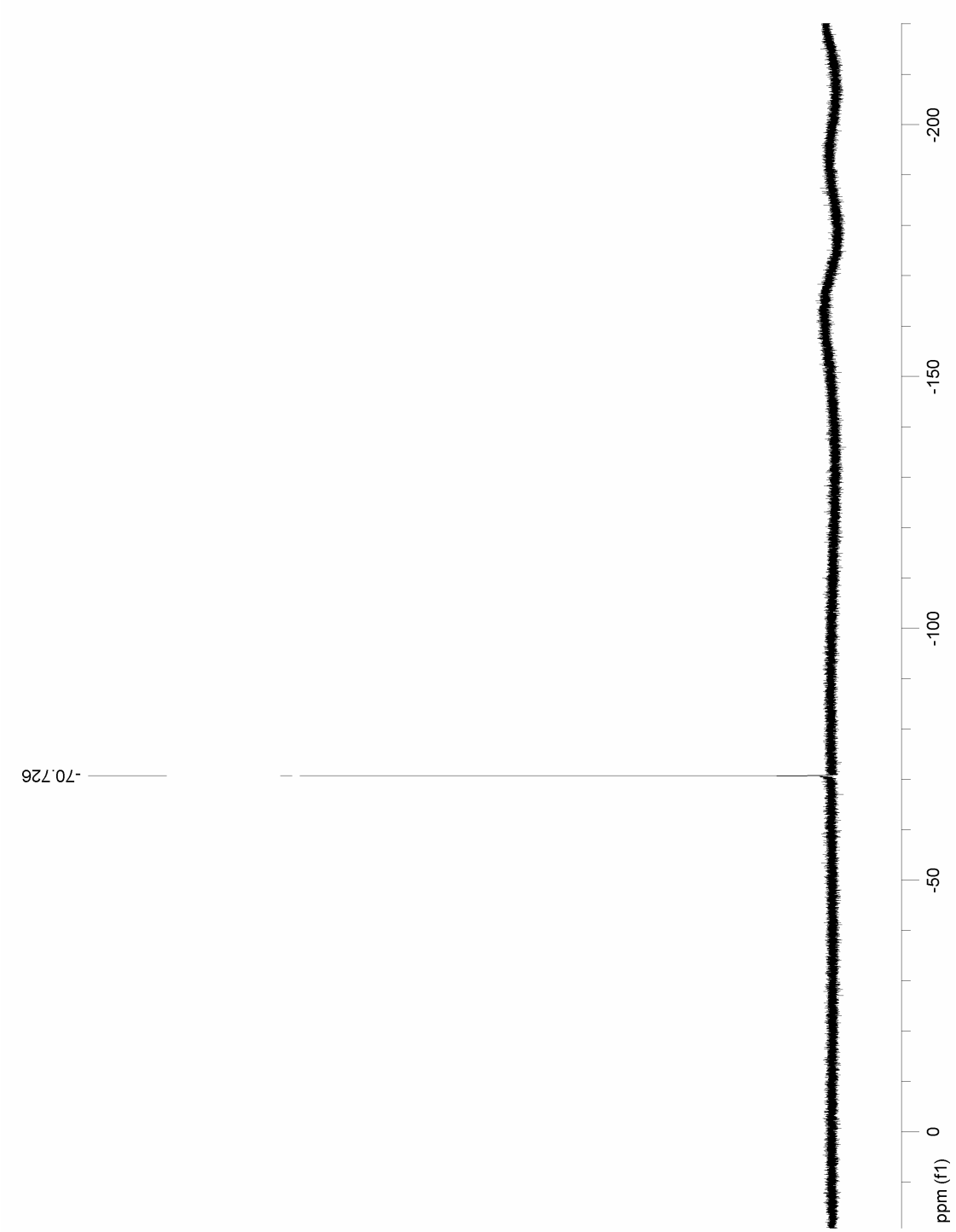

Figure A.36 ^{19}F-NMR spectrum of compound **3-26** in $^{*}CDCl_3$ (400 MHz).

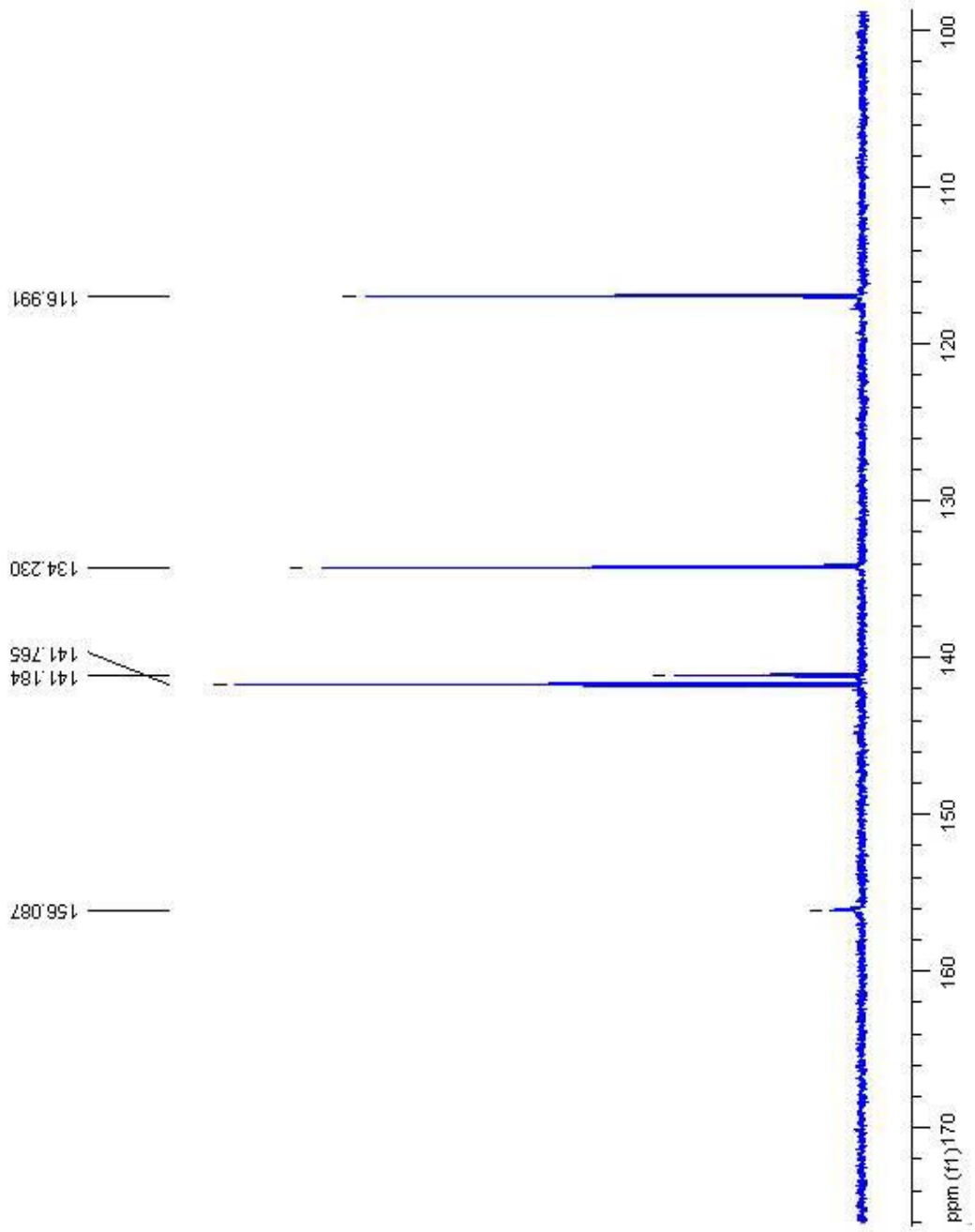

Figure A.37 ^{13}C-NMR spectrum of compound **3-23** in $^{*}CDCl_3$ (400 MHz).

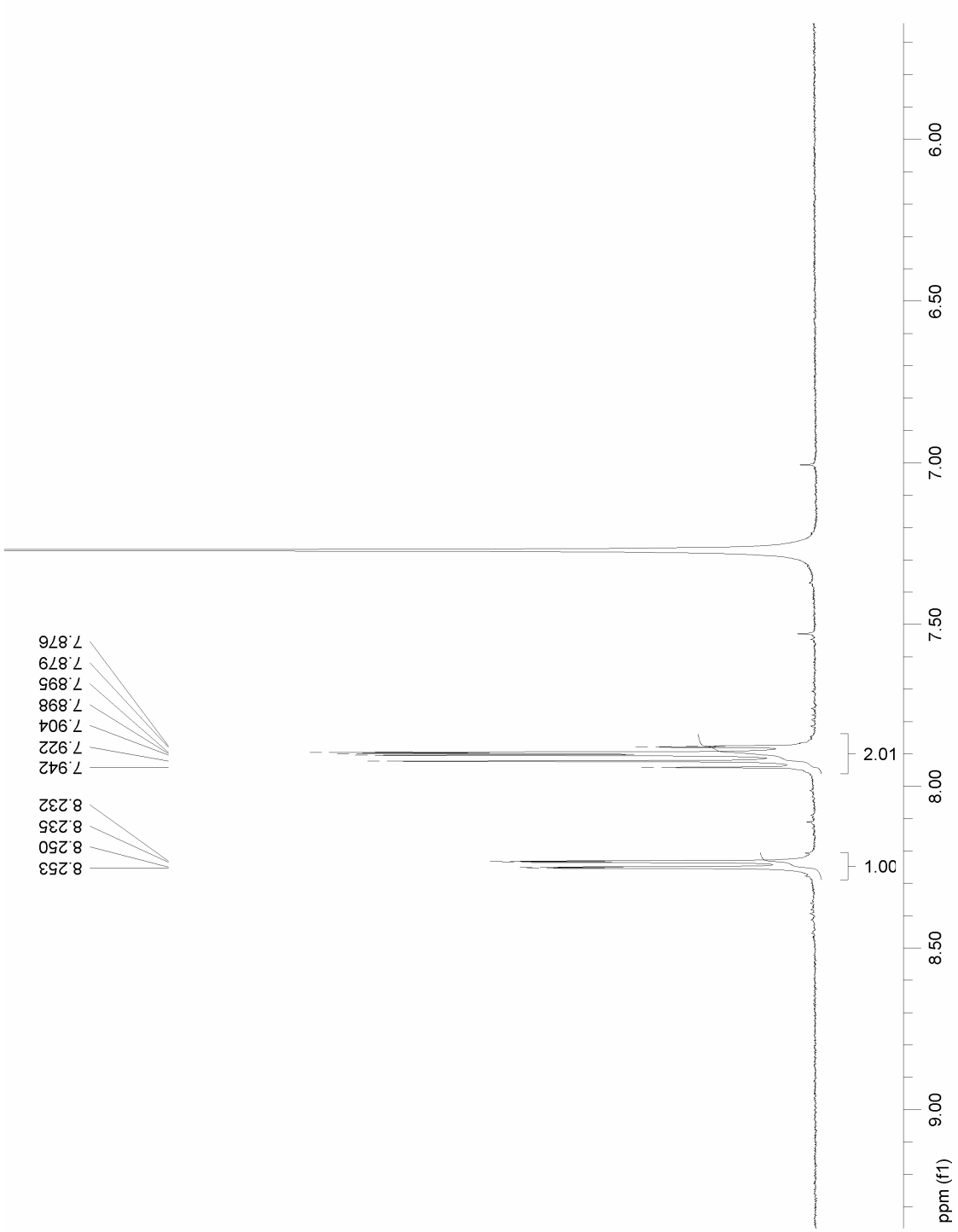

Figure A.38 ^{1}H-NMR spectrum of compound **3-23** in $^{*}CDCl_3$ (400 MHz).

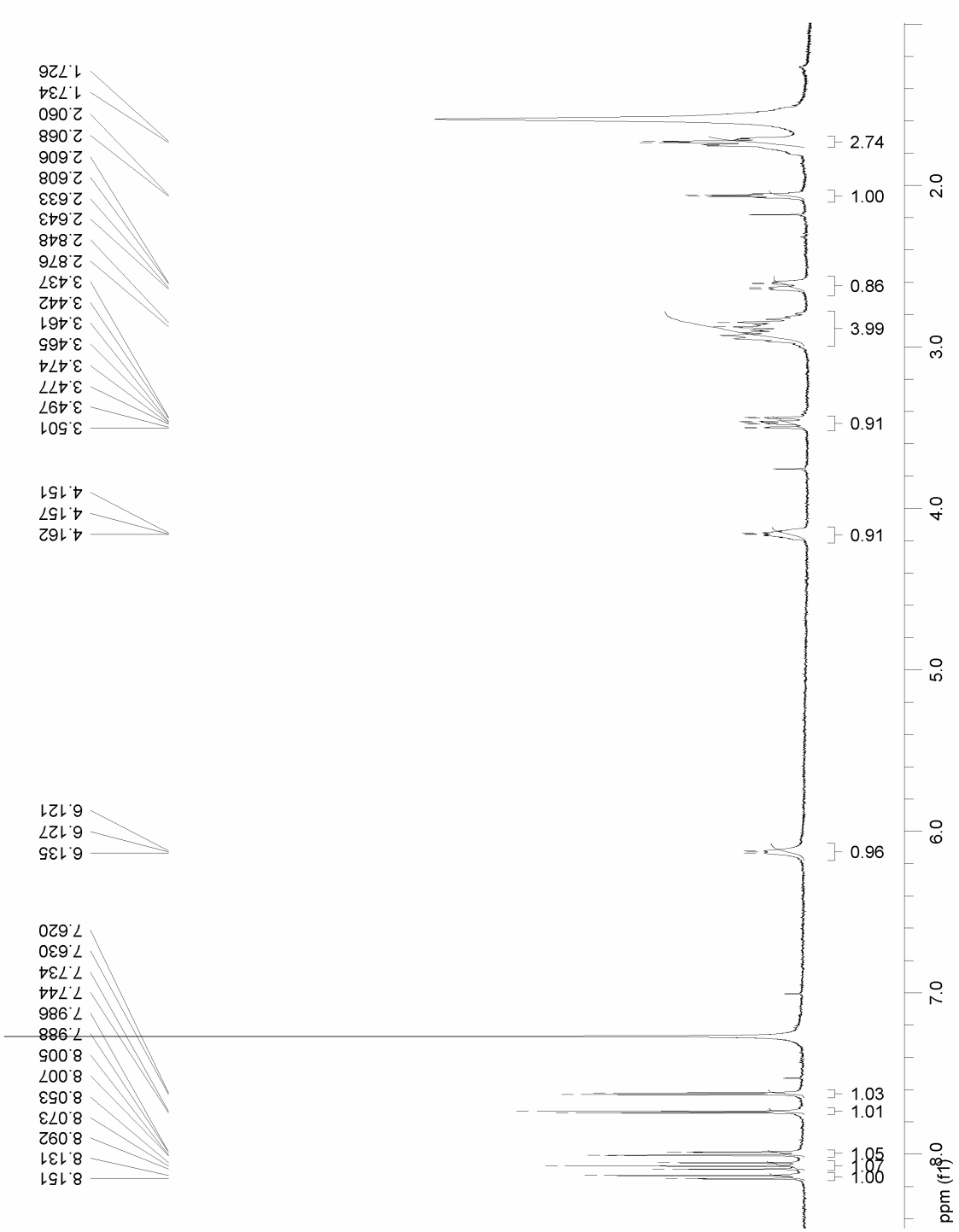

Figure A.39 ^{1}H-NMR spectrum of compound **3-25** in $^{*}CDCl_3$ (400 MHz).

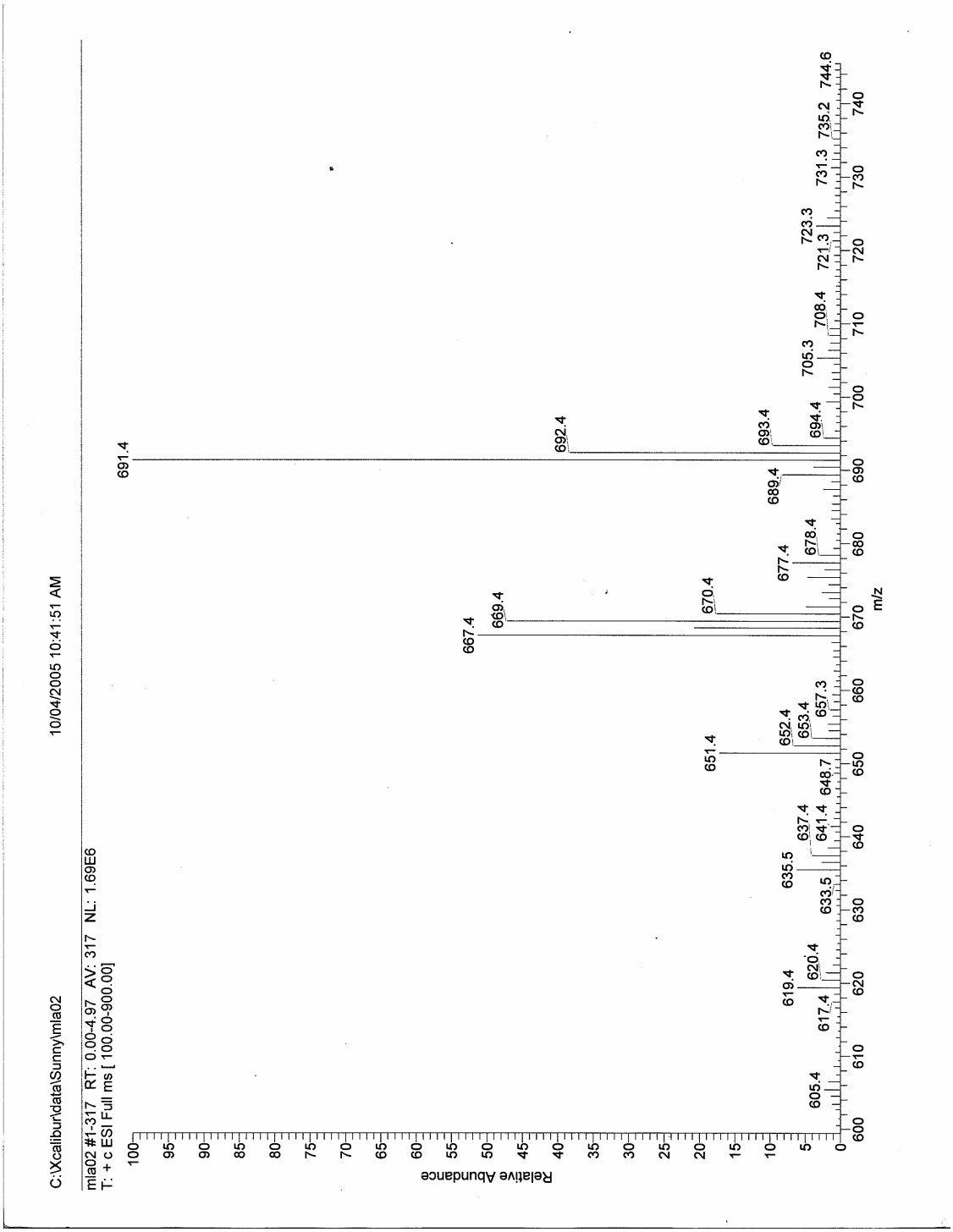

Figure A.40 Mass spectrum of compound **4-2** (ESI).